UNIVERSITÀ
DEGLI STUDI
FIRENZE

Scuola di dottorato in Scienze Biomediche

DOTTORATO DI RICERCA IN
BIOCHIMICA E BIOLOGIA APPLICATA

CICLO XXVI

COORDINATORE Prof. Stefani Massimo

"STUDY OF THE MOLECULAR BASES OF THE TOXICITY OF AMYLOID AGGREGATES"

Settore Scientifico Disciplinare BIO/10

Dottorando
Dott.ssa Conti Simona

Tutore
Dott.ssa Cecchi Cristina

Coordinatore
Prof. Dello Sbarba Persio

Anni 2011/2013

Dedication

To my family

Chapter 1- Introduction

Proteins: from synthesis to degradation

Protein folding

Maintaining the proteome to preserve the health of an organism in the face of developmental changes, environmental insults, infectious diseases, and rigors of aging is a formidable task. The challenge is magnified by the inheritance of mutations that render individual proteins subject to misfolding and/or aggregation . Maintenance of the eukaryotic protein homeostasis, or proteostasis, requires the orchestration of protein synthesis, folding, degradation, and trafficking by highly conserved and deeply integrated cellular networks that sometimes synergize and sometimes compete to regulate the function of the proteome [Morimoto RI 1998; Balch WE et al. 2008; Morimoto RI and Cuervo AM 2009; Powers ET et al. 2009; Jarosz DF et al. 2010; Taipale M et al. 2010]. Proteins are macromolecules made up of α- amino acid residues connected together by amide bonds. They range in size from approximately 35 to more than one thousand amino acid residues and are often composed of more than one independently folding domain [Lindquist and Kelly 2011]. Proteins have evolved to contain all the information required to adopt their correct architecture within their own amino acids sequences [Luheshi LM and Dobson CM 2009]. The biosynthesis of proteins occurs on the ribosome, a complex riboprotein nanomachine that translates messenger RNA (mRNA) into a polypeptide chain. The linear synthesis of proteins performed by the ribosome in the amino to carboxy-terminal direction allows individual domains to fold and/or be engaged by proteostasis network components (e.g., chaperones) before the entire protein is synthesized [Junker M et al. 2009]. Mechansisms such as the unfolded protein response have also evolved in the cell for sensing and responding to an excess of misfolded proteins and for targeting them to be degraded by proteolytic systems such as the proteosome [Luheshi LM and Dobson CM 2009]. Protein folding is the physical process by which a polypeptide chain changes its conformation to reach a biologically active threedimensional structure. Folding in vivo is in some cases co-translational and it is initiated before the completion of protein synthesis, whereas the nascent chain is still attached to the ribosome. Other

proteins, however, undergo the major part of their folding in the cytoplasm after release from the ribosome, whereas yet others fold in specific compartments, such as mitochondria or the endoplasmic reticulum (ER), after trafficking and translocation through membranes [Dobson CM 2003]. Native states of proteins almost always correspond to the structures that are most thermodynamically stable under physiological conditions [Dobson CM et al 2003]. Cyrus Levinthal in 1968 for the first time poses the problem of how, and with which mechanism, can a protein fold so quickly. If a given protein is to attain its correctly folded configuration by sequentially sampling all the possible conformations, it would require a time longer than the age of the universe to arrive at its correct native conformation [Levinthal 1969], that is the famous "Levinthal paradox". The energetics of the folding behaviour of a polypeptide chain is best described by the energy landscape of an amino acid polymer. The energy landscape contains all conformational states accessible to the polypeptide chain together with their entropy, free energy and fraction of native contacts. These species are heterogeneous, highly dynamic and disordered conformational ensembles whose structures are far from the native one (Fig 2). The protein energy landscape is encoded in the amino acid sequence and, in the case of natural proteins, is robust and has the very special appearance of a rough funnel biased towards the native state. The folding funnel view of structure acquisition makes it clear that there are multiple pathways for arriving at the folded ensemble, and when the surface is rough, partially folded intermediates are populated (confirmed by experiments) that can be prone to aggregation and proteolysis [Lindquist and Kelly 2011]. It is proposed that the key signature for a protein to fold correctly can be traced back to the pattern of hydrophobic and polar (notably charged) residues that favours preferential interactions of specific residues as the compactness of the structure progressively increases. Once these interactions have established the correct topology of the folding protein, the process evolves rapidly and invariably to generate the native compactly folded structure [Stefani M 2008]. Ptitsyn suggested that folding could occur in a hierarchical process with the initial rapid formation of secondary structures, such as α-helices or β-sheets [Fersht AR 2008]. At each step, the formation of a new layer of structure stabilized the previous one [Fersht AR 2008]. Thus, solving Levinthal's

paradox implies that folding proceeds in a step-wise manner and that several intermediates with increasing native-like structure are populated along the folding coordinate. In the past two decades major advances have been done in folding experiments and possible mechanisms of protein folding have been proposed. Presently we know that intermediate states are ubiquitous in protein self-assembly. On their way to such states, protein molecules tend to hop between transiently populated partially folded states, thus spending most of their traveling time in a few metastable minima on their free energy landscapes. This behavior can be attributed to the fact that protein self-assembly is generally driven initially by nonspecific forces, such as hydrophobic interactions, and then finetuned by more specific interactions, such as hydrogen bonding [Vendruscolo and Dobson 2013].

Characterisation of intermediates

In the last 30 years, the use of technique like hydrogen exchange pulse labelling coupled to NMR [Roder H et al. 1988] and of protein engineering methods [Matouschek A and Fersht AR 1991] allowed structural characterization of partially folded states. More recently, the development of new instrumentation, such as ultra-rapid mixing devices [Shastry MC et al. 1998] and temperature jump relaxation techniques [Mayor et al. 2003] allowed the measurements of events within dead-time of normal stopped flow experiments. Finally, the destabilization of native state has allowed to increase the equilibrium population of partially folded states [Religa TL et al. 2005]. This has allowed solution NMR methods to be applied to solve the structure of folding intermediates of small proteins [Religa TL et al. 2005]. The characterisation of partially folded states raised the question as to whether these states are productive species en-route to the native state (on pathway intermediates) or kinetic traps that slow down the process (off-pathway partially folded conformations [Bai Y 1999; Gianni S et al. 2007] (Fig 1). If many proteins were shown to form on-pathway partially folded states [Bai Y 1999; Capaldi AP et al. 2002; Travaglini-Allocatelli C et al. 2003; Jemth P et al. 2004], recent observation that non-native interactions may be observed for productive on-pathway intermediates suggests that partial protein misfolding may be an obligatory step preceding native state consolidation [Capaldi AP et al. 2002; Religa

TL et al. 2005]. Moreover, in many cases evidence emerged that parallel pathways can lead to the formation of native states [Matagne and Dobson 1998] . This led to the description of energy landscapes for protein folding [Dinner et al. 2000; Dobson 2003; Vendruscolo M and Dobson CM 2005]. This "new view" uses the idea of an energy surface to describe the conformational ensemble accessible during folding. Unfolded molecules, structurally different, follow different pathways and populate different conformational states characterised by weak interactions [Matagne and Dobson 1998]. Faster paths and local minima exist in the landscape, but Brownian motions allow each molecule to escape kinetic traps and continue the search for the native state. If the trajectories can be numerous, the transition state is unique and all pathways lead to the formation of native state as native interactions are the most stable [Dinner et al. 2000]. Thus, energy landscapes are not in contrast with the concept of folding pathway; they are instead able to join different pathways that can be detected with different experimental approaches.

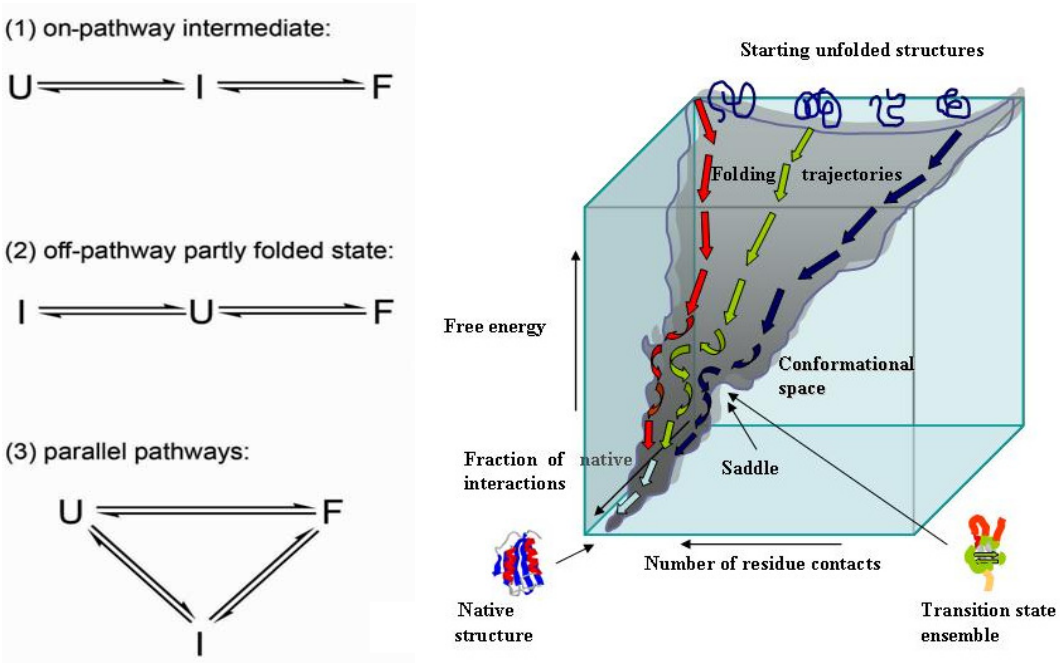

Figure 1 Partially folded states can play different roles in folding. They can be (1) onpathway intermediates, (2) off-pathway partially folded states, (3) local minima transiently populated in one of many parallel pathways that lead to the formation of the native state (F). U refers to the unfolded state.. On the right side, schematic energy landscape for protein folding. The surface is derived from a computer simulation of the folding of a highly simplified model of a small protein. The surface 'funnels' the multitude of denatured conformations to the unique native structure. Modified from [Stefani M 2008].

Protein misfolding and aggregation

The inability of a protein to adopt, or remain in, its native conformation, often referred to as protein misfolding, can be at the basis of some of the most important disorders that affect humans [Bellotti and Chiti 2008]. Many diseases, often known as misfolding or conformational diseases, ultimately result from the presence in a living system of protein molecules with structures that are 'incorrect', that differ from those in normally functioning organisms. Such diseases include conditions in which a specific protein, or protein complex, fails to fold correctly (e.g. cystic fibrosis, Marfan syndrome, amyotrophic lateral sclerosis) or is not sufficiently stable to perform its normal function (e.g. many forms of cancer) [Stefani and Dobson 2003]. Misfolding is influenced by the amino acid composition, and certain mutations are known to accelerate the process. Moreover, it also depends on environmental conditions, because once proteins are exposed to specific environmental changes such as increased temperature, high or low pH, agitation, elevated glucose, or oxidative agents, they can lose their native conformation more rapidly. The process wherein the native state is disrupted is called denaturation, and it generally results in the unfolding of the proteins. Because of the lack of arrangement, unfolded proteins are nonfunctional. Importantly, the unfolded state is thermodynamically unfavorable and unstable [Herczenik and Gebbink 2008]. Like intramolecular folding, aggregation, i.e., the association of two or more non-native protein molecules, is driven by hydrophobic forces and predominantly results in the formation of amorphous structures that lack long range order. Alternatively, aggregation can lead to the formation of ordered, fibrillar assemblies called amyloid, in which strands run perpendicular to the long fibril axis (cross structure) (Fig 3). Protein misfolding and aggregation are often coupled, with over 40 human diseases associated with formation of fibrillar aggregates. Such fibrillar structures are generally referred to as amyloid fibrils when they accumulate in the extracellular space of fundamental tissues, such as the liver, the heart, the spleen, or, in the case of neurodegenerative diseases like Alzheimer's disease, the central nervous system [Bellotti and Chiti 2008].

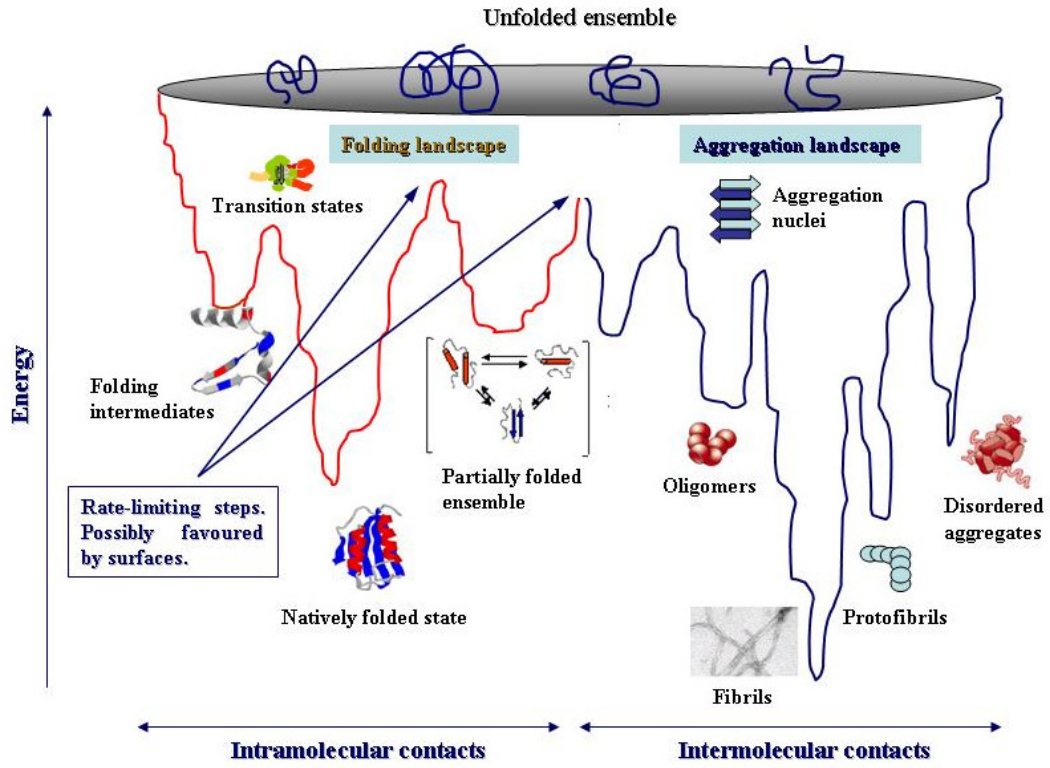

Figure 2 A combined energy landscape model for protein folding (left) and aggregation (right) starting from the unfolded ensemble. Both sides display considerable roughness, but amyloid fibrils display a remarkably higher stability and lower energy content than the natively folded structure. The picture highlights the multitude of the different conformational states available to a protein when they are stabilized by either intramolecular (monomeric protein) or intermolecular (aggregation intermediates and mature fibrils) contacts. From [Stefani M 2008]

Although about 20 different and unrelated proteins are the precursors of the amyloid fibrils in different known types of amyloidosis, the fibrils themselves are always very similar, sharing the pathognomonic tinctorial property of binding the planar azo dye, Congo red, and then giving green-red birefringence when viewed in intense cross-polarised light. This suggests a particular ordered environment for the bound dye molecules, and X-ray fibre diffraction studies identify the ordered, repeating core structure within all amyloid fibrils as an extensive cross-β conformation. Clinical amyloidosis occurs with overproduction, accumulation or even lifelong sustained normal production of inherently amyloidogenic normal proteins, or with the production of acquired or hereditary variant amyloidogenic proteins. Mature amyloid fibrils are 60-120 Å in diameter, rigid, non-branching, of indeterminate length, and

have similar dimensions, although the molecular mass of the protein subunit varies widely in different diseases.

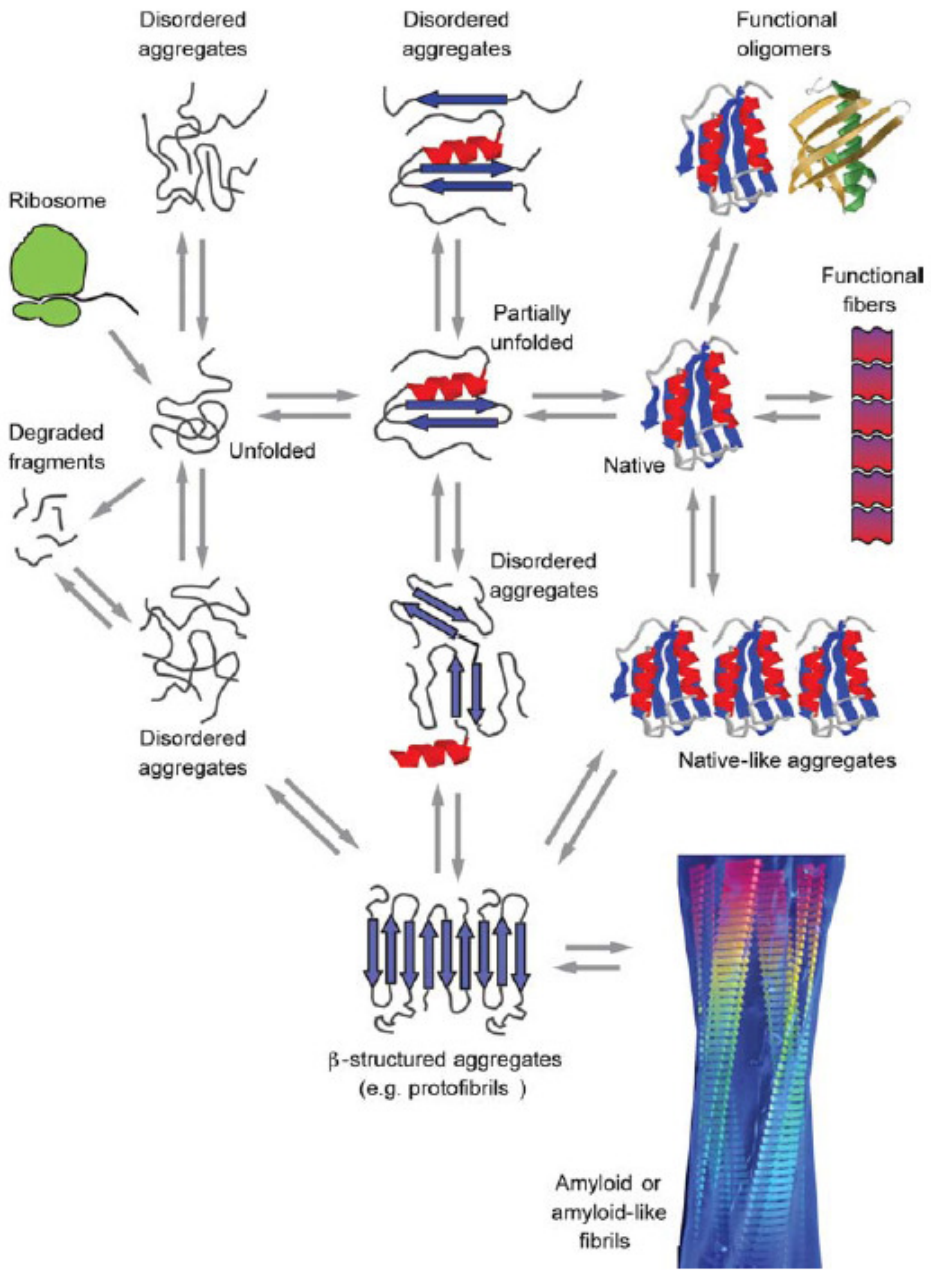

Figure 3 A schematic representation of some of the many conformational states that can be adopted by polypeptide chains and of the means by which they can be interconverted. The transition from β-structured aggregates to amyloid fibrils can occur by addition of either monomers or protofibrils (depending on protein) to preformed β-aggregates. From [Chiti F and Dobson CM 2006]

In the electron microscope, the fibrils are seen to be assembled by lateral association of a number of smaller protofilaments, and sub-fibrillar levels of structure have been reported, arising from either the observation of detail along the length of amyloid fibrils or from cross-sectional views in fibril sections [Serpell et al 2000]. Protein aggregation can occur starting from any of the conformational states adopted by the initially monomeric protein, including the fully unfolded state, the folded state, and any partially folded states, although the latter have the highest propensity to selfassemble (Fig 3). Protein aggregation is deleterious for any living organism as it prevents a protein from adopting its functional state and because the resulting protein oligomers are inherently toxic. The end product of protein aggregation processes occurring in pathology is generally represented by extracellular amyloid fibrils or structurally equivalent intracellular inclusions, often associating further to form larger assemblies that are visible with optical microscopy. However, protein oligomers forming early during the process of amyloid fibril formation or, alternatively, released by mature fibrils, have acquired increasing importance over the past 10–15 years. This is first due to the fact that formation of protein oligomers is a key event of the overall process of amyloid fibril formation and has been long regarded as the rate-limiting step, responsible for the lag phase in aggregation kinetics. Second, oligomers are thought to be the pathogenic species associated with the formation of amyloid in diseases [Bemporad and Chiti 2012]. One of the most widely accepted mechanisms proposed for the assembly of monomers into oligomers is the so-called ‘‘nucleation growth’’ mechanism. According to this mechanism, monomers convert into a nucleus through a thermodynamically unfavorable process taking place in the lag phase of amyloid aggregation kinetics. The nucleus can be defined as the least thermodynamically stable species in solution. The nucleus could even be a monomer that acts as a template for the rapid growth of the amyloid aggregate through the association of further monomers. After the nucleation growth model was proposed, the concept of nucleus was investigated in further detail and other more accurate models were proposed. In the nucleated conformational conversion, native monomers initially convert into misfolded conformations, which initiate self-assembly through a template-independent mechanism, with formation of a molten oligomer lacking

persistent structure. This aggregated species then undergoes a structural reorganization into an amyloid-like oligomer, which acts as a nucleus. The nucleus rapidly triggers aggregation as other molten oligomers acquire the amyloid conformation through a templating or induced-fit mechanism at the aggregate ends. This leads to the formation of higher order oligomers and eventually fibrils [Bemporad and Chiti 2012]. Moreover, in many cases, normally folded proteins can access amyloidogenic states without the involvement of a global unfolding reaction, for example, as a result of thermal fluctuations of the native state or disruption of the quaternary structure. In these cases, the amyloidogenic state can be described as an ensemble of native-like conformations characterized by the presence of locally unfolded elements [Bemporad et al 2012].

The protein quality control system

The functionality of the proteome depends on a delicate balance between the synthesis, folding and degradation of proteins. Cells possess a large network of proteins designed to maintain this balance. One essential group of proteins involved in proteome quality control comprises molecular chaperones, which facilitate protein folding, unfolding and remodelling. These molecular machines modulate the kinetic partitioning of polypeptides between pathways that lead to active proteins with native conformations and inactive proteins that are unfolded, misfolded or aggregated [Doyle et al. 2013]. Several different classes of structurally unrelated chaperones exist in cells, forming cooperative pathways and networks. Members of these protein families are often known as stress proteins or heat-shock proteins (HSPs), as they are up regulated under conditions of stress in which the concentrations of aggregation-prone folding intermediates increase. Chaperones are usually classified according to their molecular weight (HSP40, HSP60, HSP70, HSP90, HSP100 and the small HSPs). They are involved in a multitude of proteome-maintenance functions, including *de novo* folding, refolding of stress-denatured proteins, oligomeric assembly, protein trafficking and assistance in proteolytic degradation. The chaperones that participate broadly in *de novo* protein folding and refolding, such as the HSP70s, HSP90s and the chaperonins (HSP60s), are multicomponent molecular machines that promote folding through ATP and cofactor

regulated binding and release cycles. They typically recognize hydrophobic aminoacid side chains exposed by non-native proteins and may functionally cooperate with ATP independent chaperones, such as the small HSPs, which function as 'holdases', buffering aggregation [Hartl et al 2011]. The various chaperones have differing actions and distinct functional roles in protein quality control. For example,Hsp70 plays a role early in the protein folding process, interacting with ribosomes, growing peptide chains, and newly synthesized polypeptides. In contrast, Hsp60 andHsp90 members act further downstream to provide an enclosed environment with hydrophobic surfaces to assist in the folding of specific protein clients. Once folded, a range of physiological stressors can cause a protein to partially unfold or misfold. Chaperones such as Hsp100 and the sHsps can recognize misfolded proteins and, in cooperation with folding chaperones such as Hsp70, allow them to refold. Cells contain several systems to remove damaged or misfolded proteins when maintenance of correct protein folding is no longer possible. The ubiquitin-proteasome system recognizes, labels, and degrades stubbornly misfolded proteins. There are many hundreds of ubiquitin ligases that, through a series of highly regulated events, covalently attach polyubiquitin chains to misfolded proteins; ubiquitinated proteins are subsequently transferred to the proteasome as substrates for degradation. In addition, lysosomes can degrade damaged cytosolic proteins via three distinct mechanisms: macroautophagy, microautophagy, and chaperone-mediated autophagy. Chaperones are involved in controlling the movement of intractably misfolded proteins toward degradation machinery. For example, Hsp70 can, depending on the cofactors involved, promote folding, degradation through the ubiquitin-proteasome system, and chaperone-mediated autophagy, or even actively partition misfolded proteins into inclusions such as the aggresome [Wyatt et al 2013].

It is well established that "holdase" chaperones are vital in targeting misfolded intracellular molecules for protease degradation or for repair by "foldase" chaperones. While normally intracellular chaperones may be present in the extracellular environment, their abundance is normally extremely low (e.g., Hsp70 is present in blood plasma at <10 ng/mL). Also, ATP, which is needed to fuel intracellular protease systems and foldase chaperones, is at least 1000 times less concentrated outside of

the cell than inside. Therefore, the efficient processing of misfolded extracellular proteins is likely to be managed by abundant, normally secreted, ATP-independent mechanisms that are constitutively present in blood plasma, cerebrospinal fluid, interstitial fluid and all extracellular spaces. Three secreted glycoproteins, namely, clusterin, haptoglobin and α2-macroglobulin (α2M), are known to have ATP-independent chaperone activity *in vitro*. These structurally unrelated proteins have the ability to stably bind misfolded proteins and thereby inhibit inappropriate protein–protein interactions, prevent aggregation and maintain proteins in solution. All three extracellular chaperones demonstrate the ability to influence amyloid formation *in vitro* and are found co-localised with clinical amyloid deposits *in vivo*. Two other secreted glycoproteins, apolipoprotein E (ApoE) and serum amyloid P (SAP), that are universally found associated with amyloid deposits are also known to influence amyloid formation *in vitro*; however, less is known about their ability to stabilise misfolded proteins [Wyatt et al 2012].

In eukaryotic systems, many of the proteins that are synthesized in a cell are destined for secretion to the extracellular environment. These proteins are translocated into the ER, where folding takes place before secretion through the Golgi apparatus. The ER contains a wide range of molecular chaperones and folding catalysts, and in addition the proteins that fold here must satisfy a 'quality-control' check before being exported. This quality-control mechanism involves a remarkable series of glycosylation and deglycosylation reactions that enables correctly folded proteins to be distinguished from misfolded ones. Like the 'heat shock response' in the cytoplasm, the 'unfolded protein response' in the ER is also stimulated (upregulated) during stress and is strongly linked to the avoidance of misfolding diseases [Dobson 2003].

Folding and unfolding are the ultimate ways of generating and abolishing cellular activities, and unfolding is also the precursor to the degradation of proteins. Moreover, it is increasingly apparent that some events in the cell, such as translocation across membranes, can require proteins to be in unfolded or partially folded states. Processes as apparently diverse as trafficking, secretion, the immune response and the regulation of the cell cycle, are in fact now recognized to be directly dependent on folding and unfolding [Radford and Dobson 1999]. Indeed, it is becoming increasingly

evident that a wide range of human diseases is associated with aberrations in the folding process [Dobson 2001]. Some of these diseases (e.g. cystic fibrosis) result from the simple fact that if proteins do not fold correctly they will not be able to exercise their proper functions. In other cases, misfolded proteins escape all the protective mechanisms discussed above and form intractable aggregates within cells or in the extracellular space. An increasing number of pathologies, including Alzheimer's and Parkinson's diseases, the spongiform encephalopathies and late-onset diabetes, are known to be directly associated with the deposition of such aggregates in tissue [Thomas et al 1995]. Diseases of this type are amongst the most debilitating, socially disruptive and costly diseases in the modern world, and they are becoming increasingly prevalent as our societies age and become more dependent on new agricultural, dietary and medical practices [Dobson 2004]. It is widely accepted that protein aggregation is the cause, rather than a epiphenomenon, of the clinical manifestation of the different amyloidoses, and that the latter, at least in the case of the neurodegenerative diseases, can ultimately be traced back to the cytotoxic effects of the aggregates [Stefani 2008].

Failure of protein quality control system: protein misfolding deseases

Protein misfolding diseases comprise a group of disorders that have one central aspect in common: the appearance of non-native protein structure, which is accompanied by increased aggregation and deposition of proteins. The group contains diseases with dissimilar symptoms, and the affected organs and tissues can be drastically different [Herczenik and Gebbink 2008]. They include pathological states in which an impairment in the folding efficiency of a given protein results in a reduction in the quantity of the protein that is available to play its normal role. This reduction can arise as the result of one of several posttranslational processes, such as an increased probability of degradation via the quality control system of the endoplasmic reticulum, as occurs in cystic fibrosis [Amaral MD 2004], or the improper trafficking of a protein, as seen in early-onset emphysema [NLomas DA and Carrell RW 2002]. The largest group of misfolding diseases, however, is associated with the conversion of specific peptides or proteins from their soluble functional states ultimately into highly

organized fibrillar aggregates. These structures are generally described as amyloid fibrils or plaques when they accumulate extracellularly, whereas the term "intracellular inclusions" has been suggested as more appropriate when fibrils morphologically and structurally related to extracellular amyloid form inside the cell [Westermark P et al 2005]. However, recent studies suggest that prefibrillar aggregates, called micelles, protofibrils, or amyloid derived diffusible ligands rather than fibrils are the most potent mediators of cell damage, cytotoxicity, and neurotoxicity. These soluble oligomers are temporally unstable, and they can rapidly transform into more mature and eventually fibrillar forms. This action is supported by the finding that the severity of cognitive impairment in protein misfolding diseases correlates with the levels of small oligomeric aggregates and not with the large fibrillar species [Herczenik and Gebbink 2008].

Alzheimer desease

Among the human disorders marked by protein misfolding and aggregation, Alzheimer's disease looms large. This enormously common degeneration of limbic and associated cortices and related subcortical nuclei slowly robs its victims of their most human qualities: memory, reasoning, abstraction, and language. The disease has no doubt existed for millennia but was often confused with other syndromes that also presented as "senile dementia," that is, progressive cognitive decline after middle age [Selkoe 2011]. The global prevalence of dementia places a considerable burden on society. Currently, the prevalence is estimated to amount to 24 million and predicted to quadruple by the year 2050. In the US alone, Alzheimer disease (AD) the most frequent cause of dementia is associated with estimated health-care costs of $172 billion per year. The key pathological changes observed in AD brain tissue are amyloid-β (Aβ) peptide deposited extracellularly in diffuse and neuritic plaques, and hyperphosphorylated tau (p-tau) protein, a microtubule assembly protein accumulating intracellularly as neurofibrillary tangles (NFTs). Additional changes include reactive microgliosis and widespread loss of neurons, white matter and synapses [Reitz and Mayeux 2014].

Aβ is formed by the proteolytic processing of the amyloid precursor protein (APP) [Vardy ERLC et al 2005]. The amyloidogenic pathway of APP processing involves the initial cleavage of APP by the β-secretase (BACE1; β-site APP cleaving enzyme-1), to release a soluble N-terminal fragment, sAPPβ (Fig 4). The residual short membrane-bound C-terminal fragment of APP (C99) is subsequently cleaved by the presenilin-containing γ-secretase complex to form Aβ and the amyloid intracellular domain (AICD). The amyloidogenic cleavage of APP results in a number of Aβ isoforms from 39–43 amino acids in length. Of these isoforms, Aβ40 and Aβ42 are the most commonly found. Aβ42 is the more amyloidogenic isoform as it aggregates more readily and it is this isoform that is predominantly found in senile plaques.

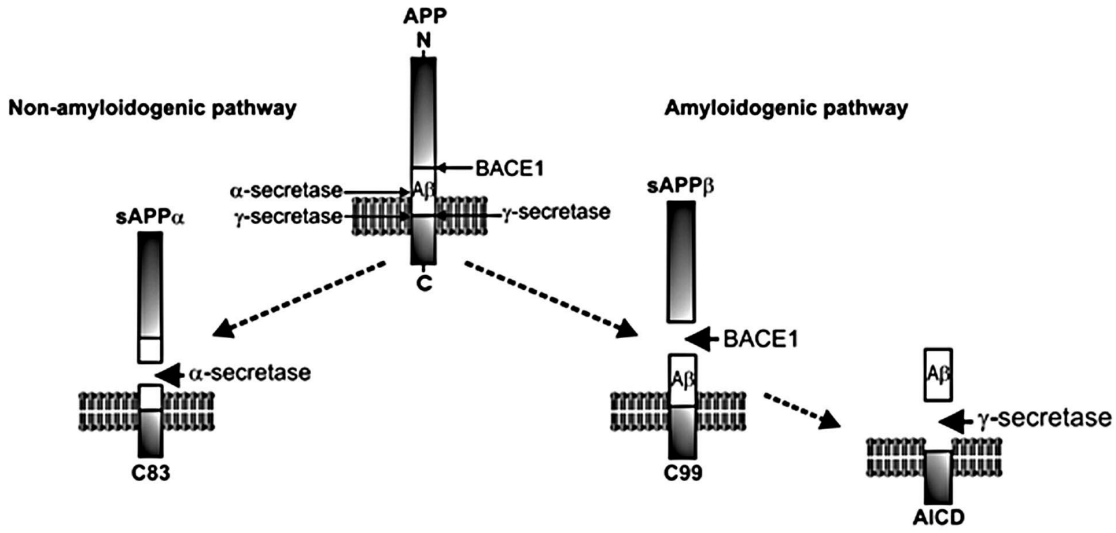

Figure 4 Proteolytic processing of APP. The amyloidogenic pathway involves the sequential cleavage of APP first by BACE1, producing sAPPβ and C99, and then by γ-secretase to release the amyloidogenic Aβ and the AICD. In the non-amyloidogenic pathway, α-secretase cleaves within the Aβ fragment, preventing the formation of Aβ peptides. From [Kellet and Hooper 2009]

Aβ peptides can self-assemble into small soluble oligomers or larger protofibrils and fibrils. While monomeric Aβ is generally non-toxic, there is growing evidence that Aβ oligomers are responsible for the synaptic dysfunction that occurs in AD [Walsh DM et

al 2002; Cleary et al 2005]. APP can alternatively be processed via the non-amyloidogenic pathway where the initial cleavage is by α-secretase, members of the ADAM (a disintegrin and metalloprotease) family [Vardy ERLC et al 2005] (Fig 4). This α-cleavage occurs within the Aβ region, thus precluding the formation of the Aβ peptide.

Tau belongs to the family of microtubule- associated proteins (MAPs) that includes MAP2. As neurons develop, tau segregates into axons, and MAP2 into dendrites [Matus A 1990]. In the axon, tau stabilizes the microtubules. Under pathological conditions tau dissociates from the microtubules, causing them to collapse, and tau starts accumulating in the somatodendritic compartment. The precise steps of this process are not fully understood. The established axonal localization of tau does not exclude the fact that under physiological conditions, this protein exerts important functions outside of the axon, such as in the dendrite [Ittner LM et al 2010]. Tau contains an unusually high number of putative phosphorylation sites (45 serines, 35 threonines, and 4 tyrosines), and for many of these, specific antibodies are available [Chen F et al 2004]. Under physiological conditions, there are on average 2–3 mol of phosphate per mol of tau, whereas under pathological conditions this ratio is increased to 7–8 mol [Kopke E et al 1993]. This posttranslational modification has been termed 'hyperphosphorylation': some sites are phosphorylated to a higher degree in the diseased than in the healthy brain; others are de novo phosphorylated. Phosphorylation tends to dissociate tau from microtubules. Tau also undergoes a conformational change that is likely to assist in differential phosphorylation [Jicha GA et al 1997]. Both tau and Aβ undergo nucleation-dependent fibril formation [Harper JD and Lansbury PT 1997].

The link between neurodegeneration and presence of amyloid plaques in AD brain was first proposed in 1990, when it was shown that aggregated Aβ was neurotoxic *in vitro* [Yankner BA et al.1990]. At the same time seminal discoveries in the AD genetics pave the way to the formulation of the ''amyloid cascade hypothesis'', stating that Aβ peptides originating from the proteolytic cleavage of their precursor protein (APP) are the main culprits of AD symptoms at the molecular level [Selkoe 1991]. Rapidly, yet with diffuse resistances in AD scientists, the ''amyloid cascade hypothesis'' replaced

previous proposals such as the ‘‘cholinergic hypothesis’’; yet, the latter has recently been reproposed, though in a modified form [Craig et al. 2011].

What is causing AD is not understood, with the exception of the rare, familial (FAD) forms; the latter, however, account for less than 5% of all cases [Delacourte A et al 2002]. In FAD, autosomal dominant mutations have been identified in three genes: in APP itself, and in the presenilin 1 (PSEN1) and presenilin 2 encoding (PSEN2) genes. In addition to the FAD genes, a series of susceptibility genes have been identified in sporadic AD (SAD); these include apolipoprotein E (APOE) as the most established risk gene [Bertram L and Tanzi RE 2008], CLU encoding clusterin, PICALM encoding the phosphatidylinositol-binding clathrin assembly protein, and CR1 encoding the complement component (3b/4b) receptor 1 [Lambert JC et al 2009]. Clinically and histopathologically, early-onset FAD cannot be discriminated from late-onset SAD [Gotz J 2001]. Moreover Alzheimer’s disease is believed to be a disease of the synapses and has hence been termed a ‘synaptic failure’ [Selkoe DJ 2002]. While Aβ can kill neurons, synaptotoxicity may be more relevant for the earlier stages of AD that are best characterized by synaptic loss rather than neuronal death. Loss of synaptic terminals or dendritic spines could cause the associated decline in cognitive functions that characterizes AD. At present, however, major research efforts of many groups concentrate on non-fibrillar soluble Aβ as the major toxic species in AD [Lambert MP et al 1998]. These have been given different names, including ADDLs, globulomers [Barghorn S et al 2005], and the dodecameric Aβ species Aβ *56 [Lesne S et al 2006]. Recent structural analysis has revealed that pentameric and hexameric oligomers may be the building blocks of the more toxic decameric and dodecameric complexes [Ahmed M et al 2010].

Neurotoxicity of Aβ

The presence of toxic aggregates inside or outside cells can impair a number of cell functions that ultimately lead to cell death by an apoptotic mechanism [Ross CA 2002; Morishima Y et al. 2001]. Many pieces of data point to a central role of modifications to the intracellular redox status and free Ca^{2+} levels in cells exposed to toxic aggregates [Kourie JI 2001; Butterfield AD et al. 2001]. A modification of the intracellular redox

status in such cells is associated with a sharp increase in the quantity of reactive oxygen species (ROS) that is reminiscent of the oxidative burst by which leukocytes destroy invading foreign cells after phagocytosis. In addition, changes have been observed in reactive nitrogen species, lipid peroxidation, deregulation of NO metabolism [Kourie JI 2001], protein nitrosylation [Guentchev M et al. 2000] and upregulation of heme oxygenase- 1, a specific marker of oxidative stress [Choi YG et al. 2000]. intracellular oxidative stress could be related to some form of destabilisation of cell membranes by toxic species leading to a failure to regulate appropriately plasma membrane proteins such as receptors and ion pumps [Mattson MP 1999] and/or to impairment of mitochondrial function. Mitochondria play a well recognised role in oxidative stress and apoptosis; in this regard, a key factor in Aβ peptide neurotoxicity could be the opening of mitochondrial permeability transition pores by Ca^{2+} entry in neuronal mitochondria [Moreira PI et al. 2002] followed by release of cytochrome *c*, a strong inducer of apoptosis. It has been suggested recently that intracellular ROS elevation following exposure to amyloid aggregates is a consequence of Ca^{2+} entry into cells followed by stimulation of oxidative metabolism aimed at providing the ATP needed to support the activity of membrane ion pumps involved in clearing excess Ca^{2+} [Squier TC 2001]. ROS elevation would in turn oxidise not only the proteins involved in ion transfer but also proteins such as calmodulin [Squier TC 2001] that when oxidised is unable to activate the Ca^{2+}-ATPase. The down-regulation of the Ca^{2+}-ATPase activity would then reduce the need for ATP, and hence ATP synthesis and ROS production by oxidative metabolism, leading to an increase in intracellular Ca^{2+} concentration [Squier TC 2001]. This hypothesis can explain the relationship between ROS, apoptosis, mitochondrial damage and intracellular free Ca^{2+} increase shown by cells exposed to toxic amyloid aggregates [Kawahara M et al. 2000, Selkoe DJ 2001].

As previously mentioned, studies from AD mouse models have lent further support to the hypothesis that Aβ causes ‘‘synaptic failure’’ before plaques develop and neuron death occurs [Selkoe 2002]. Excitatory synapses contain AMPA and NMDA ionotropic glutamate receptors as well as metabotropic type glutamate receptors (mGluRs) positioned on dendritic spines [Baude et al. 1993; Takumi et al. 1999]. Basal transmission is largely mediated by AMPA receptors. Brief periods of high synaptic

activity open NMDA receptors, leading to a long-lasting increase in postsynaptic AMPA receptor number, spine growth, and longterm potentiation (LTP) of synaptic transmission [Bliss and Lomo 1973]. Alternatively, low levels of synaptic stimulation can activate NMDA receptors to produce NMDA-dependent long-term depression (LTD) or mGluRs to produce mGluR-dependent LTD. These two forms of LTD can induce removal of postsynaptic AMPA receptors and loss of spines [Lee et al. 2002; Luscher et al. 1999; Man et al. 2000; Nagerl et al. 2004; Snyder et al. 2001; Xiao et al. 2001; Zhou et al. 2004]. It is generally believed that plasticity, such as LTP and LTD, are important processes for learning and memory. Multiple signaling pathways, which include several protein kinases and phosphatases, are required for the generation of LTP and LTD [Sheng and Kim 2002]. Neurons from transgenic APP mice that express genes encoding mutant APP or presenilin linked to familial, autosomal-dominant forms of AD (FAD) exhibit decreased synaptophysin and PSD95 staining as well as dendritic spine loss [Almeida et al. 2005; Hsia et al. 1999; Lanz et al. 2003; Mucke et al. 2000; Spires et al. 2005]. These mice develop mature amyloid plaques, are impaired on learning tasks, and can show deficits in LTP [Billings et al. 2005; Chapman et al. 1999; Giacchino et al. 2000; Larson et al. 1999; Moechars et al. 1999; Oddo et al. 2003; Stern et al. 2004]. Furthermore, application of Aβ, *in vivo* and *in vitro*, adversely affects LTP and synaptic transmission [Cleary et al. 2005; Cullen et al. 1997; Freir et al. 2001; Walsh et al. 2002]. Interestingly, learning and synaptic dysfunction appear before the formation of plaques, suggesting that a physiological deficit rather than a loss of neurons underlies the initial development of the disease [Hsia et al. 1999; Kamenetz et al. 2003; Mucke et al. 2000; Oddo et al. 2003].

Amyotrophic lateral sclerosis

Amyotrophic lateral sclerosis (ALS) is a fatal neurodegenerative disease caused by the loss of both upper and lower motor neurons. Affected patients develop progressive muscle weakness eventually leading to death due to respiratory failure, typically 3–5 years after symptom onset. ALS affects ~2 out of 100,000 individuals per year [Hardiman O et al 2011]. In the majority of patients the disease occurs sporadic and is

referred to as sporadic ALS (SALS). In 5 % of cases there is a family history of ALS (FALS) [Byrne S et al 2011]. The presence of protein aggregates in affected motor neurons is a characteristic, but still poorly understood hallmark of SALS and FALS patients. Recently, many new ALS causing gene defects have been identified including mutations in HNRNPA1, PFN1, C9ORF72, UBQLN2, OPTN, VCP, FUS and TARDBP [Al-Chalabi A et al 2012; Kim HJ et al 2013]. Most of these mutations are rare and cause ALS in a small subgroup of patients. Remarkably, however, the proteins encoded by these genes are present in protein aggregates of a large proportion of non mutation carriers indicating a more widespread role for their abnormal localization in ALS pathogenesis. Moreover, some of these proteins are present in pathological aggregates of other neurodegenerative disorders such as frontotemporal lobar degeneration (FTLD), spinocerebellar ataxia (SCA), Huntington's disease, Alzheimer's disease and inclusion body myositis (IBM), indicating a more general involvement in neurodegeneration. The central pathological hallmark of ALS is the presence of cytoplasmic inclusions or aggregates in degenerating motor neurons and surrounding oligodendrocytes. Inclusions are not restricted to the spinal cord but also present in other brain regions such as the frontal and temporal cortices, hippocampus and cerebellum. The predominant aggregates found in ALS patients are ubiquitinated aggregates that are classified as either Lewy body like hyaline inclusions or skein like inclusions. At the ultrastructural level, Lewy body like or skein like inclusions appear as randomly oriented filaments covered by fine granules [Hasegawa M et al 2008; Lin WL and Dickson DW 2008]. Other cellular abnormalities include the presence of mitochondrial vacuolization, fragmentation of the Golgi apparatus and abnormalities at the neuromuscular junction. In 1993, SOD1 was the first protein to be identified to aggregate in FALS cases carrying a mutation in the *SOD1* gene [Rosen DR et al 1993]. Later, mutations in *VAPB* were also shown to cause ALS in a group of FALS patients [Nishimura AL et al 2004].

TAR DNA-binding protein 43 (TDP43) was identified 8 years ago as the major constituent of the proteinaceous inclusions that are characteristic of most forms of ALS and frontotemporal lobar degeneration [Neumann M et al 2006]. Since then, numerous groups have confirmed this finding [Buratti E and Baralle FE 2012;

Brandmeir N J et al 2008; Strong M J et al 2007]. With over 600 studies published on TDP43 and its role in ALS and FTLD, there is now an emerging consensus that TDP43 protein is mechanistically linked to neurodegeneration. TDP43 is a 414 aminoacid protein with two RNA recognition motifs (RNA recognition motif 1 (RRM1) and RNA recognition motif 2 (RRM2)) and a carboxyterminal glycine rich domain. Nearly all of the described ALS-associated TDP43 mutations are dominant missense mutations within the glycine rich domain, suggesting that altering the function of this domain is sufficient to induce neurodegeneration [Kabashi E et al 2008; Sreedharan J et al 2008]. Normally TDP-43 predominantly localizes to the nucleus. In ALS patients, cytoplasmic aggregation is often accompanied by nuclear clearing of the protein [Mackenzie IRA et al 2007; Neumann M et al 2006]. Furthermore, the protein is cleaved in C-terminal fragments (CTFs) of 20-25 and 35 kDa and the full-length protein and 18-26 kDa fragments are hyperphosphorylated [Hasegawa M et al 2008]. Furthermore, the distribution of the TDP-43-positive aggregates is disease-specific with, for example, involvement of spinal cord motor neurons in ALS and a more widespread distribution in the brain in FTLD [Baloh RH 2011]. Mutations in *TARDBP* are unique to ALS and are not found in other neurodegenerative disorders [Brouwers N et al 2010; Van Deerlin VM et al 2008] with the exception of a small number of FTLD cases [Chio A et al 2010; Corrado L et al 2009]. TDP-43 is a DNA and RNA binding protein that binds around 30 % of the mouse transcriptome with a preference for long UG-rich sequences [Tollervey JR et al 2011]. Target sequences are mainly intronic, but also include non coding RNAs and 3' UTRs. In line with this, TDP-43 plays a role in nuclear RNA metabolism including splicing, transcriptional repression, miRNA synthesis, mRNA nucleo-cytoplasmic shuttling and RNA transport [Lagier-Tourenne C et al 2010].

Like other proteins that form neurodegenerative disease-related intracellular inclusions, such as tau and α-synuclein, pathological TDP43 aggregates are ubiquitylated and phosphorylated [Neumann M et al. 2006]. Under normal circumstances, ubiquitylated and phosphorylated TDP43 is not readily detected in brain tissue. Thus, the very presence of these modified TDP43 species in ALS is abnormal and seems to be disease specific; however, it is not clear whether these modifications lead to aggregate formation and/or neurotoxicity, or whether they

represent a normal reaction to the presence of an intracellular aggregate and are therefore indirectly related to TDP43-mediated neurodegeneration. Interestingly, human tissue studies indicate that not all TDP43 inclusions are ubiquitin positive. In particular, so-called 'pre-inclusions' (granular, less dense cytoplasmic inclusions) are often not ubiquitin positive, suggesting that ubiquitylation is a relatively late phenomenon in the disease process [Giordana M T et a.l 2010; Strong M J et al. 2007). By contrast, antibodies that specifically detect TDP43 that is phosphorylated at serine residues 409 and 410 seem to recognize most TDP43 inclusions as well as the truncated 25 kDa TPD43 CTFs [Neumann, M. et al. 2009; Hasegawa, M. et al 2008] These studies suggest that phosphorylation precedes ubiquitylation, but they do not address whether these post-translational modifications are mechanistically involved in TDP43 mediated neurodegeneration. A major unresolved question is whether TDP-43-mediated neuronal loss is caused by toxic gain of function of cytoplasmic aggregates, or by a loss of its normal function in the nucleus. We now have an idea of the key steps that occur from the onset of TDP43 mediated neurodegenerative disease through to the culmination of these events in dysfunction and death of affected neurons in ALS, FTLD-TDP and related TDP43 proteinopathies. As is often the case for disease processes, multiple pathways are likely to be involved, and the downstream consequences of TDP43 phosphorylation, aggregation, cleavage, mislocalization and clearance from the nucleus are unclear. Perhaps it is easiest to conjecture that the absence of normal nuclear TDP43 implies that there is a loss of normal TDP43 function. Given the plethora of normal nuclear TDP43 functions, this alone might lead to neurodegeneration. Alternatively, perhaps TDP43 retains its ability to bind RNA, and therefore its cytoplasmic localization acts as a peripheral sink, thereby implicating a toxic gain of function. Or maybe TDP43 CTFs act in a dominant negative fashion by occupying hnRNP binding sites without being able to bring along its usual RNA cargo.

In an attempt to understand the mechanisms of neurodegeneration, we can consider two hypothetical models of TDP43-mediated neurodegeneration. The first model, "loss of function" was proposed by two groups independently. Although the initial insult is generally unknown (aside from cases that are linked to genetic mutations), one possible initiating event may be the presence of abnormal, toxic RNA species. Cellular

stress is thought to cause a redistribution of TDP43 from the nucleus to the cytoplasm. This is akin to the formation of stress granules that has been observed experimentally, although there is currently little evidence showing an upregulation of stress granules in ALS. Alternatively, RNA transport granules that are usually localized within peripheral neurites may be abnormally distributed. According to this model, this redistribution results in the aggregation of TDP43 into preinclusions that are phosphorylated, variably ubiquitylated and difficult to degrade. These cytoplasmic inclusions lead to further redistribution of normal TDP43 from the nucleus as protein is sequestered into inclusions, accounting for nuclear clearance. If TDP43 autoregulation occurs within the nucleus, there would be a loss of TDP43 autoregulation and increased TDP43 expression, leading to increased aggregate formation. This would feed forward through a vicious cycle leading to cell death [Polymenidou M et al 2011].

Alternatively, in the second model, "gain of function" a stressor can lead to redistribution of TDP43 into the cytoplasm resulting in aggregation (similar to the first model). If autoregulation of TDP43 mRNA is a cytoplasmic event and TDP43 aggregates retain the ability to bind RNA and therefore autoregulate its cognate RNA, then an increase in cytoplasmic TDP43 may lead to increased autoregulation, thereby decreasing TDP43 mRNA and decreasing newly synthesized TDP43 protein in affected cells. This decrease in synthesis may account for the nuclear clearance phenomenon (that is, aggregates represent the existing pool of TDP43 protein and not newly synthesized protein). Given the myriad of normal TDP43 functions, loss of normal nuclear TDP43 may further increase cellular stress, again resulting in a vicious cycle leading to cell death [Kabashi E et al 2010].

HypF-N

A growing body of evidence suggests that protein aggregation is a capability of all polypeptide chains. [Chiti F et al 2002]. However, relative scarcity of aggregants in organisms and the wide range of aggregation rates under the same conditions measured *in vitro* show that the process of aggregation varies tremendously by sequence [Dubay, K F et al 2004]. This leads to the question of what determines a polypeptide chain's propensity to aggregate. Recent work has shown a strong

correlation between aggregation rates and hydrophobicity, hydrophobic patterning, and charge of a sequence; [Zbilut J P et al 2004] additionally, helix and sheet propensity correlate significantly with mutational changes in aggregation rates within a sequence [Calamai M et al 2005]. One possible mechanism is that the aggregation precursor is fairly disordered and transiently exposes hydrophobic residues to the solvent for sufficient time to form bimolecular interactions. Therefore, there may be some correlation between intramolecular diffusion rates of aggregation precursors and aggregation propensity. One particularly favourable system for investigating the fundamental principles underlying protein aggregation is the N-terminal domain of HypF from *Escherichia coli* (HypF-N), a large globular protein factor of about 82 KDa, participating in the maturation of the prokaryotic [NiFe] hydrogenase that is involved in hydrogen metabolism [Colbeau A et al 1998]. HypF-N has been shown to have one of the fastest aggregation rates *in vitro*,[Dubay, K F et al 2004) and extensive work has been done to identify the nature of the aggregation precursor [Dumoulin, M et al 2006] (Fig 5). This bacterial protein, not associated with any amyloid disease, aggregates into pre-fibrillar and fibrillar amyloid assemblies undistinguishable from those associated with amyloid diseases and endowed with the same cytotoxicity [Bucciantini, M et al 2002; Bucciantini, M et al 2004]. This conversion in amyloidlike fibrils was achieved incubation in the presence of moderate concentrations 30% (v/v) of trifluoroethanol (TFE) at pH 5.5 or 20 mM citrate buffer at pH 3.0, favoring the destabilization of hydrophobic interactions [Relini A et al. 2004; Chiti F et al. 2001]. The formation of a partially folded state is a key event in the aggregation pathway of this protein *in vitro*, even under mild destabilising conditions in which the folded state is by far the predominant species. Indeed, under mild denaturing conditions generated by moderate concentrations of trifluoroethanol [6–12% (v/v)], the partially folded state is in rapid equilibrium with the native state and populated to ca 1-2%. Indeed, a kinetic analysis has shown that aggregation does not result from those protein molecules that are in their fully native conformation, but

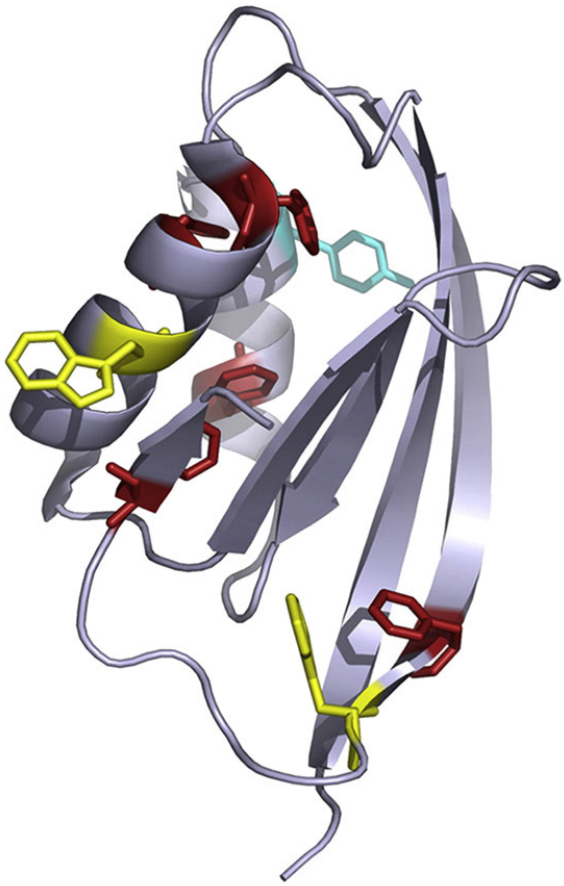

Figure 5 Three-dimensional structure of native HypF-N from X-ray crystallography. From [Campioni et al. 2008]

from the population of a partially unfolded conformational state that is in dynamic equilibrium with the former [Marcon G et al. 2005]. Recently, new aggregation conditions for HypF-N, allowing the characterization of the partially folded state populated prior undergoing aggregation, have been described, such as at pH 5.5 in the presence of 12% (v/v) TFE, or at pH 1.7 in the presence of salts (NaCl). A detailed structural investigation of this partially folded state has also been performed and achieved by means of different biophysical and biochemical methodologies [Campioni S et al. 2010]. The resulting species have been imaged with both transmission electron microscopy (TEM) and tapping mode atomic force microscopy (TM-AFM), have been shown to increase the fluorescence of thioflavin T (ThT) and to have a characteristic cross β-structure as revealed by X-ray diffraction studies, indicating the presence of

intermolecular β-sheet structure typical of amyloid aggregates [Relini A et al. 2004; Chiti F et al. 2001]. In general, the data obtained suggest that the aggregation process of this protein starts from a partially folded state that can be either fully populated or in rapid equilibrium with the native state when the latter is destabilized by mutations and/or mild unfolding conditions [Marcon G et al. 2005]. The results support an aggregation pathway in which the native protein first converts into a partially folded state separated from the native state by an energy barrier comparable to that of (un)folding. This monomeric state converts into globular small aggregates and small beaded fibrils that further associate into ring-like structures. Finally, the ring-like structures convert into ribbon-like fibrils that associate into fibrillar tangles [Relini A et al. 2004]. Since many disease-involved systems aggregate following similar pathways, HypF-N represents a valuable model system for investigating the structural basis of the amyloid formation.

In the last years it has been increasingly suggested that the oligomers formed by proteins unrelated to any amyloid disease can be toxic when added to the extracellular medium of cultured cells, whereas the same proteins in monomeric or fibrillar forms are not [Bucciantini M et al. 2002]. These prefibrillar aggregates impair cell viability interacting with the macromolecular components of living organisms, such as membranes and proteins, and interfere with their normal function. The early prefibrillar aggregates of HypF-N formed in 30% TFE were shown to be able to interact with, insert into, and eventually disassemble synthetic membranes and supported phospholipid bilayers [Relini A et al. 2004; Canale C et al. 2006]. Furthermore, these species can interact with the plasma membrane of cultured cells and be internalized inside the cytoplasm, resulting in cell impairment and death [Bucciantini M et al. 2005; Cecchi C et al. 2005]. Similarly to the protofibrillar aggregates of disease-related proteins and peptides, treatment of the cells with HypF-N protofibrils leads to an increase of reactive oxygen species (ROS) and free Ca^{2+} levels inside the cells, which ultimately die by apoptosis or necrosis [Bucciantini M et al. 2005; Cecchi C et al. 2005]. Moreover, the increase of intracellular Ca^{2+} levels is associated with both the activation of plasma membrane receptors with Ca^{2+} channel activity, such as AMPA receptor and NMDA receptor, and unspecific membrane permeabilization, with the

former effect being more important at early times [Pellistri F et al. 2008]. The susceptibility of different cells to HypF-N oligomers was shown to depend on their ability to counteract these early impairments, which increases during cell differentiation [Cecchi C et al. 2005; Cecchi C et al. 2008]. Remarkably, HypF-N protofibrils can also induce a loss of cholinergic neurons when injected into rat brains, demonstrating that these species can act as toxins even in higher organisms [Baglioni S et al. 2006]. These data strongly support the hypothesis that a common mechanism of cytotoxicity exists, which is related to the misfolded nature and oligomeric state of a protein rather than to its sequence. In spite of this advancement, a structural characterization of the conformational properties of the oligomers finalized to an understanding of the relationship with their toxic effect is still lacking, mainly due to the fact that the transient formation of these species and their structural heterogeneity have hampered considerably their investigation. The structural determinants of the protein oligomers that are responsible for cell dysfunction are starting, only these days, to be elucidated. At different destabilizing conditions (presence of rifluoroacetic acid or trifluoroethanol), HypF-N misfolds and generates morphologically similar oligomers, yet with different structural features in terms of stability, exposure of hydrophobic surface, compactness and flexibility. Recently, the functional and structural properties of the spherical aggregates formed by HypF-N in two distinct environmental conditions can be compared. It is therefore nowadays essential to determine in detail the structure of the toxic oligomeric species in order to identify new therapeutical targets, and to understand whether it represents a single common fold or rather exhibits some polymorphism. It is well known that incubation of the same protein/peptide under different experimental conditions causes the formation of oligomers or fibrils with different morphologies and that such differences result in different degrees of toxicity [Petkova AT et al. 2005; Lee S et al. 2007; Kayed R et al. 2009]. Similarly, mutations or covalent modifications result in different levels of oligomers or different fibrillar structures with completely different toxicities [Hung LW et al. 2008]. However, little experimental information is available on the structural features of oligomers grown under different conditions and on the relationship between their structure and their ability to cause cell dysfunction. Recently, it has

been found that oligomers formed from the same protein (HypF-N) under different conditions (pH 5.5 in the presence of 12%(v/v) TFE or pH 1.7 in the presence of 330 mM NaCl) exhibited similar morphological and tinctorial properties, yet differed in their molecular structure.

Comparisons of the two types of aggregates, indicated that their structural differences resulted from different degrees of packing of the hydrophobic residues within their cores with a consequent different level of structural flexibility and solvent-exposure of such residues [Campioni S et al. 2010]. Thus, whilst the ability to form amyloid-like structures is generic to polypeptide chains, whether or not such species are pathogenic will depend on their structural features, notably the extent to which hydrophobic residues are flexible and exposed on their surfaces within the environment of a living organism. These findings, however, do not seem to be limited to the HypF-N aggregates, and could indeed explain the toxic properties of the oligomers formed by disease-related systems. In fact, several studies indicated a correlation between the size and surface hydrophobicity of Aβ40 aggregates and their ability to decrease the bilayer fluidity of model membranes [Kremer JJ et al. 2000], suggesting that the exposure to the solvent of hydrophobic surfaces determines the ability of these species to interact with cell membranes. A correlation between hydrophobicity, tendency to form aggregates and aggregate cytotoxicity has also been observed in comparative studies where the behavior of different homopolymeric amino acid (HPAA) stretches was investigated [Oma Y et al. 2005]. It has been recently reported that expanded huntingtin-exon1 forms fibrillar aggregates at two different temperatures that have different structural and physical properties as well as different cytotoxicities [Petkova AT et al. 2005]. The structures and toxicities of both forms of the aggregates are comparable with those extracted from regions of mouse brains affected to different extents by huntingtin deposition. In both pairs of structures a direct relationship between structural flexibility and cytotoxicity of amyloid assemblies was found, supporting the generality of previous conclusions [Petkova AT et al. 2005]. Finally, all these data lend support to the idea that a key feature in the generation of toxicity is the conversion of a species of aggregates where stability is associated with extreme burial of hydrophobic residues to one where such residues are substantially

exposed and disorganized [Cheon M et al. 2007]. Recently, it has been suggested that for therapeutic purposes the toxicity can be dramatically reduced if the hydrophobic residues are incorporated to a greater extent within the interior of the oligomeric assemblies, even in the absence of an effective change in morphology [Campioni S et al. 2010]. Approaches of this type will facilitate the elucidation of the causative link between the molecular structure of aberrant protein oligomers and their ability to cause cell dysfunction, with the aim of understanding the pathogenesis of protein deposition diseases and identifying therapeutic strategies to combat them. Moreover, a detailed understanding of the forces that determine the structure of amyloid-like oligomers will also enable to identify the factors that can modulate it, and eventually alter the biological activities of these species.

Transthyretin

Transthyretin (TTR) is a homotetrameric protein of 55 kDa found mainly in plasma and cerebrospinal fluid and previously thought to be synthesized only in liver, choroid plexus, retinal pigment epithelium, and pancreas [Jacobsson B et al 1989; Cavallaro T et al 1990]. In the plasma TTR transports thyroxine (T_4) and the retinol binding protein charged with retinol (RBP), whereas in the cerebrospinal fluid (CSF) TTR is the primary transporter of T4 [Reixach N et al 2008]. The binding sites for its normal ligands, T4 and RBP have been well defined [Raz AJ et al. 1969; Andrea TA et al. 1980; Monaco HL 2002]. TTR is encoded by a single copy of gene located on chromosome 18 in human and chromosome 4 in mouse. The gene contains four exons with the first exon encoding the leader sequence [Buxbaum JN 2007]. In 1981, the International Union of Biochemists adopted the name ‘‘transthyretin’’ for the molecule previously designated as ‘‘thyroxine binding prealbumin’’ [Goodman DS et al 1986]. Until recently, TTR had its established clinical significance in two settings. TTR serum concentration has been utilized as a marker of nutritional/inflammatory status in a variety of conditions [Ingenbleek Y and Young VR 2002; Potter MA and Luxton G 2002]. More importantly, as an etiologic agent, TTR is one of the 30 human proteins associated with the amyloidoses, a group of disorders originally defined pathologically by the formation and aggregation of misfolded proteins which result in extracellular deposits that impair

organ function [Westermark P et al 2007]. The clinical syndromes associated with TTR aggregation are senile systemic amyloidosis (SSA), a late onset disease in which the wild-type protein deposits primarily in the heart, but also in the gut and carpal tunnel [Pitkanen P et al 1984; Kyle RA et al 1992; Rocken C et al 1994], and the familial amyloidotic polyneuropathies (FAP) and cardiomyopathies (FAC) in which point mutations in the gene encoding the protein result in deposition of aggregates in peripheral and autonomic nerves and heart, respectively [Buxbaum JN 2007]. FAP and FAC usually have an earlier onset than SSA presumably due to the decreased stability of variant TTR with respect to the wild-type protein, with the most aggressive variants depositing as early as the second decade of life [Jacobson DR et al. 1992].

In vitro studies have demonstrated that TTR forms amyloid fibrils through a process that involves tetramer dissociation followed by misfolding of the released monomers into an aggregation-prone conformation by which oligomers, soluble aggregates, insoluble amorphous aggregates, and amyloid fibrils are formed in a downhill polymerization process [Hurshman AR et al. 2004]. Whether the insoluble amorphous aggregates described first in transgenic animals [Teng MH et al. 2001] and then in humans [Sousa MM et al. 2001] are in on- or off-pathway towards the amyloidogenic structure is still a matter of debate. Tissue culture studies using cell lines derived from tissues that are targets of TTR deposition have shown that TTR monomers or small oligomers are cytotoxic to the cells, whereas the native tetramer, large soluble aggregates (100 kDa), and amyloid fibrils are not. Furthermore, amyloidogenic TTR variants were toxic to the cells whereas non-amyloidogenic TTR was not [Reixach N et al. 2004]. These results support the notion that cell death in the protein misfolding diseases is caused not by amyloid fibrils, which are the end product of the aggregation process, but rather by the intermediate oligomers that are formed during that process.

The most common amyloidogenic TTR variant is V30M-TTR, which was first isolated from a Portuguese kindred. L55P-TTR is the variant associated with the most aggressive form of FAP. Comparison between the crystal structures of WT and V30M-TTR showed a very similar global fold for both proteins. Substitution of valine 30 by methionine forces the β-sheets of the monomer resulting in the distortion of the thyroxine-binding cavity [Hamilton J A et al 1993; Terry C J et al 1993]. However, the

small differences between the crystal structures of WT and V30M-TTR have not clearly pointed out the causes for the amyloidogenicity of V30M-TTR. Very recently, based on the crystal structure of the highly amyloidogenic L55P-TTR, a model for TTR amyloid fibrils has been proposed consisting of a tubular structure with inner and outer diameters of ;30 and 100 Å, respectively, and four monomers per cross-section [Sebastião M P et al 1998]. Westermark and co-workers [Gustavsson Å et al 1990] have reported the formation of amyloid by TTR *in vitro* at low pH. This observation has led to the proposal of a low pH environment as a prerequisite for amyloid formation *in vivo* [Colon W and Kelly J W 1992]. These authors proposed that the low pH medium (present for example in the lysosomes) would induce tetramer rearrangement and dissociation to a monomeric amyloidogenic intermediate with altered tertiary structure, which in turn would self-assemble to form amyloid fibrils [Lai Z et al 1996]. However, this proposal, with lysosomal involvement, implies the formation of amyloid intermediates intracellularly, which is not consistent with the observation that TTR amyloid deposits are extracellular. Furthermore, in FAP, amyloid deposition occurs predominantly in the peripheral nerves, and both TTR mRNA and protein are not detected in the cellular components of nerves. Thus, amyloid assembly and deposition must take place extracellularly. Additionally, at low pH, both amyloidogenic and non-amyloidogenic TTR variants form amyloid *in vitro* [Adams D and Said G 1996].

Transthyretin and AD

The frequency of many of the amyloidoses increases with aging but their deposition appears to be independent, i.e. each has its own anatomically predisposed site and pattern [Wright JR et al 1969]. Thus, while there are reported instances of mixed precursor deposition, they are relatively uncommon, e.g. [Bergstrom J et al 2001; de Sousa MM et al 2000]. Nonetheless the commonality of structure that leads precursor proteins to form fibrils suggests that interaction could occur, perhaps accelerating fibril formation. The example of transthyretin (TTR) and β-amyloid (Aβ) raises the question as to whether the effect may be, in truth, to reduce fibrillogenesis. Wild type and mutant forms of TTR are the precursors in the systemic human diseases, FAP, FAC and SSA [Buxbaum JN 2007]. In contrast, Alzheimer's disease (AD) is a localized amyloid

disease of the brain. AD and the TTR amyloidoses share age dependence and are manifested as both autosomal dominant, mutation-related and sporadic (wild type protein associated) diseases. In the TTR amyloidoses the precursor is synthesized primarily by hepatocytes distant from the main sites of deposition in peripheral nerve and heart. However local synthesis and deposition can be seen in the eye, gut, kidney and choroid plexus. In AD the β-amyloid protein (Aβ) is synthesized ubiquitously but deposition and tissue compromise are restricted to the brain and even more so to specific brain regions. The first association of TTR with AD was the observation that cerebrospinal fluid (CSF) could inhibit Aβ fibril formation *in vitro* [Wisniewski T et al 1993]. TTR was the third CSF protein found to interact with Aβ after apolipoprotein E (ApoE) [Strittmatter WJ et al 1993] and ApoJ (clusterin) [Ghiso J et al 1993]. It was hypothesized at that time that these three extracellular proteins could "sequester" Aβ, thereby preventing neuronal damage, although there was little evidence presented as to how or where such sequestration could take place. Perhaps "chaperone" in the sense of "protector" might have been a better term than "sequester", but the oxymoronic phrase "pathologic chaperone" had already been utilized to describe the co-deposition of ApoE in AD plaques [Wisniewski T et al 1992]. Early immunopathologic studies, based on the premise that TTR might be the amyloid precursor in AD, gave conflicting results with respect to the presence of TTR in plaques in human AD brains [Eikelenboom P and Stam FC 1984; Shirahama T et al 1982]. More recent analyses found TTR co-localized in hippocampal plaques and vessels of AD patients [Schwarzman AL and Goldgaber D 1996; Stein TD et al 2004]. Anti-TTR serum stained the majority of neuronal bodies in AD brains but only 10% of neurons in age-matched non demented controls [Li X et al 2011]. The latter finding may be responsible for the many reports of TTR synthesis only in the choroid plexus in the normal brain since the TTR signal from the choroid plexus, ependyma and leptomeninges is much stronger than that from normal neurons [Sousa JC et al 2007; Ng L et al 2009]. TTR, ApoE and ApoJ (clusterin) are major Aβ-binding proteins in human CSF [Schwarzman AL et al 1994]. The mean CSF TTR level has been reported to be decreased in several series of AD patients [Serot JM et al 1997; Castano EM et al 2006]. However not all investigators have found this to be true [Schultz K et al 2010]. The significance of the

decrease is not clear. It has been proposed, on the basis of the decrease, that TTR sequesters Aβ but no site of sequestration has been identified. It is also possible that the CSF TTR concentration may be determined in part by neuronal TTR synthesis [Li X et al 2011], particularly in AD (as well as choroid plexus production) and that the observed reduction is related to neuronal loss. Also plausible is the possibility that patients with AD have a genetic or acquired low CSF TTR level independent of Aβ binding, which conceivably could put them at greater risk for AD. A recent analysis of TTR single nucleotide polymorphisms (SNPs) has associated 5 TTR SNPs with hippocampal atrophy [Cuenco KT et al 2011]. A prior single small study did not identify AD in carriers of amyloidogenic TTR mutations, but there is no a priori reason why such mutations would predispose to Aβ deposition [Palha JA et al 1996]. Reduced CSF TTR levels have also been reported in patients with depression (although not in those who committed suicide), normal pressure hydrocephalus and most recently in ALS [Brettschneider J et al 2010]. The variability of the finding has made it an unsuitable CSF marker for AD and made it more difficult to understand its role in AD pathogenesis. An in vivo interaction between Aβ/TTR was also noted in human kidneys [Tsuzuki K et al 2000], and in the muscle of a single patient with inclusion body myositis [Askanas V et al 2000]. However its significance in these circumstances is unclear since the subjects did not have clinical AD. It was hypothesized that TTR could inhibit Aβ related toxicity by sequestration of Aβ thus preventing Aβ aggregation and fibril formation based on the observation that first identified TTR as an Aβ-binding protein in CSF [Schwarzman AL et al 1996]. In subsequent studies of the capacity of a series of recombinant mutant TTR's to inhibit Aβ fibril formation at neutral pH in vitro was analyzed. The investigators found that the amount of Congo red binding material formed over a 24-36 hour period was reduced in the presence of many of the recombinant TTR's (at a 5:1 molar ratio of Aβ:TTR). However, the experiments suffered from the lack of non-TTR e.g. albumin, controls and the use of a relative measure of inhibitory capacity that was never quantified in terms of protein concentration. In addition the nature of the Aβ1-42 when it was added to the assay was not precisely defined. Given current knowledge regarding the propensity of Aβ to aggregate on standing, it is not clear from the publications whether the different TTR's were actually

seeing the same Aβ conformers. Nonetheless in retrospect the observation that TTR bound Aβ and inhibited fibril formation was correct, although the detailed results regarding the relative capacities of different variants are less likely to be valid. The hypothesis itself was attractive since TTR is abundant in Human CSF (5-20 µg/ml or 0.1-0.36 µM) and serum (174-420 µg/ml or 3-7 µM) [Vatassery GT et al 1991]; while Aβconcentration in CSF is relatively low (3 nM or less) [Price JM et al 2001]. However it inferred, as a second hypothesis, that the interaction would be responsible for lowering the CSF TTR concentration.

Transthyretin and Aβ interaction

Schwarzman et al studied 47 recombinant TTR variants. Most (except G42 and P55) bound to Aβ and inhibited Aβ aggregation in vitro [Schwarzman AL et al 2004]. Wild type human TTR binds to all forms of soluble Ab, monomer, oligomer and fibrils [Liu L et al 2006]. TTR binds to Ab better at 37°C than 25° C [Buxbaum JN et al 2008], binds to Ab aggregates better than Ab monomer [Liu L et al 2006; Du J, Murphy RM et al 2010], and Ab1-42 better than Ab1-40 [Buxbaum JN et al 2008]. The binding is highly dependent on the quarternary structure of TTR [Du J et al 2010]. It has been suggested that human monomeric TTR binds Aβ better than the TTR tetramer. The interaction between TTR and Aβ interferes with Ab aggregation in vitro and inhibits Ab fibril formation [Buxbaum JN et al 2008; Liu L et al 2006]. The interaction between TTR and Aβ species is apparently beneficial to cultured cells under Aβ stress. TTR prevented accumulation of the Aβ in cultured vascular smooth muscle cells [Mazur-Kolecka Bcdae et al 1995]. In the human neuroblastoma cell line SK-N-BE, TTR inhibited ultrastructural changes characteristic of apoptosis [Giunta S et al 2005]. Pre-incubation of Aβ with TTR also suppressed caspase- 3 activation in the undifferentiated human neuroblastoma SH-SY5Y cell line [Costa R et al 2008] and the cytotoxicity induced by Aβ oligomers on SH-SY5Y cells differentiated by retinoic acid treatment [Li X et al 2011]. Moreover, TTR also inhibited cytotoxicity and the induction of reactive oxygen species (ROS) by Aβspecies in cultured embryonic mouse neurons [Li X et al 2011].

Aim of the Study

We are painfully aware that the basis of that group of disorders known as protein misfolding desease is the failure of a specific peptide or protein to adopt, or remain in, its native functional conformational state. These pathological conditions include neurodegenerative disorders, systemic amyloidoses and cystic fibrosis. The pathological alterations of protein involved in these group of deseases are caused by mutations, aging or other modification of the chemical environment and ultimately leads to the formation of insoluble highly organized fibrillar aggregates, often called amyloid fibrils. There is increasing evidence that the oligomeric assemblies that precede the formation of amyloid fibrils, often kinetic intermediates in the process of amyloid fibril formation or off-pathway species, are the primary pathogenic species in many protein deposition diseases. The toxicity of these early oligomers appears to result from their intrinsic ability to impair fundamental cellular processes, for example by interacting with cellular membranes and disassembling. To better clarify this issue, in the present research, the molecular bases of cell damage induced by prefibrillar forms of different aggregates after the interaction with plasma membrane was investigated in depth. In particular, the oligomer-induced cytotoxicity throught alteration of membrane permeability, oxidative stress and apoptotic pathway activation in human SH-SY5Y neuroblastoma cells and primary neurons from rat brains were checked.

Hippocampal neurogenesis appears to play an important role in learning and memory processes and mood regulation and its abnormal regulation might account for cognitive impairments associated with Alzheimer's disease (AD). We showed that two types of extracellular chaperones (clusterin and α2-macroglobulin) suppress Aβ42-mediated impairment of rat's spatial memory, when microinjected in their brains. In addition, chaperones suppress Aβ42–induced glia inflammation and colocalization with postsynaptic markers in cultured rat hippocampal and cortical primary neurons. Our results support the idea that chaperones can protect against all the effects caused by Aβ oligomers associated with the early symptoms of AD (Result I).

Transthyretin (TTR) is an evolutionarily conserved serum and cerebrospinal fluid protein that transports the holo-retinol binding protein (RBP) and thyroxine (T4). Human TTR is an homotetrameric protein which can disassemble into its monomers, that can misfold and aggregate into fibrils whose growth is considered the cause of TTR amyloidoses. More than 100 mutations have been linked to TTR pathologies and a general trend is that the more destabilized the quaternary structure by the mutation, the more pathological is the variant. Nevertheless, an anti-amyloidogenic effect that prevents Aβ formation *in vitro* has recently been proposed for TTR. Thus, it is possible that TTR ability to bind many classes of compounds allows it to serve as an endogenous detoxifier of molecules with potential pathologic effects. Here we study the ability of three different types of TTR to suppress the toxicity of soluble oligomers formed by three different peptides/proteins. Our results show that TTR can protect SH-SY5Y cells and rat primary neurons against oligomer-induced cytotoxicity and this ability correlates with the capability of TTR to adopt a monomeric state (Result II). The implication emerging from the pieces of evidence described above is that while the physiological function of TTR is linked to the packing of its folded state into a well-defined quaternary structure, different monomeric TTR conformations may play other biological roles, be they negative/pathological or positive/protective. Although tetrameric TTR is far more populated *in vivo* than the monomer, small amounts of misfolded monomers may be sufficient to trigger aggregation, while the interaction of monomeric TTR with its target may shift the equilibrium between tetramers and monomers towards the latter. Consequently, the elucidation of the different monomeric conformational states that can be populated by TTR represents a crucial step towards understanding the properties of the protein and the relationships between those properties and its *in vivo* function (Result III).

TDP-43 is the main component of the ubiquitin-positive, tau-negative and α-synuclein-negative protein inclusions accumulating in the fronto-temporal cortex and hippocampus of the brain and in the motor neurons of the spinal cord of patients suffering from frontotemporal lobar degeneration with ubiquitin-positive inclusions (FTLD-U) and amyotrophic lateral sclerosis (ALS). Pathological TDP-43 aggregation is associated with a dislocation of this protein from the nucleus, where the protein

normally resides and plays its functions, to the cytoplasm, where the inclusions accumulate. In such cytoplasmic inclusions TDP-43 is hyperphosphorylated, ubiquitinated and cleaved to form C-terminal fragments, although in the spinal cord motor neurons the inclusions consist rather of full-length TDP-43. In this work we have overexpressed full-length and C-terminal TDP-43 in *E. coli*, purifying the resulting TDP-43 containing inclusion bodies (FL TDP-43 IBs and Ct TDP-43 IBs, respectively) and subjecting them to a number of biophysical analyses to assess their structure and morphology. In addition to performing a biophysical investigation of the TDP-43 IBs, we have transfected human SH-SY5Y neuroblastoma cells with FL TDP-43 IBs to evaluate their inherent toxicity (Result IV).

Chapter 2- Materials & Methods

Materials

Chemicals

All reagents were of analytical grade or the highest purity available. Tissue plastic ware was obtained from PBI international (Milan, Italy). Ampicillin, 8-anilino-1-naphthalenesulfonic acid (ANS), bovine serum albumin (BSA), Bradford reagent, chloroquin, congo red (CR), fetal bovine serum (FBS), dithiothreitol (DTT), hen egg white lysozyme (HEWL), hexafluoro-2-isopropanol (HFIP), hygromycin B, human and bovine Cyclophilin A, 3-MA, media for cell cultures, MG-132, phosphate buffer saline (PBS), pluronic acid F-127, proteinase K (PK), tetracycline, Vitamin E (Vit E), ATP, thioflavin T (ThT), urea and other chemicals were from Sigma (Milan, Italy). Neurobasal medium and B-27 were from Gibco (Invitrogen Corporation, Milan, Italy), and were purchased from Sigma-Aldrich.

Fluorescent probes

Calcein-acetoxymethyl (Calcein-AM), 2',7'-dichlorodihydrofluorescein diacetate,acetyl ester (CM-H2DCFDA), fluo3-acetoxymethyl ester (Fluo3-AM) and wheat germ agglutinin-conjugated with fluorescein or with Alexa Fluor 633 were purchased fromMolecular Probes (Eugene, OR, USA). All the fluorescent probes were prepared as stock solutions in DMSO, purged with nitrogen and stored in light-protected vessels at −20 °C until use.

$A\beta_{42}$ and HyPF-N: aggregation protocols and pre-incubation with chaperons or TTR

$A\beta_{42}$ were purchased from Sigma (Milan, Italy). Lyophilized $A\beta_{42}$ was initially incubated in 1 mM in hexafluoro-2-propanol (HFIP) at least for 1 h at room temperature to allow complete peptide monomerization. Then, aliquots of peptide solutions were dried under nitrogen and stored at −80 °C. Prefibrillar aggregates of the $A\beta_{42}$ peptide were obtained according to Lambert's protocol [Lambert MP et al. 2001]. Briefly, aliquots of $A\beta_{42}$ were dissolved in DMSO to a final concentration of 5.0 mM, incubated in ice-cold F12 medium to a concentration of 100 µM at 4°C for 24 h and then centrifuged at

14,000 x g for 10 min to remove insoluble structures. The supernatant, defined as the amyloid β-derived diffusible ligand (ADDL) preparation, consisted of a fibril-free solution of globular assemblies, as routinely assessed by atomic force microscopy [Cecchi C et al. 2009]. Lyophilized amylin 1–37 (Sigma, Milan, Italy) was stored as powder at −20 °C until reconstitution in HFIP at a concentration of 1.25 mM. The reconstituted peptide was stored as 10 µl aliquots at -80 °C until used.

HypF-N protein, expressed and purified as previously reported [Campioni S et al. 2010], was converted into stable oligomers by incubation to 48 µM for 4 h or for 3 and 9 days at 25 °C in two different experimental conditions: 50 mM acetate buffer, 12% (v/v) trifluoroethanol (TFE), 2 mM dithiothreitol (DTT), pH 5.5 (condition A) and 20 mM trifluoroacetic acid (TFA), 330 mM NaCl, pH 1.7 (condition B). Both types of HypF-N oligomers were centrifuged at 16100 g, dried under N2 to remove the TFE and TFA when necessary, dissolved in the appropriate culture media at 48 µM concentration and immediately added to cultured cells at differing final concentrations. Native HypFN was tested by diluting the protein stock solution in the same cell media. Tappingmode atomic force microscopy revealed the presence of spherical bead-like aggregates with heights in the range of 2-6 nm and 2-7 nm under conditions A and B, respectively [Campioni S et al. 2010].

Human clusterin and α_2-macroglobulin (α_2M) were purified as described [Wilson MR et al. 1992; French K et al. 2008; Yerbury JJ et al. 2005]. The three TTR variants were prepared and purified in an *E. Coli* expression system as described elsewhere [White JT et al. 2001; Jiang X *et al* 2001; Hammarstrom P et al 2003].

All oligomers were incubated in the appropriate media for 1h at 37°C while shaking, in the absence or presence of chaperones or TTRs, and then added to cultured cells or injected in rat brains. The HypF-N ($A\beta_{42}$/IAPP):chaperone molar ratio was 10:1 (clusterin),) and 100:1 (α_2- macroglobulin), unless stated otherwise (HypF-N, $A\beta_{42}$, IAPP, are considered as monomers, clusterin as αβ dimers and α_2-macroglobulin as a tetramer, according to the functional oligomeric state). The HypF-N:TTR molar ratio was 10:1, unless stated otherwise (hTTR, mTTR or M-TTR are considered as a tetramer, according to the functional state).

FL and Ct TDP-43 gene cloning and protein expression

The genes for full length (FL TDP-43) and its C-terminal fragment 208-414 were cloned downstream of the glutathione S-transferase (GST) gene in the pGEX-2T plasmid. In brief, the sequence coding for FL TDP-43 and that coding for Ct TDP-43 were amplified from the pINCY vector (EuroClone, Milan, Italy) by PCR, using forward and reverse primers containing the restriction sites for *BamHI* and *EcoRI* enzymes, respectively. Each amplified sequence and the pGEX-2T plasmid were digested with *BamHI* and *EcoRI* (Fermentas, Milan, Italy) and combined with the T4 DNA ligase (Fermentas) to obtain the constructs coding for the GST/FL TDP-43 and the GST/Ct TDP-43 fusion proteins. Their correct nucleotide sequence was verified by DNA sequencing. Cultures of *E. coli* XL1 Blue cells (Agilent Technologies, Milan, Italy) were transformed with the resulting plasmids containing FL TDP-43 or Ct TDP-43 and were grown overnight at 37 °C in LB medium with 100 µg/mL ampicillin under vigorous shaking. Cells were then diluted 1:10 in fresh medium and grown at 37 °C in LB until OD_{600nm} ~ 0.6. Protein expression was induced using 1 mM isopropyl β-D-1-thiogalactoside (IPTG; Inalco, Paris, France). Cells were harvested by centrifugation, resuspended in PBS buffer (137 mM NaCl, 2.7 mM KCl, 4.3 mM Na_2HPO_4, 1.4 mM KH_2PO_4, 1 mM EDTA, 1 mM β-mercaptoethanol, 0.1 mM PMSF, at pH 7.3) and then lysed by 30 min incubation with 1 mg/mL HEWL in ice, followed by sonication at 40 kHz (five cycles of 30 s each). The expression of FL and Ct TDP-43 and their presence in the supernatant or in the pellet fractions after cell lysis were checked by SDS-PAGE, using 12% (w/v) polyacrylamide gels.

Inclusion bodies purification

Inclusion bodies (IBs) were purified from IPTG induced cells harbouring the pGEX-2T/FL TDP-43 plasmid, the pGEX-2T/Ct TDP-43 plasmid and the only pGEX-2T plasmid by detergent-based procedures. Briefly, cells obtained from 1 L cultures were harvested by centrifugation at 29000 × g for 15 min at 4 °C, resuspended in 40 mL of lysis buffer (50 mM Tris-HCl, 100 mM NaCl, 1 mM EDTA, at pH 8.0) and maintained overnight at −80 °C. After thawing, 35 µL of 100 mM PMSF and 280 µL of 10 mg/mL HEWL were added and the samples were incubated for 45 min at 37 °C under gentle agitation. To cause the membrane lysis, IGEPAL was added to a final concentration of 1% (v/v) and

the mixture maintained in ice for 1 h under agitation. Then, 600 µL of 1 mg/mL DNase I and 600 µL of 1 M $MgSO_4$ were added and the resulting mixture was incubated at 37 °C for 40 min. IBs were separated by centrifugation at 29000 × g for 15 min at 4 °C. The resulting IBs were washed once with lysis buffer containing 0.5% Triton X-100 and twice with water. After a final centrifugation at 29000 × g for 15 min at 4 °C, the *pellet* was stored at −80 °C and reconstituted in PBS buffer (137.0 mM NaCl, 2.7 mM KCl, 4.3 mM Na_2HPO_4, 1.4 mM KH_2PO_4, at pH 7.3).

IBs internalization

FL TDP-43 IBs were labeled with fluorescein-5-isothiocyanate (5-FITC) using AnaTagTM 5-FITC Microscale Protein Labeling Kit (AnaSpec, San Jose, CA, USA). Transfection of both labeled and unlabeled FL TDP-43 IBs and unlabeled control IBs into SH-SY5Y neuroblastoma cells was performed using a total protein concentration of 5.7 µg/mL and 4.0 µg/mL, respectively, and the PULSin protein delivery reagent (Polyplus-transfection, Illkirch, France). Cells were also transfected with R-phycoerythrin (R-PE), a green fluorescent protein used as a positive control (excitation and emission at 488 and 575 nm, respectively). After 3 h transfection, the incubation medium without serum was replaced with fresh complete medium. After washing with PBS, cells treated with unlabeled IBs were counterstained for 10 min with 50 µg/mL Alexa Fluor 633-conjugated wheat germ agglutinin and fixed in 2% (w/v) buffered paraformaldehyde for 10 min at room temperature (20 °C). After plasma membrane permeabilization with a 3% (v/v) glycerol solution for 5 min, the coverslips were incubated for 60 min with 1:350 diluted rabbit polyclonal anti-TDP-43 antibodies (Sigma-Aldrich) and then for 90 min with 1:1000 diluted Alexa Fluor 488-conjugated anti-rabbit antibodies incubated at 37 °C. Cells were analyzed using a Leica TCS SP5 confocal scanning microscope (Leica Microsystems, Mannheim, Germany), equipped with an argon laser source and a Leica Plan Apo 639 oil immersion objective.

The colocalization of FL TDP-43 IBs or phosphorylated TDP-43 with ubiquitin was monitored using 1:350 rabbit polyclonal anti-TDP-43 antibody or 1:500 rabbit anti-TDP-43 phosphorylation sites 409/410 (Cosmo Bio Co., Ltd., Tokio, Japan) for 60 min at 37 °C, 1:150 mouse monoclonal anti-ubiquitin antibodies (Life Technologies, CA, USA) for

60 min at 37 °C, and then with 1:1000 Alexa Fluor 488-conjugated secondary antibodies (Life Technologies, CA, USA) for 60 min at 37°C and 594-conjugated secondary antibodies (Life Technologies, CA, USA) for 60 min at 37°C.

Rat models and cell culture

Three-month-old (220–250 g) male Wistar rats (Harlan Nossan, Correzzana, Italy) were housed in macrolon cages until surgery and maintained on a 12-hours light/dark cycle at 23°C. All animal manipulations were performed *in vivo*, according to the European Community guidelines for animal care (DL 116/92).

Primary hippocampal and cortical neurons were obtained from embryonic day (ED)-17 Sprague-Dawley rats (Harlan, Italy) as described in Bongers et al. [Bongers G. et al. 2007]. The experimental procedure were in accordance with the standards set forth in the Guide for the Care and Use of laboratory Animals (published by the National Academy of Science, National Academy Press, Washington, D.C.). The uteri were removed from the gravid rat under anesthesia. Cerebral hippocampi and cortices were dissociated in sterile Dulbecco's phosphate-buffered saline (D-PBS; Sigma), and neurons isolated in the same medium containing trypsin (0.5% in sterile Dulbecco's phosphate-buffered saline) for 10 min at 37° C. After centrifugation, dissociated neurons were re-suspended in neurobasal medium (NBM; Gibco, Invitrogen Corporation, Milan, Italy) supplemented with 2% B-27 (Gibco) and 0.5 mmol/L glutamine (Gibco), and then plated in poly-L-lysine-coated 96 or 24-well plates at a density of approximately 1.0 x 10^4 and 2.0 x 10^4/well, respectively. Cultures were maintained in NBM at 37° C in a 5% CO_2-humidified atmosphere. Neurons were exposed to 12.0 µM toxic oligomers 14 days after plating.

Human SH-SY5Y neuroblastoma cells (A.T.C.C., Manassas, VA, USA) were cultured in DMEM/F-12 Ham with 25 mM N-2-hydroxyethylpiperazine-N-2-ethanesulfonic acid (HEPES) and $NaHCO_3$ (1:1) supplemented with 10% FBS, 1.0% glutamine and 1.0% antibiotics. The cell culture was maintained in a 5.0% CO_2 humidified atmosphere at 37 °C and grown until 80% confluence for a maximum of 20 passages.

Methods

Analyses on rat models: Morris water maze test (MWM)

For *in vivo* studies, $A\beta_{42}$ oligomers and chaperones were suspended in F12-medium with 0.1% DMSO at final concentrations of 0.45 mg/ml (100 µM) and 0.7 mg/ml (10 µM for Clu and 1 µM for α_2M), respectively, and incubated for 1 h at 37 °C while shaking. 1.5 µl aliquots of F12-medium, F12-medium with $A\beta_{42}$ oligomers, F12-medium with $A\beta_{42}$ oligomers and Clu and F12-medium with $A\beta_{42}$ oligomer and α_2M, all containing 0.1% DMSO, were injected into the Cornu Ammonis (CA) 1 molecular layer of the right hippocampus of anaesthetised (Zoletyl, 45 mg/kg plus Carprofen, 5 mg/kg) rats for each condition, using a Hamilton microsyringe, at the following stereotaxic coordinates (in mm): AP,-3.7; L,-2.5 from bregma; and H, 3.5 below the dura [Paxinos G et al. 1980]. The injections lasted 3 min, and the microsyringe was left in the place for 5 min after completing the infusion. Rats were behaviourally tested in the MWM 1 week after the intrahippocampal injection of the different oligomers (n=6/group). This was considered a reasonable time period to allow us to detect long-term effects of the injected aggregates in light of their likely persistence in tissue.

The water maze apparatus consisted of a circular pool (160 cm diameter and 45 cm high) made of plastic. The pool was filled to a depth of 30 cm with water (22±1 °C) that was made dark by the addition of non-toxic dark paint, and virtually divided into four equivalent quadrants. Rats were tested in the reference memory version of MWM with the procedure previously described [Inostroza M et al. 2011]; briefly, all rats underwent a reference memory training with a hidden platform (13 cm diameter, submerged 0.5 cm under the water level), placed in the centre of one quadrant of the pool (northwest) for 4 days, with 4 trials per day, with the four starting locations varied between trials. Upon release into the water, the rat was allowed to search the platform for 60 s; if the platform was not located within the maximum time of 60 s, the rat was guided to the location. The rat was allowed 20 s on the platform. Extra-maze visual cues around the room remained in fixed positions throughout the experiment. For each trial, latency to find the platform (maximum 60 s) was recorded by a video-tracking/computer-digitising system (HVS Image, Hampton, UK). On day 4, five hours after the last trial, the platform was removed from the pool and each rat received one

30 s swim "probe trial". The starting point was set in the south-east quadrant. Percentage of time spent in each quadrant and the number of crossing over the platform section were recorded.

Fluorescence immunohistochemical analyses of glial activation and Neu-N

After behavioural evaluations, all rats were deeply anaesthetised with chloral hydrate (400 mg/kg, i.p.) and killed by decapitation. Four brains for each conditions were quickly extracted and fixed in phosphate-buffered 4% paraformaldehyde (pH 7.4) for 24 h at 4 °C, subsequently rinsed with PBS, dehydrated using an automated machine and embedded in paraffin. Coronal sections (5.0 µm) were cut using a microtome and mounted on slides. Sections were then incubated in xylene for 20 min at room temperature, to allow removal of paraffin, and subsequently rehydrated.

Fluorescent labeling followed previously described protocols [Rosi MC et al. 2010]. Briefly, 5 µm paraffin-embedded coronal sections (3 sections of each brain for each condition) were rinsed 3 times and placed in blocking solution (PBS, pH 7.4 + 0.3% (v/v) Triton X-100, 2 g/l bovin serum albumin (BSA) and 5% (v/v) normal goat serum (NGS)) for 30 min at room temperature (RT). Analysis of glial fibrillary acidic protein (GFAP)-immunoreactive astrocytes and ionised calcium binding adaptor molecule 1 (Iba-1)-labeled microglial cells were carried out overnight at 4 °C using 1:500 diluted rabbit polyclonal anti-GFAP (Dako, Glostrup, Denmark) or 1:300 diluted rabbit polyclonal anti-Iba 1 (Wako, Fuggerstrasse, Germany) antibodies diluted in fresh blocking solution. Sections were then washed in PBS (3x 10 min) at RT and subsequently incubated for 2 h with Alexa Fluor 488-conjugated anti-rabbit or Alexa Fluor 594-conjugated anti-rabbit polyclonal antibodies (Invitrogen, Eugene, OR), diluted 1:400 in blocking solution. Following further rinses, sections were cover-slipped using Vectashield water-based mounting medium containing DAPI (Vector Laboratories, Burlingame, CA).

Analysis of neuronal nuclei (Neu-N) were carried out overnight at 4 °C using 1:100 diluted mouse polyclonal anti-Neu-N (Chemicon, Millipore, Italy) antibodies diluted in fresh blocking solution. Sections were then washed in PBS (3x 10 min) at room temperature and subsequently incubated for 2 h with Alexa Fluor 594-conjugated anti-mouse polyclonal antibodies (Invitrogen) diluted 1:400. Following further rinses,

sections were cover-slipped using Vectashield water-based mounting medium containing DAPI (Vector Laboratories). In each study the analysis of negative controls (omission of primary antibody) was simultaneously performed in order to exclude the presence of non-specific immunofluorescent staining, cross-immunostaining, or fluorescence bleed-through. Neu-N-positive cells in the hippocampus were counted under a 10 x objective lens of an Olympus Optical (Tokyo, Japan) BX63 microscope equipped with an Olympus Optical DP50 digital camera and a cellSens Dimension software. The total number of counted Neu-N-positive cells, carried out on 3 sections of each brain for each condition, was averaged, expressed as percentage of that in the F-12-injected rats, assumed as 100% and analyzed using Prism 3.0 (GraphPad Software, San Diego, CA).

Lipid peroxidation analysis and caspase-3 activity assay in rat hippocampus

The analyses of lipid peroxidation and caspase-3 levels were performed on rat hippocampal homogenates. We microinjected 1.5 µl aliquots of F12-medium, $A\beta_{42}$ oligomers and $A\beta_{42}$ oligomer pre-incubated with Clu or α_2M for 0 h and 1 h, into the right hippocampus of anaesthetised rats. Three hippocampi for each condition were quickly extracted from rat brains and immediately stored at -80 °C. Each hippocampus was transferred to ice-cold microcentrifuge tubes with 200 µl of lysis buffer (50 mM Tris–HCl, pH 7.5, 50 mM NaCl, 10 mM EGTA, 5 mM EDTA, 2 mM sodium pyrophosphate, 4 mM para-nitrophenylphosphate, 1 mM sodium orthovanadate, 1 mM phenylmethylsulfonyl fluoride (PMSF), plus 20 µg/ml leupeptin and 30 µg/ml aprotinin), and tissues were homogenised on ice (with a Potter-Elvehjem homogeniser) directly into the Eppendorf tube (20 strokes, 1 stroke/s). Immediately after homogenisation, protein determination was performed using the method of Bradford [Bradford MM 1976]. To assess the rate of lipid peroxidation, the 8-OH isoprostane levels were measured in rat hippocampal homogenates (5 µg of proteins per well) using the 8-isoprostane EIA kit (Cayman Chemical Company, Ann Arbor, MI) at 405 nm, as previously described [Zampagni M et al. 2012].

The caspase-3 activity assay homogenates were prepared using a different buffer composition (20 mM Tris-HCl buffer, pH 7.4, containing 250 mM NaCl, 2 mM EDTA,

0.1% Triton X-100, 5 μg/ml aprotinin, 5 μg/ml leupeptin, 0.5 mM phenylmethylsulfonyl fluoride, 4 mM sodium vanadate, and 1 mM dithiothreitol (DTT)) [Donati C et al. 2007]. To evaluate the caspase-3 activation, 50 μg of total proteins were diluted in 50 mM HEPES-KOH buffer, pH 7.0, containing 10% glycerol, 0.1% 3-[(3-cholamidopropyl)dimethylammonio]- 1-propanesulfonate, 2 mM EDTA, 10 mM DTT and incubated for 4 h at 37 °C in presence of 30 μM Ac-DEVD-AFC (excitation, 400 nm; emission, 505 nm) (Biomol Research Laboratories Inc., Plymouth Meeting, PA, http://www.biomol.com).

Analyses on cell cultures

Cell exposure to aggregates

The effect of protein oligomers on cell viability was assessed using primary neurons from rat brains and SH-SY5Y cells seeded in 96-well plates. Preformed oligomers of $A\beta_{42}$ and HypF-N (12 μM monomer concentration) were incubated in cell culture medium for different time lengths (0, 5, 15, 30 and 60 min) in the absence or presence of Clu, α_2M, hTTR, muTTR, M-TTR, HEWL or BSA (protein: Clu and protein:TTR molar ratio were 10:1 unless otherwise stated; protein:α_2-macroglobulin was 100:1, protein:haptoglobin, protein:HEWL and protein:BSA molar ratio was 5:1), and then added to the cells. Each TTR (1.2 μM tetramer concentration) or 12 μM native HypF-N and $A\beta_{42}$ were also used as controls. In additional experiments, 1 μM staurosporine (Sigma Aldrich, Milan, Italy) was incubated for 1 h in cell culture medium in the absence or presence of each TTR and then added to the cells.

60 min at 37 °C, and then with 1:1000 Alexa Fluor 488-conjugated secondary antibodies (Life Technologies, CA, USA) for 60 min at 37°C and 594-conjugated secondary antibodies (Life Technologies, CA, USA) for 60 min at 37°C.

Evaluation of intracellular ROS production

Intracellular ROS production was detected by using CM-H_2DCFDA, a ROS-sensitive fluorescent dye. CM-H_2,DCFDA esterified derivative is loaded more effectively within the cytoplasm of the cells because it is more cell permeant before ester groups are

hydrolyzed by the cellular esterases. Only a negligible leakage of the probe occurred, since chloromethyl-DCF is negatively charged at physiological intracellular pH. SHSY5Y cells were first cultured on glass coverslips and exposed to native protein or to HypF-N aggregates for different times at 37°C. Cells were also exposed to HypF-N aggregates in a Ca^{2+} free medium or pre-treated for 24 hours with 100 μM vitamin E prior to aggregate exposure in Ca^{2+} containing medium. In other set of experiments, SH-SY5Y cells and rat neurons were incubated for 60 min with 12 μM HypF-N type A oligomers or $A\beta_{42}$ oligomers pre-incubated with or without different chaperones or TTRs for different lengths of time. The cells were then incubated with 5 μM CMH_2DCFDA, dissolved in 0.1% DMSO and Pluronic acid F-127 (0.01% w/v), in the final 10 min of aggregate exposure. The cells were then fixed in 2.0% buffered paraformaldehyde for 10 min at room temperature and the emitted CM-H_2DCFDA fluorescence was detected at 488-nm excitation by the confocal Leica TCS SP5 scanning microscope (Mannheim, Germany) equipped with an argon laser source for fluorescence measurements at 488 nm and 633 nm and a Leica Plan Apo 63 x oil immersion objective. A series of optical sections (1024 X 1024 pixels) 1.0 μm in thickness was taken through the cell depth for each examined sample.

The levels of intracellular ROS production were analysed also 24 h after transfection or extracellular addition of FL TDP-43 IBs and control IBs to SH-SY5Y cells seeded on glass coverslips and loaded with CM-H_2DCFDA. Final protein concentration were 4.0 μg/mL and 215 μg/mL (plus 30% for FL TDP-43 IBs) for the intracellular and extracellular analyses, respectively. $A\beta_{42}$ oligomers at a final protein concentration of 60 μg/mL were also used as a positive control. To quantify the signal intensity of CM-H_2DCFDA, 10-22 cells were analyzed using ImageJ software (NIH, Bethesda, MD), and the fluorescence intensities were expressed as arbitrary units.

Analysis of membrane permeability

In order to assess whether HypF-N aggregates disrupt cell membrane integrity, neuroblastoma cells were pre-treated for 20 min at 37°C with 2.0 μM calcein-AM, dissolved in DMSO and resuspended in cell culture medium [Cecchi C et al. 2008]. The decay in fluorescence was analyzed by confocal microscopy at 488 nm excitation

wavelength after cell exposure to 12 μM HypF-N aggregates at 37°C for differing length of time. In a set of experiments, SH-SY5Y cells were incubated for 60 min with 12 μM HypF-N type A oligomers pre-incubated with or without different chaperones or TTRs for different lengths of time.

Analysis of cytosolic Ca^{2+} dyshomeostasis

The effect of HypF-N aggregates on cytosolic free Ca^{2+} levels was analyzed in SH-SY5Y cells plated on glass coverslips and loaded with Fluo3-AM, a Ca^{2+} specific fluorescent probe. The cells were first exposed to 12 μM HypF-N aggregates for differing length of times at 37°C. Cytosolic Ca^{2+} levels were also examined in SH-SY5Y cells exposed to HypF-N aggregates in Ca^{2+} free medium or in cells pre-treated for 24 h with 100 μM vitamin E prior to aggregate exposure in Ca^{2+} containing medium. In a set of experiments SH-SY5Y cells and rat neurons were exposed for 60 min at 37°C to 12 μM HypF-N type A aggregates or $A\beta_{42}$ oligomers pre-incubated with or without different chaperones/TTRs for for different lengths of time. The cells were then loaded for 30 min at 37°C with 10 μM Fluo3-AM, 0.01% (w/v) pluronic acid F-127 in Hank's Balanced Salt Solution (HBSS) and subsequently fixed in 2.0% buffered paraformaldehyde for 10 min at room temperature. Fluorescence was detected at 488 nm excitation by collecting the emitted fluorescence with the confocal scanning system described above.

Apoptotic and necrotic markers

Caspase-3 activity

The extent of the apoptotic program activation in SH-SY5Y cells was evaluated by confocal microscope and flow cytometric analyses of caspase-3 activity, which is the main effector caspase in apoptosis. The cells were exposed to 12 μM native or aggregated HypF-N aggregates for 24 h at 37 °C in culture medium. In a series of experiments, the cells were also treated with HypF-N type A oligomers pre-incubated with or without different chaperones/TTRs for different lengths of time. After the appropriate treatment, the culture media were removed and replaced with FAM-FLICA

Caspases 3&7 solution (Caspase 3&7 FLICA kit; FAM-DEVDFMK; Immunochemistry Technologies, LLC, Bloomington, MN, USA) for 60 min and the emitted fluorescence was detected at 488 nm excitation by the confocal scanning system described above. The levels of caspase-3 activity were analysed also 24 h after transfection or extracellular addition of FL TDP-43 IBs and control IBs to SH-SY5Y cells seeded on glass coverslips. Final protein concentration were 4.0 μg/mL and 215 μg/mL (plus 30% for FL TDP-43 IBs) for the intracellular and extracellular analyses, respectively. $A\beta_{42}$ oligomers at a final protein concentration of 60 μg/mL were also used as a positive control. To quantify the signal intensity of CM-H_2DCFDA, 10-22 cells were analyzed using ImageJ software (NIH, Bethesda, MD), and the fluorescence intensities were expressed as arbitrary units

Hoechst staining

Nuclear alterations eventually induced by HypF-N aggregates were investigated by Hoechst 33342 dye staining. Briefly, SH-SY5Y cells were exposed to 12 μM HypF-N type A oligomers pre-incubated with or without different TTRs for 24 h at 37 °C. Then, the cells were incubated with 20 μg/ml Hoechst for 15 min at 37 °C and fixed in 2% buffered paraformaldehyde for 10 min at room temperature. Blue fluorescence micrographs of cells were obtained under UV illumination in an epifluorescence inverted microscope (Nikon, Diaphot TMD-EF) with an appropriate filter set.

Mitochondrial status

Cytotoxicity assay

The toxic effect of the differing aggregates on metabolic cell functions was assessed in cell models by the 3-(4,5-dimethylthiazol-2-yl)-2,5-diphenyltetrazolium bromide (MTT) assay in 96-well plates [Cecchi C et al. 2007]. Native or aggregated HypF-N (12 μM) were added to the SH-SY5Y or rat neuron cell culture media for 24 h at 37 °C. In a set of experiments, SH-SY5Y cells were exposed for 24 h at 37 °C to 12 μM HypF-N type A, Aβ42 or IAPP oligomers, pre-incubated with or without chaperones, TTRs, HEWL or BSA for 1 h. In another set of experiments SH-SY5Y cells were exposed 1 μM

staurosporine pre-incubated with or without chaperones or TTRs, for 24 h at 37°C. Rat neurons were exposed for 24 h at 37°C to 12 µM HypF-N type A or Aβ42 oligomers pre-incubated with or without chaperones.

The MTT assay was also carried out 24 h after cell transfection or addition to the extracellular medium of SH-SY5Y cells of FL TDP-43 IBs, control IBs and R-PE. The final protein concentrations were 4.0 µg/mL for the cell internalization analysis and ranged from 7.5 to 860 µg/ml for the extracellular analysis (plus 30% for FL TDP-43 IBs). In a set of experiments cells were treated with either 5 µM MG-132, 10 mM 3-MA or 40 µM chloroquin, which were added immediately after cell transfection with FL TDP-43 IBs and control IBs. After cell treatments, 100 µl of 0.5 mg/ml MTT solution in PBS was added to the cell cultures and the samples were incubated for 4 h at 37°C. Finally, 100 µl of cell lysis buffer (20% SDS, 50% N,N-dimethylformamide, pH 4.7) was added to each well and the samples were incubated for at least 3 h at 37°C in a humidified incubator, before determination of absorbance value of blue formazan at 590 nm with an ELISA plate reader. Cell viability was expressed as a percentage of MTT reduction in aggregate or transfected cells compared to untreated cells (assumed as 100%).

Colocalization of $A\beta_{42}$ aggregates with PSD-95 in cultured neurons

Preformed oligomers of $A\beta_{42}$ (12 µM monomer concentration) were incubated for 1 h in the cell culture medium with or without Clu or α_2M ($A\beta_{42}$:chaperone molar ratio as described above) and then added to rat neurons seeded on glass coverslips for 1 h or 24 h at 37 °C. Immunolabeling of cultured primary neurons was performed as previously described [Lacor PN et al. 2004]. The colocalization of $A\beta_{42}$ aggregates with PSD-95 was monitored using 1:200 mouse monoclonal 6E10 antibody and 1:500 rabbit polyclonal anti-PSD-95 antibody (Pierce Biothecnology, USA) for 60 min at 37 °C, and then with Alexa Fluor 488- and 594-conjugated antibody (Sigma-Aldrich, St. Louis, MO) for 2 h at room temperature. Cell fluorescence was analyzed by confocal Leica TCS SP5 scanning microscope (Mannheim, Germany) equipped with laser sources for fluorescence measurements at 488 and 594 nm and a Leica Plan Apo 63X oil immersion objective. A series of optical sections (1024x1024 pixels), 1.0 µm in thickness, were taken through the cell depth for each examined sample. Settings were

maintained constant for each analysis. The colocalization of oligomers with PSD-95 was estimated on regions of interest (12–13 cells) using the ImageJ (NIH, Bethesda, MD, USA) and JACOP plugin (rsb.info.nih.gov) softwares [Rasband WS 1997-2008].

Confocal microscopy analysis for TTR-HypF-N oligomer binding

HypF-N oligomers (at a corresponding monomer concentration of 48 µM) were incubated for different time lengths (0, 5, 15, 30 and 60 min) in the absence or presence of TTRs and then centrifuged to obtain pellet that were resuspended and incubated subsequently for 30 min at 37 °C in solutions containing: (I) 1:4,000 rabbit polyclonal anti–HypF-N antibodies (Primm) and mouse monoclonal anti-TTR antibodies (Santa Cruz Biotechnology), (II) 1:1,000 Alexa Fluor 488-conjugated anti-rabbit secondary antibodies (Life technologies, CA, USA), and (III) Alexa Fluor 594-conjugated anti-mouse secondary antibodies (Life technologies, CA, USA). After every incubation, samples were centrifuged for 10 min at 16,100 × g, washed in PBS, and centrifuged again. Finally, the pellet was resuspended in 20 µl PBS and spotted on glass coverslips. The cross-reactivity of oligomers was tested by subsequent incubations with primary and secondary anti-TTR antibodies. Confocal microscope images were acquired as described above.

Confocal microscopy analysis for TTR- $A\beta_{42}$ oligomer binding

$A\beta_{42}$ oligomers (at a corresponding monomer concentration of 48 µM) were incubated for different time lengths (0, 5, 15, 30 and 60 min) in the absence or presence of M-TTR, spotted on glass coverslips and incubated for 30 min at 37 °C in solutions containing (i) 1:300 diluted rabbit polyclonal A11 anti-Aβ antibodies (Life technologies, CA, USA) and mouse monoclonal anti-TTR antibodies (Santa Cruz Biotechnology), (ii) 1:1,000 Alexa Fluor 488-conjugated anti-rabbit secondary antibodies (Life technologies, CA, USA), and (iii) Alexa Fluor 594-conjugated anti-mouse secondary antibodies (Life technologies, CA, USA). After every incubation, samples were washed in PBS. The cross-reactivity of oligomers was tested by subsequent incubations with primary and secondary anti-TTR antibodies. Confocal microscope images were acquired as described in the Material and Methods section.

Biophysical methods

Thioflavin T assay

Preformed HypF-N oligomers (12 µM monomer concentration) were incubated for 1 h at 37 °C with shaking in the presence or absence of each TTR (HypF-N:TTR molar ratio as described above). Aliquots of these samples were added to a solution of 25 µM Thioflavin T (ThT) dissolved in 25 mM phosphate buffer at pH 6.0, in order to obtain a 3.7-fold molar excess of dye. Final protein concentration was 6 µM. The steady-state intensity of fluorescence emission at 485 nm (excitation at 440 nm) was recorded at 37 °C. Each TTR (1.2 µM tetramer concentration) and 12 µM native HypF-N were also used as controls.

In a set of experiment FL TDP-43 IBs, Ct TDP-43 IBs and control IBs at the same concentrations were incubated at 25 °C and an aliquot of 60 µL of each sample was mixed with 440 µL of a 25 mM NaH2PO4 buffer at pH 6.0 containing 25 µM ThT. The resulting fluorescence was measured at 25 °C using a Perkin-Elmer LS 55 spectrofluorimeter (Waltham, MA, USA) equipped with a thermostated cell holder attached to a Haake F8 water bath (Karlsruhe, Germany), using excitation and emission wavelengths of 440 and 450-600 nm, respectively. A 2 x 10 mm quartz cuvette was used. The ThT spectrum obtained in the presence of the same buffer without IBs was subtracted from those acquired in the presence of FL TDP-43 IBs, Ct TDP-43 IBs and control IBs. The ThT fluorescence obtained after incubation with native HypF-N is reported as negative control.

Pyrene fluorescence emission spectra

HypF-N variants carrying a single cysteine residue were labeled with N-(1-pyrene)maleimide and converted into toxic aggregates as previously reported [Zampagni M et al. 2011] and then 4-fold diluted into 20 mM potassium phosphate buffer at pH 7.0. Fluorescence emission spectra of these samples were measured after 1 h of incubation at 37 °C under shaking in the absence and presence of each TTR. The spectra were acquired with 12 µM HypF-N, at 37 °C, with an excitation of 344 nm using a Perkin-Elmer LS 55 spectrofluorimeter (Wellesley, MA) equipped with a

thermostated cell holder attached to a Haake F8 water bath (Karlsruhe, Germany), and a 1.5 × 1.5 mm quartz cell. The spectra were normalized to the intensity of the peak centered at 375 nm.

Intrinsic fluorescence

HypF-N oligomers and each TTR incubated in isolation and in combination as described before were centrifuged for 10 min at 16100 rcf. The intrinsic fluorescence of the supernatants (SNs) were measured at 37 °C with excitation at 280 nm using a Perkin-Elmer LS 55 spectrofluorimeter (Wellesley, MA) equipped with a thermostated cell holder attached to a Haake F8 water bath (Karlsruhe, Germany), and a 2 × 10 mm quartz cell. The spectrum of HypF-N oligomers has been subtracted from that of TTR+HypF-N oligomers.

SDS-PAGE

HypF-N oligomers and each TTR incubated in isolation and in combination as described above were centrifuged for 10 min at 16100 rcf. Pellets and SN aliquotes were collected and mixed with 4× sample buffer with 20 % 2-mercaptoethanol. Sodium dodecylsulfate polyacrylamide gel electrophoresis (SDS-PAGE) analysis was performed in accordance with Laemmli [Oberg K et al. 1994] using a 16% polyacrylamide gels. Proteins were visualized by Coomassie Blue staining (0.1% Coomassie Blue, 10% acetic acid, 40% methanol). The densitometric analysis was obtained using ImageJ software (NIH, Bethesda, MD,USA).

Atomic force microscopy

HypF-N/Aβ_{42} oligomers (12 μM monomer concentration) were incubated for 1 h at 37 °C under shaking in 20 mM potassium phosphate buffer at pH 7.0, in the presence or absence of each TTR. Samples were diluted 1000-fold and immediately deposited on a freshly cleaved mica substrate and dried under a gentle nitrogen flux. Non-contact AC mode atomic force microscopy (AFM) images were acquired in air using a PicoSPM microscope equipped with an AC-mode controller (Molecular Imaging, Phoenix, AZ).

Rectangular non-contact cantilever (model NSG01, NT-MDT Moscow, Russia), with typical resonance frequency of 150 Khz, were used. Oligomer sizes were measured from the height in cross section of the topographic AFM images.

In another set of experiment purified IBs were resuspended in water at a protein concentration of 2 mg/mL and diluted 10 or 100 times. A 10 µL aliquot was deposited on freshly cleaved mica and dried under mild vacuum. Digestion with PK was performed by incubating 40 µL of undiluted IBs with 3.2 µL of a 10 mg/mL PK stock solution for 60 min at 37 °C. Digested samples were then diluted 100 times and a 10 µL aliquot was deposited on freshly cleaved mica and dried under mild vacuum. Tapping mode AFM images were acquired in air using a Dimension 3000 SPM, equipped with a "G" scanning head (maximum scan size of 100 µm) and driven by a Nanoscope IIIa controller, and a Multimode SPM equipped with a "E" scanning head (maximum scan size of 10 µm) and driven by a Nanoscope V controller (Digital Instruments, Veeco). Single-beam uncoated silicon cantilevers (type OMCL-AC160TS, Olympus) were used. The drive frequency was between 260 and 330 kHz; the scan rate was 0.4-0.8 Hz. CR absorbance

CR absorbance

CR interaction with IBs was tested using a Jasco V-630 spectrophotometer (Tokyo, Japan) by recording the absorbance spectra from 400 nm to 700 nm using a 10 mm quartz cell. FL TDP-43 IBs, Ct TDP-43 IBs and control IBs at 1.0, 1.0 and 0.7 mg/mL concentrations, respectively, were incubated at 25 °C and an aliquot of 60 µL of each sample was mixed with 440 µL of a 5 mM NaH_2PO_4, 150 mM NaCl buffer at pH 7.4 containing 20 µM CR. Spectra were also recorded for similar samples devoid of CR and similar samples devoid of IBs. The difference spectrum obtained by subtracting the spectra of CR alone and IBs alone from that of CR plus IBs indicated the spectrum of CR bound to β-sheet structure. The CR spectra obtained for the native HypF-N protein are also reported as a further control.

Far-UV CD

FL TDP-43 IBs, Ct TDP-43 IBs and control IBs at 2.8, 2.8 and 2 mg/mL concentrations, respectively, were prepared in 25 mM NaH_2PO_4 buffer at pH 7.3, 25 °C. The far-UV circular dichroism (far-UV CD) spectra were collected over the 190-260 nm wavelength range at 25 °C using a Jasco J-810 Spectropolarimeter (Tokyo, Japan) equipped with a thermostated cell holder attached to a Thermo Haake C25P water bath (Karlsruhe, Germany). A 1 mm path-length cell was used. All spectra were blank subtracted. For the calculation of the molar ellipticity [θ] we used the following formula:

$$[\theta] = \frac{\theta}{\left(\frac{10 * N° residues * optical\ path * concentration}{molecular\ weight}\right)} \quad (1)$$

were [θ] is the molar ellipticity in deg cm^2dmol^{-1}, θ is the ellipticity in mdeg, optical path is in cm, concentration is in g/L, molecular weight is in g/mol.

Fourier transformed infrared spectroscopy (FTIR)

Purified IBs were resuspended in D_2O to achieve a final protein concentration of 21 mg/mL for FL TDP-43 IBs and Ct TDP-43 IBs and 15 mg/mL for control IBs. Each sample was deposited on a potassium bromide window in a semipermanent liquid cell using a spacer of 25 µm, and the Fourier transformed infrared spectroscopy (FTIR) spectrum was recorded at room temperature using a Jasco FTIR 4200 spectrophotometer (Tokyo, Japan). The system was constantly purged with N_2. The resulting spectra were background subtracted and baseline corrected.

PK proteolysis

FL TDP-43 IBs and control IBs were prepared in water at a final protein concentration of 14.3 mg/mL and 10 mg/mL, respectively, and digested with 250 µg/mL PK at 37 °C. The digestion was followed for 500 s observing the turbidity decrease at 350 nm using a Jasco V-630 spectrophotometer (Tokyo, Japan) and a 5 mm quartz cell. The digestion kinetics were analysed using a procedure of best fitting obtained with the following single exponential equation:

$$N(t) = k + (N_0 - k)e^{-\lambda t} \quad (2)$$

where *N(t)* is the turbidimetry at time *t*, *k* is the final value of the turbidimetry, N_0 is the initial turbidimetry, *t* is the time in *s*, λ is the rate constant in s^{-1}. The FL TDP-43 IBs and Ct TDP-43 IBs digestions were also followed by SDS-PAGE. The FL TDP-43 IBs sample at a total protein concentration of 14.3 mg/mL was treated at 37 °C with 250 µg/mL and 20 µg/mL PK, for a total time of 300 s, while the Ct TDP-43 IBs sample at the same concentration of FL TDP-43 was treated at 37 °C with 20 µg/mL PK, for a longer time (1200 s). Aliquots of both samples were taken at defined times and tested by SDS-PAGE using 12% (w/v) polyacrylamide gels. The progressive FL TDP-43 and Ct TDP-43 digestions were monitored observing the intensity changes of their corresponding bands.

Thermal Unfolding Experiments

Thermal unfolding measurements were carried out following the CD signal emitted by M-TTR at 216 nm using a Jasco J-810 spectropolarimeter (Tokyo, Japan) equipped with a thermostated cell holder attached to a Thermo Haake C25P water bath (Karlsruhe, Germany). Thermal unfolding was achieved by heating the protein sample from 25 to 80°C in a 1 mm path length quartz cell at a rate of 1 degree/minute. Sample was then kept at this temperature for 20 minutes and subsequently cooled down to 25°C at a rate of 1 degree/minute. Conditions were 29.1 µM M-TTR in phosphate buffer. The reversibility of the unfolding transitions was checked by measuring the CD signal at room temperature upon cooling down after the end of the transition. Each spectrum was recorded as the average of many scans, blank-subtracted and smoothed.

Dynamic Light Scattering (DLS) measurements

DLS measurements were performed using a Zetasizer Nano S device from Malvern Instruments (Malvern, Worcestershire, UK) thermostated with a Peltier system. Low-volume 12.5×4.5-mm disposable cells were used. Refractive index and viscosity of

phosphate buffer was calculated using the software provided with the instrument; a refractive index of 1.45 was used for M-TTR. Samples were prepared at a final protein concentration of 29.1 µM in phosphate buffer. Before the measurements, the protein sample was heated from 25 to 80°C, maintained at this temperature for 20 minutes and subsequently cooled to 25°C and filtered with an anotop filter having a cut-off of 20 nm. Protein concentration was 29.1 µM. The presented size distributions were the average of three consecutive measurements.

In another set of experiment HypF-N oligomers (12 µM monomer concentration) were incubated for 1 h at 37 °C under shaking in 20 mM potassium phosphate buffer at pH 7.0 in the absence or presence of each TTR. Samples containing TTRs were also used as controls and filtered using 20 nm anotop filters (Sigma-Aldrich, Milan, Italy). Size distributions by intensity and total light-scattering intensity were determined at regular time-intervals over a period of 10 minutes. The temperature was maintained at 37° C and the parameters were set manually on the instrument to allow the same settings in the various distributions acquired at different time-values. These included ten acquisitions each of ten seconds duration, with cell position 4.2 cm and attenuator index 7. The reported data are the average of three consecutive measurements.

Equilibrium unfolding experiments

Equilibrium denaturation studies were performed exploiting tryptophan fluorescence and CD in the near-UV and far-UV as probes. 28 to 34 samples were prepared containing M-TTR in phosphate buffer with urea at concentrations ranging from 0 to 7.6 M. Measurements were carried out at 37 °C. Resulting plots were analysed with the method provided by Santoro & Bolen [Santoro MM and Bolen DW 1988] in order to obtain quantitative measurements of the free energy change upon denaturation in the absence of denaturant the concentration of middle denaturation (Cm) and dependence of free energy change upon denaturation on urea concentration (m). In the case of fluorescence, spectra from 300 to 450 nm (excitation at 280 nm) were acquired for 28 equilibrated samples containing 2.9 µM M-TTR. A 10x2 mm quartz cuvette was used. Spectra were acquired using a PerkinElmer LS 55 (Waltham, Massachusetts). The ratio between the fluorescence intensity at 365 and 335 was used

to analyse the collected data as previously described [Jiang X et al. 2001]. CD spectra from 200 to 260 nm were also acquired for 34 equilibrated samples containing 29.1 µM M-TTR. Spectra were acquired using a Jasco J-810 spectropolarimeter (Tokyo, Japan) and a 1 mm path length cuvette. Mean residue ellipticity at 219 nm was calculated and plotted Vs urea concentration. CD spectra were also measured from 275 to 300 nm for 28 equilibrated samples containing 145.5 µM M-TTR. The Jasco J-810 spectropolarimeter was used with a 0.1 mm path length cuvette. Mean residue ellipticity at 290 nm was calculated and plotted versus urea concentration.

Stopped flow kinetics coupled to intrinsic fluorescence

Unfolding and refolding reactions were followed using a Bio-logic SFM-3 stopped-flow device equipped with an FC-15 cuvette and coupled to a fluorescence detection system (Claix, France). An excitation wavelength of 280 nm and a band-pass filter to monitor emitted fluorescence above 320 nm were used. All the experiments were performed in phosphate buffer at 37 °C, at final protein concentrations of 1.5-2.9 µM. For the unfolding experiments native M-TTR was diluted into solutions containing urea at final concentrations ranging from 3.5 to 6.5 M. Refolding reactions were initiated by a 10-fold dilution of the urea denatured protein into solutions containing low concentrations of urea. Final [urea] ranged from 0.2 M to 3.5 M. The dead time was generally 10.4 ms. In another set of experiments, the equilibrium signal measured at the end of unfolding kinetics was plotted Vs urea concentration so as to linearly extrapolate the fluorescence of the unfolded protein under native conditions.

T-jump experiments

Relaxation kinetics was measured as a function of urea concentration by using a Hi-Tech PTJ-64 capacitor-discharge T-jump apparatus (Hi-Tech). Temperature was rapidly changed from 28 °C to 37 °C. 10 to 20 individual traces were averaged at given denaturant concentrations. Protein concentration was typically 29.1 µM. The excitation wavelength was 280 nm, and the fluorescence emission was measured using a 320 nm cut-off glass filter.

Kinetic analysis

Unfolding and refolding traces were fitted to multi exponential functions to determine the rate constants of unfolding and of folding, together with their relative amplitudes. The fitting procedure was made using the general equation

$$y(t)=m\cdot t+q+\Sigma Aini=1exp(-\lambda i\cdot t) \quad (3)$$

where $y(t)$ is the fluorescence signal recorded as a function of time, t is the time, Ai and λi are the apparent amplitude and rate constant of the *i*th phase, respectively, q is the fluorescence value at equilibrium, m is the dependence of equilibrium fluorescence on time and *n* is the number of observed phases.

We then plotted the apparent rate constants of the major refolding phase (λ2) observed in stopped-flow kinetics together with the rate constants obtained from T-jump experiments (λ1). The logarithm of each rate constant was assumed to vary linearly with denaturant concentration. The observed chevron plots were fitted globally with shared m-values using three-state on-pathway and off-pathway models [Gianni S et al. 2007]. Data of λ1 were also analysed with a two state model [Jackson SE and Fersht AR 1991]. In the latter case refolding rate constants in the absence of denaturant was linearly extrapolated from unfolding kinetics at high urea concentration. Free energy change upon denaturation in the absence of denaturant ($\Delta G_{U-F}^{H_2O}$) was obtained from equilibrium unfolding. The global fit was obtained with Prism software (Graphpad). Values obtained from this analysis were then used to run numerical simulations of the refolding process with the COPASI software and to calculate the equilibrium concentrations of each species.

Stopped-flow CD

Folding of M-TTR was also monitored by far-UV CD at 219 nm using a Bio-Logic SFM-20 stopped-flow device coupled to the Jasco J-810 CD detection system described previously. Final conditions were 0.585 M urea in the phosphate buffer at 37 °C, at a protein concentration of 14.5 µM. The dead time of the experiment was 19 ms. The signal of the buffered solution with no protein was subtracted from the averaged

trace. In the same experiment, the CD signal of the unfolded protein was measured at different urea concentrations in order to extrapolate the signal of the unfolded protein under native conditions.

Stopped-flow ANS

Kinetic measurements were performed in the presence of ANS using the Bio-logic SFM-3 stopped-flow device. An excitation wavelength of 370 nm and a band-pass filter to monitor emitted fluorescence above 475 nm were used. All the experiments were performed in phosphate buffer with 100 µM ANS, 0.5 M urea, pH 7.4, 37 °C, at final protein concentrations of 2.91 µM.

Double jump experiments

Two sets of double jump experiments were employed. Interrupted refolding experiments were carried out on an Applied Photophysics DX-17MV stopped-flow instrument with double jumpfacility (Leatherhead, UK) in order to assess the time dependence of accumulation of the native state. Refolding (first jump) and unfolding (second jump) were initiated by a symmetric mixing of the denatured and native protein with the appropriate buffer. In the first jump 16 µM M-TTR denatured in 3 M urea with 2 mM DTT at pH 3.2 was diluted into a phosphate buffer at pH 7.4 to a final urea concentration of 5 M. After a given delay time, the solution obtained at the end of the first jump was diluted 1:1 into another solution containing 8.5 M urea to achieve denaturation. Final conditions were 4 µM M-TTR in phosphate buffer pH 7.4 with 5 M urea. Delay time ranged from 12 to 350 ms. Excitation wavelength was 280 nm and the fluorescence emission was measured using a 320 nm cut-off glass filter.
Interrupted unfolding experiments were performed with the Bio-logic SFM-3 stopped-flow to assess the occurrence of X-Pro peptide bonds isomerism during refolding. In the first jump M-TTR in 1 M urea was diluted 1:4 into a buffer containing 6 M urea to a final urea concentration of 5 M. After the delay time, the solution was diluted 1:4 into phosphate buffer. Final conditions were 2.2 µM M-TTR in phosphate buffer pH 7.4 with 1 M urea. Delay time ranged from 44 ms to 30 s.

Folding in the Presence of CypA

Folding of M-TTR was studied in the presence of human and bovine CypA on the Bio-Logic SFM-3 stopped-flow apparatus by monitoring intrinsic fluorescence emission above 320 nm with excitation wavelength of 280 nm. Folding was initiated at 37 °C by mixing 21.8 μM TTR denatured in 5 M urea into a refolding buffer containing phosphate buffer and 0.5 M urea, pH 7.4 and CypA concentrations ranging from 0 to 0.67 μM. Obtained traces were fitted to equation (3).

Statistical analysis

All data are expressed as mean ± standard deviation (SD). Comparisons between the different groups were performed by ANOVA followed by Bonferroni's t-test. A p value less than 0.05 was accepted as statistically significant.

Chapter 3- Results

Results I: Extracellular chaperones prevent $A\beta_{42}$-induced toxicity in rat brains

Alzheimer's disease (AD) is a progressive neurodegenerative disorder characterised by cognitive decline, formation of the extracellular amyloid β ($A\beta_{42}$) plaques, neuronal and synapse loss, and activated microglia and astrocytes. Extracellular chaperones, which are known to inhibit amyloid fibril formation and promote clearance of misfolded aggregates, have recently been shown to reduce efficiently the toxicity of HypF-N misfolded oligomers to immortalized cell lines, by binding and clustering them into large species. However, the role of extracellular chaperones on Aβ oligomer toxicity remains unclear, with reports often appearing contradictory. In this study we microinjected into the hippocampus of rat brains $A\beta_{42}$ oligomers pre-incubated for 1 h with two extracellular chaperones, namely clusterin and α_2-macroglobulin. The chaperones were found to prevent $A\beta_{42}$-induced learning and memory impairments, as assessed by the Morris Water Maze test, and reduce $A\beta_{42}$-induced glia inflammation and neuronal degeneration in rat brains, as probed by fluorescent immunohistochemical analyses. Moreover, the chaperones were able to prevent $A\beta_{42}$ colocalization with PSD-95 at post-synaptic terminals of rat primary neurons, suppressing oligomer cytotoxicity. All such effects were not effective by adding pre-formed oligomers and chaperones without preincubation. Molecular chaperones have therefore the potential to prevent the early symptoms of AD, not just by inhibiting $A\beta_{42}$ aggregation, as previously demonstrated, but also by suppressing the toxicity of $A\beta_{42}$ oligomers after they are formed. These findings elect them as novel neuroprotectors against amyloid-induced injury and excellent candidates for the design of therapeutic strategies against AD.

Chaperones prevented learning and memory impairment in intra-hippocampus $A\beta_{42}$ injected rats

$A\beta_{42}$ oligomers were incubated for 1 h in F-12 medium in the absence or presence of two types of extracellular chaperones, namely clusterin (Clu) and α_2-macroglobulin (α_2M). 1.5 µl aliquots (0.7 µg $A\beta_{42}$ with. 1 µg Clu or α_2M) were microinjected into the right hippocampus of rat brains. Seven days after unilateral injection into the hippocampus, rats were trained for four days in the Morris water maze (MWM) to learn where the hidden platform was located. The ability of rats to acquire, process, and recall spatial information was assessed by evaluation of the time required to find the platform (escape latency), time in quadrant where the platform is located (target quadrant), time in the opposite quadrant, time in the small area where the platform is located (platform section) and number of crossings over the platform section. The animals were naive to the water maze and showed no deficiencies in swimming abilities, directional swimming toward the platform, or climbing onto a hidden platform during training trials. Rats injected only with F12-medium shortened the escape latency during the 4-days training phase (Fig. 6A). They were good swimmers and responded to being placed in water with an appropriate swim-search response. Conversely, $A\beta_{42}$ oligomer-injected rats showed only a slow decrease in escape latency during the 4 days of training (Fig. 6A). When we pre-incubated $A\beta_{42}$ oligomers with Clu or α_2M for 1 h and then injected these solutions intra hippocampus, we obtained a significant decrease ($p<0.05$) in escape latency, compared with the $A\beta_{42}$ oligomer-administered group, particularly at day 3 and 4 (Fig. 6A). Five h after the last test on day 4 it was found that rats treated with $A\beta_{42}$ oligomers pre-incubated with Clu or α_2M for 1 h spent a significantly higher percentage of time in the target quadrant ($p<0.05$), with respect the animals treated with only $A\beta_{42}$ oligomers (Fig. 6B, top left). We also observed a marked reduction of the percentage of time spent in the opposite quadrant ($P<0.05$) in rats treated with $A\beta_{42}$ oligomers plus Clu or α_2M, compared to $A\beta_{42}$ oligomer-injected rats (Fig. 6B top right). The percentage of time spent in the adjacent quadrants and the swim speed in target quadrant during this session was comparable among the groups (data not shown), indicating that the motility of rats injected with the different samples was not impaired. The analysis of the percentage of time in the

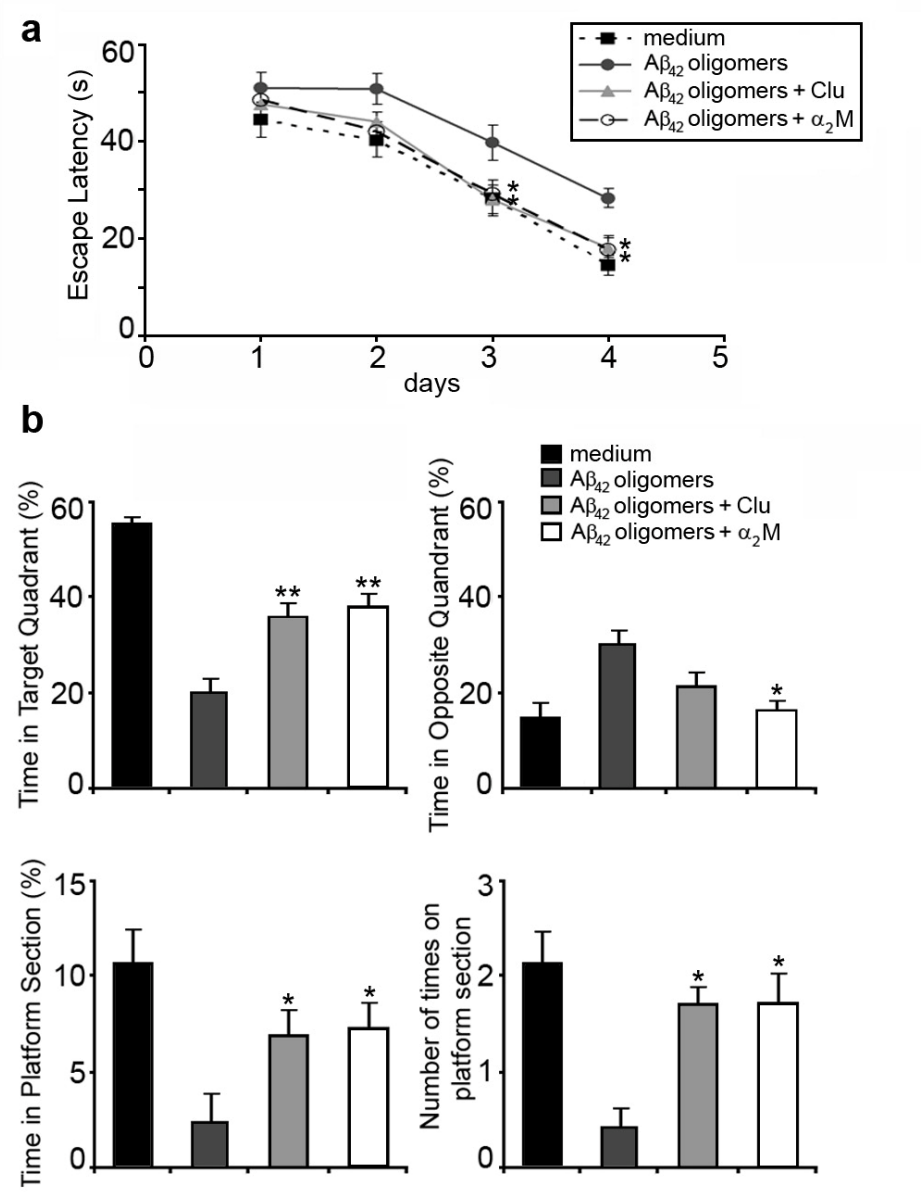

Fig. 6 Effect of hippocampal injection of $A\beta_{42}$ oligomers pre-incubated with two extracellular chaperones (Clu and α_2M) on MWM performance of rats. Rats were injected with 1.5 µl of 0.45 mg/ml $A\beta_{42}$ oligomers in the absence or presence of 0.7 mg/ml chaperones (protein:Clu molar ratio was 10:1; protein:α_2M molar ratio was 100:1). Control rats were injected with 1.5 µl of medium. **(A)** Time lengths employed to find the platform during the training session (escape latencies) are reported as mean ± SEM. Each point represents the mean daily value of four trials of each experimental group (n=6 per group). **(B)** Percentage of time in the target and opposite quadrants (top panels), percentage of time in the platform section and number of crossings over the platform position (bottom panels) measured for 30 s on day 4. Data are expressed as mean ± SEM. (n=6 per group). The asterisks and the double asterisks indicate significant differences ($p \leq 0.05$ and $p \leq 0.01$, respectively) versus $A\beta_{42}$-injected rats.

platform section showed a significant increase in rats treated with $A\beta_{42}$ oligomers plus chaperones, with respect to the $A\beta_{42}$ oligomer-treated group (Fig. 6B, bottom left). Finally, the number of crossings over the platform position revealed a significant increase in rats injected with $A\beta_{42}$ oligomers plus chaperones, compared to the $A\beta_{42}$ oligomer-administered group (Fig 6B, bottom right). Taken together, these data demonstrated that both types of extracellular chaperones have the ability to prevent the learning and memory impairment mediated by the intra hippocampus injection of $A\beta_{42}$ oligomers.

Chaperones reduced glial reaction in Aβ42 exposed rat hippocampus

We then investigated whether chaperones could neutralise $A\beta_{42}$-mediated glial inflammation, by evaluating glial fibrillary acidic protein (GFAP)-immunoreactive astrocytes and Iba 1-labelled microglial cells. Immunofluorescence analyses revealed diminished glial reaction in rats treated with $A\beta_{42}$ oligomers and chaperones compared to rats treated with $A\beta_{42}$ oligomers only (Fig. 7). Such a decrease was evident by monitoring both GFAP-immunoreactive astrocytes (Fig. 7A) and Iba 1-labelled microglial cells (Fig. 7B). Hypertrophic astrocytes with long, thick branches were detected by GFAP immunostaining in $A\beta_{42}$-injected rats (Fig. 7A). In contrast, in rats treated with $A\beta_{42}$ and chaperones, astrocyte activation occurred to a much lesser extent (Fig. 7A). Labeling with anti-Iba-1 antibodies revealed microglia with small cell bodies and thin, elongated processes in rats treated with $A\beta_{42}$ plus Clu or α_2M, compared to $A\beta_{42}$-injected rats, where microglia with enlarged cell bodies and short, thickened processes were found (Fig. 7B). This data therefore suggests that these two extracellular chaperones can protect against the $A\beta_{42}$ oligomer-mediated glial inflammation.

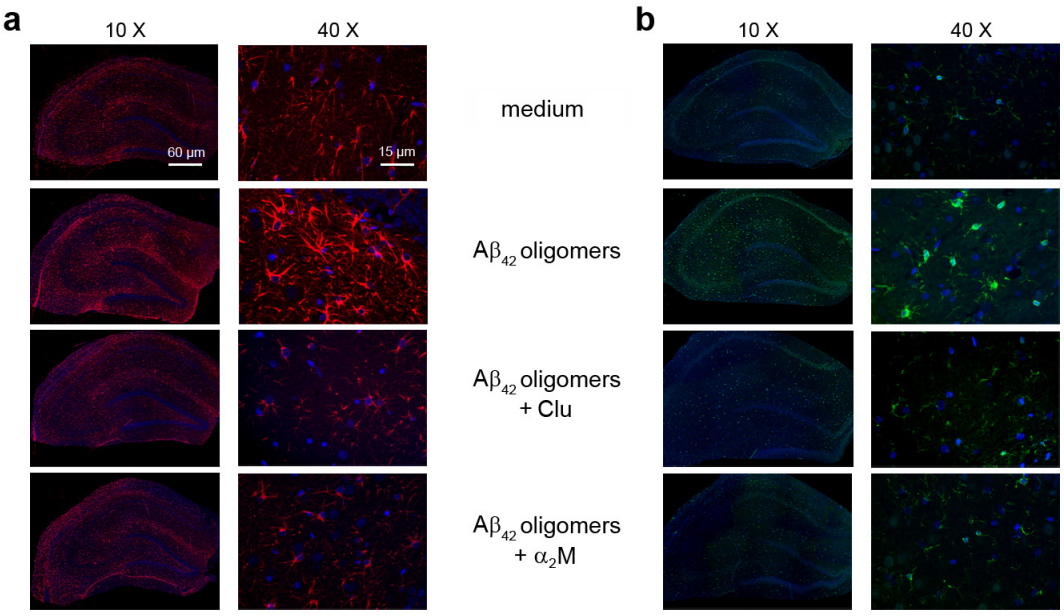

Fig. 7 Analyses of glial activation in the hippocampus of 3-month-old male Wistar rats treated with $A\beta_{42}$ oligomers pre-incubated with extracellular chaperones. Representative photomicrographs (10 x and 40 x magnifications) of fluorescence immunohistochemical analyses of GFAP immunoreactivity **(A)** and Iba-1-labeled microglial cells **(B)** obtained 14 d after injection of 1.5 µl medium, or 1.5 µl of 0.45 mg/ml $A\beta_{42}$ oligomers in the absence or presence of 0.7 mg/ml chaperones (protein:chaperone molar ratios as described in the Materials and Methods section). GFAP immunoreactivity and Iba-1-labeling are indicated by red and green colours, respectively.

Chaperones prevented neuronal degeneration in Aβ42 exposed rat hippocampus

In AD, the aggregated species of Aβ peptides interact with the plasma membrane of the affected cells, triggering a free radical-mediated injury that ultimately results in cell degeneration [Varadarajan S et al. 2000]. The survival of neurons after treatment with $A\beta_{42}$ oligomers plus Clu or α_2M was examined by using the Neu-N marker. The group injected with $A\beta_{42}$ oligomers showed a decreased number of mature neurons compared to the medium-administered group (Fig. 8A). Conversely, rats treated with $A\beta_{42}$ oligomers preincubated for 1h with Clu or α_2M showed a high improvement in neuron survival, suggesting that chaperones can prevent $A\beta_{42}$-mediated neurodegeneration.

We next evaluated the protective role of the two extracellular chaperones against $A\beta_{42}$-induced lipid peroxidation, determined by measuring 8-OH isoprostane levels. The results showed that 8-OH isoprostane levels were significantly higher in the

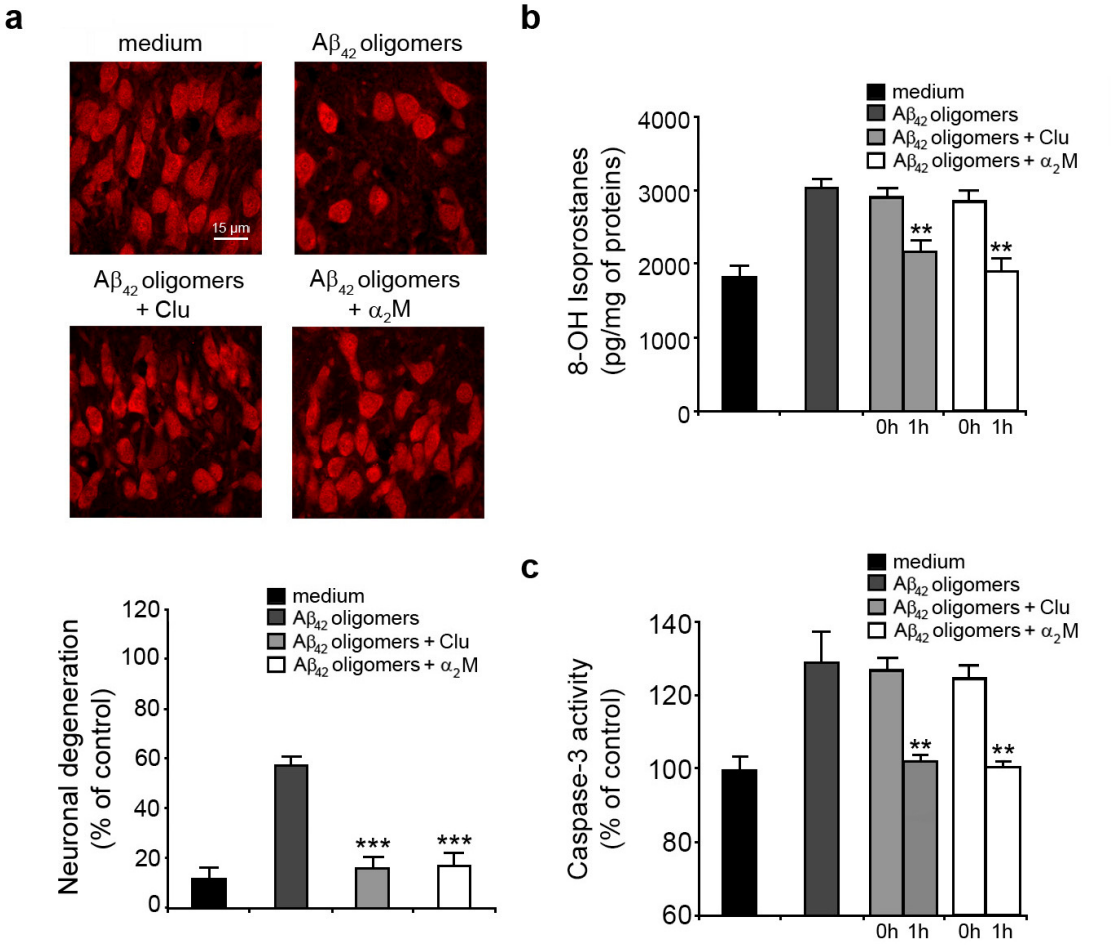

Fig. 8 Analyses of neuronal degeneration, lipid peroxidation and apoptosis in the hippocampus of 3-month-old male Wistar rats treated with $A\beta_{42}$ oligomers pre-incubated with extracellular chaperones. **(A)** Representative photomicrographs (40 x magnifications) of fluorescence immunohistochemical analysis of Neu-N obtained 14 d after injection of 1.5 µl medium, or 1.5 µl of 0.45 mg/ml $A\beta_{42}$ oligomers in the absence or presence of 0.7 mg/ml chaperones (protein:chaperone molar ratio as described in the Materials and Methods section). The quantification of Neu-N immunoreactivity in the hippocampus after the injections are shown below the images. **(B)** 8-OH isoprostane levels, a correlate of lipid peroxidation, in rat hippocampal homogenates (5 µg of proteins per well) at the indicated time lengths of pre-incubation between $A\beta_{42}$ oligomers and chaperones. (**C**) Caspase-3 levels assessed by a fluorimetric assay using the Ac-DEVD-AFC probe, at the indicated time lengths of pre-incubation between $A\beta_{42}$ oligomers and chaperones. The reported values (means ± SD) are representative of three independent experiments carried out in triplicate for each experimental group (n=6 per group). The double and the triple asterisks indicate significant differences ($p \leq 0.01$ and $p \leq 0.001$, respectively) versus $A\beta_{42}$-injected rats.

hippocampal homogenates of rats treated with $A\beta_{42}$ oligomers, compared to the medium-injected groups (Fig. 8B), suggesting an oxidative-stressed condition associated with $A\beta_{42}$ oligomer exposure. 8-OH isoprostane levels were also high after injection of $A\beta_{42}$ oligomers with Clu or α_2M in the absence of pre-incubation (Fig. 8B). In contrast, the hippocampi of rats treated with $A\beta_{42}$ oligomers and either chaperone in the presence of preincubation for 1 h before injection showed no difference in the lipid peroxidation levels with respect to medium-injected rats (Fig. 8B).

We then analyzed whether the two chaperones can prevent the $A\beta_{42}$-induced cell death, by measuring the activity of caspase-3, a well-recognised apoptotic marker, in rat hippocampal homogenates [Donati C et al. 2007]. Caspase-3 activation was significantly increased in the hippocampal homogenates of rats injected with $A\beta_{42}$ oligomers, with respect to the rats injected only with F12-medium (Fig. 8C), indicating apoptotic cell death associated with $A\beta_{42}$ oligomer treatment. Caspase-3 activation was also increased in the hippocampal homogenates of rats injected with $A\beta_{42}$ oligomers plus Clu or α_2M in the absence of pre-incubation (Fig. 8C). On the other hand, the level of caspase-3 activation in hippocampi of rats treated with $A\beta_{42}$ oligomers pre-incubated with chaperones for 1 h was not significantly different to that of rats injected only with F12-medium (Fig. 8C).

These results suggest that the pre-incubation of $A\beta_{42}$ oligomers with chaperones prevents the oxidative-stress conditions associated with $A\beta_{42}$ oligomer exposure, avoiding the induction of apoptosis by the oligomers.

Chaperones suppress $A\beta_{42}$ oligomer-induced cytotoxicity in rat hippocampal and cortical neurons

To assess the protective role of the two extracellular chaperones against $A\beta_{42}$ oligomers, we also used cultures of hippocampal and cortical neurons extracted from embryonic day (ED)-17 rats and analyzed in their mature form at day 21. In a first set of experiments we incubated preformed oligomers of $A\beta_{42}$ in the cell culture medium in the absence or presence of Clu or α_2M for different time lengths, and then added the resulting mixture to the extracellular medium of cultured primary hippocampal neurons. $A\beta_{42}$ oligomers showed their toxic action (Fig. 9A), whereas the neurons

treated with oligomers pre-incubated with Clu or α_2M were found to reduce MTT to levels similar to medium-administered cells (Fig. 9A) and to cells treated with native

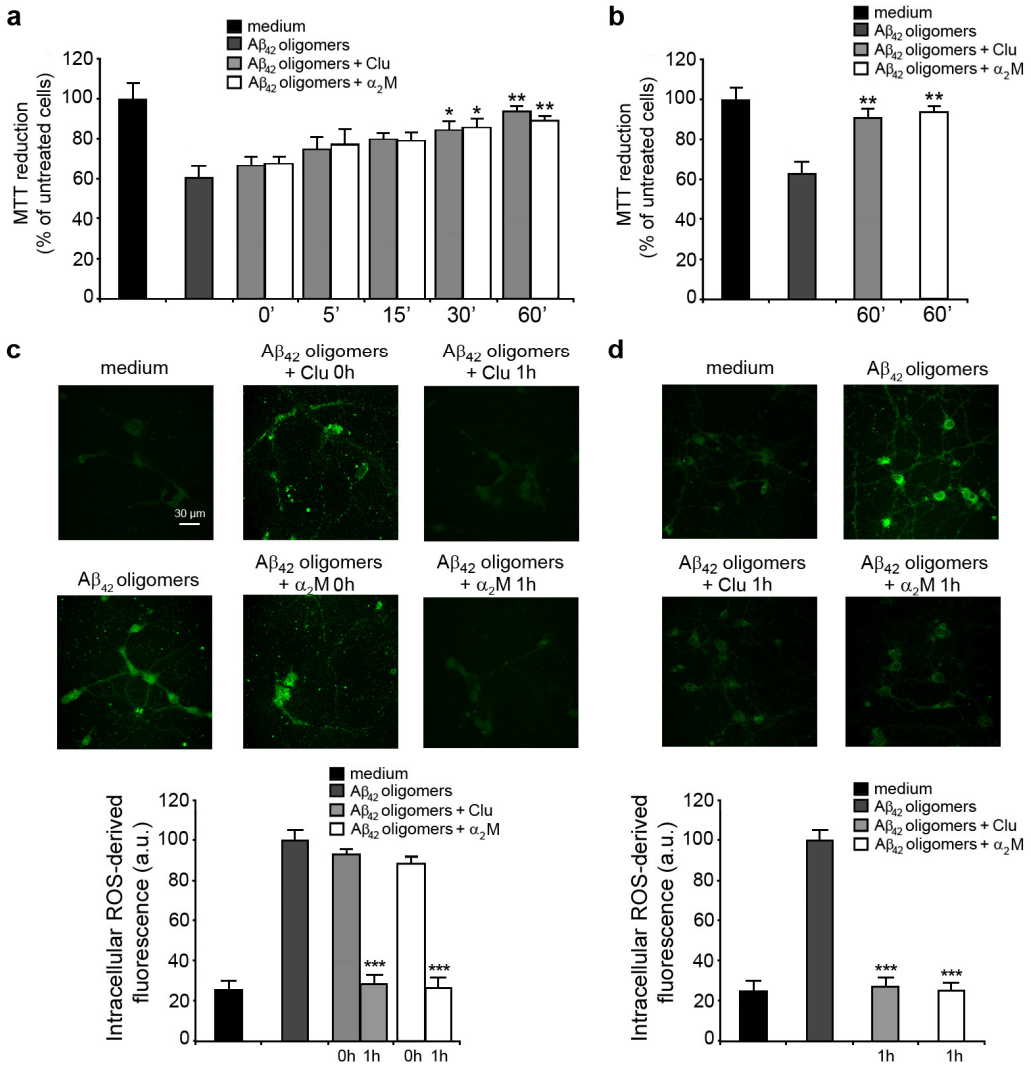

Fig. 9 Suppression of $A\beta_{42}$ oligomer toxicity by chaperones in rat primary neurons. Preformed $A\beta_{42}$ oligomers were incubated in the absence or presence of the indicated chaperones ($A\beta_{42}$:chaperone molar ratios as described in the Materials and Methods section) for the indicated time lengths **(A)** and for 1 h **(B)** and then added to the extracellular medium of hippocampal **(A)** or cortical **(B)** neurons for 24 h. **(C,D)** Representative confocal scanning microscope images showing intracellular ROS levels in primary hippocampal **(C)** and cortical **(D)** neurons from rat brains. Preformed $A\beta_{42}$ oligomers were incubated in the absence or presence of the indicated chaperones (protein:chaperone molar ratio as described in the Materials and Methods section) for the indicated time lengths and then added to the extracellular medium of hippocampal **(C)** or cortical **(D)** neurons for 1 h. The green fluorescence arises from the CM-H_2DCFDA probe that has reacted with ROS. The corresponding semi-quantitative values of the green fluorescence signal are shown below the confocal images. In all histograms, the values reported are means ± SD of three independent experiments carried out in triplicate. The single, double and triple asterisks indicate significant differences ($p \leq 0.05$, $p \leq 0.01$ and $p \leq 0.001$, respectively) versus neurons treated with $A\beta_{42}$ oligomers.

$A\beta_{42}$ (data not shown), with an effect dependent on the time of preincubation of the oligomers with the chaperones. Similar data was obtained by pre-incubating $A\beta_{42}$ oligomers plus chaperones for 1 h in cultured primary cortical neurons (Fig. 9B). Comparable results were achieved with preformed oligomers of the N-terminal domain of the HypF protein from Escherichia coli (HypF-N) (Fig. 10A and B). HypF-N is a valuable model system for investigating the structural basis of the cellular dysfunction caused by misfolded protein oligomers, because this protein have the same morphological and tinctorial features as those formed by disease-related peptides and proteins [Campioni S et al. 2010].

Then we compared the ability of the two extracellular chaperones to suppress the intracellular ROS production and Ca^{2+} dyshomeostasis induced by $A\beta_{42}$ oligomers. $A\beta_{42}$ oligomers induced a sharp increase in ROS (Fig. 9C,D) and cytosolic free Ca^{2+} (Fig. 11) in rat neurons, which was inhibited by Clu and α_2M (Fig. 9C and D and Fig. 11). Such inhibitory effects were not found when the oligomers and the chaperones were added to the rat neurons in the absence of pre-incubation (Fig. 9C and Fig. 11A), suggesting the importance of the pre-incubation time. Comparable results were obtained with HypF-N oligomers (Fig. 10C and D and Suppl. Fig. 8).

These results therefore indicate that pre-incubation of $A\beta_{42}$ oligomers with the two chaperones can suppress or decrease markedly the oxidative stress, calcium dishomeostasis and toxicity caused by $A\beta_{42}$.

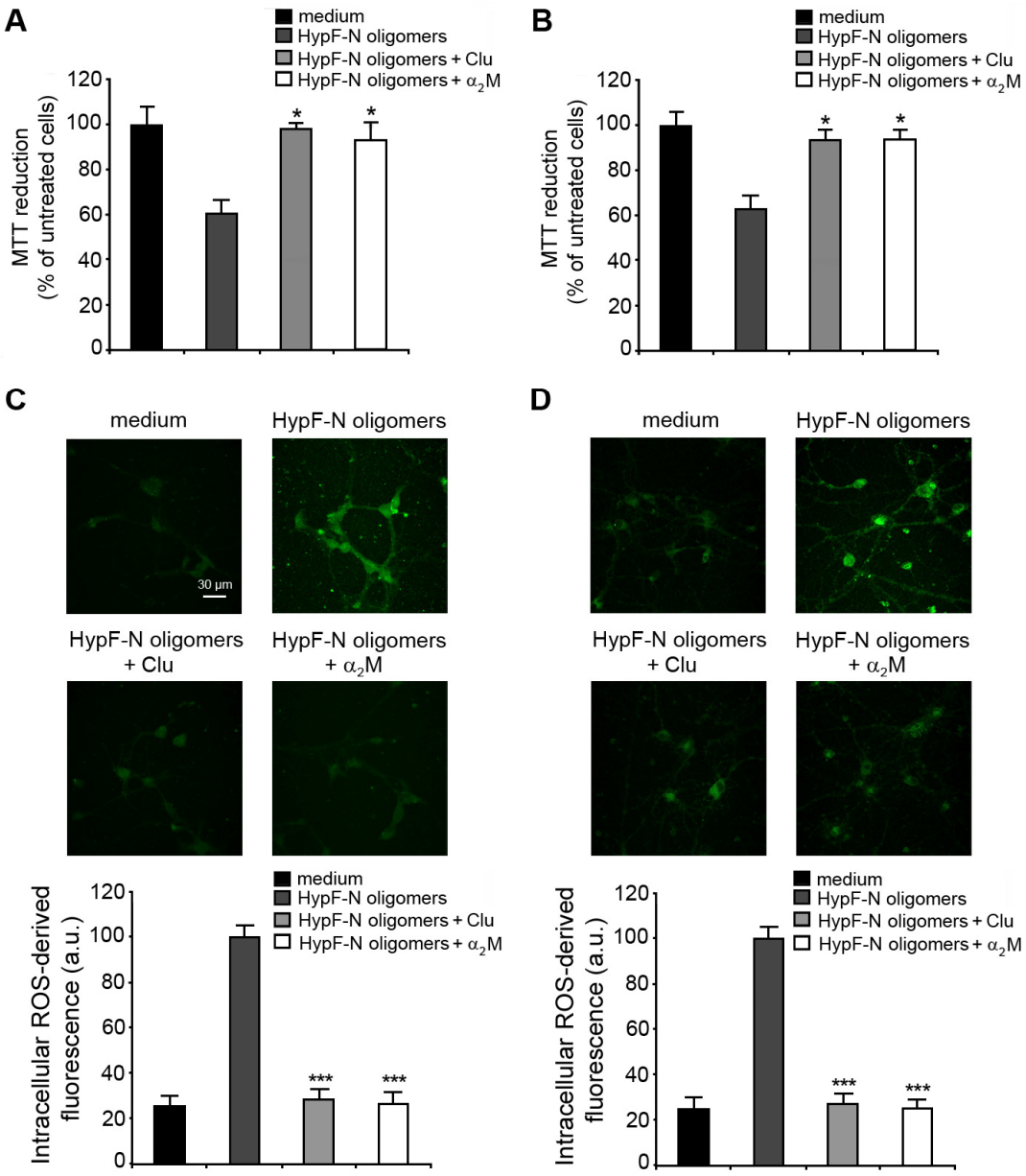

Figure. 10. Suppression of HypF-N oligomer toxicity by chaperones in rat primary neurons. Preformed HypF-N oligomers were incubated for 1 h in the absence or presence of the indicated chaperones (protein:chaperone molar ratio as described above) and then added to the extracellular medium of hippocampal **(A)** or cortical **(B)** neurons for 24 h. Cell viability was expressed as percent of MTT reduction in treated cells with respect to medium-administered cells (taken as 100%). (**C,D**) Representative confocal scanning microscope images showing intracellular ROS levels in primary hippocampal (**C**) and cortical (**D**) neurons from rat brains. Preformed HypF-N oligomers were incubated in the absence or presence of the indicated chaperones (protein:chaperone molar ratio as described above) and then added to the extracellular medium of the neurons for 1 h. The green fluorescence arises from the CM-H_2DCFDA probe that has reacted with ROS. The corresponding semi-quantitative values of the green fluorescence signal are shown below the confocal images. The values reported are means ± SD of three independent experiments carried out in triplicate. The asterisk and the triple asterisks indicate significant differences ($p \leq 0.05$ and $p \leq 0.001$, respectively) *vs* neurons treated with HypF-N oligomers.

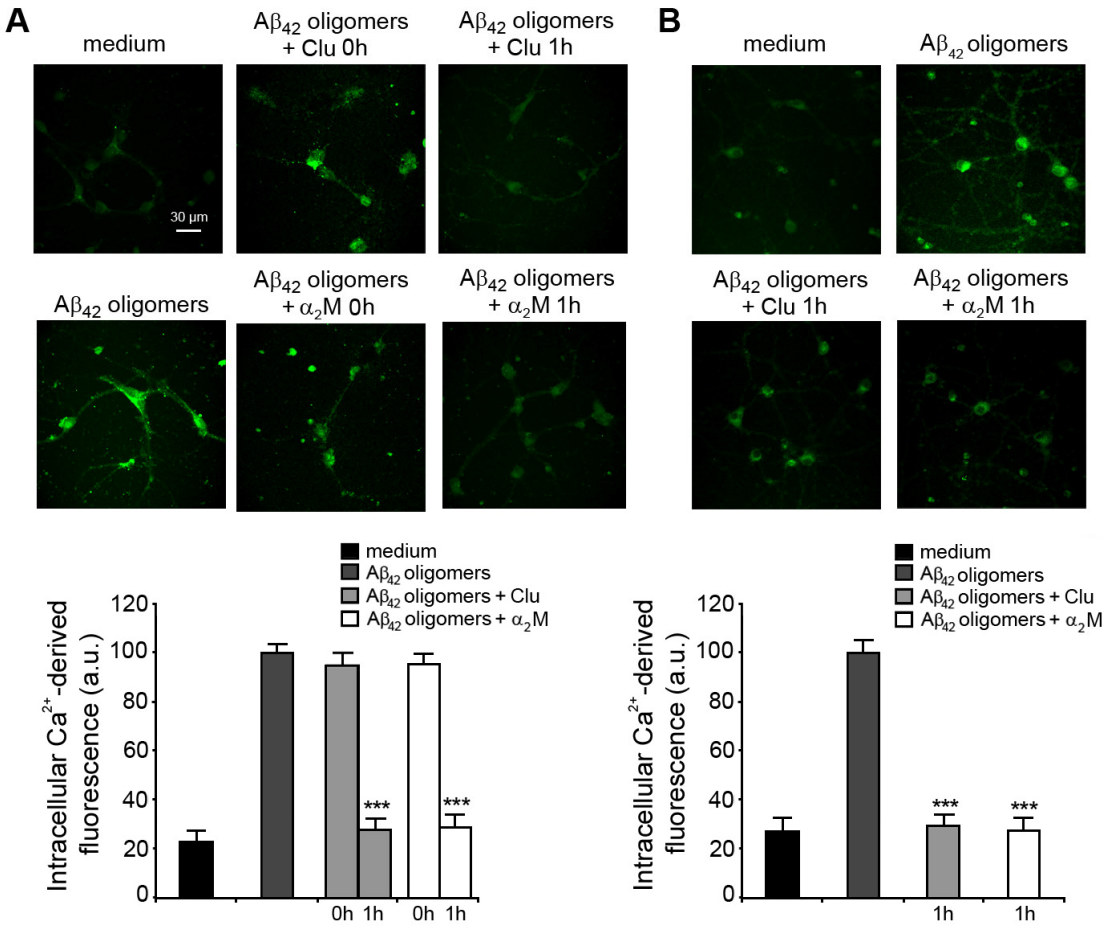

Figure. 11. Representative confocal scanning microscope images showing intracellular Ca^{2+} levels in primary hippocampal **(A)** and cortical **(B)** neurons from rat brains. **(A)** Preformed $A\beta_{42}$ oligomers were incubated in the absence or presence of the indicated chaperones (protein:chaperone molar ratio as described in the Materials and Methods section) for the indicated time lenghts and then added to the extracellular medium of the hippocampal neurons for 1 h. (**B**) Preformed $A\beta_{42}$ oligomers were incubated in the absence or presence of the indicated chaperones (protein:chaperone molar ratio as described in the Materials and Methods section) for 1 h and then added to the extracellular medium of cortical neurons for 1 h. In all images the green fluorescence arises from the intracellular Fluo3 probe bound to Ca^{2+}. The corresponding semi-quantitative values of the green fluorescence signal are shown below the confocal images. The values reported are means ± SD of three independent experiments. The triple asterisks indicate significant differences ($p \leq 0.001$) *vs* neurons treated with $A\beta_{42}$ oligomers.

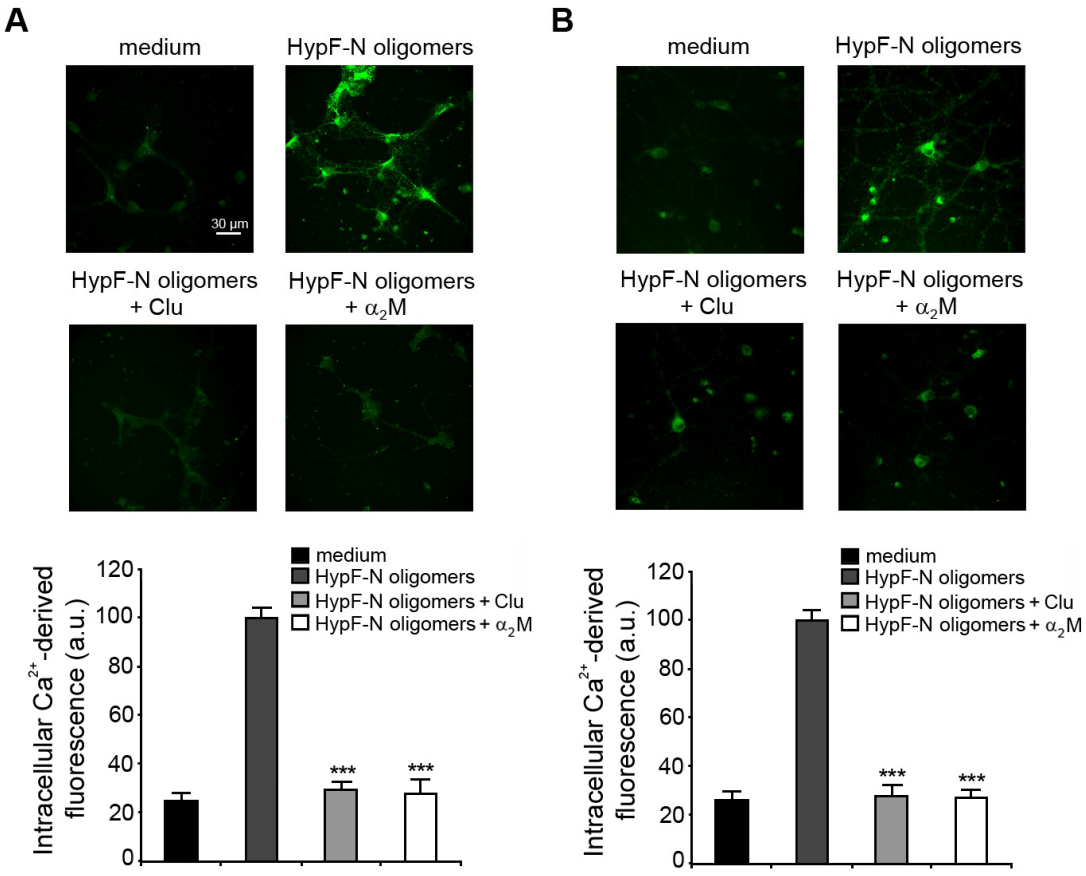

Figure. 12. Representative confocal scanning microscope images showing intracellular Ca^{2+} levels in primary hippocampal (A) and cortical (B) neurons from rat brains. Preformed HypF-N oligomers were incubated in the absence or presence of the indicated chaperones (protein:chaperone molar ratio as described above) and then added to the extracellular medium of the neurons for 1 h. In all images the green fluorescence arises from the intracellular Fluo3 probe bound to Ca^{2+}. The corresponding semi-quantitative values of the green fluorescence signal are shown below the confocal images. The values reported are means ± SD of three independent experiments. The triple asterisk indicates significant differences ($p \leq 0.001$) *vs* neurons treated with HypF-N oligomers.

Chaperones inhibit colocalization of $A\beta_{42}$ aggregates with PSD-95 preventing synaptic dysfunction

We next investigated by confocal microscopy whether chaperones prevent the colocalization of $A\beta_{42}$ aggregates with PSD-95. The scatter plots of fluorescence signals over the highlighted areas are shown in Fig. 13. A notable degree of colocalization between $A\beta_{42}$ oligomers and PSD-95 was observed in neurons treated for 1 h with $A\beta_{42}$ oligomers, with respect to medium-administered neurons (Fig. 13).

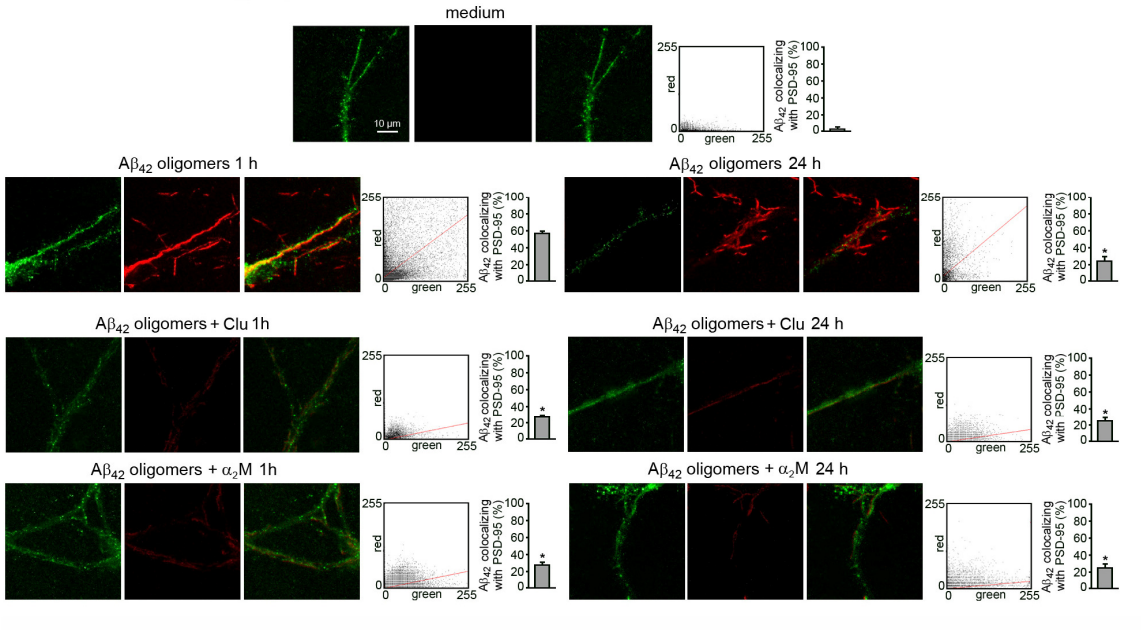

Fig. 13 Representative confocal scanning microscope images showing $A\beta_{42}$ oligomers colocalizing with post synaptic densities in rat primary hippocampal neurons. Preformed $A\beta_{42}$ oligomers were incubated in the absence or presence of the indicated chaperones (protein:chaperone molar ratios as described in the Materials and Methods section) for 1 h and then added to the extracellular medium of rat neurons for 1 h or 24 h, as indicated. $A\beta_{42}$ aggregates and PSD-95 were monitored using mouse monoclonal 6E10 antibody and rabbit polyclonal anti-PSD-95 antibody, respectively, and then with Alexa Fluor 488- and Alexa Fluor 594-conjugated antibody (red and green fluorescence, respectively). The first line showed medium-administered neurons; the second line shows neurons treated for 1 h (left) or 24 h (right) with $A\beta_{42}$ oligomers (12 µM monomer concentration); the third and fourth lines shows neurons treated for 1 h (left) or 24 h (right) with Aβ42 oligomers plus Clu (third line) or α_2M (fourth line). The cytofluorograms of dendrite sections show the red fluorescence intensity (as pixel intensity, y axis) versus green fluorescence intensity (x axis). For each sample, 18 cytofluorograms were analyzed, each considering one dendrite section. The histograms show the percentage of colocalization on regions of interest (12–13 cells) using the ImageJ (NIH, Bethesda, MD, USA) and JACOP plugin (rsb.info.nih.gov) softwares. Data are expressed as mean ± S.D. (n=18 per group). The asterisks indicate significant differences ($p \leq 0.05$) with respect to neurons treated for 1 h with $A\beta_{42}$ oligomers.

Conversely, when we treated the neurons for 1 h with $A\beta_{42}$ oligomers pre-incubated with either Clu or α_2M, the chaperones were found to inhibit oligomer binding to the cell membrane thus preventing the colocalization with PSD-95 (Fig. 13, 18 dendrite sections were analyzed for each samples).

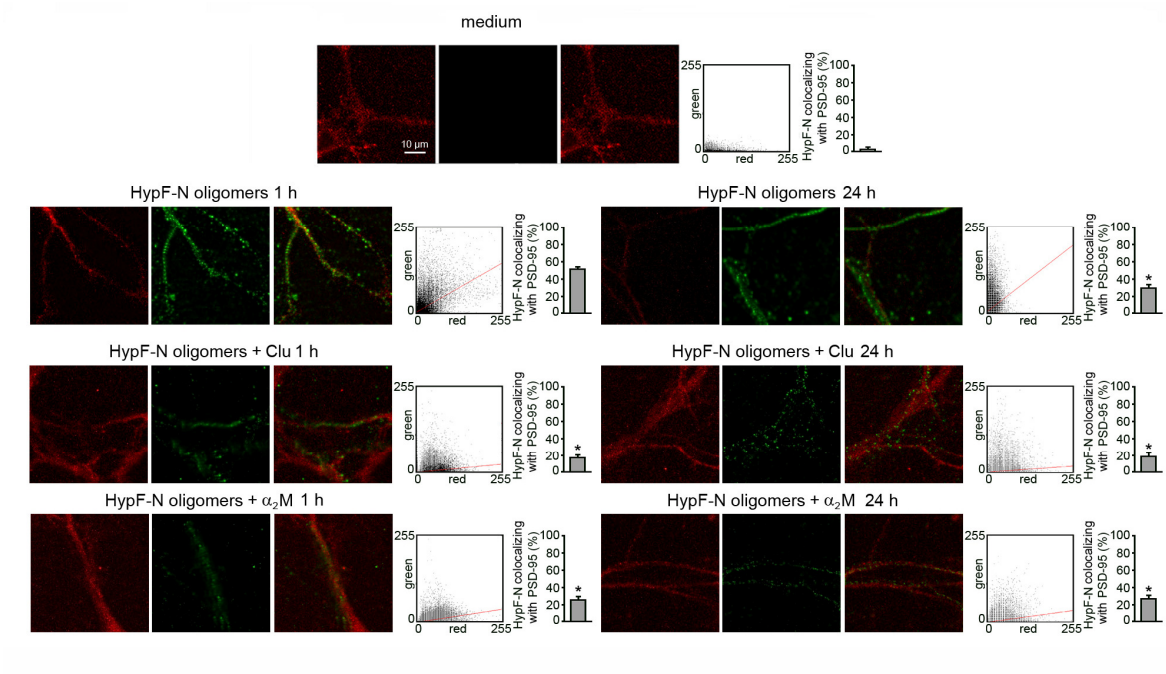

Figure. 14. Representative confocal scanning microscope images showing HypF-N oligomers colocalising with post synaptic densities in rat primary hippocampal neurons. Preformed HypF-N oligomers were incubated in the absence or presence of the indicated chaperones (protein:chaperone molar ratio as described above) for 1 h and then added to the extracellular medium of rat neurons for 1 h or 24 h, as indicated. HypF-N aggregates and PSD-95 was monitored using 1:200 diluted rabbit polyclonal anti-HypF-N antibody and 1:500 mouse monoclonal anti-psd-95 antibody, respectively, and then with Alexa Fluor 488- and Alexa Fluor 594-conjugated antibody (green and red fluorescence, respectively). The first line showed medium-administered neurons, the second line shows neurons treated for 1 h (left) or 24 h (right) with HypF-N oligomers (12 µM monomer concentration) the third and fourth lines shows neurons treated for 1 h (left) or 24 h (right) with HypF-N oligomers plus Clu (third line) or α_2M (fourth line). The cytofluorograms of dendrite sections show the green fluorescence intensity (as pixel intensity, y axis) vs red fluorescence intensity (x axis). For each samples, 18 cytofluorograms were analysed, each considering one dendrite section. The histograms show the percentage of colocalisation. Data are expressed as mean ± S.D. (n=18 per group). The asterisk indicates significant differences ($p \leq 0.05$) with respect to neurons treated for 1 h with HypF-N oligomers.

The fraction of $A\beta_{42}$ puncta colocalizing with PSD-95 puncta was 1.2 ± 0.5% for medium-administered neurons, 59.9 ± 2.0% for neurons treated for 1 h with $A\beta_{42}$ oligomers, 26.3 ± 1.8% for neurons treated for 1 h with $A\beta_{42}$ oligomers plus Clu, 26.9 ± 1.9% for neurons treated for 1 h with $A\beta_{42}$ oligomers plus α_2M. Similar data was achieved analyzing the colocalization between HypF-N oligomers and PSD-95 (Fig. 14). The concentration of PSD-95 has been found to be significantly lower in the brain of AD patients with respect to normal brains [Lovell MA et al. 2006]. Thus, we evaluated whether the prolonged treatment of rat hippocampal neurons with $A\beta_{42}$ oligomers decrease PSD-95 levels. When we treated the neurons with $A\beta_{42}$ oligomers for 24 h, we observed a lower degree of colocalization with PSD-95 caused by a decreased expression of PSD-95 (Fig. 13). In particular, in neurons treated for 24 h with $A\beta_{42}$ oligomers the fraction of $A\beta_{42}$ puncta colocalizing with PSD-95 puncta (29.3 ± 2.8%) was comparable to that observed in neurons treated for 24 h with $A\beta_{42}$ oligomers plus Clu or α_2M (24.6 ± 1.9% or 24.5 ± 1.7%, respectively). Similar data was achieved analyzing the colocalization between HypF-N oligomers and PSD-95 (Fig.14).

These results show that $A\beta_{42}$ oligomers induce a decrease in PSD-95 levels in a time-dependent manner, as previously reported with $A\beta_{40}$ [Roselli F et al. 2005], supporting a model of AD pathogenesis in which soluble Aβ may be responsible for the cognitive impairment through synaptic dysfunction [Walsh DM et al. 2004]. In addition, the two extracellular chaperones studied here are able to recover PSD-95 expression, avoiding oligomer binding to the synapses, suggesting an important protective effect of chaperones against oligomer-induced synaptic dysfunction.

Results II: Transthyretin suppress the toxicity of oligomers formed by misfolded proteins *in vitro*

Although human transthyretin (TTR) is associated with systemic amyloidoses, an anti-amyloidogenic effect that prevents Aβ fibril formation *in vitro* and in animal models has been observed. Here we studied the ability of three different types of TTR, namely human tetramers (hTTR), mouse tetramers (muTTR) and an engineered monomer of the human protein (M-TTR), to suppress the toxicity of oligomers formed by two different amyloidogenic peptides/proteins (HypF-N and $A\beta_{42}$). muTTR is the most stable homotetramer, hTTR can dissociate into partially unfolded monomers, whereas M-TTR maintains a monomeric state. Preformed toxic HypF-N and $A\beta_{42}$ oligomers were incubated in the presence of each TTR then added to cell culture media. hTTR, and to a greater extent M-TTR, were found to protect human neuroblastoma cells and rat primary neurons against oligomer-induced toxicity, whereas muTTR had no protective effect. The thioflavin T assay and site-directed labeling experiments using pyrene ruled out disaggregation and structural reorganization within the discrete oligomers following incubation with TTRs, while confocal microscopy, SDS-PAGE, and intrinsic fluorescence measurements indicated tight binding between oligomers and hTTR, particularly M-TTR. Moreover, AFM, light scattering and turbidimetry analyses indicated that larger assemblies of oligomers are formed in the presence of M-TTR and, to a lesser extent, with hTTR. Overall, the data suggest a generic capacity of TTR to efficiently neutralize the toxicity of oligomers formed by misfolded proteins and reveal that such neutralization occurs through a mechanism of TTR-mediated assembly of protein oligomers into larger species, with an efficiency that correlates inversely with TTR tetramer stability.

TTRs prevent oligomer-induced cytotoxicity in SH-SY5Y cells

We incubated oligomers formed from HypF-N and $A\beta_{42}$ in cell culture medium in the absence or presence of hTTR, muTTR or M-TTR for 1 h, then added the resulting mixtures to SH-SY5Y cells and measured the resulting cell viability using the MTT reduction assay. The two types of oligomers were toxic (Fig. 15A,B), as previously demonstrated [Mannini B et al 2012]. The cells treated with oligomers preincubated with hTTR and M-TTR displayed no toxic effect showing MTT reduction similar to that of untreated cells, to cells treated with the native proteins or to cells treated with oligomers preincubated with haptoglobin or α_2-macroglobulin, two well known extracellular chaperones used here as positive controls for inhibition of oligomer toxicity (Fig. 15A,B). Conversely, muTTR shows a small insignificant protective effect (Fig. 15A,B). In addition, when the two oligomer types were incubated in the cell culture medium for 1 h with proteins that are not expected to possess chaperone properties, such as hen egg white lysozyme (HEWL) or bovine serum albumin (BSA), the oligomers maintained their toxicity (Fig. 15A,B). In these studies we did not examine the effect of the various TTRs on $A\beta_{42}$ and HypF-N oligomer formation.

We repeated the experiments described above for HypF-N and $A\beta_{42}$ oligomers by varying the concentration of each TTR in the 1 h preincubation solution, while maintaining a constant concentration of HypF-N and $A\beta_{42}$. M-TTR was found to suppress the toxicity of HypF-N and $A\beta_{42}$ oligomers even at low concentration with an efficacy similar to haptoglobin and α_2-macroglobulin, (Fig. 15C,D). M-TTR remained effective even at an HypF-N:TTR and $A\beta_{42}$:TTR molar ratio of 400:1, becoming ineffective at a molar ratio of 1000:1 both for HypF-N and $A\beta_{42}$ (Fig. 15C,D). hTTR is also effective, but at higher concentrations; indeed, hTTR inhibited toxicity until a HypF-N:TTR and $A\beta_{42}$:TTR molar ratio of 40:1 and 100:1, respectively, only becoming ineffective at molar ratios of 100:1 for HypF-N and 200:1 for $A\beta_{42}$. muTTR did not show any protective effect, even at low molar ratios (Fig. 15C,D).

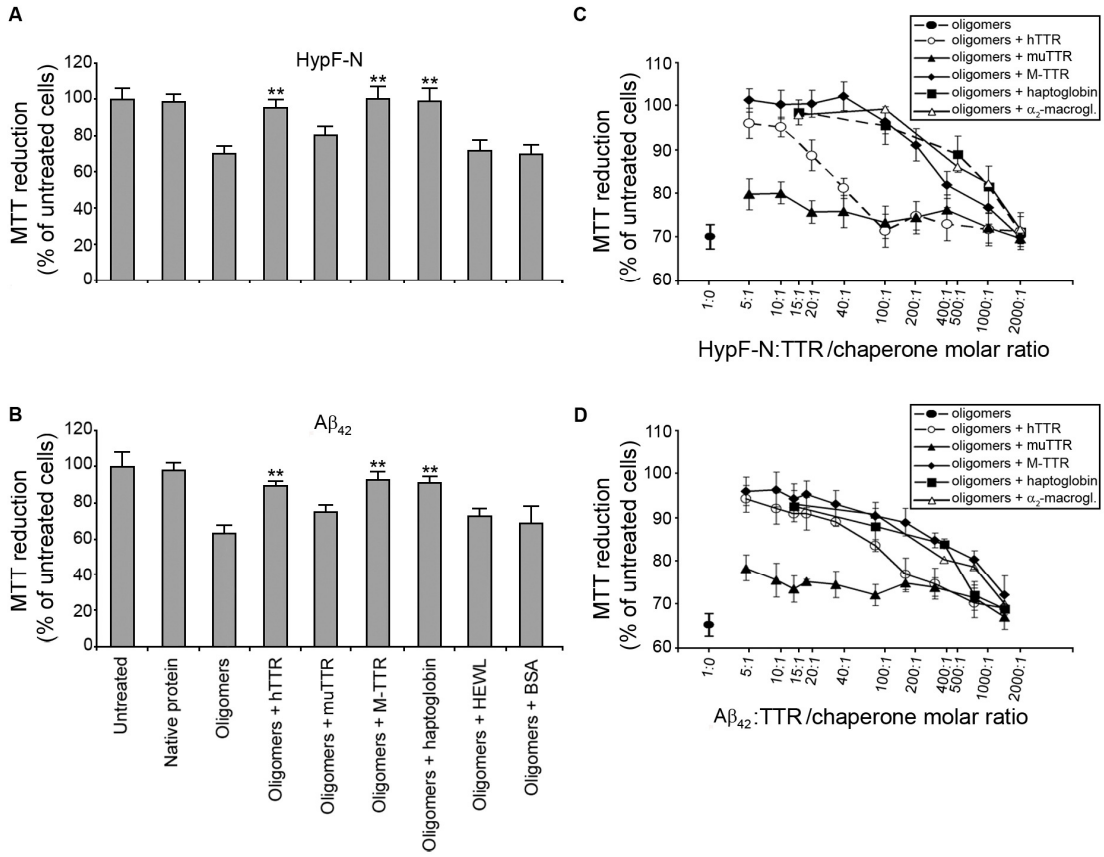

Fig. 15 Suppression of protein oligomer toxicity by TTRs. Preformed oligomers of HypF-N (**A**) and $A\beta_{42}$ (**B**) were resuspended in the cell culture medium, incubated for 1 h at a corresponding monomer concentration of 12 μM in the absence or presence of the indicated TTRs (protein:TTR molar ratio was 10:1), human haptoglobin (protein:haptoglobin molar ratio was 15:1), human α_2-macroglobulin (protein:α_2-macroglobulin molar ratio was 100:1), HEWL (protein:HEWL molar ratio was 5:1), or BSA (protein:BSA molar ratio was 5:1) and then added to SH-SY5Y cells. (**C**-**D**) Dose-dependent suppression of HypF-N (**C**) and $A\beta_{42}$ (**D**) oligomer toxicity by TTRs. Preformed oligomers of HypF-N and $A\beta_{42}$ were resuspended in the cell culture medium, incubated for 1 h in the absence (●) or presence of the indicated HypF-N:TTR/chaperone (**C**) and $A\beta_{42}$:TTR/chaperone (**D**) molar ratios and then added to SH-SY5Y cells. TTRs were always considered as tetramers in all HypF-N/$A\beta_{42}$:TTR molar ratio values. The scale on the *x* axis is logarithmic. Cell viability was expressed as percent of MTT reduction in treated cells with respect to untreated cells (taken as 100%). The values shown are means ± SD of three independent experiments carried out in quadruplicate. The single, double and triple asterisks indicate a significant difference ($p \leq 0.05$, $p \leq 0.01$, $p \leq 0.001$, respectevily) relative to the experiment with oligomers only.

We also evaluated the intrinsic cytotoxic effect of each TTR variant in the absence of the oligomers. Our results showed that under our experimental condition (preincubation for 1 h at 37 °C) M-TTR significantly decreased the MTT reduction of the SH-SY5Y cells by ca. 20% (Fig. 16A); conversely, hTTR and muTTR did not show significant toxic effects (Fig. 16A), whereas it has been demonstrated that hTTR is cytotoxic if produced or exposed to cold temperature [Sörgjerd K et al.2008, Choi S et al. 2010]. These results indicate that M-TTR alone is toxic to cells, as previously demonstrated [Reixach N et al.2004], whereas preincubation of M-TTR with toxic HypF-N and $A\beta_{42}$ oligomers suppresses both toxic effects, suggesting an interaction between oligomers and monomeric TTR with mutual suppression of toxicity.

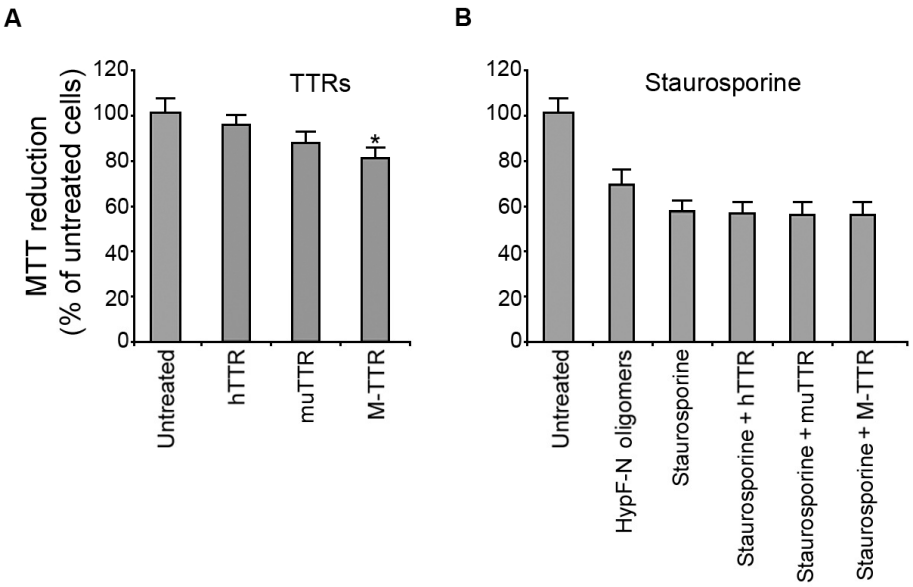

Figure. 16. (**A**) Intrinsic cytotoxic effect of TTRs. Each TTR was dissolved in the cell culture medium, incubated for 1 h at a corresponding tetramer concentration of 1.2 µM (M-TTR concentration was 4.8 µM) and then added to SH-SY5Y cells. (**B**) Effect of TTRs on staurosporine toxicity. 1 µM staurosporine was incubated for 1 h in the cell culture medium in the absence or presence of the indicated TTRs (staurosporine:TTR molar ratio was 10:1) and then added to SH-SY5Y cells. In both panels cell viability was expressed as percent of MTT reduction in treated cells with respect to untreated cells (taken as 100%). The values shown are means ± SD of three independent experiments carried out in triplicate. The asterisk indicates a significant difference ($p \leq 0.05$) relative to the untreated cells.

To assess whether the three types of TTR can protect the cells from other forms of stress, or if they are specific for protein oligomers, we incubated the cells with staurosporine, a well-known apoptosis inducer. We found that a concentration of 1 μM of staurosporine decreased the MTT reduction of the cells to a level similar to that of preformed protein oligomers under our conditions. The staurosporine toxicity was not reduced by any of the three TTRs (Fig. 16B).

These results indicate that hTTR and M-TTR can suppress or markedly decrease the toxicity of oligomers formed by two different peptides and proteins. The suppression is specific for TTRs or chaperones (relative to other proteins) with respect to toxicity induced by preformed protein oligomers (not other forms of stress).

TTRs inhibit oligomer-mediated intracellular Ca^{2+} influx, ROS production and membrane permeabilization

The influx of Ca^{2+} ions from the extracellular space into the cytosol across the cell membrane has been recognised to be an early biochemical change undergone by cells exposed to deleterious protein oligomers including HypF-N and $A\beta_{42}$ oligomers [Zampagni M et al. 2011, Orrenius S et al.2003, Demuro A et al. 2005, Canale C et al. 2006, Bojarski L et al. 2008, Evangelisti E et al.2012]. Here we compared the ability of the different types of TTR to inhibit the influx of Ca^{2+} caused by soluble oligomers of HypF-N and $A\beta_{42}$ after their preincubation for 1 h in the cell culture medium before addition to the SH-SY5Y cells. Both HypF-N and $A\beta_{42}$ oligomers induced a sharp increase in cytosolic free Ca^{2+} levels (Fig. 17). Preincubation with hTTR and M-TTR was found to inhibit the increase of intracellular Ca^{2+} levels caused by the oligomers, whereas muTTR showed a lower protective effect (Fig. 17). In addition, the degree of Ca^{2+}-derived fluorescence was found to decrease exponentially with the time of preincubation with M-TTR and hTTR (Fig. 18); in particular, M-TTR prevented the Ca^{2+} spike after only 15 min of preincubation (Fig. 18).

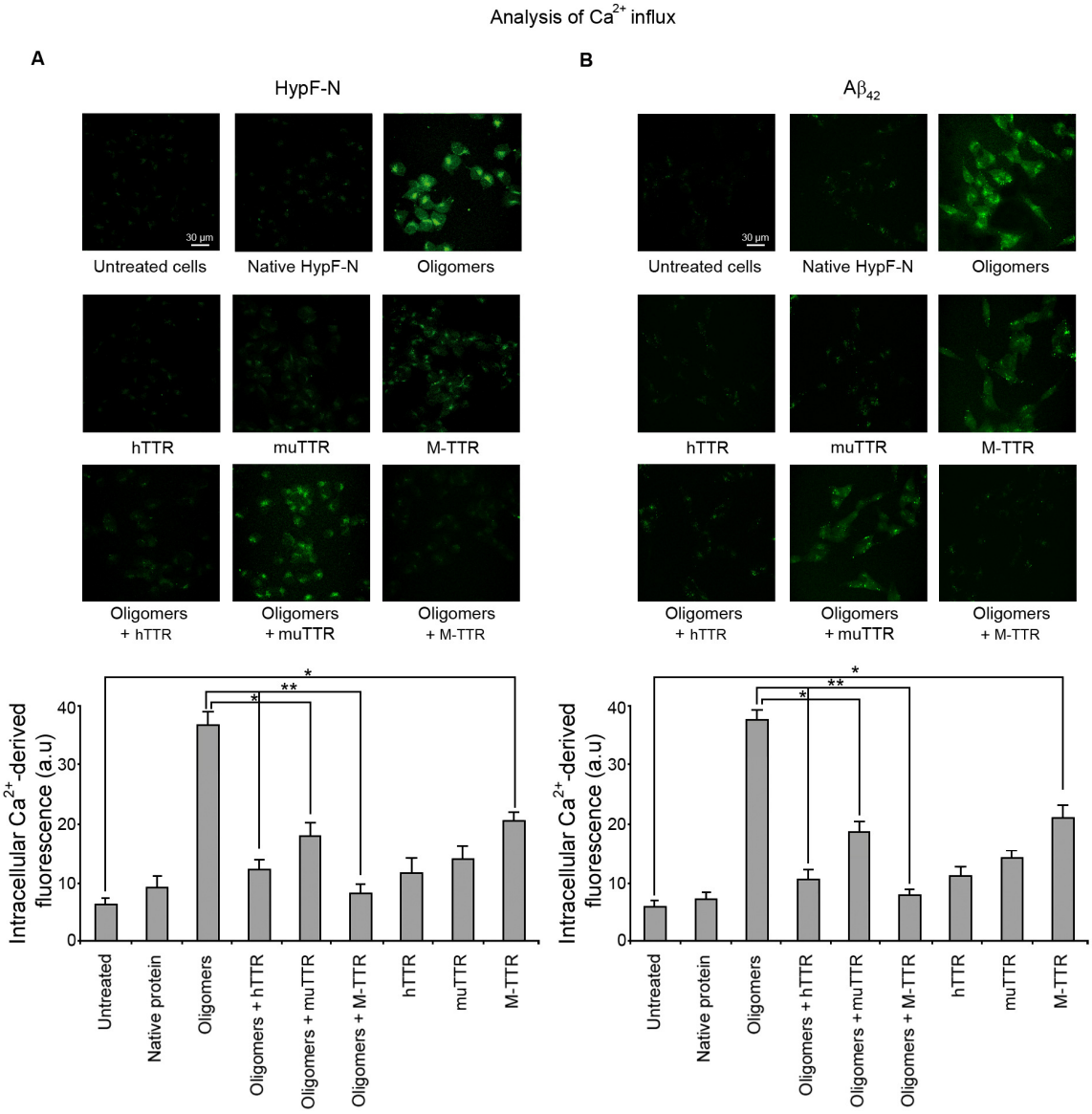

Fig. 17 Representative confocal scanning microscope images showing intracellular Ca^{2+} levels in SH-SY5Y cells. Preformed oligomers of HypF-N (**A**) and $A\beta_{42}$ (**B**) were resuspended in the cell culture medium, incubated for 1 h at a corresponding monomer concentration of 12 µM with or without the indicated TTRs (protein:TTR molar ratio was 10:1) and then added to SH-SY5Y cells for 1 h. The figure also shows untreated cells, cells exposed for 1 h to the native protein, to toxic oligomers (12 µM monomer) and to the indicated TTRs alone (1.2 µM tetramer or 4.8 µM monomer). The green fluorescence arises from the intracellular Fluo3 probe bound to Ca^{2+}. The corresponding semi-quantitative values of the green fluorescence signals are shown below each set of images. Statistics as in Fig. 15.

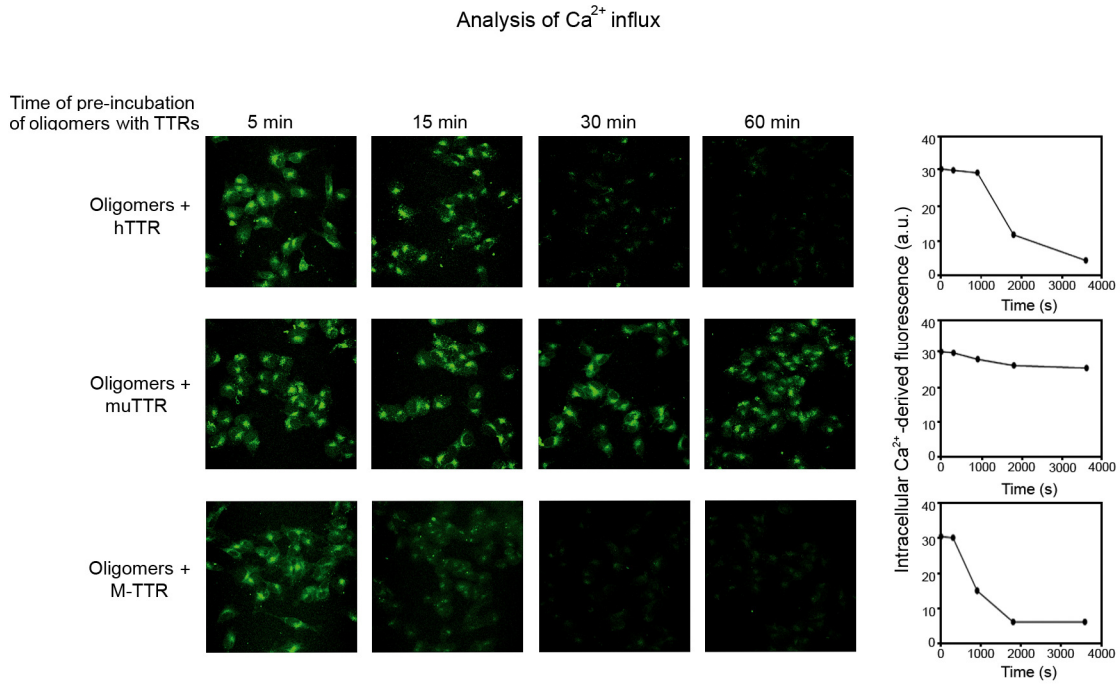

Figure. 18. Representative confocal scanning microscope images showing intracellular Ca^{2+} levels in SH-SY5Y cells. Preformed oligomers of HypF-N were resuspended in the cell culture medium, incubated at a corresponding monomer concentration of 12 µM in the absence or presence of the indicated TTRs (protein:TTR molar ratio was 10:1) for the indicated time lengths and then added to SH-SY5Y cells for 1 h. The green fluorescence arises from the intracellular Fluo3 probe bound to Ca^{2+}. The kinetic plots show the fluorescence associated with intracellular Ca^{2+} versus time elapsed after preincubation of oligomers with TTRs.

Similar results were obtained analysing intracellular ROS production and membrane permeability. HypF-N oligomers induced a sharp increase in ROS levels in our cell model (Fig. 19A). hTTR and M-TTR inhibited the increase of intracellular ROS levels caused by the oligomers, with the degree of ROS-derived fluorescence decreasing exponentially with the time of preincubation (Fig. 19A); M-TTR prevented the ROS production after only 15 min of preincubation (Fig. 19A). In contrast, mTTR did not show any protective effect (Fig. 19A).

Confocal microscopy analysis of SH-SY5Y cells pre-loaded with calcein-AM showed that cell exposure to HypF-N toxic oligomers resulted in a significant decrease of fluorescence intensity in our cells, indicating increased membrane permeabilization (Fig. 19B). In contrast, the reduction in calcein fluorescence was prevented when

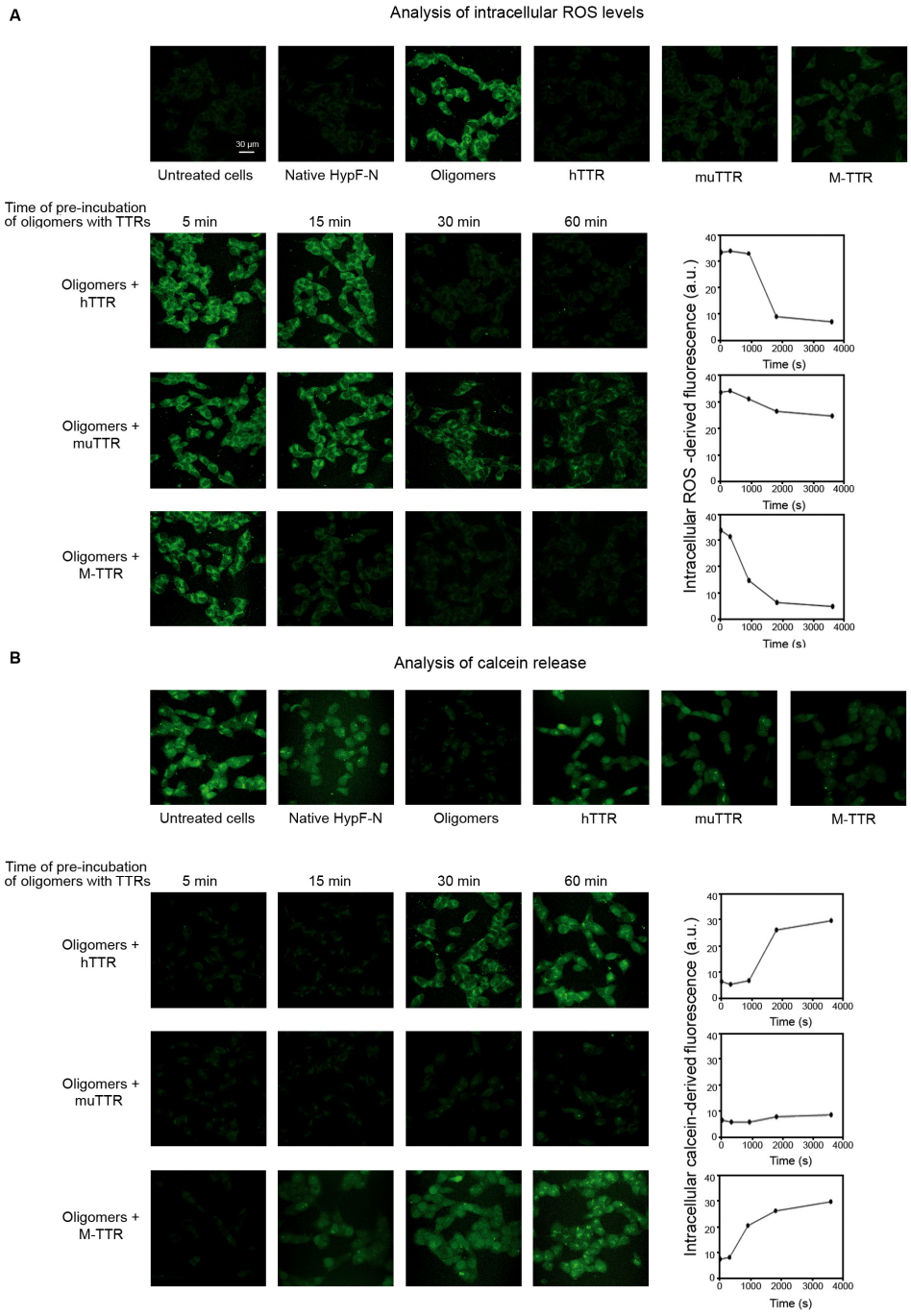

Figure. 19. Representative confocal scanning microscope images of SH-SY5Y cells showing intracellular ROS levels (**A**) and the release of intracellular calcein (**B**). Preformed oligomers of HypF-N were resuspended in the cell culture medium, incubated at a corresponding monomer concentration of 12 µM in the absence or presence of the indicated TTRs (protein:TTR molar ratio was 10:1) for the indicated time lengths and then added to SH-SY5Y cells for 1 h. The kinetic plots show the fluorescence associated with intracellular ROS or calcein versus time elapsed after pre-incubation of oligomers with TTRs. Top panel images show untreated cells, cells exposed for 1 h to the native protein, to toxic oligomers (12 µM monomer concentration) and to the indicated TTRs without oligomers (1.2 µM tetramer or 4.8 monomer concentration). The green fluorescence arises from the CM-H_2DCFDA probe that has reacted with ROS (**A**) and calcein (**B**) entrapped inside cells, respectively.

the cells were treated with oligomers preincubated with hTTR and M-TTR, with the degree of calcein-derived fluorescence increasing exponentially with the time of preincubation (Fig. 19B). In particular, the reduction of permeabilization occurred even more quickly in the presence of M-TTR. mTTR did not show any protective effect (Fig. 19B).

TTRs prevent oligomer-induced apoptosis

We then evaluated whether the different capacities of TTRs to protect cytosolic Ca2+ influx, ROS production and membrane permeabilization induced by HypF-N and Aβ42 oligomers also resulted in different abilities to prevent cell death. We measured caspase-3 activity, a well recognised apoptotic marker, using confocal microscopy (Fig. 20) [Thornberry N.A. et al.1997]. Fluorescence microscopy images and the corresponding semi-quantitative values of the green fluorescence signal show that hTTR and M-TTR significantly prevented the apoptotic response induced by HypF-N and Aβ42 oligomers (Fig. 20A,B; $p<0.01$). muTTR also showed a significant protection but it was less marked than that of the other TTRs (Fig. 20A,B; $p<0.05$). A similar trend was observed analyzing chromatin condensation by using the Hoechst 33342 dye, a fluorescent marker that binds to the highly condensed chromatin present in the nuclei of apoptotic cells [Yerbury JJ et al.2007] (Fig. 21).

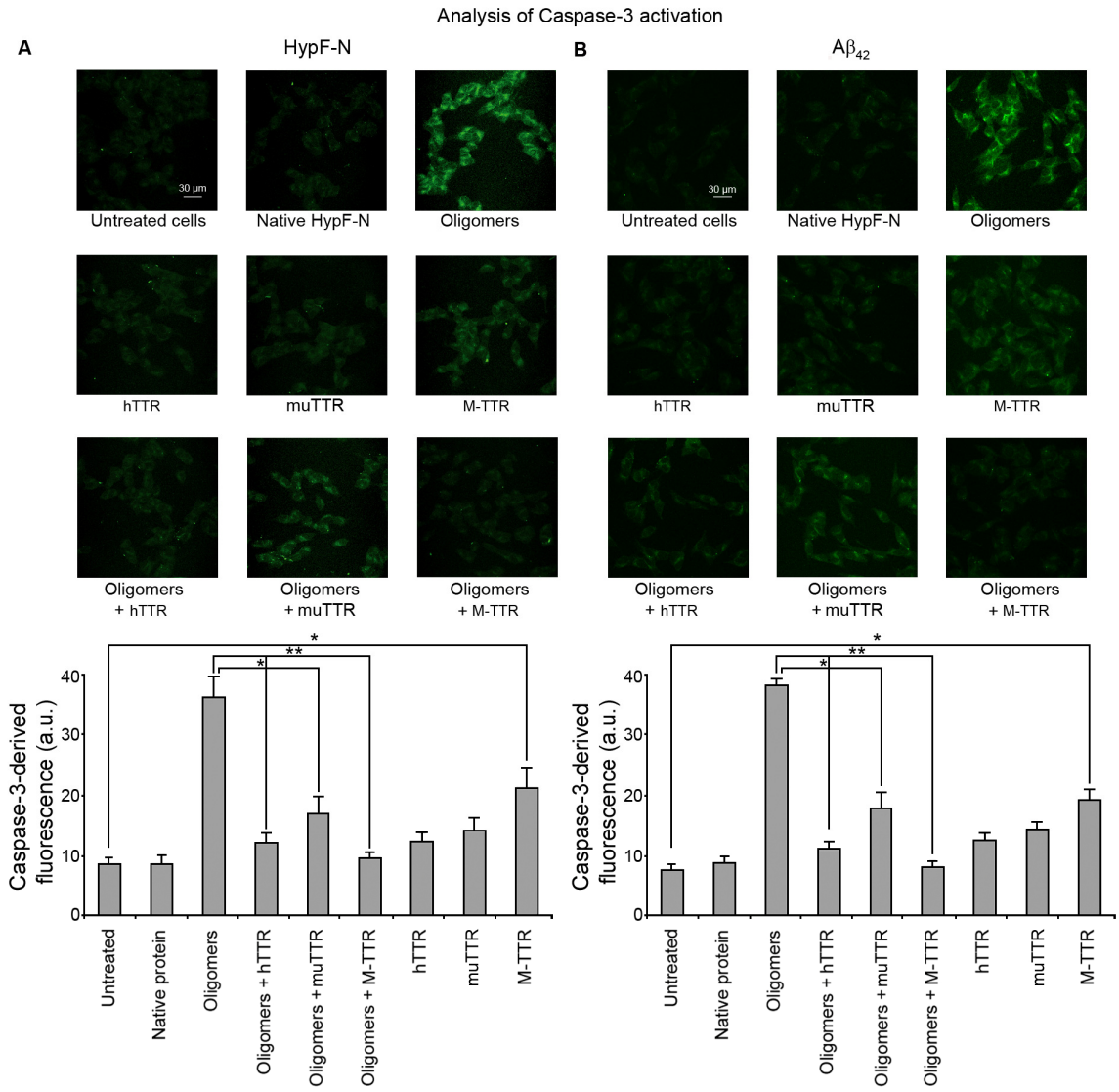

Fig. 20 Representative confocal microscope images showing caspase-3 activation in SH-SY5Y cells. Preformed oligomers of HypF-N (**A**) and $A\beta_{42}$ (**B**) were resuspended in the cell culture medium, incubated at a corresponding monomer concentration of 12 µM with or without the indicated TTRs (protein:TTR molar ratio was 10:1) for 1 h and then added to SH-SY5Y cells for 24 h. The figure also shows untreated cells, cells exposed for 1 h to the native protein, to toxic oligomers (12 µM monomer) and to the indicated TTRs alone (1.2 µM tetramer or 4.8 µM monomer). Caspase-3 activity, assessed using the fluorescent probe FAM-FLICA™ Caspase 3&7, is indicated by green fluorescence. The corresponding semi-quantitative values of the green fluorescence signals are shown below each set of images. Statistics as in Fig. 15.

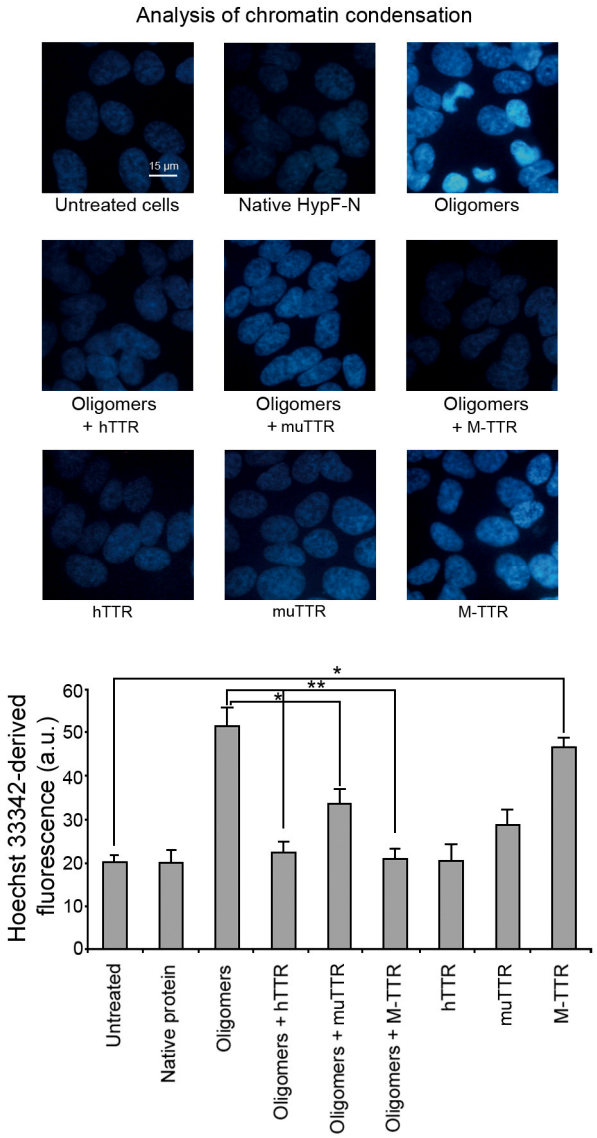

Figure. 21 Representative microscope images showing chromatin condensation using the Hoechst staining test in SH-SY5Y cells. Preformed oligomers of HypF-N were resuspended in the cell culture medium, incubated at a corresponding monomer concentration of 12 µM in the absence or presence of the indicated TTRs (protein:TTR molar ratio was 10:1) for 1h and then added to SH-SY5Y cells for 24 h. The figure also shows untreated cells, cells exposed for 1 h to the native protein, to toxic oligomers (12 µM monomer concentration) and to the indicated TTRs alone (1.2 µM tetramer or 4.8 monomer concentration). Small and bright nuclei indicate apoptosis. The corresponding semi-quantitative values of the blue and green fluorescence signals are shown below each set of images, respectively. The values reported are means ± S.D. of three independent experiments. In both panels the asterisk and the double asterisk indicate significant differences ($p \leq 0.05$ and $p \leq 0.01$, respectively).

TTRs prevent oligomer-induced toxicity and inhibit colocalization of HypF-N aggregates with PSD-95 in rat primary neurons

We assessed the relative protective capacity of the three different TTRs for rat hippocampal and cortical neurons using the MTT reduction assay. The HypF-N oligomers were toxic to rat hippocampal and cortical neurons (Fig. 22A,B). The neurons treated with HypF-N oligomers pre-incubated with hTTR and M-TTR were found to reduce MTT to levels similar to untreated cells and to cells treated with the native protein (Fig. 22A,B); conversely, muTTR showed a small and non-significant protective effect (Fig. 22A,B). We also evaluated the intrinsic cytotoxic effect of each TTR variant in the absence of the oligomers. M-TTR significantly decreased the MTT reduction of neurons by 25% (Fig. 22A,B); conversely hTTR and muTTR did not show any significant toxic effect (Fig. 22A,B). These results indicate that as previously shown for Aβ induced cytotoxity, hTTR and M-TTR are able to suppress HypF-N oligomer-induced toxic effects in both immortalized cell cultures and primary neurons.

To investigate the mechanism of action by which TTRs protect cultured primary neurons from toxic HypF-N oligomers, we examined the colocalization between oligomers and PSD-95 in cultured primary hippocampal neurons. It has previously been shown that binding sites of Aβ42 and HypF-N oligomers on neurons overlap with PSD-95 [Cascella R et al. 2013, Lacor PNet al.2004, Tatini F et al. 2013]. A remarkable degree of colocalization was observed between HypF-N oligomers and PSD-95, whereas no colocalization was observed in untreated cells or in cells treated with native HypF-N (Fig. 22C). Preincubation of HypF-N oligomers with hTTR or M-TTR for 1 h was found to inhibit oligomer binding to the cell membrane, thus preventing the colocalization with PSD-95 (Fig. 22C). Preincubation of HypF-N oligomers with muTTR also decreased colocalization, but to a lower level than observed for the other TTRs (Fig. 22C). In particular, the fraction of HypF-N puncta colocalizing with PSD-95 puncta was 21.4±3.1% (n=18) for oligomers preincubated with hTTR for 1 h, 35.7±1.2% (n=18) for oligomers preincubated with muTTR for 1 h and 16.5±1.2% (n=18) for oligomers preincubated with M-TTR for 1 h.

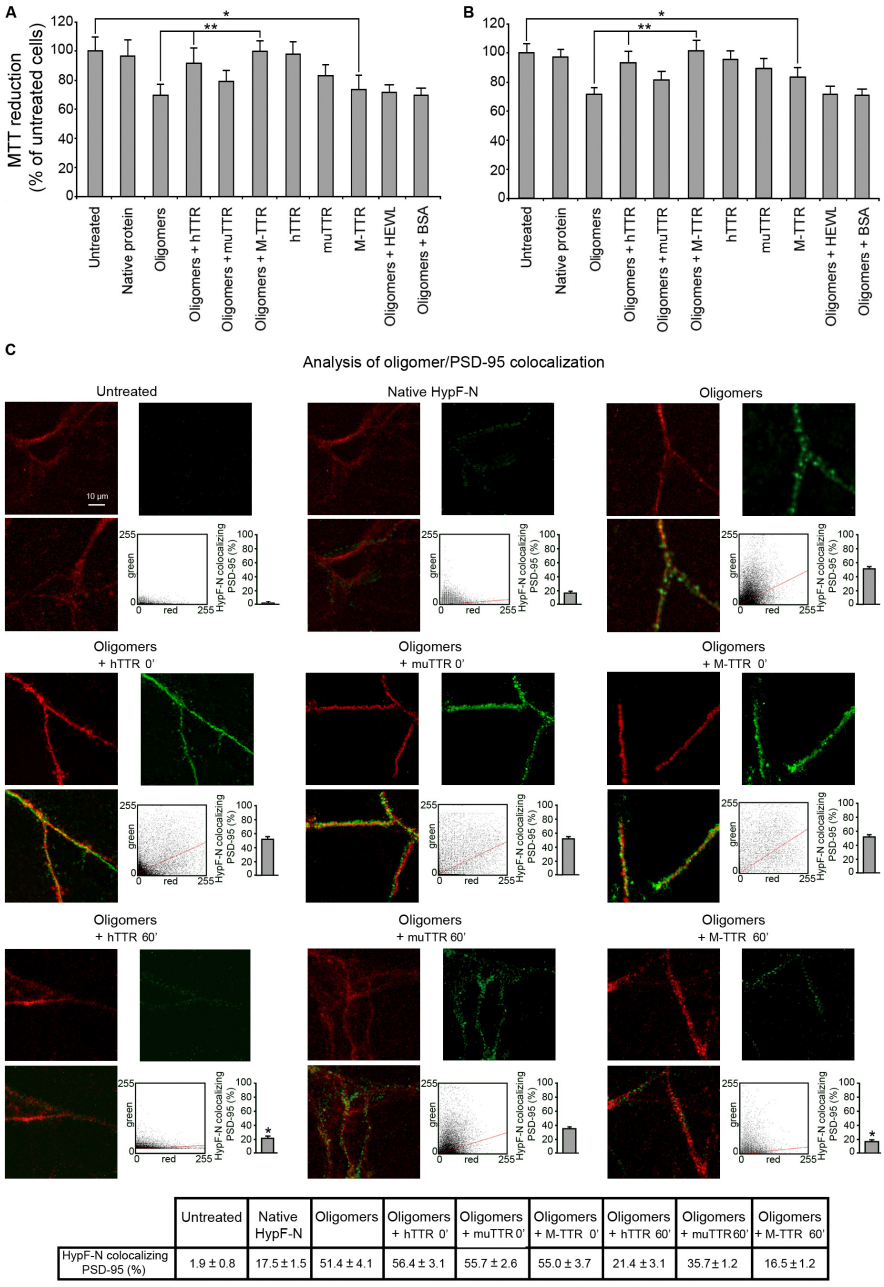

	Untreated	Native HypF-N	Oligomers	Oligomers + hTTR 0'	Oligomers + muTTR 0'	Oligomers + M-TTR 0'	Oligomers + hTTR 60'	Oligomers + muTTR 60'	Oligomers + M-TTR 60'
HypF-N colocalizing PSD-95 (%)	1.9 ± 0.8	17.5 ± 1.5	51.4 ± 4.1	56.4 ± 3.1	55.7 ± 2.6	55.0 ± 3.7	21.4 ± 3.1	35.7 ± 1.2	16.5 ± 1.2

Figure. 22 Suppression of protein oligomer toxicity by TTRs in rat hippocampal (**A**) and cortical (**B**) neurons. See Fig. 1 legend for details. (**C**) Representative confocal scanning microscope images at high magnification showing oligomer colocalization with PSD-95 in rat primary hippocampal neurons. Preformed oligomers of HypF-N were resuspended in the cell culture medium, incubated at a corresponding monomer concentration of 12 µM in the absence or presence of the indicated TTRs (protein:TTR molar ratio was 10:1) for 0 h and 1 h and then added to neurons for 30 min. The colocalization of HypF-N aggregates with PSD-95 was monitored using anti-HypF-N and anti-PSD-95 antibodies and then with Alexa Fluor 488- and 594-conjugated secondary antibodies (green and red, respectively). Top panel images showed untreated cells, cells exposed to the native protein and toxic oligomers (12 µM monomer concentration). The cytofluorograms of dendrite sections show the green fluorescence intensity (as pixel intensity, *y* axis) *versus* red fluorescence intensity (*x* axis). For each sample, 18 cytofluorograms were analysed, each considering one dendrite section. The histograms show the percentage of colocalization, also reported in the table.

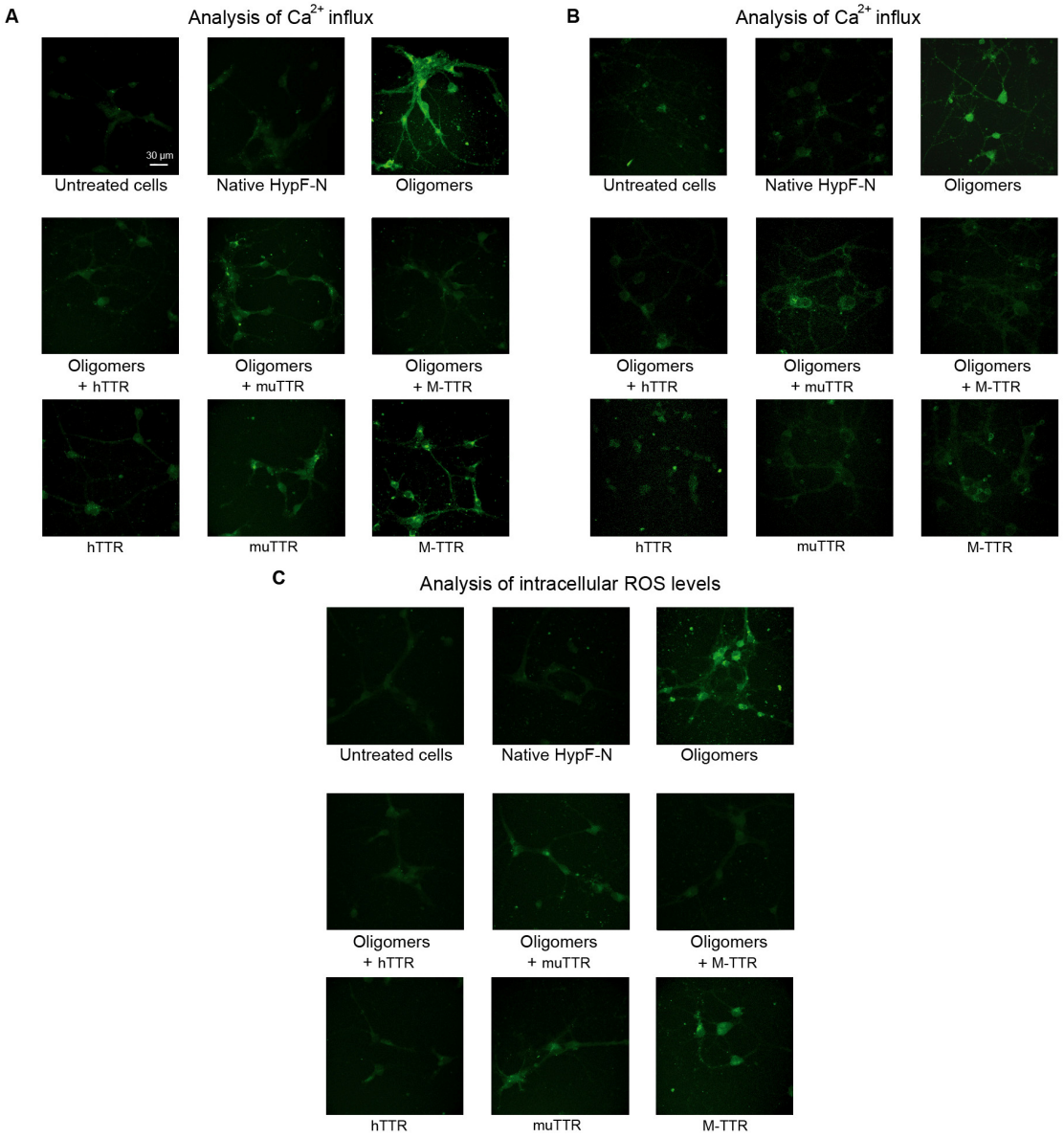

Figure. 23. (**A, B**) Representative confocal scanning microscope images showing intracellular Ca^{2+} levels in primary hippocampal (**A**) and cortical (**B**) neurons from rat brains. Preformed oligomers of HypF-N were resuspended in the cell culture medium, incubated at 12 µM with or without the indicated TTRs (protein:TTR molar ratio was 10:1) for 1 h and then added to rat neurons for 1 h. Each panel also show untreated cells, cells exposed for 1 h to the native protein, toxic oligomers (12 µM monomer concentration) and to the indicated TTRs without oligomers (1.2 µM tetramer or 4.8 monomer concentration). In all images the green fluorescence arises from the intracellular Fluo3 probe bound to Ca^{2+}. (**C**) Representative confocal scanning microscope images showing intracellular ROS levels in primary hippocampal neurons from rat brains. Conditions as in A, B. The green fluorescence arises from the CM-H_2DCFDA probe that has reacted with ROS.

hTTR and M-TTR were also found to prevent the oligomer-mediated intracellular Ca2+ increase in both hippocampal (Fig. 23A) and cortical neurons (Fig. 23B). They also inhibited intracellular ROS production in hippocampal neurons (Fig. 23C). These results show that preincubation of the HypF-N oligomers with hTTR and M-TTR, and to a lesser extent muTTR, inhibit the binding of the oligomers at PSD-95 containing sites and reduce the toxicity of the oligomers for neurons.

The molecular structure of HypF-N oligomers is preserved in the complexes with TTRs

In order to investigate the mechanism by which TTRs suppress the toxicity of protein oligomers, we have chosen to focus on the toxic oligomers of HypF-N. Indeed, under different experimental conditions, HypF-N can aggregate into toxic (type A, the same used in the present work) or non toxic (type B) oligomers; using atomic force microscopy (AFM) the two species are morphologically similar (ca. 2-6 nm in height) and bind ThT to similar levels, making it possible to carry out valuable control experiments [Campioni S et al. 2010]. Thus, HypF-N oligomers appear to be highly stable, making them easy to handle in our experiments [Campioni S et al. 2010]. We have, however, carried out the key experiments also on Aβ42 oligomers (see below).
To shed light on the behaviors of the various TTRs and on the molecular mechanism by which they exert their protection against HypF-N oligomers we investigated the oligomeric state and the molecular structure of HypF-N oligomers after preincubation with various TTRs. To assess whether the oligomers can be dissolved by the different types of TTR, we exploited the ability of the HypF-N oligomers, unlike native HypF-N, to bind to ThT and increase its fluorescence [S. Campioni et al.2010] (Fig. 24A). HypF-N oligomers incubated for 1 h in a phosphate buffer at neutral pH cause a seven to eight fold increase of ThT fluorescence, and the same increase was observed when the oligomers were preincubated in the same buffer for 1 h with each of the TTRs (Fig. 24A). To exclude the possibility that TTRs bind ThT, in parallel we also analysed samples containing only TTRs under identical conditions and detected no increase of ThT fluorescence in these cases (Fig. 24A). Overall, these results show that HypF-N oligomers remain stable and do not undergo disaggregation after TTR treatment.

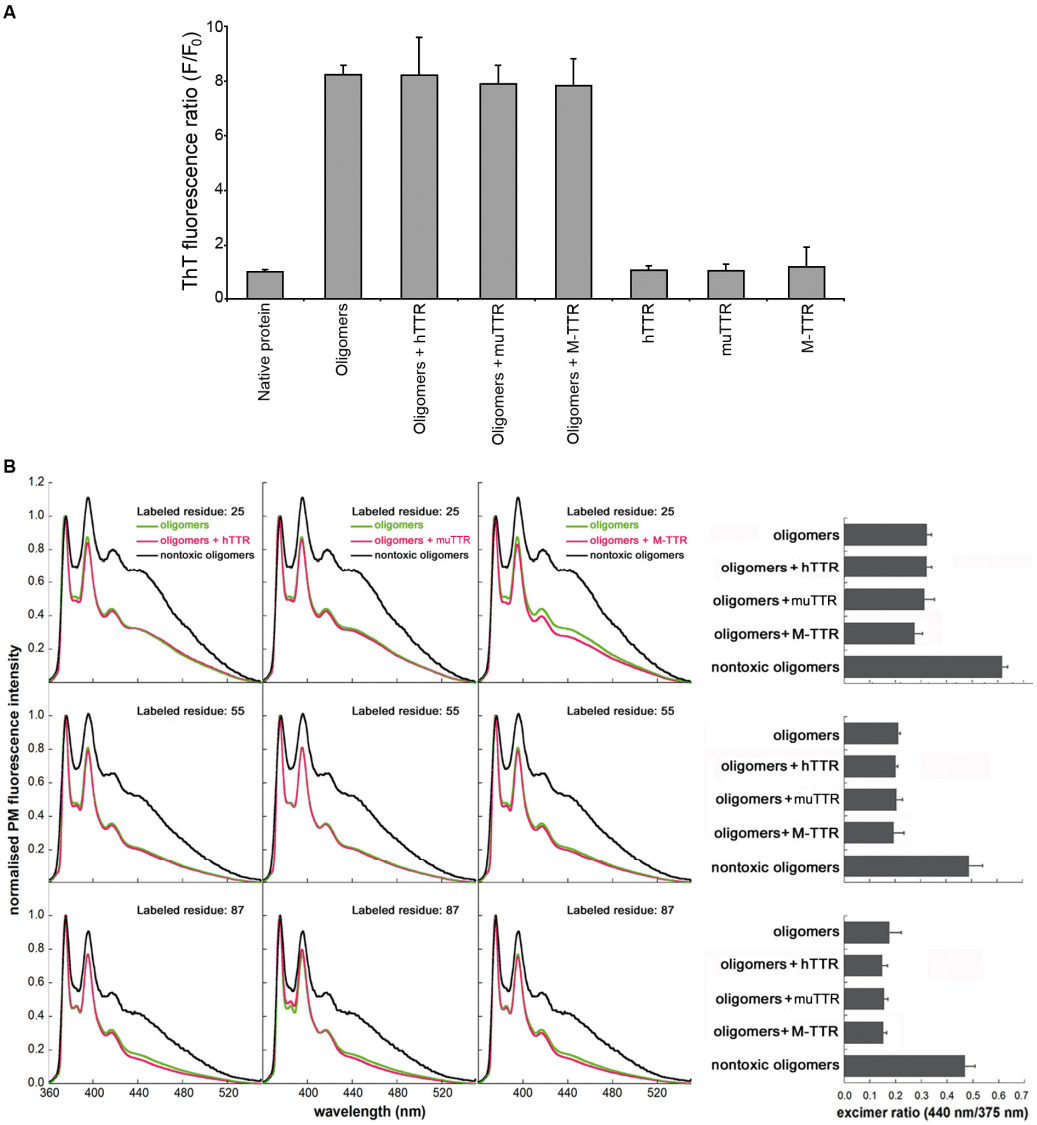

Fig. 24 TTRs do not dissolve and do not remodel HypF-N oligomers. (**A**) ThT fluorescence at 485 nm (excitation 440 nm) in the presence of the indicated protein components following preincubation for 1h in 20 mM phosphate buffer at pH 7.0 in the absence or presence of different types of TTR. The ratio between the ThT fluorescence in the presence (F) and absence (F_0) of proteins is reported; data are means ± SD of three independent experiments. The HypF-N concentration was 48 µM (in monomer units) and the HypF-N:TTR molar ratio was 10:1. (**B**) Fluorescence emission spectra of samples containing HypF-N oligomers labeled with pyrene at positions 25 (top), 55 (middle) and 87 (bottom). The spectra were acquired at 12 µM HypF-N concentration following 1 h incubation in the absence (green) or presence (pink) of hTTR (left panels), muTTR (middle panels) or M-TTR (right panels). For comparison, the corresponding spectra of nontoxic oligomers are reported in each graph (black). The spectra have been normalized to the intensity of the peak centered at 375 nm. The molar ratio of HypF-N:TTR was 10:1. On the right, the exicimer-to-monomer fluorescence intensity (FI_{440}nm/FI_{375}nm) of each sample and of the nontoxic oligomers is reported.

Subsequently, we asked whether the oligomers are structurally re-organised at the molecular level by the TTRs (Fig. 24B). Differences in the structure of toxic and non toxic oligomers have been detected using the fluorescent probe pyrene, a structural probe for changes in oligomers exposed to chaperones [Campioni S et al. 2010]. We determined the degree of packing of the oligomers through the acquisition of fluorescence spectra of oligomers labeled with pyrene. This method consists in creating HypF-N variants containing a single cysteine at different positions along the sequence, label them with pyrene and allow the labeled mutants to aggregate. When two pyrene molecules are close to each other (within 10 Å of distance), excited state dimers called excimers form and can be detected as a peak at 440-470 nm [Birks J.B et al 1967, P. Hammarström et al.1999, R. Krishnan et al.2005]. It has been shown that toxic and non toxic HypF-N oligomers can be distinguished by differences in their pyrene emission spectra [Campioni S et al.2010].

Three variants of HypF-N containing a single cysteine residue at position 25, 55 or 87, all located in the major hydrophobic regions, were labeled with pyrene, allowed to aggregate and transferred to phosphate buffer at neutral pH for 1 h with or without the different forms of TTR. The fluorescence spectra acquired for the oligomers in either the presence or absence of the TTRs were very similar with none showing an excimer band (Fig. 24B). Moreover, the ratio of the excimer-to-monomer fluorescence intensity (FI440nm/FI375nm) did not change following preincubation with any TTR, remaining lower in all cases than the corresponding value measured for the nontoxic oligomers (Fig. 24B). These results show that none of the TTRs promotes structural re-organization of the toxic HypF-N oligomers.

TTRs bind to the oligomers

To determine whether TTRs bind to the oligomers we used TTR-derived intrinsic fluorescence and SDS-PAGE. HypF-N oligomers sediment at relatively low centrifugal force; therefore, if the TTRs bind to the oligomers and the interaction between them is stable, the concentration of the TTRs in the supernatant will decrease following centrifugation, depending on the strength of the interaction. HypF-N oligomers and TTRs were incubated for 1h in phosphate buffer at pH 7.0 then centrifuged to separate

the pellet fraction (P), which contains the TTR bound to the oligomers, from the supernatant (SN), which contains the soluble unbound TTR. The amount of TTR in the SN was measured by its intrinsic fluorescence (Fig. 25A-C).

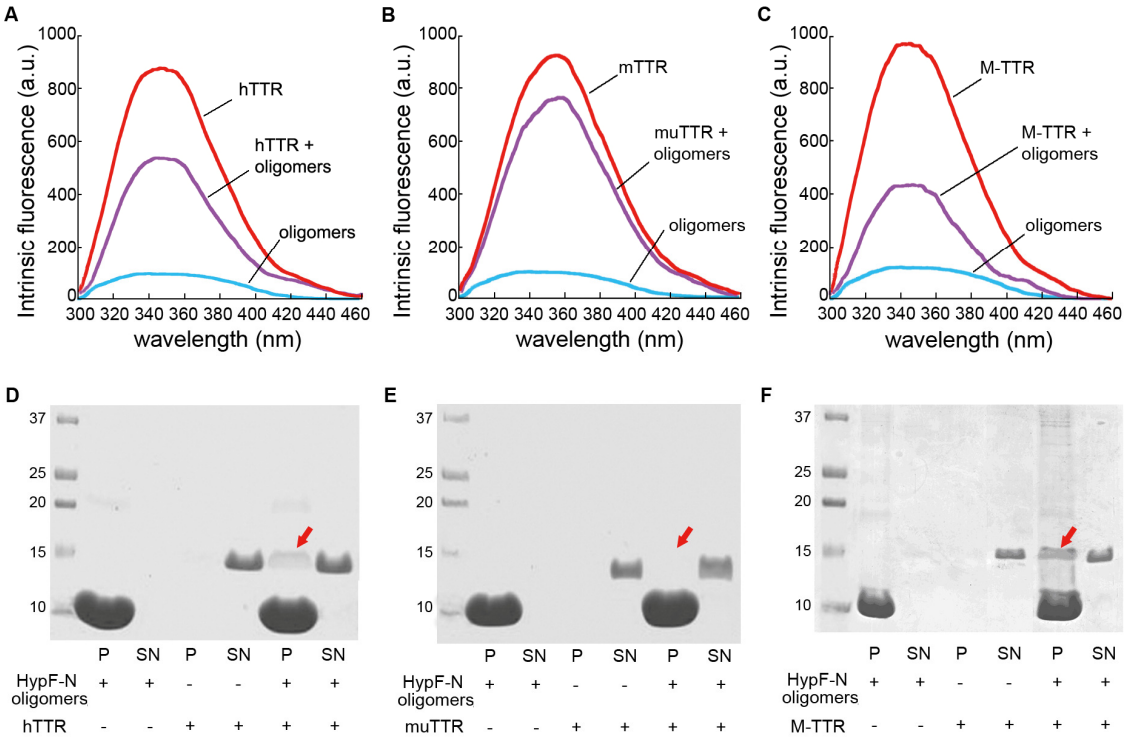

Fig. 25 TTRs interact with HypF-N oligomers. (**A-C**) Intrinsic fluorescence spectra of the SN fractions obtained after centrifugation of samples containing preformed HypF-N oligomers (blue), TTR (red) and HypF-N oligomers + TTR (purple). The fluorescence emission spectra (excitation at 280 nm) were acquired at 37 °C. The spectrum of HypF-N oligomers has been subtracted from that of TTR + HypF-N oligomers to eliminate its contribution. (**D-F**) SDS-PAGE analysis of the insoluble (P) and soluble (SN) fractions obtained from samples containing preformed HypF-N oligomers (lanes 2, 3), TTR (lanes 4, 5) and preformed oligomers treated for 1 h with TTR (lanes 6, 7). The HypF-N concentration was 48 µM (in monomer units) and the molar ratio of HypF-N:TTR was 10:1.

The fluorescence spectra of the SNs collected from the samples in which oligomers and hTTR or M-TTR were present were less intense than the corresponding ones in which only the TTRs were present, indicating that a fraction of hTTR, and to a greater extent M-TTR, is bound to the oligomers. In contrast, the fluorescence spectrum of the SN

collected from the sample containing oligomers and muTTR was similar to that in which only muTTR was present.

As a further evidence of binding, the pellet and supernatant fractions collected in each experiment were analysed by SDS-PAGE. In the samples containing oligomers or TTR alone, the HypF-N monomer (MW ~10.5 kDa) and the TTR monomer (MW ~14 kDa) were found only in the Pellet and SN fractions, respectively (Fig. 25D-F). In the sample containing both HypF-N oligomers and M-TTR, the HypF-N band was present only in the pellet fraction, whereas M-TTR was found to partition between the pellet (49.8 % ± 2.6) and SN fractions (Fig. 25F). This result confirms that a fraction of M-TTR is bound to the oligomers. Similar results, but with evidence of a smaller fraction bound in the pellet (24.1 % ± 3.1), were obtained with hTTR (Fig. 25D). In contrast, we found muTTR only in the SN fraction, suggesting that muTTR did not bind to HypF-N oligomers under these conditions (Fig. 25E). These results suggest that the ability of TTRs to bind HypF-N oligomers correlates inversely with TTR tetramer stability.

TTRs promote the assembly of the oligomers into larger species

To investigate whether the binding of TTRs to the oligomers promotes their further assembly, we first used AFM. Discrete HypF-N oligomers with a height of 1–4 nm were observed by AFM in the absence of TTR (Fig. 26A), but significantly larger aggregates were evident after 1 h incubation in the presence of M-TTR and, to a lower extent, hTTR (Fig. 26A). More complex structures were observed in the presence of M-TTR, consisting of very large aggregates of irregular shape with typical heights of a few tens of nanometers. Large assemblies were not observed in samples containing oligomers with muTTR (Fig. 26A), or in samples containing only TTR. Similar results were obtained with Aβ42 oligomers and TTRs (Fig. 28A).

As additional evidence of the ability of TTRs to promote oligomer assembly, we took advantage of light scattering measurements. In the presence of M-TTR, and hTTR to a lower extent, light scattering intensity increased, indicating that the oligomers were larger in size (Fig. 26B). Accordingly, these results were confirmed with turbidimetry measurements at 500 nm, which revealed a similar trend, presumably related to the lower sensitivity of this method (Fig. 26C).

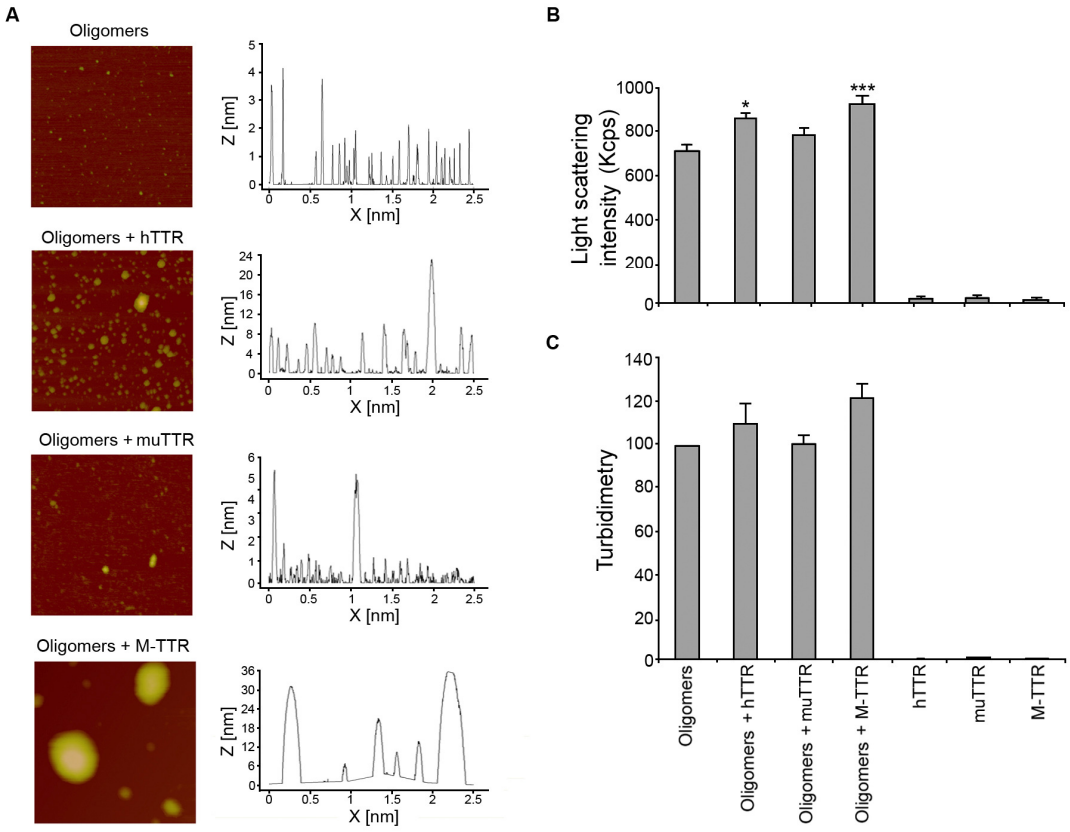

Fig. 26 Assembly of HypF-N oligomers induced by TTRs. (**A)** AFM images and corresponding height analysis of HypF-N oligomers preincubated with or without TTRs. Preformed oligomers of HypF-N were resuspended in phosphate buffer pH 7.0, incubated for 1 h at a corresponding monomer concentration of 48 µM in the absence or presence of the indicated TTRs (HypF-N:TTR molar ratio was 10:1) and then deposited on mica; the scan size is 1 µm. Z range: 5 nm (oligomers), 24 nm (oligomers + hTTR), 6 nm (oligomers + muTTR), 36 nm (oligomers + M-TTR). (**B)** Light scattering intensity measurements of HypF-N oligomers preincubated with or without TTRs and TTRs alone. The light scattering intensity were measured at 48 µM HypF-N and at a HypF-N:TTR molar ratio of 10:1. (**C**) Measurements of turbidimetry at 500 nm of HypF-N oligomers incubated with or without TTRs and TTRs alone. Conditions as in (**B**). The values shown are means ± SEM of five independent experiments. The single and the triple asterisks indicate significant difference ($p \leq 0.05$ and $p \leq 0.001$, respectively) relative to the experiment with oligomers only.

The AFM, light scattering and turbidity results show that M-TTR and hTTR promote the assembly of the HypF-N oligomers into larger species but do not provide information on whether or not the large HypF-N aggregates include the TTRs. The oligomers can also be observed with confocal microscopy because, unlike free TTRs, they readily adhere to the glass coverslips (Fig. 27).

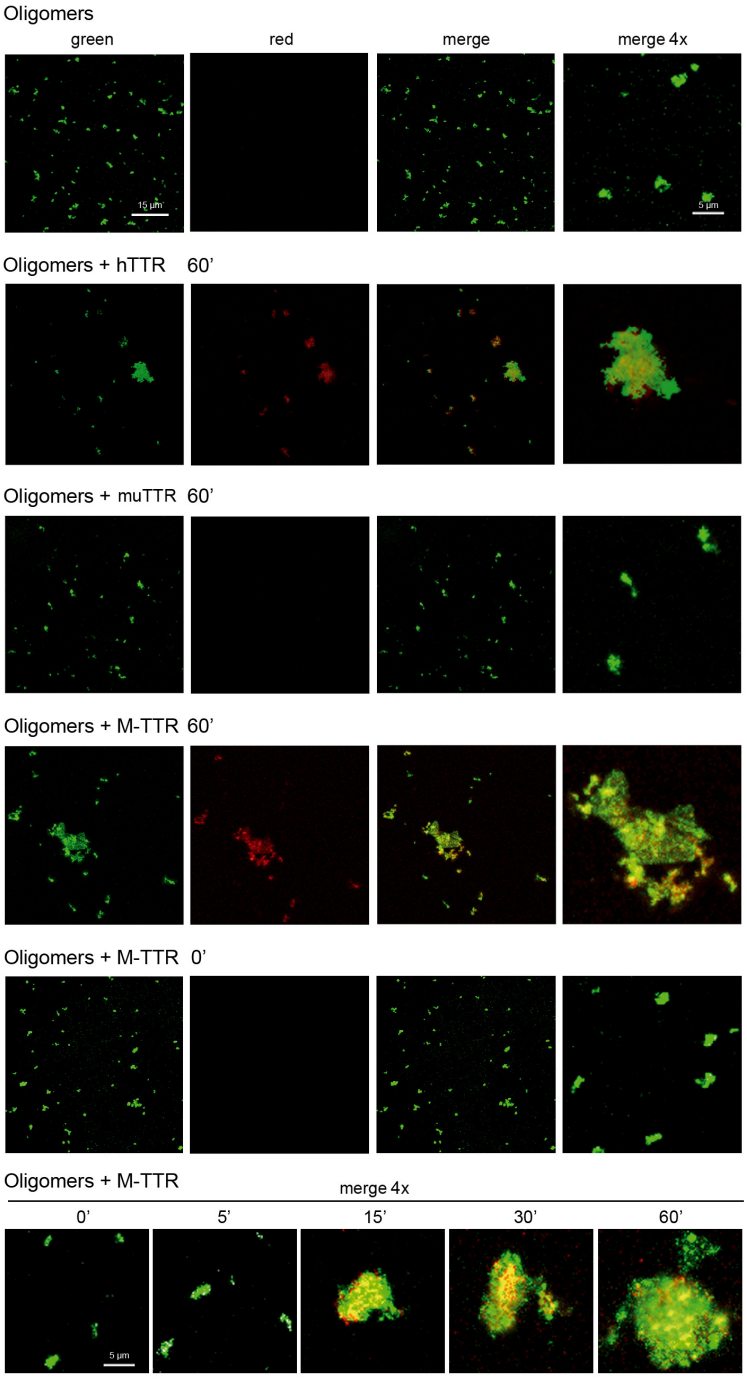

Fig. 27 Colocalization of HypF-N oligomers and TTRs. Representative confocal microscope images with HypF-N oligomers incubated for the indicated time lengths in the absence or presence of the indicated TTRs and treated with anti-HypF-N (green) and anti-TTR (red) antibodies. The colocalization of oligomers and TTRs is shown in the merged images (yellow dots). The HypF-N concentration was 48 µM (in monomer units) and the molar ratio of HypF-N:TTR was 10:1.

Images obtained using HypF-N oligomers incubated for 1 h with TTRs show larger aggregates, with M-TTR and hTTR colocalizing with the large oligomer clusters (Fig. 27).

By contrast, images obtained using HypF-N oligomers and TTRs in the absence of 1 h incubation showed no large oligomers (Fig. 27). Indeed, incubation of HypF-N oligomers with M-TTR promoted formation of large aggregates in a time-dependent manner (Fig. 27, bottom panel). Interestingly, the TTRs appear within the structural core rather than on the surface of these larger aggregates, suggesting that they promote the formation of such large aggregates rather than binding and stabilizing them after they are formed (Fig. 27). On the other hand, mTTR did not colocalize with the oligomers. This technique also showed that the M-TTR and hTTR were bound only to the large clusters of oligomers, not to single oligomers, confirming that the binding promotes their further assembly into clusters. Similar results were obtained with $A\beta_{42}$ oligomers and M-TTR (Fig. 28B).

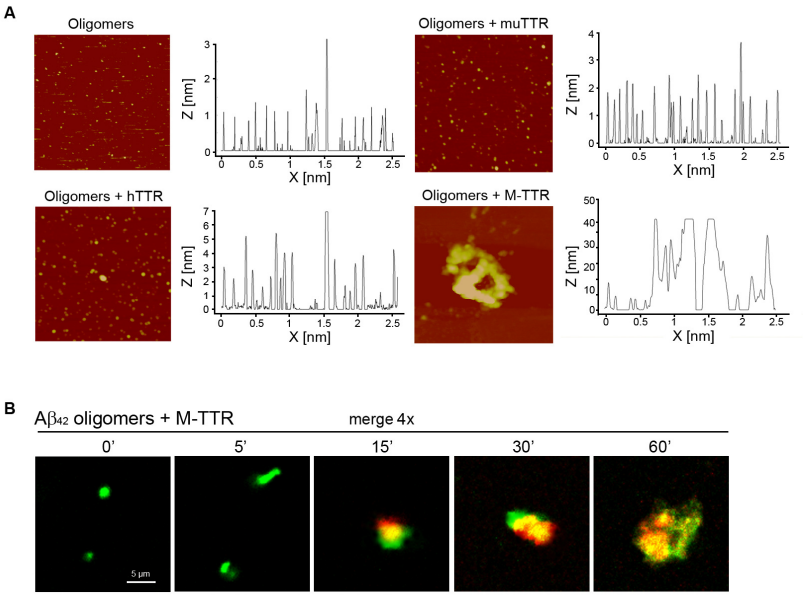

Figure. 28. Assembly of $A\beta_{42}$ oligomers induced by TTRs. (**A)** AFM images and corresponding height analysis of $A\beta_{42}$ oligomers preincubated with or without TTRs. Preformed oligomers of $A\beta_{42}$ were resuspended in phosphate buffer pH 7.0, incubated for 1 h at a corresponding monomer concentration of 48 µM in the absence or presence of the indicated TTRs ($A\beta_{42}$:TTR molar ratio was 10:1) and then deposited on mica; the scan size is 1 µm. Z range: 3 nm (oligomers), 7 nm (oligomers + hTTR), 4 nm (oligomers + muTTR), 50 nm (oligomers + M-TTR). (**B**) Colocalization of $A\beta_{42}$ oligomers and M-TTR. Representative confocal microscope images with $A\beta_{42}$ oligomers incubated for the indicated time lengths in the presence of M-TTR and treated with A11 anti-Aβ (green) and anti-TTR (red) antibodies. The colocalization of oligomers and M-TTR is shown in the merged images (yellow dots). The $A\beta_{42}$ concentration was 48 µM (in monomer units) and the molar ratio of $A\beta_{42}$:M-TTR was 10:1.

Results III: A complex equilibrium between partially unfolded conformations in monomeric transthyretin

Aggregation and deposition of the homotetrameric protein transthyretin (TTR) is known to be linked to the onset of several localised amyloidoses. It is also emerging that TTR exerts a protective role against aggregation of the Aβ peptide, a process linked to Alzheimer's disease. Both processes correlate with the ability of TTR to populate a monomeric state, yet a complete description of the possible conformational states populated by monomeric TTR under physiological conditions is missing. Using an array of biophysical method and kinetic tests, we show that once monomers of transthyretin are released by the quaternary structure, an equilibrium is established between a set of conformational states possessing different amounts of disorders. A molten globular state appears in equilibrium with the fully folded monomer, whereas an off-pathway species accumulates transiently during refolding of TTR. These two conformational ensembles are distinct in terms of structure, dynamics, kinetics and pathway of formation. Further subpopulations of the protein fold slower due to the occurrence of proline isomerism. The identification of two conformational states remained undisclosed in previous studies paves the way to the characterization of the amyloidogenicity and protective role of TTR.

Thermal denaturation of M-TTR is an irreversible process

In order to characterize the unfolding/refolding pathway of M-TTR, we first studied thermal unfolding of the protein in phosphate buffer by means of CD spectroscopy at 216 nm, where the biggest difference between the signal of native and thermally unfolded protein was observed (Figure 29A). The CD signal did not vary as the sample was heated up to a temperature of about 50 °C (Figure 29B). After that, the protein denatured and the transition was complete at 70 °C in our experimental setup. However, when the sample was cooled down to 25 °C, the CD signal did not recover the initial value (Figure 29B). The irreversibility of thermal denaturation was further confirmed by the differences observed between CD spectra recorded at 25 °C before and after thermal denaturation, which revealed a decrease in β-sheet structure and an increase in disordered segments following denaturation (Figure 29A).

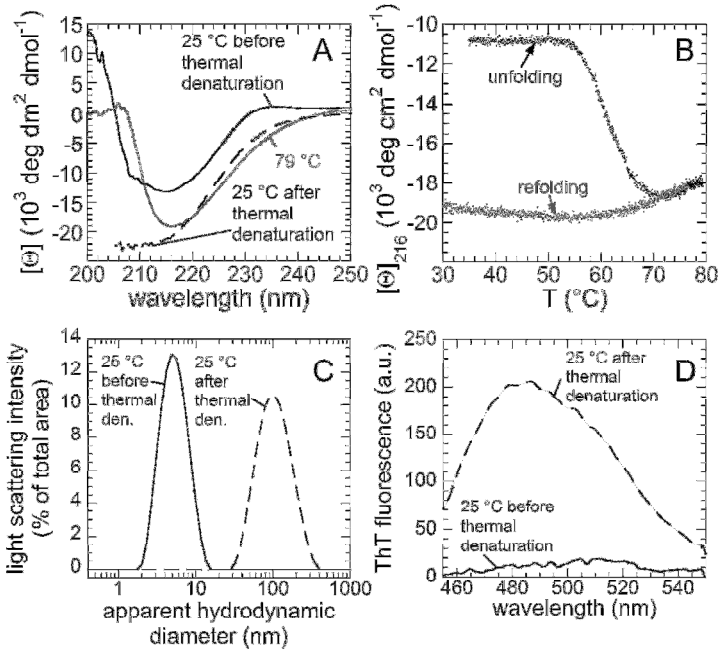

Figure 29 Thermal denaturation of M-TTR. (A) CD spectra of M-TTR recorded at different temperatures. Spectra are shown for the protein at 25 °C before (black continuous line) and after (black dashed line) thermal unfolding and for thermally unfolded protein at 79 °C (grey continuous line). (B) CD signal at 216 nm Vs temperature during unfolding (black) and refolding (grey). (C) DLS distribution of M-TTR before (continuous line) and after (dashed line) thermal denaturation. (D) ThT fluorescence measured at 25°C in the presence of M-TTR before (continuous line) and after (dashed line) thermal unfolding.

In order to get insight into this thermally unfolded state we investigated the process by means of DLS. DLS analysis revealed that M-TTR is prevalently monomeric before thermal denaturation, with an apparent hydrodynamic diameter of 4.5 ± 1.0 nm (Figure 29C), which is compatible with that determined with X-ray crystallography [Jiang, X et al.2001]. By contrast, M-TTR was converted into oligomers exhibiting an apparent hydrodynamic diameter of about 100 nm after thermal denaturation and cooling (Figure 29C). Unlike native M-TTR, these aggregated particles bound to the dye Thioflavin T (Figure 29D), a fact reminiscent of the presence of amyloid-like structure in the sample [Biancalana, M. et al.2010]The same set of experiments was repeated in the presence of 1.5 M urea so as to verify whether small amounts of the denaturant might be able to inhibit aggregation in the sample. However, the results showed that thermal denaturation of M-TTR is irreversible even in the presence of urea (Figure 30).

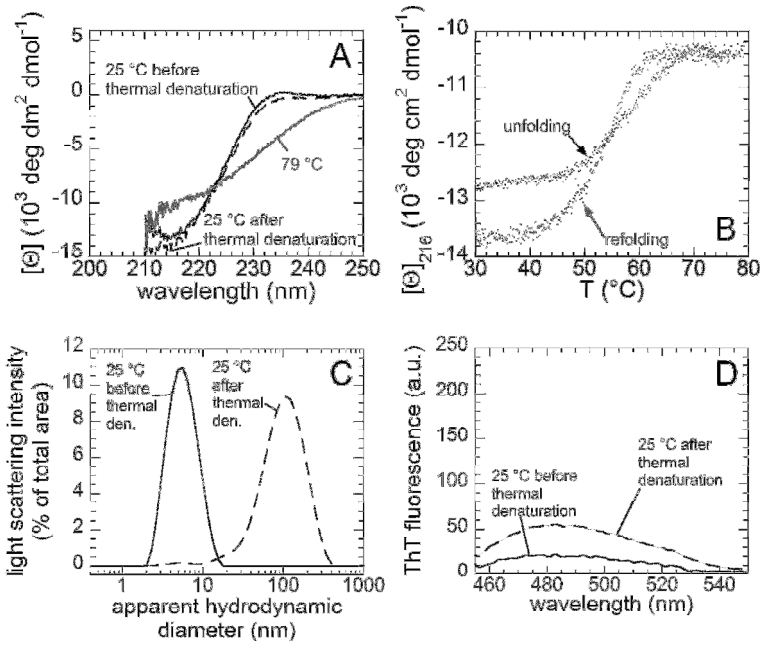

Figure 30 Thermal denaturation of M-TTR in phosphate buffer containing 1.5 M urea. (A) CD spectra of M-TTR recorded at different temperatures. Spectra are shown for the protein at 25 °C before (black continuous line) and after (black dashed line) thermal unfolding and for thermally unfolded protein at 79 °C (grey continuous line). (B) CD signal at 216 nm Vs temperature during unfolding (black) and refolding (grey). (C) DLS distribution of M-TTR at 25° C before (continuous line) and after (dashed line) thermal denaturation. (D) ThT fluorescence measured at 25° C in the presence of M-TTR before (continuous line) and after (dashed line) thermal unfolding.

Urea induced denaturation of M-TTR revealed a molten globule

Given the difficulties associated with studying M-TTR unfolding by means of thermally induced denaturation, we investigated the process by means of urea equilibrium titration experiments. Different probes were used for the analysis, namely CD in the far-UV to assess secondary structure changes and CD in the near–UV and tryptophan fluorescence to investigate tertiary structure. Spectra at urea concentrations ranging from 0 to 7.6 M and obtained with the three spectroscopic probes are shown in figure 31A, 31B and 31C; the corresponding unfolding traces (spectroscopic signal Vs [urea]) are shown in figure 32A, 32B and 32C while the corresponding native fraction plots are shown in Figure 31D. All probes indicated a major cooperative unfolding transition taking place between 2 and 4 M urea. Unfolding traces were analysed with a two-state transition model [Santoro, M. M.et al.1988] in order to determine thermodynamic parameters associated with conversion of the folded state (F) into the unfolded (U) state (Figure 31D and 31E). This analysis yielded values of conformational stability in the absence of denaturant ($\Delta G_{U-F}^{H_2O}$) of 4.8± 0.2, 5.2 ± 0.3 and 4.9 ± 0.2 kcal mol^{-1} for far-UV CD, near-UV CD and fluorescence, respectively and *m* values of 1.64 ± 0.10, 1.56 ± 0.10 and 1.63 ± 0.10 kcal mol^{-1} M^{-1} for far-UV CD, near-UV CD and fluorescence, respectively. The average $\Delta G_{U-F}^{H_2O}$ and *m* are 5.0 ± 0.2 kcal mol^{-1} and 1.61 ± 0.10 kcal mol^{-1}M^{-1}, respectively. These values are in reasonable agreement with those from similar experiments previously carried out under slightly different conditions (Jiang, X., et al.2001, Hurshman Babbes, A. R., et al. 2008).

Importantly, the analysis carried out with far-UV CD revealed the presence of a second transition located between 0 and 2.4 M urea and involving a remarkable change in CD signal between 195 nm and 210 nm (light grey region in Figure 31B).

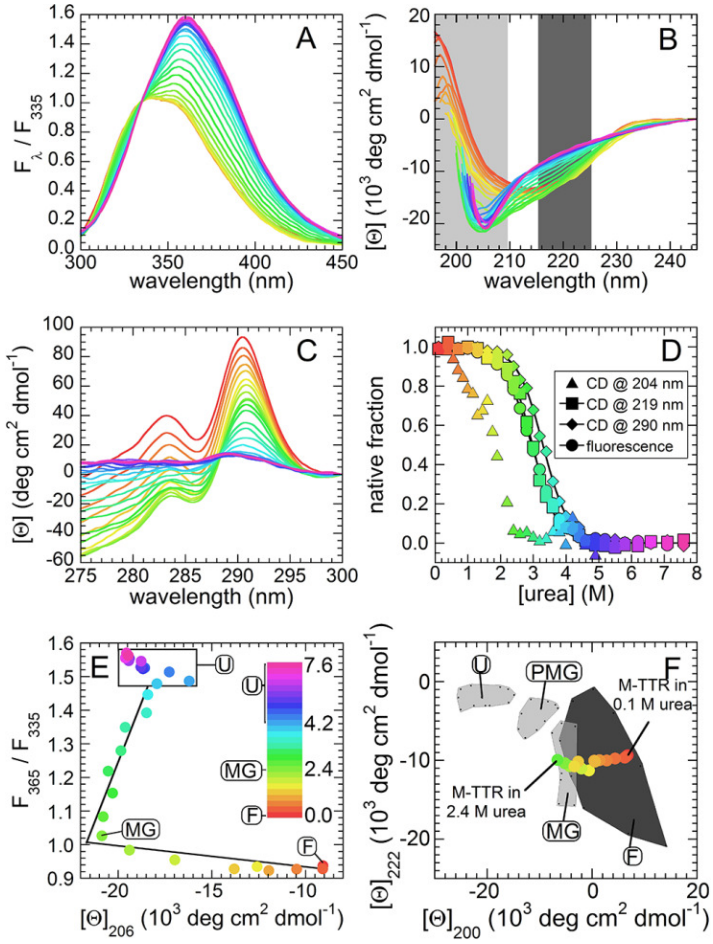

Figure 31 Urea induced denaturation of M-TTR, followed with several spectroscopic probes. The color scale refers to urea concentration according to the legend displayed in panel (E). (A) Equilibrium unfolding followed by intrinsic (tryptophan) fluorescence. Spectra are shownas ratio between fluorescence at a given wavelength λand that at 335 nm. (B)Equilibrium unfolding followed by far-UV CD, revealing two transitions: transition 1 is visible from 195 to 205 nm (light grey), andtransition 2 at 215-225 nm (dark grey).(C)Equilibrium unfolding followed by near-UV CD.(D) Native fraction as measured from best fits to a two state model of data reported in panel (A), (B) and (C).Tryptophan fluorescence (circles), CD at 219 nm (squares) and at 290 nm (diamonds) indicated a cooperative transition between 2 and 4 M urea, whereas CD at 204 nm illustrated a non-cooperative transition occurring between 0 and 2.4 M urea (triangles). (E) Phase diagram consisting of the plot of tryptophan fluorescence(F_{365}/F_{335})Vs CD signal at 206 nm; this analysis suggestedtwotransitions: (i) a transition from a fully folded state to a molten globular (MG) state; (ii) conversion of MGinto an unfolded (U) state. (F) Plot of CD signal at 222 nm Vs the signal at 200 nm: this analysis is able to distinguish between folded (F), unfolded (U), pre-molten globular (PMG) and molten globular (MG) states.

Comparison between near-UV and far-UV CD spectra of M-TTR in 0 M and 2.4 M urea indicated that in the latter condition the protein is folded in terms of tertiary structure but exhibits a decrease in β-sheet structure and an increase in random coil structure. Such a transition involving the F state and a hidden conformation could be investigated by plotting the signal at 204 nm *Vs* [urea] (Figure 31D and 32D). The obtained plot is reminiscent of a cooperative transition and illustrates that the second transition is well separated from the first one (Figure 31D and 32D). An exhaustive analysis of the thermodynamic parameters showed that the concentration of middle denaturation (C_m) depended on wavelength, a fact reminiscent of a non-cooperative transition. Although this effect might reflect the low signal to noise ratio observed below 200 nm, which limits the possibility of getting information at urea concentrations higher than 2 M, the present data do not allow assigning the transition as a cooperative one.

Thus, the two transitions can be recapitulated by a phase diagram approach [Kuznetsova, I. M et al. 2004]: indeed, the plot of a spectroscopic probe able to detect the first transition (e.g. the ratio of fluorescence at 365 and 335 nm) *Vs* a second probe able to detect the second transition (CD at 206 nm) illustrates that a hidden conformation forms along the unfolding pathway of M-TTR and is maximally populated at 2.4 M urea (Figure 31E). After the denaturation of such hidden conformation the unfolded state becomes populated.

In order to characterize the conformational ensemble dominant at 2.4 M urea we plotted the CD signal at 222 nm Vs the signal at 200 nm (Figure 31F). It was reported that such an analysis is able to distinguish between folded, unfolded and molten globular (MG) states [Uversky, V. N et al. 2004]. In the case of M-TTR the analysis revealed that, as denaturant concentration increases from 0 to 2.4 M, the protein moves from a folded zone to a predominantly molten globular region (Figure 29F). This interpretation was corroborated by near-UV CD spectra, which showed a slight decrease in the tryptophan peak at 290 nm and in the tyrosine peak at 283 nm (Figure 3C and S2C), a fact reminiscent of a more dynamic environment surrounding aromatic side chains [Kelly, S. M., et al.2005] . Thus, a transition F -> MG takes place before M-TTR undergoes a complete denaturation (MG -> U).

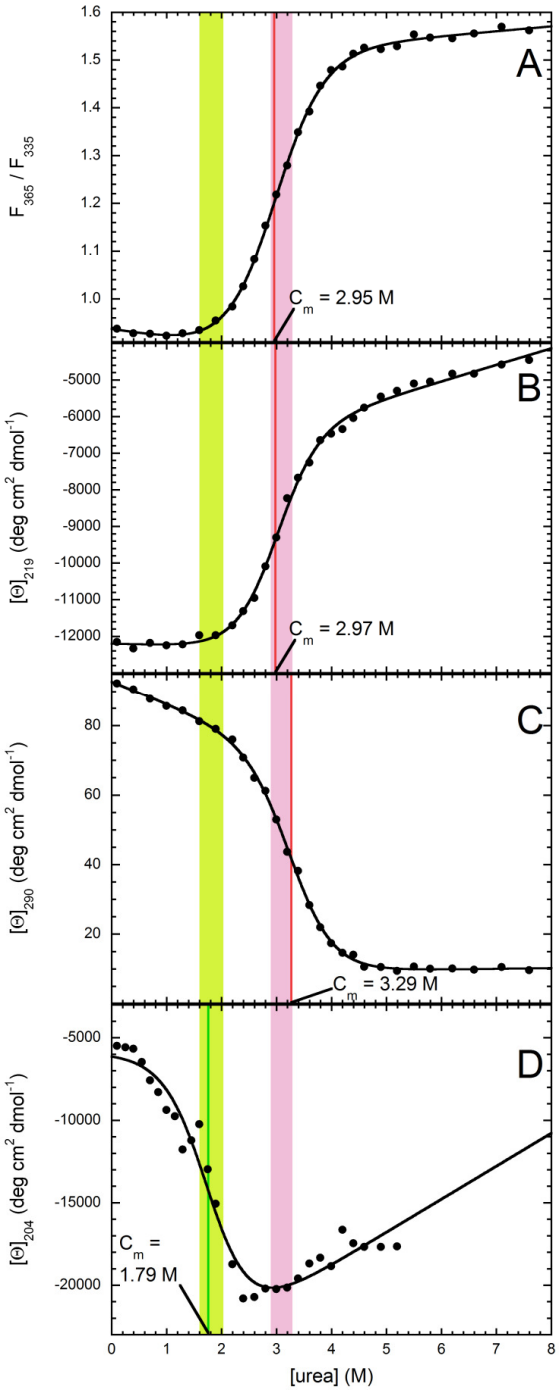

Figure 32 Urea induced denaturation followed with different spectroscopic probes, namely the ratio between tryptophan fluorescence at 365 and 335 nm (A), far-UV CD at 219 nm (B), near-UV CD at 290 nm (C) and far-UV CD at 204 nm (D). Data show that there are two transitions: the first one (highlighted in green) occurs at low urea concentration and has a C_m value of ~ 1.79 M; the second one (highlighted in pink) has a $C_m$value of roughly 3.1 M.

Folding and unfolding kinetics revealed a transiently populated state

We set out to investigate folding and unfolding kinetics of M-TTR by means of a stopped-flow device coupled to fluorescence or CD detection systems. Folding kinetics in the presence of 0.5 M urea involved a decrease in tryptophan fluorescence as M-TTR underwent refolding (Figure 33A). Such a decrease was complete after ca. 50 ms in 0.5 M urea. We gauged the signal of the unfolded protein under native conditions by linear extrapolation from measurements at high urea concentrations, where the protein is 100% unfolded (not shown). This analysis revealed that fluorescence of the unfolded state is significantly different than the signal at the beginning of the refolding kinetics. This suggested the occurrence of one further refolding phase within the dead-time of our stopped-flow experiments (Figure 33A). We will refer to the fast phase occurring in the dead-time of our stopped-flow experiments as to λ_1 and to the major refolding phase as to λ_2 (λ_2= 80 s-1 in the absence of denaturant). The occurrence of the fast λ_1 phase was further confirmed by other spectroscopic probes, such as ANS binding to characterize exposure to solvent of hydrophobic clusters (Figure 33B) and far-UV CD to assess secondary structure content (Figure 33C).The conformational state populated at the beginning of the refolding kinetics exhibited a higher ANS binding than the unfolded state, suggesting hydrophobic clusters partially exposed to the solvent (Figure 4B). The CD signal did not vary during refolding, indicating that the conformational state at the beginning of the refolding kinetics has a secondary structure similar to that of the folded state (Figure 33C). However, a dramatic change took place within the dead-time, as the unfolded state was found to lack any secondary structure (Figure 33C). Consequently, both ANS fluorescence and CD confirmed the occurrence of the fast λ_1 phase.

In order to get direct evidence of such a phase, we investigated M-TTR refolding by means of T-jump relaxation experiments using tryptophan fluorescence as a probe (Figure 33D). Results confirmed a rapid decrease in tryptophan fluorescence (λ_1), complete in ca. 10 ms. As expected, the time-scale of this process was within the dead-time of our stopped-flow experiments and was therefore masked in this latter case. Hence, T-jump relaxation kinetics provided direct evidence of the formation of a

transiently populated state. After λ_1 and λ_2 were complete, refolding of M-TTR followed by means of tryptophan fluorescence exhibited two more exponential phases (Figure 33E). The third and fourth phases were complete in ca. 2.5 s (λ3 = 2 s-1) and 30 s (λ4 = 0.15 s-1), respectively.

As far as unfolding is concerned, the process, monitored at urea concentration higher than 4 Mby means of tryptophan fluorescence, involved an increase in fluorescence (Figure 33F). Two exponential phases could be distinguished: the first phase was complete in ca. 50 ms in 5 M urea (inset of Figure 33F), which is on the same time-scale of similar experiments previously reported under slightly different conditions [Stéphan A. et al.2001]. The second phase lasted ca. 5 s (Figure 33F).

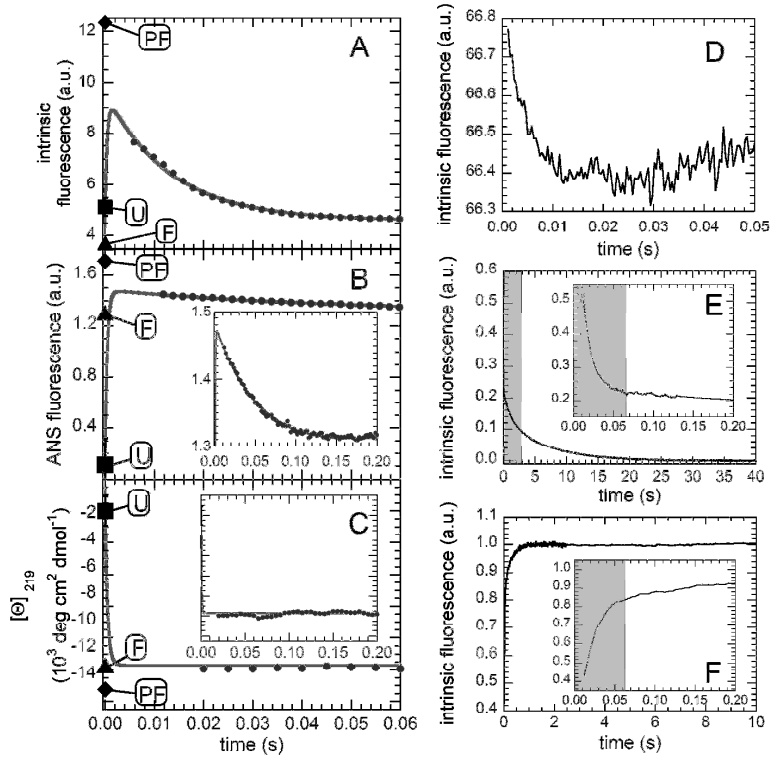

Figure 33 M-TTR refolding and unfolding kinetics, followed by means ofdifferent spectroscopic probes. (A-C) M-TTR refolding kinetics monitored by means ofdifferenttechniques: tryptophan fluorescence (A), ANS binding (B), far-UV CD (C). In each panel the spectroscopic probe was monitored in stopped-flow refolding experiments at 0.25 M urea. Signal for the folded (F), partially folded (PF) and unfolded states (U) are shown. Insets show the same kinetics up to 200 ms. (D) T-jump relaxation kinetics at 2.5 M urea illustrates the presence of a fast phase (λ_1), complete inca. 10ms.(E) Refolding kinetics in phosphate buffer with 0.5 M urea show that, after λ_1 and λ_2 are complete (grey zone in the inset) two slow phases can be detected, consistingin a further decrease in tryptophan fluorescence:λ_3, complete in ca. 2.5 s (grey zone in main panel) and λ_4, complete in ca. 40 s. (F) M-TTR unfolding kinetics, showing the occurrence of two phases, which are complete in ca. 50 ms (grey zone in the inset, λ_1) and 1 s (λ_2).

The transiently populated state is a partially folded off–pathway ensemble

We built the chevron plot for M-TTR (Figure 34A). In particular, T-jump experiments were carried out in the urea concentration range 0.5 – 4.5 M to obtain the plot of ln (λ_1) *Vs* [urea] (triangles in Figure 34A). Rate constants for the major folding/unfolding transition (λ_2) were obtained from best fits of experimental kinetic traces to multi-exponential equations and these values were used to build plot of ln (λ_2) *Vs* [urea] (circles in Figure 34A). The C_m value obtained from the analysis of this plot -calculated as the urea concentration at which extrapolated refolding and unfolding rate constants are equal- was in good agreement with that determined for the MG -> U transition observed at equilibrium. Indeed, kinetic and equilibrium experiments indicated C_m values of 3.2 ± 0.2 and 3.1 ± 0.2 M urea, respectively. However, a downward curvature could be observed in the folding limb of the plot. Such a deviation from the expected plot for a two state folder [Jackson, S. E et al. 1991] is usually referred to as roll-over [Matouschek, A., et al.1990, Ferguson, N et al.1999, Bemporad, F., et al.2004], and can be recapitulated in kinetic terms as follows. The extrapolated unfolding rate constant in the absence of denaturant was 1.82 s-1. Given the conformational stability obtained by equilibrium experiments the folding rate constant under the same conditions was expected to be ~ 6100 s-1 for a two state folder (Figure 34A). Refolding rate constant extrapolated by experimental data was ca. 81 s^{-1}, two orders of magnitude lower than the expected value.

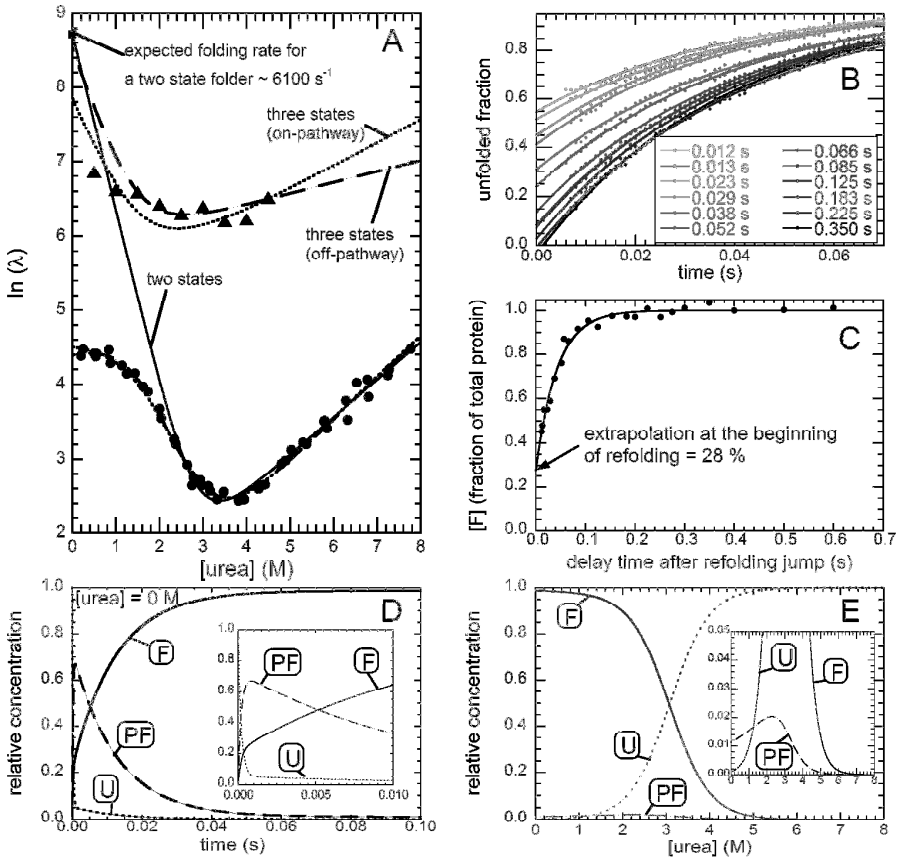

Figure 34 Characterization of the transiently populated state.(A) Natural logarithm of the observed folding/unfolding microscopic constants λ_1 (triangles) and λ_2(circles), plotted as a function of urea concentration (chevron plot). The refolding limb of the chevron plot deviates from linearity at urea concentrations lower than 2 M, where a downward curvature, generally referred to as "rollover," is observed. The continuous line represents the best fit of the data to the equation for a two-state transition. Dashed and dotted lines represents best global fits to three-state off-pathway and on-pathway models, respectively. (B-C)Interrupted refolding double jump experiment. The protein unfolded in 3M urea at pH 3.2 was first refolded by dilution into a refolding phosphate bufferat pH 7.4. After agiven delay time, the protein was denatured in a second jump through dilution into a solution containing 5 M urea at pH 7.4. (B)experimental traces obtained at different delay times (see legend); (C) calculated folded fraction Vsdelay time. The amount of folded protein present at the beginning of the refolding experiment was extrapolated from a single exponential fit. (D-E) Transient (D) and equilibrium (E) concentrations for the folded (F, continuous line), unfolded (U, dotted line) and partially folded (PF, dashed line) states according to the off-pathway model at 0 M urea (D) and plotted Vs urea concentration (E). Insets show magnifications to illustrate PF concentrations.

While roll-over in M-TTR chevron plot probably reflects the transient formation of a hidden conformation [Gianni, S et al. 2007], other interpretations were previously proposed for this phenomenon, including Hammond effect [Narita M er al. 1997] and aggregation artefacts [Zlokovic BV 1996]. We performed refolding kinetics at different [M-TTR] so as to detect possible aggregation phenomena occurring during refolding (figure 35A and 35B). Indeed, any intermolecular process would be affected by varying protein concentration. However, neither kinetic constants (Figure 35C) nor phase amplitudes (Figure 35D) obtained from best fits of experimental data to equation [Johnson, S. M., et al. 2012] significantly changed as [M-TTR] ranged from 0.007 to 0.07 mg ml^{-1} and this confirms that a conformational state different from the folded and unfolded states forms transiently during refolding of M-TTR.

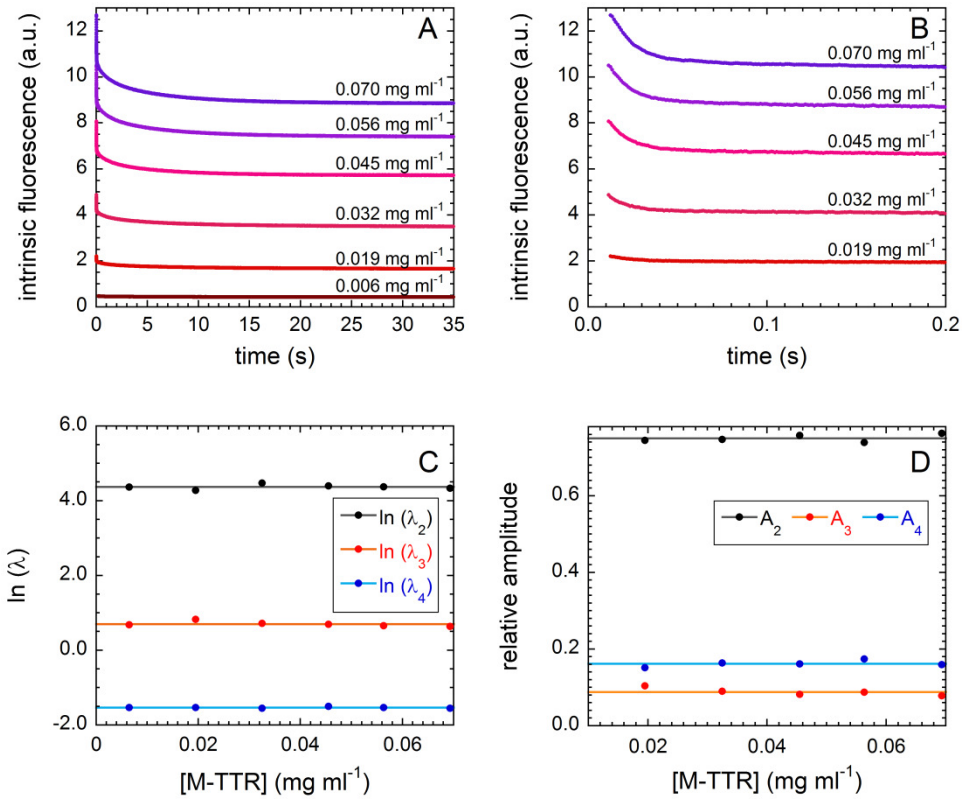

Figure 35 Folding traces obtained at different M-TTR concentrations. (A) Experimental traces; color ranges from red to purple as M-TTR concentration ranges from 0.5 to 5.1 µM. (B) Magnification of panel (A) to show the first refolding phase. (C) Natural logarithm of the three microscopic refolding rates plotted *Vs* protein concentration. (D) Relative amplitudes of refolding phases plotted *Vs* protein concentration. Panels (C) and (D) demonstrate that folding rates and relative amplitudes do not vary as protein concentration increases.

Folding slow phases arise from proline isomerism

Another important question to answer was the characterization of the two folding slow phasesλ3 and λ4(Figure 33E). The rate constants of such phases lacked dependence on urea concentration and this suggested that they could arise from proline isomerism [Schmid, F. X. 2001]. M-TTR possesses 8 X-Pro bonds (Fig 36), all populating a transconfiguration in the folded state [Jiang, X.et al. 2001, Palmieri Lde, C. et al. 2010].

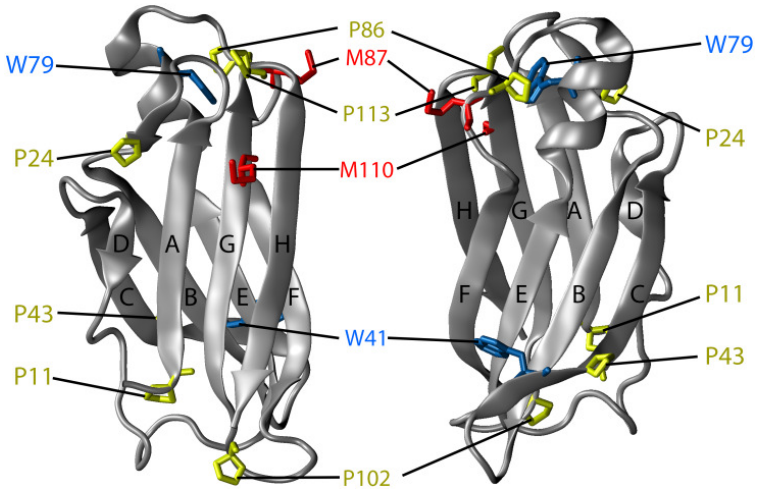

Figure 36 Front and back view of F87M/L110M TTR (M-TTR). Strands have been labelled to highlight topology. Mutated residues are labelled in red. Tryptophan side chains are labelled in blue. Proline residues are labelled in yellow. The figure was drawn using the PDB entry 1GKO(34).

To confirm this hypothesis, we performed folding kinetics experiments in the presence of cyclophilin A (cypA), a peptidyl-prolylisomerase that catalyses the *cis-trans* interconversion of X-Pro peptide bonds [Schmid, F. X. 2001]. While bovine cypA did not have any effect on M-TTR refolding (data not shown) human cypA was able to accelerate the process as enzyme concentration increased from 0 to 0.6 µM (Fig 37A). Analysis of the traces revealed that λ_2 was not affected by the presence of cypA whereas slow phases (λ_3 and λ_4) were both significantly accelerated (Figure 37B).

To further confirm the occurrence of proline isomerism during M-TTR refolding, interrupted unfolding double jump experiments were carried out. Briefly, M-TTR was first unfolded in 5 M urea and, after a delay time, refolded in 1 M urea. The rationale in this case is that by varying the delay time between the first (unfolding) and second (refolding) jump, one can vary the time the protein is allowed to refold. As proline isomerism requires several seconds to reach its equilibrium, slow phases are expected to decrease in amplitude and eventually disappear as delay time decreases. While the amplitude of the fast phase did not depend on delay time, those of the slow phases decreased as delay time decreased (Figure 37C). The plot of the amplitudes *Vs* delay time showed two exponential processeswhose amplitudessatisfactorily extrapolated to 0.00 ± 0.02 (A_3) and 0.04 ± 0.02 (A_4) when delay time is o (Figure 37D).

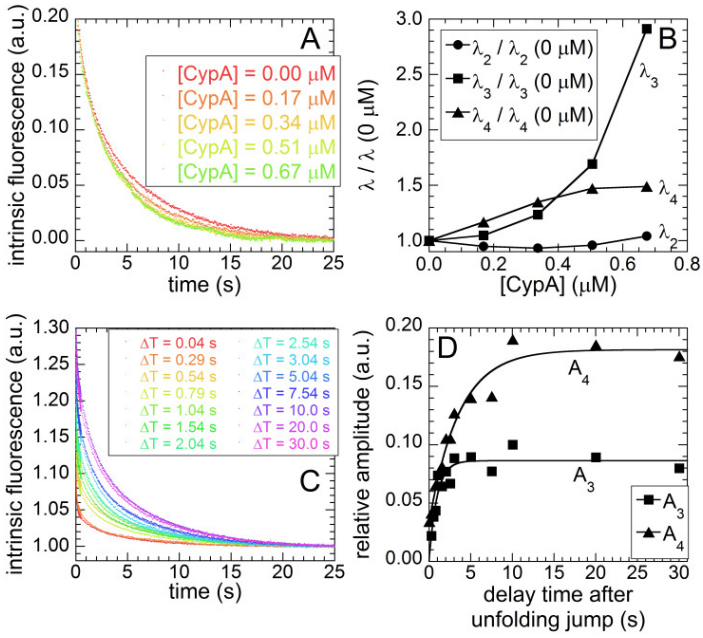

Figure 37 Characterization of M-TTR refolding slow phases (λ_3 and λ_4).(A) Effect of human CypA on M-TTR folding. The folding reaction was monitored in phosphate buffer containing 0.5 M urea,in the presence of increasing quantities of human CypA. Color refers to cypA concentration, according to the table shown in the figure.(B) Microscopic refolding rate constants reported as ratios of the value obtained for the different phases in the presence of CypA and the corresponding value in its absence. (C) Double jump interrupted unfolding experiment: the protein was first denatured ina phosphate buffer containing 5 M urea (first jump) and then, after a given delay time, refoldedin a phosphate buffer containing 1 M urea (second jump). Color refers to delay time, according to the table shown in the figure. (D) Plot displaying phase relative amplitudes obtained from best fits of experimental data to equation (1) *Vs* delay time. These traces were analyzed with a single exponential rise function(solid lines).

Kinetic constants obtained by fitting the data of A_3 and A_4*Vs* delay time to a single exponential functionwere in reasonable agreement with the values obtained from single jump refolding experiments under the same conditions.This corroborated the idea that both slow phasesarise from proline isomerism. However, it should be noticed that while λ_4 occurs on the typical time-scale for proline isomerism, λ_3 appears too fast for such process. It is therefore possible that only λ_4 should be attributed to proline isomerism while results for $\lambda_3$originate from partial overlapping of the two slow phases.

In order to assess whether the transiently populated state forming after the first fast phase of folding (λ_1) represented a true folding intermediate or rather a kinetic trap which is off the refolding pathway and slows down the bulk process, we analysed our chevron plot with on-pathway and off-pathway models [Gianni, S. et al 2007]. Results of such analysis are shown in Figure 34A and summarized in table 1. In principle, the analysis can discriminate between the two models because only the on-pathway model allows λ_2 to be higher than λ_1 in the absence of denaturant [Gianni, S. et al 2007, Bai, Y 1999]. If the experimental analysis shows that λ_2 is higher than λ_1, the off-pathway model can be ruled out. However, in the case of M-TTR, both models successfully interpreted data. Consequently, while the analysis yielded all the kinetic parameters for the refolding of M-TTR and the transient and equilibrium concentrations of the species involved in the process, it was not conclusivein terms of folding pathway.

In order to shed light on the on- or off-pathway nature of the transiently populated state, we performed an interrupted refolding double jump experiment [Haq, S. R et al.2010, Jemth, P. et al. 2004] In this experiment M-TTR was first unfolded in 3 M urea at pH 3.2 (Figure 38). It was then refolded in 1.5 M urea at pH 7.4 (first jump) and after a delay time unfolded back in 5 M urea at pH 7.4 (second jump). By varying the delay time after (Figure 34B)the first jump (refolding), one can vary the amount of protein undergoing unfolding in the second jump (unfolding), as described elsewhere Jemth, P. et al. 2004, Travaglini-Allocatelli, C. et al.2003]. Consequently,this experiment allowed the relative amount of native protein to be reconstructed during refolding time (Figure 34C). The rationale behind the approach is that only in the off-pathway model the

amount of native protein extrapolated at the beginning of the refolding experiment can be higher than 0. In the case of M-TTR, the extrapolated amount of native protein at the beginning of the refolding experiment was 28% (Figure 34C). Consequently, the transiently populated state is an off-pathway kinetic trap. Only after its denaturation the protein can convert into the correctly folded state.

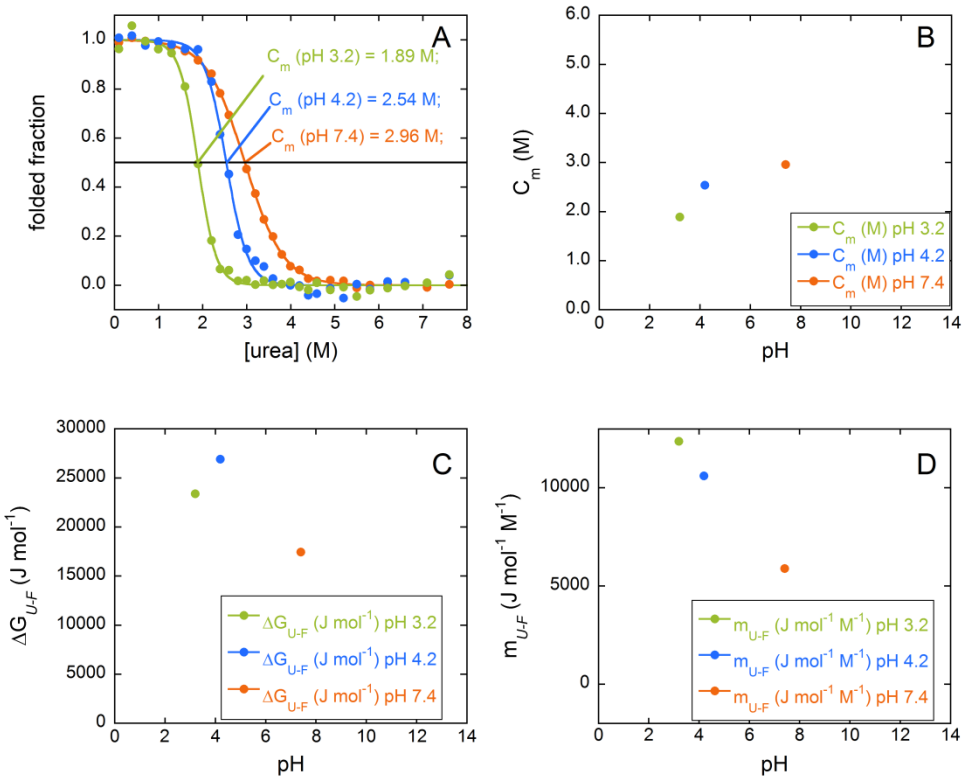

Figure 38 M-TTR equilibrium unfolding experiments monitored via tryptophan fluorescence at different pH values. In all panels green, blue and orange refer to data at pH 3.2, 4.2 and 7.4, respectively. (A) Folded fraction *Vs* urea concentration; C_m values are indicated. (B-D) Plots showing (B) the concentration of middle denaturation (C_m)*Vs* pH, (C) free energy change upon denaturation in the absence of denaturant ($\Delta G_{U-F}^{H_2O}$) *Vs* pH and (D) *m* value *Vs*pH.

The kinetic constants obtained from the off-pathway model were thus used to calculate transient and equilibrium concentrations of F, U and PF(Figure 34D and 34E) and the spectroscopic signals of PF (Figure 33A, 33B, 33C). Results revealed that the transiently populated state is hyperfluorescent relative to the fully folded state (Figure

33A), a fact reminiscent of an environment surrounding tryptophan side chains where quenching is lower. Furthermore, the transiently populated exhibits a higher ANS binding than the fully folded state (Figure 33B). However, its CD signal at 219 nm is comparable to that of the native state (Figure 33C). Consequently, the transiently populated state can be described as a partially folded (PF) conformation possessing secondary structure globally comparable to those of the fully folded state, some hydrophobic clusters exposed to solvent and some non-native contacts that must be dismantled before M-TTR can convert into the fully folded state.

Results IV: TDP-43 inclusion bodies formed in bacteria are structurally amorphous, non-amyloid and inherently toxic to neuroblastoma cells

Accumulation of ubiquitin-positive, tau and α-synuclein-negative intracellular inclusions of TDP-43 in the central nervous system represents the major hallmark correlated to amyotrophic lateral sclerosis and frontotemporal lobar degeneration with ubiquitin-positive inclusions. Such inclusions have variably been described as amorphous aggregates or more structured deposits having an amyloid structure. Following the observations that bacterial inclusion bodies generally consist of amyloid aggregates, we have overexpressed full-length TDP-43 and C-terminal TDP-43 in *E. coli*, purified the resulting full-length and C-terminal TDP-43 containing inclusion bodies (FL and Ct TDP-43 IBs) and subjected them to biophysical analyses to assess their structure/morphology. We show that both FL and Ct TDP-43 aggregates contained in the bacterial IBs do not bind amyloid dyes such as thioflavin T and Congo red, possess a disordered secondary structure, as inferred using circular dichroism and infrared spectroscopies, and are susceptible to proteinase K digestion, thus possessing none of the hallmarks for amyloid. Moreover, atomic force microscopy revealed an irregular structure for both types of TDP-43 IBs and confirmed the absence of amyloid-like species after proteinase K treatment. Cell biology experiments showed that FL TDP-43 IBs were able to impair the viability of cultured neuroblastoma cells when added to their extracellular medium and, more markedly, when transfected into their cytosol, where they are at least in part ubiquitinated and phosphorylated. These data reveal an inherently propensity of TDP-43 to form amorphous aggregates, which possess, however, an inherently ability to cause cell dysfunction. This indicates that a gain of toxic function caused by TDP-43 deposits is effective in TDP-43 pathologies, in addition to possible loss of function mechanisms originating from the cellular mistrafficking of the protein.

Aggregation of FL TDP-43 and Ct TDP-43 in IBs of E. coli cells

The cDNA encoding FL TDP-43 and Ct TDP-43 were cloned downstream of the GST gene in the pGEX-2T plasmid. XL1-Blue cells of *E. coli* were then transformed with the two resulting engineered plasmids.

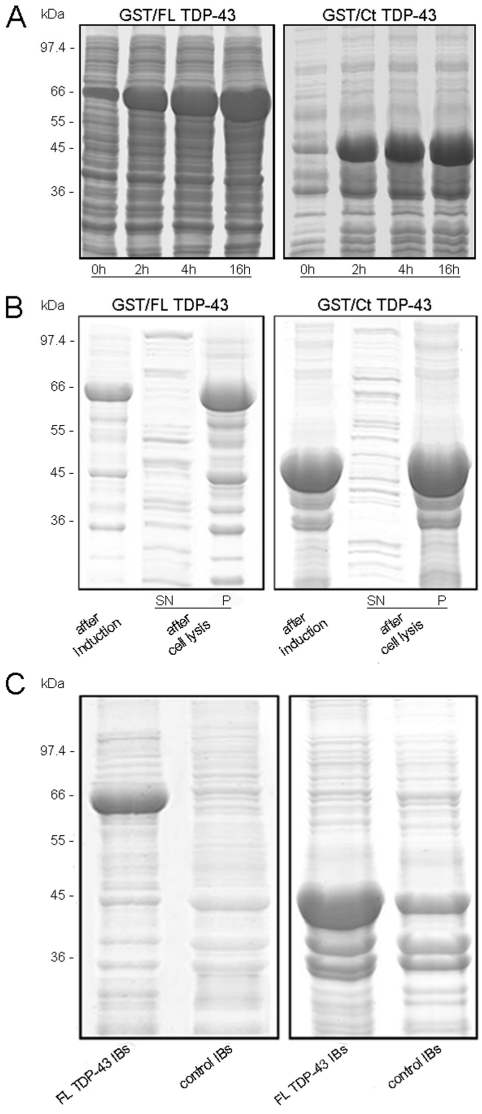

Figure 39. FL and Ct TDP-43 expression in *E. coli* cells. (A) SDS-PAGE analysis of bacterial proteins at different GST/FL TDP-43 (left) and GST/Ct TDP-43 (right) induction times (0 h, 2 h, 4 h and 16 h) with 1 mM IPTG at the temperature of 37 °C. The band at ~ 69 kDa indicates GST/FL TDP-43 (left) and that at ~ 46 kDa represents GST/Ct TDP-43 (right). (B) SDS-PAGE analysis of total bacterial proteins after GST/FL TDP-43 (left) and GST/Ct TDP-43 (right) inductions with 1 mM IPTG for 16 h at 37 °C and of the P and SN fractions of the same samples after cell lysis. (C) SDS-PAGE analysis of purified FL TDP-43 IBs, Ct TDP-43 IBs and control IBs obtained with 1 mM IPTG expression for 16 h at 37 °C. The bands at ~ 69 kDa and ~ 46 kDa indicates the GST/FL TDP-43 and GST/Ct TDP-43 proteins, respectively, that are absent in the control IBs sample.

To test whether bacterial cells expressed the fusion GST/FL TDP-43 protein, we evaluated the expression at 37 °C with 1 mM IPTG concentration and using SDS-PAGE (Fig. 39A).

The GST/FL TDP-43 band corresponds to a molecular weight of ~ 69 kDa, i.e. the sum of the molecular weights of GST (~ 26 kDa) and FL TDP-43 (~ 43 kDa). Immediately before adding IPTG (0 h), a basal protein expression was present. At 2 h and 4 h from induction a greater quantity of expressed protein was evident. However, the major expression of the fusion protein was observed at 16 h. The same conditions were used to evaluate the bacterial expression of the fusion GST/Ct TDP-43 protein. A similar expression level to that of the GST/FL TDP-43 protein was observed by SDS-PAGE, with a band corresponding to a molecular weight of ~ 46 kDa, that is the sum of the molecular weights of GST (~ 26 kDa) and Ct TDP-43 (~ 20 kDa) (Fig. 39A).

After cell growth for 8 h and protein expression for 16 h at 37 °C, the bacteria cells were harvested, lysed and centrifuged and the resulting supernatant (SN) and *pellet* (P) were analysed by SDS-PAGE (Fig. 39B). Both GST/FL TDP-43 and GST/Ct TDP-43 were found entirely in the P fraction indicating that they precipitated in IBs (Fig. 39B). Bacterial IBs have been shown to contain amyloid-like aggregates, as determined with CR and ThT binding, FTIR, X-ray diffraction, AFM and transmission electron microscopy (TEM) [Wang L et al 2008, Sabaté R et al 2009, García Fruitós E et al 2011, de Groot NS et al 2009, Wang L 2009, Gatti-Lafranconi P et al. 2011]. The presence of residual native-like structures and disordered chain segments has also been described, their content depending on the particular IB-forming protein [Oberg K, et al.1994, Przybycien TM et al. 1994, Fink AL 1998, Umetsu M et al 2004, Ventura S et al.2006]. Therefore, bacterial IBs are a physiological system consisting of several types of protein aggregates, both amyloid and amorphous, depending on the aggregating proteins. Thus, the aggregation of GST/FL TDP-43 and GST/Ct TDP-43 into IBs offered the possibility of investigating whether full-length TDP-43 or its C-terminal fragment have the propensity to form amyloid or other forms of self-assembly when aggregating in the highly crowded environment existing in a living organism.

The IBs formed from cells expressing GST/FL TDP-43 (FL TDP-43 IBs), GST/Ct TDP-43 (Ct TDP-43 IBs) and GST (control IBs) were purified as described in *2.3*. Using a

densitometric analysis of the SDS-PAGE bands we evaluated that the GST/FL TDP-43 band was 29 ± 3% of all proteins present in FL TDP-43 IBs (Fig. 39C), while the GST/Ct TDP-43 band was 32 ± 2.9% of all proteins present in Ct TDP-43 IBs (Fig. 39C). Therefore, for all the biophysical data present in this work, we analysed TDP-43 IBs with a total protein concentration higher than that present in control IBs by ~ 30%, so that the three IBs samples contained the same amount of proteins distinct from TDP-43. Using this approach, it was possible to evaluate the contribution of TDP-43 relative to other proteins present in IBs by difference, for example by subtracting the FTIR spectrum of control IBs from that of FL TDP-43 IBs or from that of Ct TDP-43 IBs.

FL TDP-43 and Ct TDP-43 aggregates do not bind CR and ThT

We used the amyloid diagnostic CR dye to assess whether FL TDP-43 and Ct TDP-43 contained in IBs display typical amyloid properties.

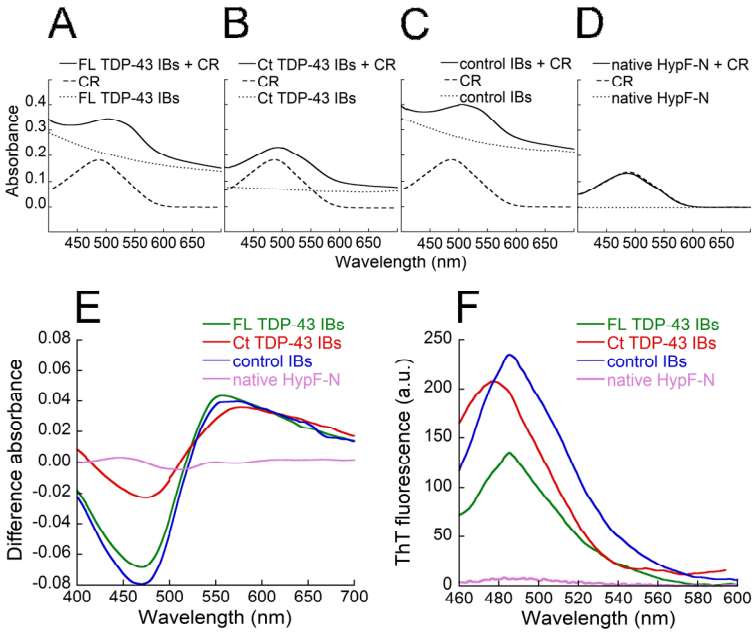

Figure 40. CR and ThT binding of FL TDP-43 IBs, Ct TDP-43 IBs and control IBs. (A) Absorbance spectra of FL TDP-43 IBs + CR (solid line), CR (dashed line) and FL TDP-43 IBs (dotted line). (B) Absorbance spectra of Ct TDP-43 IBs + CR (solid line), CR (dashed line) and Ct TDP-43 IBs (dotted line). (C) Absorbance spectra of control IBs + CR (solid line), CR (dashed line) and control IBs (dotted line). (D) Absorbance spectra of native HypF-N + CR (solid line), CR (dashed line) and native HypF-N (dotted line). (E) Difference absorbance spectra obtained for FL TDP-43 IBs (green), Ct TDP-43 IBs (red), control IBs (blue) and native HypF-N (purple). (F) ThT fluorescence spectra in the presence of FL TDP-43 IBs (green), Ct TDP-43 IBs (red), control IBs (blue) and native HypF-N (purple).

The CR absorbance increased in the presence of FL TDP-43 IBs and the wavelength of maximum absorption red-shifted to ~ 508 nm (Fig. 40A). This spectral change was very similar to that observed in the presence of control IBs (Fig. 40C).

The CR absorbance increased also in the presence of Ct TDP-43 IBs, although less markedly than in the presence of FL TDP-43 IBs, with a maximum absorption at ~ 495 nm (Fig. 40B). Spectral changes of CR were not observed in the presence of native HypF-N, used here as a soluble protein and, thus, as a negative control (Fig. 40D). For the three IBs samples, the difference spectrum obtained subtracting the CR spectrum and the IBs spectrum from the CR spectrum in the presence of IBs, showed a characteristic peak at ~ 550 nm, typical of CR bound to amyloid aggregates (Fig. 40E). By contrast, the difference spectrum obtained by subtracting the CR spectrum and the native HypF-N spectrum from the CR spectrum in the presence of native HypF-N was flat (Fig. 40E). The observation that the difference spectra obtained with FL TDP-43 IBs, Ct TDP-43 IBs and control IBs are superimposable at ~550 nm, indicates that TDP-43 does not seem to contribute to the amyloid-like structures present in IBs.

We then analyzed the capacity of the same samples to bind the ThT dye and increase its fluorescence. FL TDP-43 IBs increased the ThT fluorescence less markedly than control IBs, although this difference was not statistically significant ($p>0.05$); moreover, Ct TDP-43 increased the ThT fluorescence similarly to control IBs (Fig. 40F). Hence, the ThT assay confirms that the FL and Ct TDP-43 aggregates present in IBs do not have an amyloid-like structure (Fig. 40F). As expected, no ThT fluorescence increase was observed in the presence of non-aggregated native HypF-N (Fig. 40F).

As a positive control for *E. coli* IBs containing amyloid-like aggregates, we purified IBs formed after expression of the second acylphosphatase from D. melanogaster (AcPDro2), a protein previously shown to form amyloid-like fibrils in vitro [Powers JM et al.1981]. In particular, we purified IBs formed after expression of the destabilised C43S mutant of the protein (C43S AcPDro2 IBs), since the wild-type protein was soluble after expression and the resulting IBs contained little protein (wt AcPDro2 IBs). Unlike the wt AcPDro2 IBs, the C43S AcPDro2 IBs were found to bind CR, with a maximum at ~ 550 nm in the difference spectrum, and to bind ThT, with a remarkable increase of its fluorescence (Fig. 41).

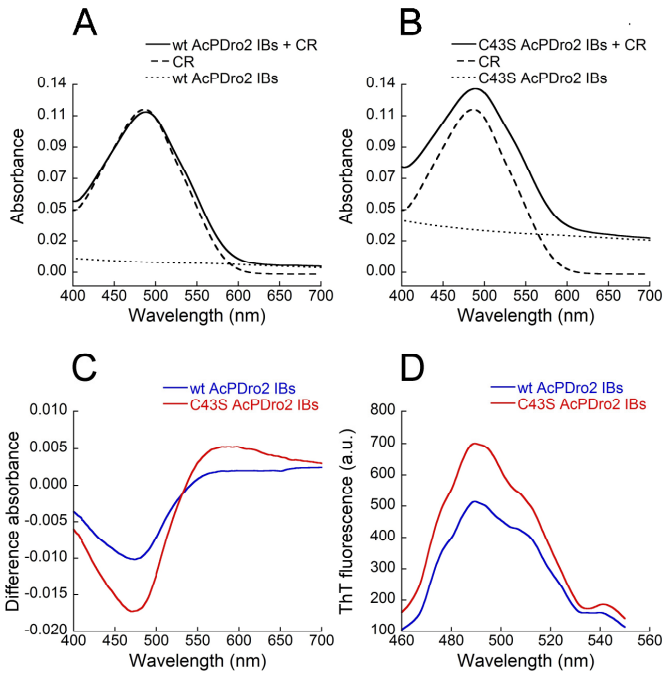

Figure 41. CR and ThT binding of wt AcPDro2 IBs and C43S AcPDro2 IBs. (A) Absorbance spectra of wt AcPDro2 IBs + CR (solid line), CR (dashed line) and wt AcPDro2 IBs (dotted line). (B) Absorbance spectra of C43S AcPDro2 IBs + CR (solid line), CR (dashed line) and C43S AcPDro2 IBs (dotted line). (C) Difference absorbance spectra obtained for wt AcPDro2 IBs (blue) and C43S AcPDro2 IBs (red). (D) ThT fluorescence spectra in the presence of wt AcPDro2 IBs (blue) and C43S AcPDro2 IBs (red). The CR and ThT analyses show that IBs containing the destabilised and amyloidogenic C43S mutant of AcPDro2 bind CR and ThT more markedly than IBs formed after expression of the less stable and less amyloidogenic wt AcPDro2. The C43S AcPDro2 IBs, therefore, can act as a positive control showing the presence of amyloid-like aggregates in IBs arising from the expressed protein

FL TDP-43 and Ct TDP-43 aggregates are composed of a random coil structure

Amyloid fibrils are closely associated with a β-sheet content that can be typically detected with either far-UV CD, FTIR or X-ray fiber diffraction. The CD spectra obtained in the presence of FL TDP-43 IBs and control IBs display a negative peak at ca. 220-230 nm and a positive peak at ca. 190-200 nm (Fig. 42A), which is typical of large aggregates containing amyloid fibrils [Nyrkova IA et al.2000, Sicorello A et al.2009]. The difference spectrum between them discloses the secondary structure of FL TDP-43 aggregates wherein the presence of a random coil structure is evident, as shown by a negative peak at ~ 198 nm (Fig. 42A). A similar result was obtained with Ct TDP-43 IBs and control IBs, with the CD spectra displaying a negative peak at ~ 230 nm and a

positive peak below 197 nm (Fig. 42B). Similarly to the result obtained with FL TDP-43 aggregates, a largely random coil structure emerges from the difference spectrum, with a negative peak at ca. 198 nm (Fig. 42B).

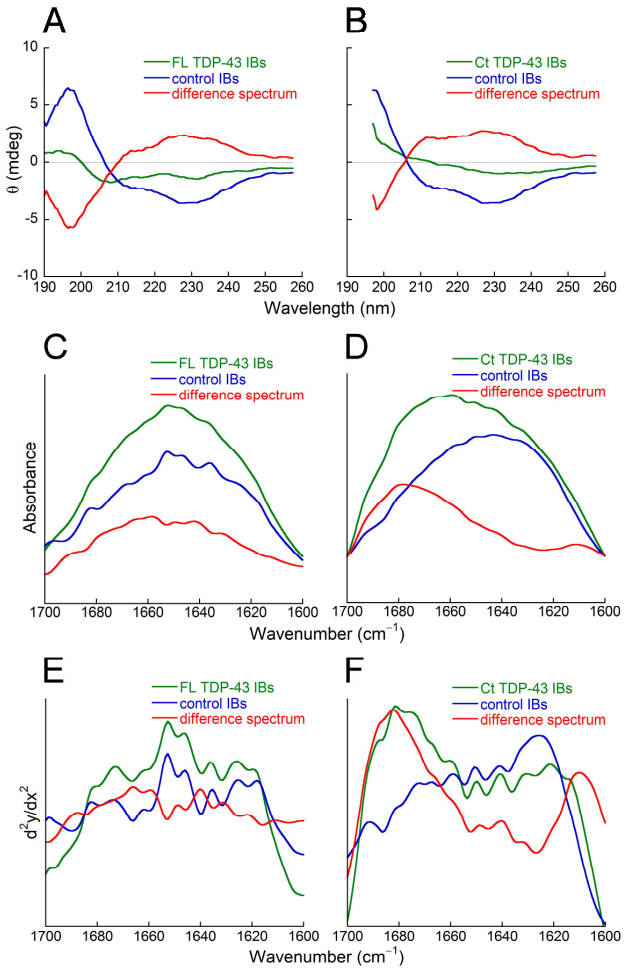

Figure 42. Secondary structure analysis of FL TDP-43 IBs, Ct TDP-43 IBs and control IBs. CD spectra (A,B), amide I regions of FTIR spectra (C,D) and second derivative of FTIR spectra (E,F) of FL TDP-43 IBs (A,C,E) and Ct TDP-43 IBs (B,D,F). In both analyses, the spectra are those of TDP-43 IBs (green), control IBs (blue) and difference spectra obtained subtracting the latter from the former (red).

The Amide I regions of FTIR spectra of FL TDP-43 IBs and control IBs obtained in D_2O, as well as their second derivative spectra, display a prominent peak at ~ 1650 cm^{-1} corresponding to α-helix and unordered structures, another peak at ~ 1675 cm^{-1} corresponding to β-turn structure and the characteristic peak at ~ 1625 cm^{-1} associated with the presence of intermolecular β-sheet structures (Fig. 42C,E). The

difference spectrum obtained from them shows two major bands at ~ 1667 cm^{-1}, corresponding to β-turn structure, and ~ 1640 cm^{-1}, corresponding to unordered structure for an FTIR spectrum obtained in D_2O (Fig. 42C,E). Importantly, the difference spectrum shows a clear disappearance of the peak in the intermolecular β-sheet region (Fig. 42C,E), providing further evidence for the lack of β-sheet structure and presence of disordered structure in the FL TDP-43 aggregates present in IBs.

The Amide I region of the FTIR spectrum of Ct TDP-43 IBs in D_2O and its second derivative, along with those of control IBs obtained concomitantly, display a similar peak at ~ 1650 cm^{-1} associated with α-helix and unordered structures (Fig. 42D,F). Besides, Ct TDP-43 IBs spectra show a prominent peak at ~ 1680 cm^{-1} associated with β-turn structure and a secondary peak at ~ 1620 cm^{-1} corresponding to intermolecular β-sheet structures, while control IBs spectra show the major peak at ~ 1620 cm^{-1} indicating the presence of intermolecular β-sheet structures and a smaller peak at ~ 1670 cm^{-1} associated with β-turn structure (Fig. 42D,F). The difference spectrum obtained from them shows a major peak at ~ 1680 cm^{-1} associated with β-turn structure and another smaller peak at ~ 1645 cm^{-1} corresponding to unordered structure (Fig. 42D,F). Again, the difference spectrum shows no peaks in the intermolecular β-sheet region, indicating a largely disordered structure in the Ct TDP-43 aggregates present in IBs.

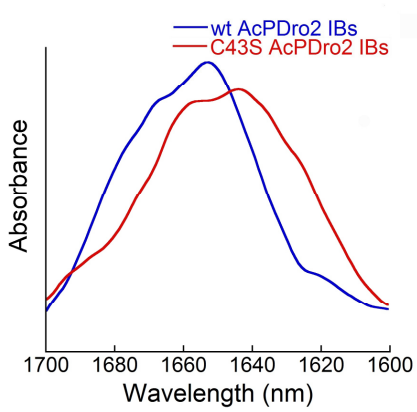

Figure 43. Amide I regions of FTIR spectra of wt AcPDro2 IBs (blue) and C43S AcPDro2 (red)**.** The analysis shows that IBs containing the destabilised and amyloidogenic C43S mutant of AcPDro2 have a large amount of β-sheet structure with respect to IBs formed after expression of the less stable and less amyloidogenic wt AcPDro2. The C43S AcPDro2 IBs, therefore, can act as a positive control showing the presence of amyloid-like aggregates in IBs arising from the expressed protein, confirming the CR and ThT analyses.

The amide I region of the FTIR spectrum obtained with C43S AcPDro2 IBs, used here as a positive control for bacterial IBs containing amyloid-like aggregates, features a remarkable peak in the β-sheet region, unlike the wt AcPDro2 IBs, indicating the presence of a largly β-sheet structure in the C43S AcPDro2 aggregates (Fig. 43).

PK digests FL TDP-43 and Ct TDP-43 aggregates contained in IBs

PK is a protease usually used to map the protected core of amyloid fibrils because it is highly active against peptide bonds of globular and disordered proteins, but it cannot attack the highly packed backbones in amyloid β-sheet structures [Hughes SR et al.1998]. Both FL TDP-43 IBs and Ct TDP-43 IBs were treated with 20 μg/mL of PK and their protein content was analyzed using SDS-PAGE. At this PK concentration a fast cleavage of FL TDP-43 was observed, with its band disappearing after 5 min of incubation (Fig. 44A,B). A fast cleavage was also observed for Ct TDP-43 (Fig. 44C,D). In this case the Ct TDP-43 band does not seem to disappear completely after 20 min of incubation, but it is reasonable to assume that the apparent remaining band was associated with an *E. coli* protein present in IBs having a molecular weight superimposed to that of Ct TDP-43 (compare Ct TDP-43 IBs and control IBs in Fig. 39C). FL TDP-43 IBs were also treated with a higher PK concentration (250 μg/mL), which induced a rapid disappearance after only 120 s (Fig. 44E,F). Other *E. coli* proteins present in TDP-43 IBs were susceptible to the action of PK, but they were generally more resistant, indicating the presence of amyloid-like structures in the IBs (Fig. 44A-F). Thus, these data confirm further the absence of an amyloid core in the FL TDP-43 and Ct TDP-43 aggregates contained in IBs.

The higher PK concentration (250 μg/mL) was also utilized for treating both FL TDP-43 IBs and control IBs and follow the decrease in the turbidimetry signal at 350 nm (Fig. 4G). At time zero the turbidimetry caused by FL TDP-43 IBs was greater than that of control IBs, because of the 30% protein concentration difference present in FL TDP-43 IBs relative to control IBs. A time dependent decrease in the absorbance value was found to occur for both FL TDP-43 IBs and control IBs, due to digestion of non-amyloid aggregates. After 140 s the two curves were apparently superimposable and reached gradually a plateau. This implies that the FL TDP-43 aggregates were entirely digested

by PK within 140 s, confirming the absence of a PK-resistant cross-β organization in these aggregates.

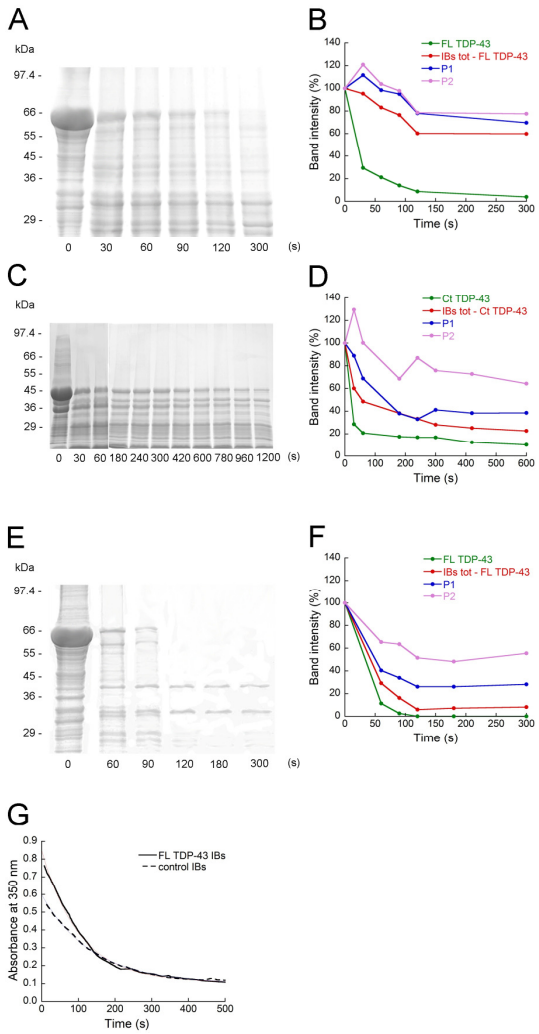

Figure 44. PK proteolysis of FL TDP-43 IBs, Ct TDP-43 IBs and control IBs**.** (A) SDS-PAGE of FL TDP-43 IBs after incubation with PK at the indicated times. The temperature was 37 °C, the total protein concentration of FL TDP-43 IBs was 14.3 mg/mL and the PK concentration was 20 µg/mL. The band at ~ 69 kDa indicates GST/FL TDP-43. (B) Corresponding densitometric analysis graph of SDS-PAGE bands representing FL TDP-43 (green), proteins other than FL TDP-43 (red) and two *E. coli* proteins labeled P1 and P2 (blue and purple). (C) SDS-PAGE of Ct TDP-43 IBs after incubation with PK at the indicated times. Conditions were as in panel A. The band at ~ 46 kDa indicates GST/Ct TDP-43. (D) Corresponding densitometric analysis graph of SDS-PAGE bands representing Ct TDP-43 (green), proteins other than Ct TDP-43 (red) and two *E. coli* proteins labeled P1 and P2 (blue and purple). (E) SDS-PAGE of FL TDP-43 IBs after incubation with PK at the indicated times. The temperature was 37 °C, the total protein concentration of FL TDP-43 IBs was 14.3 mg/mL and the PK concentration was 250 µg/mL. (F) Corresponding densitometric analysis graph of SDS-PAGE bands representing FL TDP-43 (green), proteins other than FL TDP-43 (red) and two *E. coli* proteins labeled P1 and P2 (blue and purple). (G) Kinetics at 37 °C of PK digestion of FL TDP-43 IBs and control IBs monitored by turbidimetry at 350 nm. The total protein concentration for FL TDP-43 IBs and control IBs was 14.3 mg/mL and 10 mg/mL, respectively, and the PK concentration was 250 µg/mL.

FL TDP-43 IBs, Ct TDP-43 IBs and control IBs appear morphologically irregular

AFM was used to investigate the morphology of FL TDP-43 IBs, Ct TDP-43 IBs and control IBs. All IBs samples appeared as irregular structures with heights of 33 ± 2 nm for FL TDP-43 IBs (Fig. 45A), 36 ± 3 nm for Ct TDP-43 IBs (Fig. 45B) and 32 ± 2 nm for control IBs (Fig. 45C). Such structures were formed by a variable number of disk or crescent-shaped subunits having a height of 7-8 nm (Fig. 45A-C). After 1 h digestion with 20 µg/mL PK all IBs were proteolysed and only a large number of small structures having a height of ~ 3 nm remained in the samples (as exampled by FL TDP-43 IBs digestion reported in Fig. 45D), possibly representing small aggregates of the lipids and polypeptides that are known to be present in bacterial IBs [Valax P et al 1993, Jürgen B et al.2010, Maachupalli-Reddy J et al.1997]. Interestingly, the absence of fibrillar structures after PK treatment indicates that the TDP-43 aggregates present in the IBs are not amyloid-like. Moreover, although the ThT and CR assays, as well as CD and FTIR spectra, show the existence of amyloid aggregates in both FL TDP-43 IBs and Ct TDP-43 IBs and arising from non-TDP-43 proteins, AFM imaging after PK digestion reveals that such structures are unstable and less packed and organized then the known amyloid aggregates.

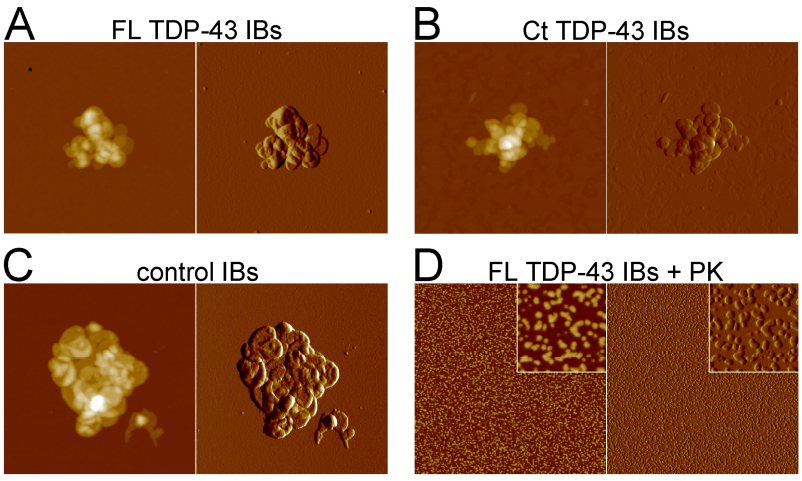

Figure 45. Morphology of FL TDP-43 IBs, Ct TDP-43 IBs and control IBs observed with AFM**.** (A-C) FL TDP-43 IBs, Ct TDP-43 IBs and control IBs, respectively. The scan size is 2 µm. (D) FL TDP-43 IBs after 1 h incubation with 20 µg/mL PK. The scan size is 2 µm. The inset shows a detail of the main panel at higher magnification (scan size 250 nm). In all panels left and right images represent height and amplitude data, respectively. Z range: 130 nm (A), 100 nm (B), 90 nm (C), 10 nm (D).

Transfected FL TDP-43 IBs are toxic to cultured neuronal cells

FL TDP-43 IBs and control IBs were also tested for their ability to cause cellular dysfunction in cultured neuroblastoma SH-SY5Y cells. Both forms of IBs were used to transfect the cells by means of the PULSin protein delivery reagent (Polyplus-transfection, Illkirch, France), which contains a cationic amphiphilic molecule thus facilitating the entry of the IBs in the cellular cytoplasm. In a first experiment, carried out to verify directly the presence of the FL TDP-43 IBs inside the cytoplasm following transfection, FL TDP-43 IBs were labeled with 5-FITC and then used to transfect the cells. The images obtained with confocal microscopy show the presence of abundant exogenous TDP-43 aggregates in the cytoplasm, indicating the high yield of FL TDP-43 IBs transfection (Fig. 46A).

In another set of experiments, both FL TDP-43 IBs and control IBs were used to transfect the cells and the presence of FL TDP-43 in the transfected cells was assessed using anti-TDP-43 polyclonal antibodies. Untreated (non-transfected) cells showed the presence of abundant TDP-43 in the nuclei, as expected for cells expressing endogenous TDP-43 which has a nuclear localization signal (Fig. 46B). Cells transfected with control IBs showed a similar high abundance of endogenous TDP-43 in the nuclei, whereas cells transfected with FL TDP-43 IBs showed a combination of nuclear endogenous TDP-43 and exogenous cytoplasmic TDP-43 (Fig. 46B). Cells were also transfected with R-PE, a green fluorescent protein used as a positive control and indeed shown to be present abundantly in the cytoplasm following transfection (Fig. 46B).

The viability of SH-SY5Y cells treated with FL TDP-43 IBs and control IBs was assessed by measuring their ability to reduce MTT, their levels of intracellular ROS and their caspase-3 activity. All such tests are widely used to assess the toxicity of TDP-43 expressed in eukaryotic cell cultures [Guo W et al.2011, Duan W et al.2010, Liu-Yesucevitz L al.2010]. In all such tests, cells treated with control IBs were found to be less viable than untreated cells, which are cells treated with the transfection mix only (Fig. 46C-E). However, a significantly lower level of viability was found in cells treated

with FL TDP-43 IBs, showing that the presence of FL TDP-43 in the IBs increases their toxicity.

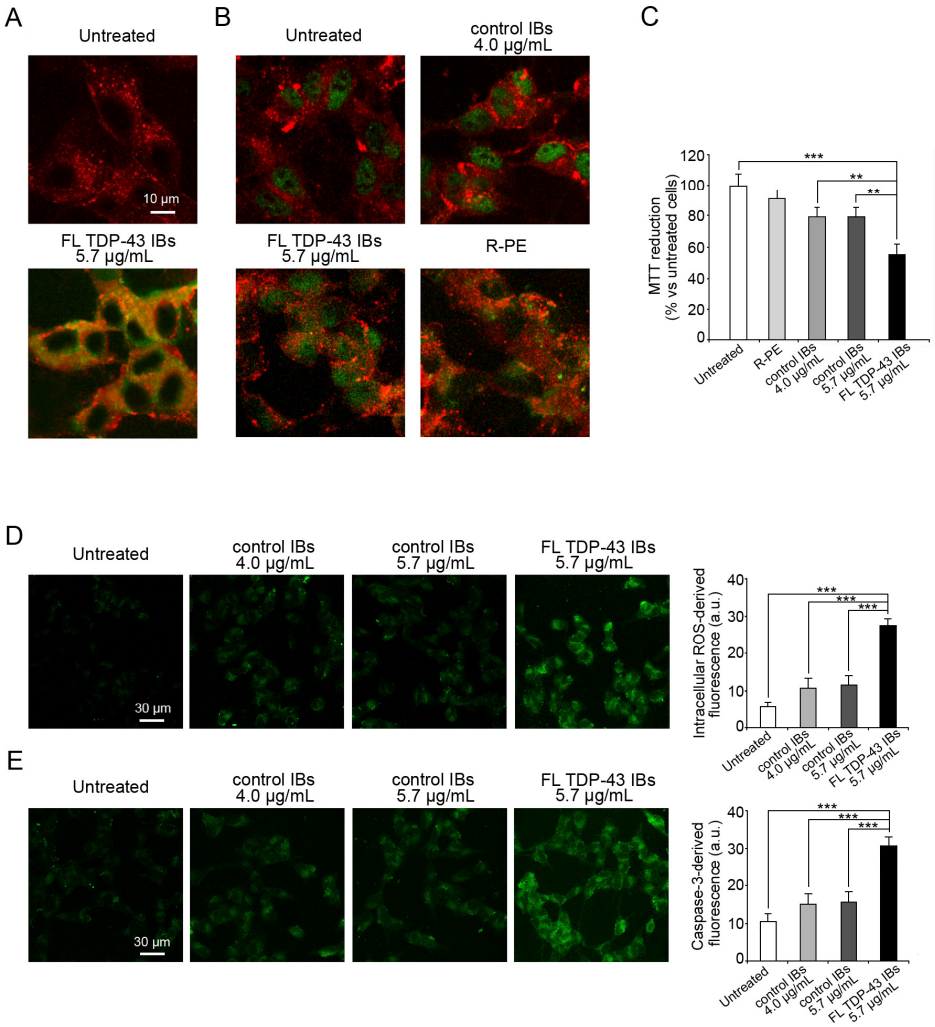

Figure 46. Toxicity of FL TDP-43 IBs and control IBs delivered intracellularly**.** (A) Representative confocal scanning microscope images of SH-SY5Y cells transfected with FL TDP-43 IBs labeled with 5-FITC. Red and green fluorescences indicate cell profiles and labeled FL TDP-43 IBs, respectively; the images were analysed at median planes parallel to the coverslip. (B) Representative confocal scanning microscope images of SH-SY5Y cells transfected with FL TDP-43 IBs, control IBs and R-PE. Red fluorescence indicates cells profiles and green fluorescence indicates TDP-43 detected with immunofluorescence or R-PE. (C) MTT reduction of SH-SY5Y cells following transfection with FL TDP-43 IBs (5.7 µg/mL), control IBs (4.0 µg/mL and 5.7 µg/mL) and R-PE (4.0 µg/mL). (D,E) Representative confocal scanning microscope images of SH-SY5Y cells showing intracellular ROS levels (D) and caspase-3 activation (E) after transfection with FL TDP-43 IBs (5.7 µg/mL) and control IBs (4.0 µg/mL and 5.7 µg/mL). The green fluorescence arises from the CM-H_2DCFDA probe that has reacted with ROS and from FAM-FLICA™ Caspase 3&7. The histograms show the quantitative fluorescence values in both cases. In panels C-E untreated cell means cells treated with the transfection mix only without proteins. The double (**) and triple (***) asterisks refer to p values lower than 0.01 and 0.001, respectively.

Importantly, the FL TDP-43 concentration was 1.7 μg/mL in the samples used to transfect the cells in all such tests, indicating that the protein aggregated in the non-amyloid form described above is highly toxic.

For the reasons explained above, the FL TDP-43 IBs contained a total protein concentration higher by ca. 30% (5.7 μg/mL) than that of control IBs (4.0 μg/mL). To assess whether the higher toxicity observed for FL-TDP-43 IBs was due to its higher protein content, the cells were also treated with control IBs containing a total protein quantity similar to that of FL TDP-43 IBs (5.7 μg/mL), but the FL-TDP-43 IBs still maintained a significantly higher toxicity with all probes of cell viability (Fig. 46C-E). All the values of toxicity reported here refer to cells transfected with the transfection mix only, ruling out that the observed toxicity of internalized FL TDP-43 IBs originates from the transfection procedure. Moreover, R-PE was not found to decrease significantly the MTT reduction following transfection, ruling out that transfected protein samples are *per se* toxic (Fig. 46C).

Transfected FL TDP-43 IBs are partially ubiquitinated and phosphorylated in cultured neuronal cells

In order to assess whether the exogenous cytoplasmic FL TDP-43 IBs were ubiquitinated, we analyzed the colocalization of FL TDP-43 IBs with ubiquitin. The images obtained with confocal microscopy showed a weak and diffuse cytoplasmic ubiquitin staining in the cytoplasm of SH-SY5Y cells transfected with control IBs, whereas a marked staining and the presence of inclusions was evident in cells transfected with FL TDP-43 IBs (Fig. 47A). In particular, a partial colocalization between cytoplasmic TDP-43 IBs and ubiquitin was observed (Fig. 47A). To investigate whether the exogenous cytoplasmic FL TDP-43 IBs were phosphorylated, we employed antibodies that recognize phosphorylated S409/410 in TDP-43 (Fig. 47B). The confocal images showed a clear phosphorylation of FL TDP-43 IBs (Fig. 47B) and these phosphorylated sites appeared to partially colocalize with ubiquitin (Fig.47B). All these data suggest that FL TDP-43 IBs are partially ubiquitinated and phosphorylated, recapitulating major features of the endogenous cytoplasmic inclusions found in ALS and FTLD-U.

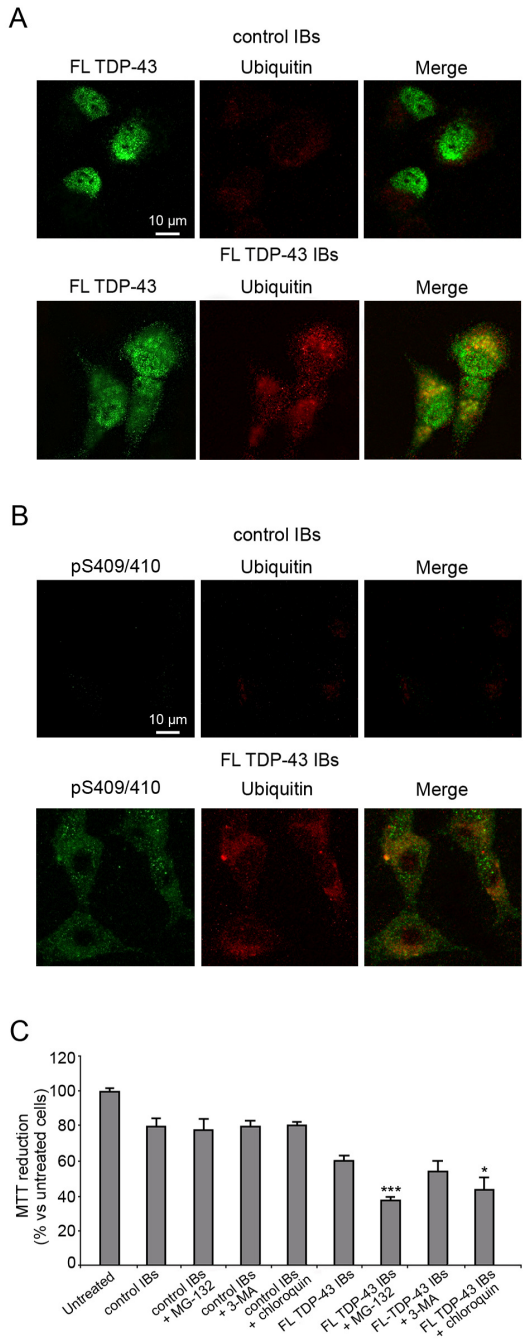

Figure 47. Ubiquitination and phosphorilation of FL TDP-43 IBs and control IBs delivered intracellularly. (A) Representative confocal scanning microscope images showing partial colocalization of exogenous cytoplasmic TDP-43 with ubiquitin-positive aggregates in SH-SY5Y cells transfected with control IBs FL and TDP-43 IBs. Green and red fluorescences indicates TDP-43 and ubiquitin, respectively. (B) Representative confocal scanning microscope images showing partial colocalization of phosphorylated S409/410 of TDP-43 and ubiquitin-positive aggregates in SH-SY5Y cells transfected with control IBs FL and TDP-43 IBs. Green and red fluorescences indicates pS409/410 TDP-43 and ubiquitin, respectively. (C) MTT reduction of SH-SY5Y cells following transfection with FL TDP-43 IBs (5.7 µg/mL), control IBs (4.0 µg/mL) in the absence or presence of 5 µM MG-132, 10 mM 3-MA and 40 µM chloroquin. The single (*) and triple (***) asterisks refer to p values lower than 0.05 and 0.001, respectively.

The toxicity of FL TDP-43 IBs and control IBs was also assessed in the presence of specific inhibitors of the proteasome, authophagy and lisosomes systems, such as MG-132, 3-MA and chloroquin, respectively (Fig. 47C). Cells treated with control IBs in the presence of the three inhibitors were found to decrease MTT reduction to a level similar to control IBs alone (Fig. 47C). Interestingly, a significantly lower level of viability was found in cells treated with FL TDP-43 IBs in the presence of MG-132 with respect to cells treated with FL TDP-43 IBs alone, showing that the inhibition of the proteasome system increases their toxicity (Fig. 47C). The cells treated with FL TDP-43 IBs in the presence of chloroquin also showed a significant decrease of cell viability with respect to cells treated with FL TDP-43 IBs alone, whereas cell treatment with FL TDP-43 IBs in the presence of 3-MA was not found to modify cell viability to a significant extent (Fig. 47C). These data indicate that the TDP-43 aggregates contained in FL TDP-43 IBs are toxic to the transfected cells, which react to their presence via mechanisms dedicated to the clearance of misfolded proteins.

Extracellular FL TDP-43 IBs are toxic to cultured neuronal cells

The toxicity of FL TDP-43 IBs and control IBs was also assessed by adding them to the extracellular medium of the SH-SY5Y cells in the absence of any transfection procedure. We first evaluated the toxic effect of both forms of IBs by measuring the ability of treated cells to reduce MTT (Fig. 48A). Their toxic effect was analysed at different protein concentrations, ranging from 7.5 μg/mL to 860 μg/mL (plus 30% for FL TDP-43 IBs). $A\beta_{42}$ oligomers were also used as a positive control of toxicity in a range of concentrations varying from 7.5 μg/mL to 215 μg/mL (Fig. 48A). It was found that FL TDP-43 IBs, unlike control IBs, were able to decrease MTT reduction at concentrations of 171 μg/mL or higher (Fig. 48A). FL TDP-43 IBs were also found to cause an increase of intracellular ROS production and caspase-3 activation, whereas control IBs induced only small changes (Fig. 48B,C).

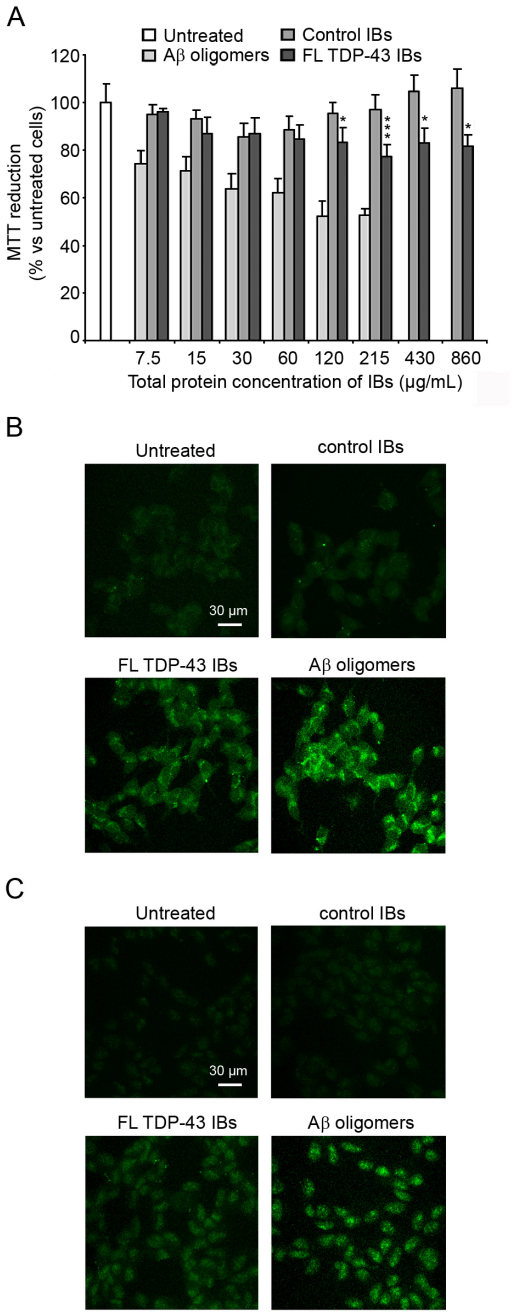

Figure 48. Toxicity of FL TDP-43 IBs and control IBs added extracellularly. (A) MTT reduction of SH-SY5Y cells following extracellular addition of FL TDP-43 IBs, control IBs and $A\beta_{42}$ oligomers. The indicated protein concentration refer to control IBs and correspond to values higher by 30% for FL TDP-43. The single (*) and triple (***) asterisks indicate a statistically significant difference between FL TDP-43 IBs and untreated cells ($p<0.05$ and $p<0.001$, respectively). (B,C) Representative confocal scanning microscope images of SH-SY5Y cells showing intracellular ROS levels (B) and caspase-3 activation (C) after extracellular addition of FL TDP-43 IBs, control IBs and $A\beta_{42}$ oligomers. The green fluorescence arises from the CM-H_2DCFDA probe that has reacted with ROS and from FAM-FLICA™ Caspase 3&7. Total protein concentrations were 280, 215 and 60 µg/mL for FL TDP-43 IBs, control IBs and $A\beta_{42}$ oligomers, respectively.

Chapter 4 – Discussion

Extracellular chaperones prevent $A\beta_{42}$-induced toxicity in rat brains

Clusterin (Clu) and α_2-macroglobulin (α_2M) are markedly induced in neuropathological conditions such as AD, where they are found associated with Aβ plaques, suggesting a physiological interaction with Aβ [Kida E et al.1995, Powers JM et al.1981, Strauss S et al. 1992, Barral JM er al.2004, Businaro R et al.1992, Trougakos IP et al 2006]. Clu and α2M are also known to inhibit amyloid fibril formation in vitro [Du Y et al. 1998, Hughes SR et al.1998, Kumita JR et al. 2007, Yerbury JJ et al. 2007, Yerbury JJ et al.2009]. In particular, it has been shown that Clu binds to all types of soluble oligomers found to be present during the aggregation and disaggregation of Aβ40, preventing further growth and proliferation of aggregated species [Humphreys DT et al 1999, Luheshi LM et al. 2010, Narayan P et al. 2012, Nielsen HM et al.2009, Wyatt AR et al.2011]. α2M was also found to bind small oligomers, preventing their growth and/or conversion into fibrils [Yerbury JJ et al. 2009]. Furthermore, Clu and α_2M are known to mediate the clearance of extracellular protein oligomers via endocytosis [48-50]. It is unclear, however, if extracellular chaperones have an ability to inhibit intrinsically the toxicity of Aβ misfolded oligomers, with evidence that has being very sparse and often contradictory so far. Indeed, some reports supported a toxicity-enhancing role for extracellular chaperones [Lambert MP et al.1998, Fabrizi C et al.2001, Oda T et al.2005], others claimed a protective action [Du Y et al.1998, Boggs LN et al.1996, Mannini B et al.2012] while one study demonstrated that the ratio of chaperone:Aβ could determine whether the effect was protective or enhanced toxicity [Yerbury JJ et al.2007].

Important suggestions have been obtained using chaperones distinct from extracellular ones, or protein oligomers distinct from Aβ oligomers. Indeed, it has been demonstrated that intracellular chaperones can prevent the toxicity of Aβ oligomers, sequestering and converting them into large non toxic aggregates [Ojha J et al.2011]. Our recent data showed that different chaperones, including Clu and α_2M, can inhibit efficiently the toxicity of extracellularly added protein oligomers formed by three

different peptides and proteins in SH-SY5Y neuroblastoma cells, provided the chaperones are incubated with the preformed oligomers before the resulting mixtures are added to the extracellular medium of the cells [Mannini B et al.2012]. Such an inhibition is very effective as it occurs even at low chaperone concentration [Mannini B et al.2012]. Using HypF-N oligomers as a toxic species, the protective effect of the chaperones was found to result from the ability of these proteins to bind to the oligomers and promote their further assembly into larger species, in the absence of any significant reorganisation of their internal molecular structure [Mannini B et al.2012].

The present work originated from this previous study and was targeted to Aβ oligomers, extracellular chaperones and a context closely related to AD, such as rat brains and cultured neurons. We demonstrated that chaperones can inhibit *in vivo* the neurotoxicity of high concentrations of pre-formed extracellular Aβ oligomers. Such an ability adds to the well-established functions of extracellular chaperones in inhibiting protein aggregation [Du Y et al. 1998, Hughes SR et al.1998, Kumita JR et al. 2007, Yerbury JJ et al. 2007, Yerbury JJ et al.2009] and promoting the clearance of protein aggregates [Zlokovic BV et al 1996, Hammad SM et al.1997]. In all our experiments, the oligomers are formed before adding the chaperones, showing that the protective action of the latter also includes neutralisation of toxic oligomers after they have formed. Thus we can hypothesize that chaperones neutralize $A\beta_{42}$ oligomers through a binding mechanism that promote the seeding of larger species, as previously demonstrated with HypF-N oligomers [Mannini B et al.2012]. The accumulation of Aβ fibrils as large plaques visible with optical microscopy and the association of such plaques with extracellular chaperones is indeed suggestive of this possibility.

Multiple lines of evidence indicate that there are two locales in which Aβ oligomers play a role in AD pathogenesis and are implicated in a synaptic failure, namely the intraneuronal and extracellular compartments [Laferla FM et al.2007, Wegiel J et al.2007]. A dynamic equilibrium seems to exist between the pools of Aβ oligomers in the two locales; extracellular Aβ appears to originate from intraneuronal Aβ [Oddo S et al.2004]. Since Aβ is released extracellularly from a membrane precursor protein, Aβ plaques accumulate extracellularly and Aβ oligomers have an ability to impair cell

viability from the extracellular space, we have chosen to focus on extracellularly added oligomers rather than intracellular ones in all our experiments.

This is the first report that molecular chaperones prevent $A\beta_{42}$-induced learning and memory impairments in hippocampal-injected rat brains *in vivo*. Associated with this prevention is the reduction of astroglial activation, astrogliosis, lipoperoxidation, and caspase-3 activation in these brains. In addition, chaperones were found to be able to protect primary hippocampal and cortical neurons against injuries caused by misfolded $A\beta_{42}$ oligomers, by preventing $A\beta_{42}$ binding to the dendrites. In future experiments it will be crucial to determine whether chaperone-mediated neutralization of $A\beta_{42}$ oligomers also act in transgenic mouse models.

Hence, these data elect extracellular chaperones as novel molecules that are neuroprotective against amyloid-induced injury and excellent candidates for the design and development of therapeutic strategies for the prophylaxis and treatment of AD.

Transthyretin suppresses the toxicity of oligomers formed by misfolded proteins *in vitro*

TTR was shown to inhibit aggregation and amyloid plaque formation of Aβ both *in vitro* and in vivo [Du J et al.2010,]. Analyses carried out in vitro have shown that TTR binds monomeric Aβ, explaining its ability to prevent aggregation of the peptide [J. Du et al.2010,]. However, in experiments using various forms of Aβ fixed to solid surfaces (e.g. nitrocellulose membranes or Biacore chips) TTR-Aβ binding was found to occur with higher affinity for aggregated Aβ, such as oligomers and fibrils, relative to monomeric Aβ, with monomeric TTR exhibiting stronger binding than tetrameric TTR [L. Liu et al.2006]. The high affinity between monomeric TTR and aggregated Aβ suggests an important role for such an interaction *in vitro*. Indeed, TTR was shown to bind to preformed Aβ oligomers and reduce their toxicity to murine primary neurons and human neuroblastoma SH-SY5Y cells [X. Li et al.2011]. In those studies, the suppression of TTR-mediated toxicity was not due to the ability of TTR to inhibit Aβ aggregation, but appeared to act on preformed oligomers. Subsequent studies have

shown that hTTR both inhibits Aβ oligomer formation and interacts with small Aβ oligomers to prevent the formation of nucleation competent seeds [Li et al, in preparation].

Here, we found that TTR is able to suppress the toxicity of extracellularly added oligomers formed by two different peptides/proteins, namely $A\beta_{42}$ and HypF-N, adding new data to the preliminary observation obtained with $A\beta_{42}$ [X. Li et al.2011]. TTR was found to inhibit the influx of Ca^{2+} caused by the oligomers, thus eliminating the occurrence of later effects, manifested as oxidative stress, membrane leakage and apoptosis. In addition, the observed dependence of the degree of protection on the time of preincubation between oligomers and TTR indicates that TTR suppresses oligomer toxicity by interacting with the oligomers, rather than through a separate protective pathway mediated by direct interaction of TTR with the cells. Overall, therefore, these findings reveal that the deleterious effects produced by interaction of misfolded protein oligomers with cell membranes can be abolished by TTR.

The three types of TTR examined here, namely hTTR, muTTR and M-TTR, were found to display different protective effects against oligomer-induced cytotoxicity. Indeed, monomeric M-TTR was able to protect SH-SY5Y neuroblastoma cells and rat primary neurons against oligomer-induced cytotoxicity; the highly stable tetrameric muTTR only showed only a small non-significant protective effect, whereas the less stable tetrameric hTTR had an effect intermediate between the two forms, or displayed a protective action more slowly or at higher concentrations than M-TTR. Hence, the ability of TTR to protect neuronal cells and neurons against these misfolded protein oligomers *in vitro* correlates inversely with the stability of the tetramer.

To shed light on the molecular mechanism by which TTR prevents cytotoxicity, we focused on HypF-N oligomers, probing their oligomeric state and molecular structure after the incubation with TTRs *in vitro*. Using ThT fluorescence we found that TTR does not disaggregate the preformed oligomers. Nor does it appear to promote a structural re-organization of the discrete oligomers, as shown by site-directed pyrene labeling. Rather, TTR was found to bind to the oligomers, as determined with SDS-PAGE, intrinsic fluorescence and confocal scanning microscopy, and promote their further assembly into larger aggregates, as shown by AFM, light scattering measurements and

turbidimetry. The ability of TTR to bind to the oligomers and cause their clustering was also found for $A\beta_{42}$ oligomers, using AFM and confocal scanning microscopy. Clearly, the ability of TTR to bind to and further assemble preformed HypF-N and $A\beta_{42}$ oligomers correlated again inversely with its stability, as the efficiency of such process followed the same order as that found for toxicity suppression, i.e. M-TTR > hTTR > mTTR. These data also suggest that the size of extracellular protein aggregates is an inverse correlate of their toxicity. The TTR-induced oligomer clusters are characterized by a reduction in their exposed hydrophobic surface and diffusional mobility, both of which are expected to reduce their toxicity to cells [Ojha J et al.2011].

Recent structural analyses of the TTR/Aβ interaction have revealed a complex set of interactions with hTTR tetramers binding the Aβ monomer in the T4 binding pocket to inhibit Aβ aggregation and cytotoxicity [Li et al, in preparation]. By contrast, M-TTR was found to interact preferentially with Aβ oligomers [Li et al, in preparation], and this observation is consistent with the better binding of M-TTR to HypF-N oligomers shown here. Nevertheless, the M-TTR/Aβ oligomer interaction was not found to be associated with a size increase of the oligomers [Li et al, in preparation], whereas in our experimental conditions the interaction between M-TTR and HypF-N/$A\beta_{42}$ oligomers was found to involve further clustering of the oligomers. The interaction showed by Li et al. was obtained under different conditions compared to those used in the present study. M-TTR was added to the aggregation assay where Aβ was initially monomeric [Li et al, in preparation]. Here we added M-TTR to pre-formed HypF-N/$A\beta_{42}$oligomers. Such a difference parallels the data showed by Ojha et al. showing that the chaperone HspB1 converted the pre-formed oligomers of Aβ into large aggregates, whereas, the incubation with Aβ monomer did not produce such larger species [J. Ojha et al.2011]. Hence, it appears that *in vitro* the different experimental conditions, i.e. the use of monomeric aggregating protein with respect to oligomeric species, may determine a different mode of M-TTR/oligomer interaction and suppression of oligomer toxicity. Further experimental studies are necessary to clarify this issue.

Overall, the molecular mechanism by which TTR protects cells against the deleterious effects of protein aggregation seems to involve two different levels of intervention,

inhibition of protein aggregation and fibril formation, as previously demonstrated [J. Du et al.2010], and neutralization of protein oligomer toxicity once the oligomers are formed, as shown here. Such dual protective behavior has also been demonstrated *in vitro* for a number of proteins that have been widely recognized as molecular chaperones, such as αB-crystallin, Hsp70 (both with and without ATP), clusterin, α2-macroglobulin and haptoglobin [K. Sörgjerd et al.2006], showing that TTR can also behave as a molecule with ATP-independent chaperone activity and have a relevant functional role *in vivo*.

A complex equilibrium between partially unfolded conformations in monomeric transthyretin

A model for M-TTR folding

In the present work we exploited a battery of biophysical methods and performed a number of kinetic tests to investigate the mechanisms of M-TTR refolding, with the final goal of proposing a model for the process.Such a model is presented in Figure 49.

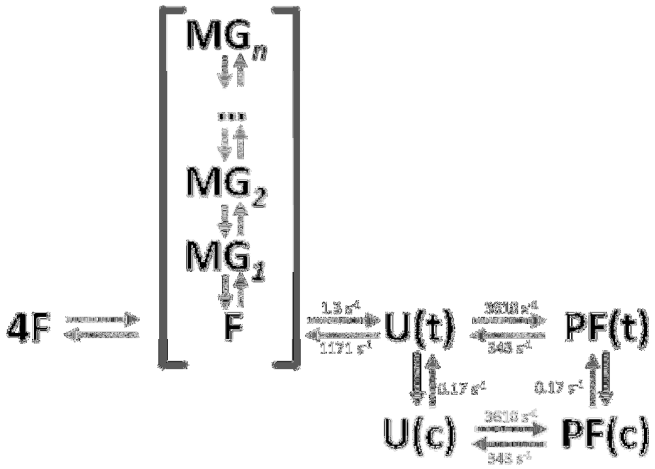

Figure 49 Model for the folding process of TTR. 4F defines the tetramer; F defines the folded monomer; MG_1 , MG_2,…MG_n correspond to a set of molten globular conformations; U(t) and U(c) refer to the unfolded state with one or more X-Pro peptide bonds in the *trans* or*cis*configuration, respectively. PF(t) and PF(c) refer to the partially folded state with one or more X-Pro peptide bonds in the *trans* or*cis*configuration, respectively.

Once a monomer of TTR(F) is released from the tetramer (4F) the protein establishes a complex equilibrium and can access a set of conformational ensembles. First, the

protein can convert from the fully folded state into an ensemble of molten globular (MG_1 … MG_n) conformations bearing increasing amounts of disorder. When compared to F, such MG ensemble possesses enhanced dynamics, a decrease in -sheet structure and an increase in random coil segments, in the presence of a substantially unaltered tertiary structure. Furthermore, the folded/molten globular ensemble is in equilibrium with the unfolded state (U). However, before the unfolded state can convert back into F, a kinetic trap can be transiently populated, consisting of a partially folded (PF) state. The PF state can be described as an ensemble of conformations exhibiting secondary structure content comparable to that of the folded state but a higher amount of hydrophobic clusters exposed to solvent compared to F. Notwithstanding that and given the off-pathway nature of PF, one can speculate that such ensemble possesses at least a few non-native contactsthat must be dismantled before M-TTR can convert into the correctly folded state. One further conformational ensemble can be identified thanks to the characterization of slow phases. Indeed, we showed that refolding of a subpopulation of M-TTR is decelerated due to the incorrect (*cis*) configuration of one or more X-Pro peptide bonds. Only after such bonds are converted into the right (*trans*)configuration, refolding can proceed.

Importantly, the MG and the PF states do not refer to the same conformational state, as revealed by differences between these two states in terms of structure, kinetics and pathway: (i) the MG ensemble can be observed in equilibrium experiments and is the dominant species at ureaconcentrationsaround 2.4 M (Figure 31). Conversely, our kinetic analysis illustrates that PF is populated only transiently. Its population at the equilibrium is not higher than 2 % under the same conditions (Figure 34);(ii)MG is directly in equilibrium with F and its formation precedes denaturation, whereas the PF ensemble must convert into U before accessing the F state; (iii) the F -> PF transition appears to be cooperative, while conversionof F into MG lacks cooperativity; (iv) MG and F are indistinguishable in terms of tryptophan fluorescence (Figure 31A and 32A), while PF has a significantly higher fluorescence than F as assessed by our stopped-flow kinetics (Figure 33A), suggesting a different environment surrounding aromatic side chains; (v) CD analysis reveals that secondary structure content of PF is globally native-like, while MG bears disordered segments. Consequently, our identification of the PF

and MG states illustrates two conformational ensembles that differ in terms of dynamics, kinetics and pathway of formation.

It is also important to point out the abundance of the PF and MG conformations. The PF state is populated only transiently: calculations based on kinetic data show that more than 1 % of the protein populates the PF state at the equilibrium in the absence of denaturant (Figure 34D). As far as the MG state is concerned, the lack of cooperativity displayed by the F -> MG transition makes it difficult to quantify the amount of protein populating theMG state. However, data in Figure 31D suggest that the transition begins at very low urea concentrations. Consequently, the amount of protein experiencing a molten globular conformation may be significant even in the absence of denaturant, especially in the presence of destabilizing mutations.

The importance of partially folded states in TTR

Several decades of research on TTR have highlighted the importance of characterising partially folded conformations populated by this protein. First, it is now clear that transient conformational fluctuations induce the conversion of the fully folded state into an ensemble of aggregation prone conformations [Lai, Z. et al.1996]. The characterization of this aggregation prone state is therefore crucial to understand the mechanisms underlying TTR aggregation. Several investigations by means of limited proteolysis and spectroscopic methods reported that the major event during the misfolding of monomeric TTR is the local unfolding and subsequent displacement of the two peripheral □-strands C and D (Figure 36)and the loop connecting them [Lai, Z. et al.1996]. The dislocation of this edge region unmasks amyloid prone segments normally buried in the TTR folded state and solvent exposure of these segmentsmediates the establishment of the inter-molecular interactions that initiate aggregation. More recently, it was proposed, by means of NMR relaxation dispersion experiments, that the amyloidogenic state of TTR possesses a largely native-like CBEF sheet while the DAGH sheet is disrupted, especially in strands D and H (Lim, K. H et al. 2013). This description is corroborated by molecular dynamics simulations suggesting that the CBEF sheet undergoes significant structural changes under conditions that promote aggregation(Armen, R. S.,et al.2004). Importantly, complete unfolding of TTR

inhibits aggregation [Lai, Z. et al.1996]. Thus, while the characteristicsthat enable the TTR amyloidogenic state to self-assemble must yet be clarified, there is consensus about the idea that such a state(s) must possess partial and local unfolding.

Second, evidence is accumulating that TTR may play a protective role against AD (Li, X., et al.2011). Different mechanisms have been proposed for such protective activity. These include direct facilitation of Aβ degradation(Costa, R.,et al.2008), transport of Aβ from the central nervous system to serum(Schwarzman, A. L., et al.1994), inhibition of Aβ aggregation(Li, X.et al.2011) and suppression of Aβ oligomer toxicity ((Li, X.et al.2011). While the mechanisms of the TTR-mediated protection against AD must be yet understood, it was recently proposed that *in vitro*interactions between TTR and Aβ can be mediated by either tetrameric or monomeric TTR, the two processes involving somewhat different mechanisms(Li, X et al.2011). In both cases it is reasonable that binding is mediated by a protein conformationable to bind peptide segments as hydrophobic as Aβ. In the TTR tetramer this appears to be the highly hydrophobic T4 binding site. The more hydrophobic structure of the TTR monomer appears to allow it to interact with relatively small oligomers, rather than the monomer, in essence increasing its valence with respect to Aβ monomer. This conformation is likely to be different from the fully folded state and displaysome extent of partial unfolding.

Therefore, the identification and characterization of partially folded states of TTR represents a crucial step towards understanding the peculiar properties of this protein. Here we showed that once a monomeris released from tetrameric TTR, a complex equilibrium is established between the fully folded monomer and at least two partially folded states. A small yet significant population of the protein populates two conformational states distinct from the fully folded one and possessing some degree of improper or incomplete folding. Future studies will clarify whether such conformational states correspond to the TTR amyloidogenic state and whether or not they may play an important role with respect to the protective effectexerted by TTR against AD.

TDP-43 inclusion bodies formed in bacteria are structurally amorphous, non-amyloid and inherently toxic to neuroblastoma cells

In 2006 it was reported, for the first time, that ubiquitin-positive, tau- and α-synuclein-negative intracellular inclusions found in the spinal cord motor neurons, in the hippocampus and neocortex of sporadic ALS and FTLD-U patients, contained the previously unidentified TDP-43 protein or its C-terminal fragments [Neumann M et al.2006]. Such inclusions appear to be phosphorylated and ubiquitinated [Neumann M et al.2006], but the structure adopted by TDP-43 in such deposits is currently a matter of debate. The IBs formed in *E. coli* cells following the over-expression of TDP-43 are informative in this regard, as bacterial IBs have been shown to consist mainly of amyloid-like deposits, providing an opportunity to emphasise the propensity of this protein to form amorphous aggregates if the amyloid form is not found in the TDP-43 component of the IBs. Our results indicate that both FL and Ct TDP-43 aggregates present in *E. coli* IBs do not possess any of the hallmarks of amyloid fibrils, allowing them to be classified as amorphous. CD and FTIR both show the presence of a secondary random-coil and β-turn structure in the absence of any detectable β-sheet structure. The aggregates bind neither ThT nor CR and are highly susceptible to PK digestion. The AFM analysis does not allow to visualize the morphology of the TDP-43 aggregates within the IBs. However, the IBs containing both FL and Ct TDP-43 appear to have an irregular morphology like that of the control IBs devoid of TDP-43.

The question naturally arises as to whether our findings resolve the current dispute on the structural/morphological type of inclusions present in TDP-43 pathology or rather add one more contribution to the ongoing debate. In order to address this issue we can try to survey the current literature critically. The first reports aimed at characterizing the structure/morphology of TDP-43 inclusions accumulating in ALS and FTLD-U patients have excluded the presence of amyloid-like structures. Although the ultrastructure of TDP-43 inclusions analyzed with TEM have highlighted the presence of 10-20 nm filaments [Neumann M et al.2006], the aggregates were found to be unable to bind ThT, ThS or CR, ruling out the presence of an amyloid-like structure [Kerman A et al.2010, Cairns NJ et al.2007]. A very recent report has emphasized that

TDP-43 inclusions may consist of amyloid fibrils, following the observation of a few ThS-positive inclusions [Robinson JL et al.2013]. Nevertheless, the ThS positivity was found only in a small fraction of skein-like inclusions of the spinal cord; it was indeed absent in most spinal cord skeins and absent altogether in other types of TDP-43 inclusions of the spinal cord [Robinson JL et al.2013]. All inclusions of the brain were also ThS negative [Robinson JL et al.2013]. By contrast, the most recent paper reporting a diffuse ThS positivity in all TDP-43 inclusions analysed in ALS spinal cords and FTLD-U brains raises important questions on the results obtained previously [Bigio EH et al.2013]. This study originated from a chemically harsh treatment of the tissue sections isolated from ALS and FTLD-U patients, based on the sequential use of potent oxidants, reductants, acids and bases, such as permanganate, metabisulfite, oxalic acid, sodium hydroxide and hydrogen peroxide, all known to chemically modify proteins and hydrolyse peptide bonds. It cannot be ruled out that the biological inclusions undergo a heavy structural reorganization under such circumstances.

The difficulty of purifying TDP-43 has limited the study of TDP-43 aggregation *in vitro* and is likely to be a limiting factor in future research on TDP-43. One report exists, however, on the characterization of the aggregates formed in vitro from TDP-43 after its purification [Johnson BS et al.2009]. This study has confirmed a filamentous morphology of TDP-43 aggregates, in the absence of ThT and CR binding [Johnson BS et al.2009]. By contrast, four other reports have emphasized an amyloid-like structure of TDP-43 aggregates, but all of them have referred to short peptides of 13 to 50 residues, all obtained from the sequence of TDP-43 [Saini A et al.2011, Jiang LL et al.2013]. It is well known that protein fragments have generally aggregation properties different from those of the full-length protein and it was recently reported that amyloid-like aggregation, as opposed to structurally undefined aggregation, is favored by small peptides and proteins [Ramshini H et al.2011].

Hence, our data and analysis suggest that FL and Ct TDP-43 form amorphous aggregates rather than amyloid-like. The finding that most, if not all, TDP-43 aggregates are amorphous in the spinal cord and brain of ALS and FTLD-U patients, in bacterial IBs and finally in aggregates formed *in vitro* from purified TDP-43, suggests that this protein has an intrinsic propensity to form amorphous aggregates and that

such a propensity is not affected remarkably by specific factors present in the biological compartments where aggregation occurs.

The bacterial TDP-43 IBs characterized here were found to be highly toxic to cultured neuronal cells, particularly following their internalization in the cytoplasm, where they are at least in part ubiquitinated and phosphorylated. A significant toxicity was found using intracellularly delivered IBs where TDP-43 was present at a concentration as low as 1.7 μg/mL before internalization. It is debated whether aggregation of TDP-43 in the cytoplasm of ALS and FTLD-U patients causes neurodegeneration due to formation of toxic protein aggregates (gain of function) or to the translocation of TDP-43 from the nucleus, which represents its physiological location, to the cytoplasm (loss of function), or both. Our results show that delivery of exogenous TDP-43 into the cytoplasm occurs in the absence of a significant loss of endogenous TDP-43 in the nucleus. Indeed, the images acquired after delivery show cytoplasmic TDP-43 in the absence of detectable clearance of nuclear TDP-43. Thus, the non-amyloid, amorphous aggregates formed from TDP-43 are inherently highly toxic to neuronal cells, indicating that a gain of function mechanism caused by TDP-43 deposits is effective in such pathology. The data do not exclude that a loss of function mechanism originating from the cellular mistrafficking of TDP-43 also contributes to pathology, but shows the inherent toxicity of TDP-43 aggregates.

In conclusion we have shown, using bacterial IBs containing aggregated TDP-43 as a model system, that both FL and Ct TDP-43 aggregates consist of non-amyloid assemblies that have an intrinsically high ability to cause neuronal dysfunction when delivered into the cytoplasm, contributing to elucidate the pathogenesis of TDP-43 proteinopathies such as FTLD-U and ALS.

References

A. Demuro, E. Mina, R. Kayed, S.C. Milton, I. Parker, C.G. Glabe. Calcium dysregulation and membrane disruption as a ubiquitous neurotoxic mechanism of soluble amyloid oligomers, J. Biol. Chem. 280 (2005) 17294–17300.

Adams D and Said G (1996). Ultrastructural immunolabelling of amyloid fibrils in acquired and hereditary amyloid neuropathies. J. Neurol*.* **243,** 73–76

Ahmed M, Davis J, Aucoin D, Sato T, Ahuja S, Aimoto S, Elliott JI, Van Nostrand WE, Smith SO (2010) Structural conversion of neurotoxic amyloid-beta(1–42) oligomers to fibrils. Nat Struct Mol Biol 17:561–567

Al-Chalabi A, Jones A, Troakes C, King A, Al-Sarraj S, van den Berg LH (2012) The genetics and neuropathology of amyotrophic lateral sclerosis. Acta Neuropathol 124:339–352. doi:10.1007/s00401-012-1022-4

Amaral MD (2004). CFTR and chaperones: processing and degradation. J Mol Neurosci.;23(1-2):41-8.

Andrea TA, Cavalieri RR, Goldfine ID, Jorgensen EC (1980). Binding of thyroid hormones and analogues to the human plasma protein prealbumin. Biochemistry 19: 55-63.

Armen, R. S., Alonso, D. O., and Daggett, V. (2004) *Structure***12**, 1847-1863

Askanas V, Engel WK, Alvarez RB, Frangione B, Ghiso J, Vidal R: Inclusion body myositis, muscle blood vessel and cardiac amyloidosis, and transthyretin Val122Ile allele. Annals of Neurol 2000, 47:544-549.

B. Mannini, R. Cascella, M. Zampagni, M. van Waarde-Verhagen, S. Meehan, C. Roodveldt, S. Campioni, M. Boninsegna, A. Penco, A. Relini, H.H. Kampinga, C.M. Dobson, M.R. Wilson, C. Cecchi, F. Chiti. Molecular mechanisms used by chaperones to reduce the toxicity of aberrant protein oligomers, Proc. Natl. Acad. Sci. U.S.A. 109 (2012) 12479-12484.

Bai Y Kinetic evidence for an on-pathway intermediate in the folding of cytochrome c. Proc Natl Acad Sci U S A. 1999 Jan 19;96(2):477-80.

Bai, Y. (1999) *Proceedings of the National Academy of Sciences of the United States of America***96**, 477-480

Balch WE,Morimoto RI, Dillin A, Kelly JW. 2008. Adapting proteostasis for disease intervention. Science 319: 916–919.

Baloh RH (2011) TDP-43: the relationship between protein aggregation and neurodegeneration in amyotrophic lateral sclerosis and frontotemporal lobar degeneration. FEBS J 278:3539– 3549. doi:10.1111/j.1742-4658.2011.08256.x

Barghorn S, Nimmrich V, Striebinger A, Krantz C, Keller P, Janson B, Bahr M, Schmidt M, Bitner RS, Harlan J, Barlow E, Ebert U, Hillen H (2005) Globular amyloid beta-peptide oligomer— a homogenous and stable neuropathological protein in Alzheimer's disease. J Neurochem 95:834–847

Barral JM, Broadley SA, Schaffar G, Hartl FU, Roles of molecular chaperones in protein misfolding diseases, Semin. Cell Dev. Biol. 15 (2004) 17-29.

Bellotti V, Chiti F. Amyloidogenesis in its biological environment: challenging a fundamental issue in protein misfolding diseases. Curr Opin Struct Biol. 2008 Dec;18(6):771-9.

Bemporad F, Chiti F. Protein misfolded oligomers: experimental approaches, mechanism of formation, and structure-toxicity relationships. Chem Biol. 2012 Mar 23;19(3):315-27.

Bemporad, F., Capanni, C., Calamai, M., Tutino, M. L., Stefani, M., and Chiti, F. (2004) *Biochemistry***43**, 9116-9126

Bergstrom J, Murphy C, Eulitz M, Weiss DT, Westermark GT, Solomon A, Westermark P: Codeposition of apolipoprotein A-IV and transthyretin in senile systemic (ATTR) amyloidosis. Biochem Biophys Res Commun 2001, 285:903-908.

Bertram L, Tanzi RE (2008) Thirty years of Alzheimer's disease genetics: the implications of systematic meta-analyses. Nat Rev Neurosci 9:768–778

Biancalana, M., and Koide, S. (2010) *Biochimica et biophysica acta***1804**, 1405-1412

Bigio EH, Wu JY, Deng HX, Bit-Ivan EN, Mao Q, et al. (2013) Inclusions in frontotemporal lobar degeneration with TDP-43 proteinopathy (FTLD-TDP) and amyotrophic lateral sclerosis (ALS), but not FTLD with FUS proteinopathy (FTLD-FUS) have properties of amyloid. Acta Neuropathol 125: 463-465.

Boggs LN, Fuson KS, Baez M, Churgay L, McClure D, Becker G, May PC Clusterin (Apo J) protects against in vitro amyloid-beta (1-40) neurotoxicity, J. Neurochem. 67 (1996) 1324-1327.

Bradford MM, A rapid and sensitive method for the quantitation of microgram quantities of protein utilizing the principle of protein-dye binding, Anal. Biochem. 72 (1976) 248-254.

Brandmeir, N. J. *et al.* Severe subcortical TDP-43 pathology in sporadic frontotemporal lobar degeneration with motor neuron disease. Acta Neuropathol. **115**, 123–131 (2008)

Brettschneider J, Lehmensiek V, Mogel H, Pfeifle M, Dorst J, Hendrich C, Ludolph AC, Tumani H: Proteome analysis reveals candidate markers of disease progression in amyotrophic lateral sclerosis (ALS). Neurosci Lett 2010, 468:23-27.

Broadley S A, Hartl FU, The role of molecular chaperones in human misfolding diseases, FEBS Lett. 583 (2009) 2647-2653.

Brouwers N, Bettens K, Gijselinck I et al (2010) Contribution of TARDBP to Alzheimer's disease genetic etiology. J Alzheimers Dis 21:423–430. doi:10.3233/JAD-2010-100198

Bucciantini, M., Calloni, G., Chiti, F., Formigli, L., Nosi, D., Dobson, C.M., Stefani, M., 2004. Pre-fibrillar amyloid protein aggregates share common features of cytotoxicity. J. Biol. Chem. 279, 31374–31382.

Bucciantini, M., Giannoni, E., Chiti, F., Baroni, F., Formigli, L., Zurdo, J., Taddei, N., Ramponi, G., Dobson, C.M., Stefani, M., 2002. Inherent toxicity of aggregates implies a common mechanism for protein misfolding diseases. Nature 416, 507–511.

Buratti E, Baralle FE (2012) TDP-43: gumming up neurons through protein-protein and protein-RNA interactions. Trends Biochem Sci 37: 237-247)

Businaro R, Fabrizi C, Fumagalli L, Lauro GM Synthesis and secretion of alpha 2-macroglobulin by human glioma established cell lines, Exp. Brain Res. 88 (1992) 213-218.

Butterfield AD, Drake J, Pocernich C, Castegna A (2001) Evidence of oxidative damage in Alzheimer's disease brain: central role for amyloid β-peptide. Trends Mol Med 7:548– 554

Buxbaum JN, Ye Z, Reixach N, Friske L, Levy C, Das P, Golde T, Masliah E, Roberts AR, Bartfai T: Transthyretin protects Alzheimer's mice from the behavioral and biochemical effects of A beta toxicity. Proc Natl Acad Sci USA 2008, 105:2681-2686.

Buxbaum JN. Edited by Uversky VN, Fink A. Santa Cruz, California: Springer. 2007; 259-283

Buxbaum, J. N. (2007) Transthyretin and the Transthyretin Amyloidoses. in *Protein Misfolding, Aggregation, and Conformational Diseases* (Uversky, V. N., and Fink, A. L. eds.), Springer, Santa Cruz (California). pp 259-283

Buxbaum, J. N., Ye, Z., Reixach, N., Friske, L., Levy, C., Das, P., Golde, T., Masliah, E., Roberts, A. R., and Bartfai, T. (2008) *Proceedings of the National Academy of Sciences of the United States of America***105**, 2681-2686

Byrne S, Walsh C, Lynch C et al (2011) Rate of familial amyotrophic lateral sclerosis: a systematic review and meta-analysis. J Neurol Neurosurg Psychiatry 82:623–627. doi:10.1136/j nnp.2010.224501

C. Canale, S. Torrassa, P. Rispoli, A. Relini, R. Rolandi, M. Bucciantini, M. Stefani, A. Gliozzi. Natively folded HypF-N and its early amyloid aggregates interact with phospholipid monolayers and destabilize supported phospholipid bilayers, Biophys. J. 91 (2006) 4575–4588.

Cairns NJ, Neumann M, Bigio EH, Holm IE, Troost D, et al. (2007) TDP-43 in familial and sporadic frontotemporal lobar degeneration with ubiquitin inclusions. Am J Pathol 171: 227-240.

Calamai M, Chiti F, Dobson CM Amyloid fibril formation can proceed from different conformations of a partially unfolded protein. Biophys J. 2005 Dec;89(6):4201-10.

Campioni S, Mannini B, Zampagni M, Pensalfini A, Parrini C, Evangelisti E, Relini A, Stefani M, Dobson CM, Cecchi C, Chiti F A causative link between the structure of aberrant protein oligomers and their toxicity, Nat. Chem. Biol. 6 (2010) 140-147.

Canet, D., Last, A. M., Tito, P., Sunde, M., Spencer, A., Archer, D. B., Redfield, C., Robinson, C. V., and Dobson, C. M. (2002) *Nature structural biology***9**, 308-315

Capaldi A.P., Kleanthous C., and Radford S.E. (2002) Im7 folding mechanism: misfolding on a path to the native state. *Nat Struct Biol* 9, 209-216.

Cascella, R., Conti, S., Mannini, B., Li, X., Buxbaum, J. N., Tiribilli, B., Chiti, F., and Cecchi, C. (2013) *Biochimica et biophysica acta*

Castano EM, Roher AE, Esh CL, Kokjohn TA, Beach T: Comparative proteomics of cerebrospinal fluid in neuropathologically-confirmed Alzheimer's disease and non-demented elderly subjects. Neurol Res 2006, 28:155-163.

Cavallaro T, Martone RL, Dwork AJ, Schon EA, Herbert J (1990) The retinal pigment epithelium is the unique site of transthyretin synthesis in the rat eye. Invest Ophthalmol Vis Sci 31:497–501

Chen F, David D, Ferrari A, Gotz J (2004) Posttranslational modifications of tau—role in human tauopathies and modeling in transgenic animals. Curr Drug Targets 5:503–515

Chio A, Calvo A, Moglia C et al (2010) Amyotrophic lateral sclerosis-frontotemporal lobar dementia in 3 families with p.Ala382Thr TARDBP mutations. Arch Neurol 67:1002–1009. doi:10.1001/archneurol.2010.173,

Chiti F, Taddei N, Baroni F, Capanni C, Stefani M, Ramponi G, Dobson CM Kinetic partitioning of protein folding and aggregation. Nat Struct Biol. 2002 Feb;9(2):137-43.

Chiti, F., Mangione, P., Andreola, A., Giorgetti, S., Stefani, M., Dobson, C. M., Bellotti, V., and Taddei, N. (2001) *Journal of molecular biology***307**, 379-391

Choi YG, Kim JL, Lee HP, Jin JK, Choi EK, Carp. RI, Kim YS (2000) Induction of heme oxygenase-1 in the brain of scrapie-infected mice. Neurosci Lett 11:173–176

Choi, S. H., Leight, S. N., Lee, V. M., Li, T., Wong, P. C., Johnson, J. A., Saraiva, M. J., and Sisodia, S. S. (2007) *The Journal of neuroscience : the official journal of the Society for Neuroscience***27**, 7006-7010

Cleary JP, Walsh DM, Hofmeister JJ, Shankar GM, Kuskowski MA, Selkoe DJ, et al. Natural oligomers of the amyloid-beta protein specifically disrupt cognitive function. Nat Neurosci 2005; 8:79-84

Colbeau A, Elsen S, Tomiyama M, Zorin NA, Dimon B, Vignais PM. Rhodobacter capsulatus HypF is involved in regulation of hydrogenase synthesis through the HupUV proteins. Eur J Biochem. 1998 Jan 15;251(1-2):65-71.

Colon W, Kelly JW. Partial denaturation of transthyretin is sufficient for amyloid fibril formation in vitro. Biochemistry. 1992 Sep 15;31(36):8654-60.

Colon, W., and Kelly, J. W. (1992) *Biochemistry***31**, 8654-8660

Cooper NR, Bradt BM, O'Barr S, Yu JX, Focal inflammation in the brain: role in Alzheimer's disease, Immunol. Res. 21 (2000) 159-165.

Corrado L, Ratti A, Gellera C et al (2009) High frequency of TARDBP gene mutations in Italian patients with amyotrophic lateral sclerosis. Hum Mutat 30:688–694. doi:10.1002/h umu.20950)

Costa R, Goncalves A, Saralva MJ, Cardoso I: Transthyretin binding to ABeta peptide - Impact on A-Beta fibrillogenesis and toxicity. FEBS Lett 2008, 582:936-942.

Costa, R., Ferreira-da-Silva, F., Saraiva, M. J., and Cardoso, I. (2008) *PloS one***3**, e2899

Costa, R., Goncalves, A., Saraiva, M. J., and Cardoso, I. (2008) *FEBS letters***582**, 936-942

Cuenco KT, Friedland R, Baldwin CT, Guo J, Vardarajan B, Lunetta KL, Cupples LA, Green RC, Decarli C, Farrer LA: Association of TTR polymorphisms with hippocampal atrophy in Alzheimer disease families. Neurobiol Aging 2011, 32:249-256.

de Groot NS, Sabate R, Ventura S (2009) Amyloids in bacterial inclusion bodies. Trends Biochem Sci 34: 408-416.

de Sousa MM, Vital C, Ostler D, Fernandes R, Pouget-Abadie J, Carles D, Saraiva MJ: Apolipoprotein AI and transthyretin as components of amyloid fibrils in a kindred with apoAI Leu178His amyloidosis. Am J Pathol 2000, 156:1911-1917.

Delacourte A, Sergeant N, Champain D, Wattez A, Maurage CA, Lebert F, Pasquier F, David JP (2002) Nonoverlapping but synergetic tau and APP pathologies in sporadic Alzheimer's disease. Neurology 59:398–407

Dinner AR, Sali A, Smith LJ, Dobson CM, Karplus M. Understanding protein folding via free-energy surfaces from theory and experiment. Trends Biochem Sci. 2000 Jul;25(7):331-9.

Dobson CM. Chemical space and biology. Nature. 2004 Dec 16;432(7019):824-8.

Dobson CMNature. Protein folding and misfolding 2003 Dec 18;426(6968):884-90.

Donati C, Cencetti F, Nincheri P, Bernacchioni C, Brunelli S, Clementi E, Cossu G, Bruni P Sphingosine 1-phosphate mediates proliferation and survival of mesoangioblasts, Stem. Cells. 25 (2007) 1713-1719.

Doyle SM, Genest O, Wickner S Protein rescue from aggregates by powerful molecular chaperone machines. Nat Rev Mol Cell Biol. 2013 Oct;14(10):617-29.

Du J, Murphy RM: Characterization of the interaction of beta-amyloid with transthyretin monomers and tetramers. Biochemistry (Mosc) 2010, 49:8276-8289.

Du Y, Bales KR, Dodel RC, Liu X, Glinn MA, Horn JW, Little SP, Paul SM, Alpha2-macroglobulin attenuates beta-amyloid peptide 1-40 fibril formation and associated neurotoxicity of cultured fetal rat cortical neurons, J. Neurochem. 70 (1998) 1182-1188.

Du, J., and Murphy, R. M. (2010) *Biochemistry***49**, 8276-8289

Du, J., Cho, P. Y., Yang, D. T., and Murphy, R. M. (2012) *Protein engineering, design & selection : PEDS***25**, 337-345

Duan W, Li X, Shi J, Guo Y, Li Z, et al. (2010) Mutant TAR DNA-binding protein-43 induces oxidative injury in motor neuron-like cell. Neurosci 169: 1621-1629.

DuBay KF, Pawar AP, Chiti F, Zurdo J, Dobson CM, Vendruscolo M Prediction of the absolute aggregation rates of amyloidogenic polypeptide chains. J Mol Biol. 2004 Aug 27;341(5):1317-26.

Dumoulin M, Kumita JR, Dobson CM Normal and aberrant biological self-assembly: Insights from studies of human lysozyme and its amyloidogenic variants. Acc Chem Res. 2006 Sep;39(9):603-10.

E. Evangelisti, C. Cecchi, R. Cascella, C. Sgromo, M. Becatti, C.M. Dobson, F. Chiti, M. Stefani. Membrane lipid composition and its physicochemical properties define cell vulnerability to aberrant protein oligomers, J. Cell Sci. 125 (2012) 2416-2427.

Eikelenboom P, Stam FC (1984). An immunohistochemical study on cerebral vascular and senile plaque amyloid in Alzheimer's dementiaVirchows Arch B Cell Pathol Incl Mol Pathol.;47(1):17-25

F. Tatini, A.M. Pugliese, C. Traini, S. Niccoli, G. Maraula, T.E. Dami, B. Mannini, T. Scartabelli, F. Pedata, F. Casamenti, F. Chiti. Amyloid-β oligomer synaptotoxicity is mimicked by oligomers of the model protein HypF-N, Neurobiol Aging (2013) doi:pii: S0197-4580(13)00133-4. 10.1016/j.neurobiolaging.2013.03.020. [Epub ahead of print].

Fabrizi C, Businaro R, Lauro GM, Fumagalli L, Role of alpha2-macroglobulin in regulating amyloid beta-protein neurotoxicity: protective or detrimental factor?, J. Neurochem. 78 (2001) 406-412.

Fabrizi C, Businaro R, Lauro GM, Fumagalli L, Role of alpha2-macroglobulin in regulating amyloid beta-protein neurotoxicity: protective or detrimental factor?, J. Neurochem. 78 (2001) 406-412.

Fearns, C., Connelly, S., Powers, E. T., and Kelly, J. W. (2013) Development of Therapeutic Strategies for the Transthyretin Amyloidoses. in *Amyloid Fibrils and Prefibrillar Aggregates* (Otzen, D. E. ed.), Wiley-VCH, Weinheim. pp 373-394

Ferguson, N., Capaldi, A. P., James, R., Kleanthous, C., and Radford, S. E. (1999) *Journal of molecular biology***286**, 1597-1608

Fersht AR. From the first protein structures to our current knowledge of protein folding: delights and scepticisms. Nat Rev Mol Cell Biol. 2008 Aug;9(8):650-4. doi: 10.1038/nrm2446. Epub 2008 Jun 25.

Fink AL (1998) Protein aggregation: folding aggregates, inclusion bodies and amyloid. Fold Des 3: R9-23.

French K, Yerbury JJ, Wilson MR, Protease activation of alpha2-macroglobulin modulates a chaperone-like action with broad specificity, Biochemistry. 47 (2008) 1176-1185.

García Fruitós E, Sabate R, de Groot NS, Villaverde A, Ventura S (2011) Biological role of bacterial inclusion bodies: a model for amyloid aggregation. FEBS J 278: 2419-2427.

Gatti-Lafranconi P, Natalello A, Ami D, Doglia SM, Lotti M (2011) Concepts and tools to exploit the potential of bacterial inclusion bodies in protein science and biotechnology. FEBS J 278: 2408-2418.

Geng, Y, Li C, Liu J, Xing G, Zhou L, Dong M, Li X, Niu Y, Beta-asarone improves cognitive function by suppressing neuronal apoptosis in the beta-amyloid hippocampus injection rats, Biol. Pharm. Bull. 33 (2010) 836-843.

Ghiso J, Matsubara E, Koudinov A, Choi-Miura NH, Tomita M, Wisniewski T, Frangione B: The cerebrospinal-fluid soluble form of Alzheimer's amyloid beta is complexed to SP-40,40 (apolipoprotein J), an inhibitor of the complement membrane-attack complex. Biochem J 1993, 293(Pt 1):27-30.

Gianni S, Ivarsson Y, Jemth P, Brunori M, Travaglini-Allocatelli C. Identification and characterization of protein folding intermediates. Biophys Chem. 2007 Jul;128(2-3):105-13. Epub 2007 Apr 24.

Gianni, S., Ivarsson, Y., Jemth, P., Brunori, M., and Travaglini-Allocatelli, C. (2007) *Biophysical chemistry***128**, 105-113

Giordana, M. T. *et al.* TDP-43 redistribution is an early event in sporadic amyotrophic lateral sclerosis. Brain Pathol. **20**, 351–360 (2010).

Giunta S, Valli MB, Galeazzi R, Fattoretti P, Corder EH, Galeazzi L: Transthyretin inhibition of amyloid beta aggregation and toxicity. Clin Biochem 2005, 38:1112-1119.

Glabe CG. Structural classification of toxic amyloid oligomers. J Biol Chem. 2008 Oct 31;283(44):29639-43.

Goedert M, Spillantini MG, A century of Alzheimer's disease, Science. 314 (2006) 777-781.

Goodman DS (1986) Statement regarding nomenclature for the protein known as prealbumin, which is also (recently) called transthyretin. In: Glenner GG, Osserman EF, Benditt EP, Calkins E, Cohen AS, Zucker-Franklin D (eds)Amyloidosis. Plenum, New York, pp 287–288

Gotz J (2001) Tau and transgenic animal models. Brain Res Brain Res Rev 35:266–286

Guentchev M, Voigtlander T, Haberler C, Groschup MH, Budka H (2000) Evidence for oxidative stress in experimental prion disease. Neurobiol Dis 7:270–273

Guo W, Chen Y, Zhou X, Kar A, Ray P, et al. (2011) An ALS-associated mutation affecting TDP-43 enhances protein aggregation, fibril formation and neurotoxicity. Nat Struct Mol Biol 18: 822-830.

Gustavsson, Å., Engstro¨m, U., and Westermark, P. (1990) *Biochem. Biophys. Res. Commun.* **175,** 1159–1164

Hamilton, J. A., Steinrauf, L. K., Braden, B. C., Liepnieks, J., Benson, M. D., Holmgren, G., Sandgren, O., and Steen, L. (1993) *J. Biol. Chem.* **268,** 2416–2424

Hammad SM, Ranganathan S, Loukinova E, Twal WO, Argraves WS, Interaction of apolipoprotein J-amyloid beta-peptide complex with low density lipoprotein receptor-related protein-2/megalin. A mechanism to prevent pathological accumulation of amyloid beta-peptide, J. Biol. Chem. 272 (1997) 18644-18649.

Hammarstrom, P., Jiang, X., Hurshman, A. R., Powers, E. T., and Kelly, J. W. (2002) *Proceedings of the National Academy of Sciences of the United States of America***99 Suppl 4**, 16427-16432

Hammarstrom, P., Sekijima, Y., White, J. T., Wiseman, R. L., Lim, A., Costello, C. E., Altland, K., Garzuly, F., Budka, H., and Kelly, J. W. (2003) *Biochemistry***42**, 6656-6663

Hammarstrom, P., Wiseman, R. L., Powers, E. T., and Kelly, J. W. (2003) *Science***299**, 713-716

Haq, S. R., Jurgens, M. C., Chi, C. N., Koh, C. S., Elfstrom, L., Selmer, M., Gianni, S., and Jemth, P. (2010) *The Journal of biological chemistry***285**, 18051-18059

Hardiman O, van den Berg LH, Kiernan MC (2011) Clinical diagnosis and management of amyotrophic lateral sclerosis. Nat Rev Neurol 7:639–649. doi:10.1038/nrneurol.2011.153

Harper JD, Lansbury PT Jr (1997) Models of amyloid seeding in Alzheimer's disease and scrapie: mechanistic truths and physiological consequences of the time-dependent solubility of amyloid proteins. Annu Rev Biochem 66:385–407

Hartl FU, Bracher A, Hayer-Hartl M Molecular chaperones in protein folding and proteostasis. Nature 2011 Jul 20;475(7356):324-32.

Hasegawa M, Arai T, Nonaka T, Kametani F, Yoshida M, Hashizume Y, Beach TG, Buratti E, Baralle F, Morita M, Nakano I, Oda T, Tsuchiya K, Akiyama H (2008). Phosphorylated TDP-43 in frontotemporal lobar degeneration and amyotrophic lateral sclerosis. Ann Neurol. Jul;64(1):60-70. doi: 10.1002/ana.21425.

Herczenik E, Gebbink MF Molecular and cellular aspects of protein misfolding and disease. FASEB J. 2008 Jul;22(7):2115-33. doi: 10.1096/fj.07-099671. Epub 2008 Feb 26.

Hughes SR, Khorkova O, Goyal S, Knaeblein J, Heroux J, Riedel NG, Sahasrabudhe S, Alpha2-macroglobulin associates with beta-amyloid peptide and prevents fibril formation, Proc. Natl. Acad. Sci. U. S. A. 95 (1998) 3275-3280.

Hughes SR, Khorkova O, Goyal S, Knaeblein J, Heroux J, Riedel NG, Sahasrabudhe S, Alpha2-macroglobulin associates with beta-amyloid peptide and prevents fibril formation, Proc. Natl. Acad. Sci. U. S. A. 95 (1998) 3275-3280.

Humphreys DT, Carver JA, Easterbrook-Smith SB, Wilson MR, Clusterin has chaperone-like activity similar to that of small heat shock proteins, J. Biol. Chem. 274 (1999) 6875-6881.

Hurshman AR, White JT, Powers ET, Kelly JW (2004) Transthyretin aggregation under partially denaturing conditions is a downhill polymerization. Biochemistry 43:7365–7381

Hurshman Babbes, A. R., Powers, E. T., and Kelly, J. W. (2008) *Biochemistry***47**, 6969-6984

Hurshman, A. R., White, J. T., Powers, E. T., and Kelly, J. W. (2004) *Biochemistry***43**, 7365-7381

Ingenbleek Y, Young VR (2002) Significance of transthyretin in protein metabolism. Clin Chem Lab Med 40:1281–1291

Inostroza M, Cid E, Brotons-Mas J, Gal B, Aivar P, Uzcategui YG, Sandi C, Menendez de la Prida L, Hippocampal-dependent spatial memory in the water maze is preserved in an experimental model of temporal lobe epilepsy in rats, PLoS One. 6 (2011) e22372.

Ittner LM, Ke YD, Delerue F, Bi M, Gladbach A, van Eersel J, Wolfing H, Chieng BC, Christie MJ, Napier IA, Eckert A, Staufenbiel M, Hardeman E, Gotz J (2010) Dendritic function of tau mediates amyloid-beta toxicity in Alzheimer's disease mouse models. Cell 142:387–397

J. Du , R.M. Murphy. Characterization of the interaction of β-amyloid with transthyretin monomers and tetramers, Biochemistry 28 (2010) 8276-8289

J. Ojha, G. Masilamoni, D. Dunlap, R.A. Udoff, A.G. Cashikar. Sequestration of toxic oligomers by HspB1 as a cytoprotective mechanism, Mol. Cell Biol. 31 (2011) 3146-3157.

J.B. Birks, I.H. Munro. Progress in Reaction Kinetics, Pergamon Press 4(1967).

Jackson SE, Fersht AR Folding of chymotrypsin inhibitor 2. 1. Evidence for a two-state transition. Biochemistry. 1991 Oct 29;30(43):10428-35.

Jackson, S. E., and Fersht, A. R. (1991) *Biochemistry***30**, 10428-10435

Jacobson DR, McFarlin DE, Kane I, Buxbaum JN (1992) Transthyretin Pro55, a variant associated with early-onset, aggressive, diffuse amyloidosis with cardiac and neurologic involvement. Hum Genet 89:353–356

Jacobsson B, Collins VP, Grimelius L, Pettersson T, Sandstedt B, Carlstrom A (1989) Transthyretin immunoreactivity in human and porcine liver, choroid plexus, and pancreatic islets. J Histochem Cytochem 37:31–37

Jarosz DF, Taipale M, Lindquist S. 2010. Protein homeostasis and the phenotypic manifestation of genetic diversity:Principles and mechanisms. Annu Rev Genet 44: 189– 216.

Jemth P, Gianni S, Day R, Li B, Johnson CM, Daggett V, Fersht AR. Demonstration of a low-energy on-pathway intermediate in a fast-folding protein by kinetics, protein engineering, and simulation. Proc Natl Acad Sci U S A. 2004 Apr 27;101(17):6450-5. Epub 2004 Apr 19.

Jemth, P., Gianni, S., Day, R., Li, B., Johnson, C. M., Daggett, V., and Fersht, A. R. (2004) *Proceedings of the National Academy of Sciences of the United States of America***101**, 6450-6455

Jiang LL, Che MX, Zhao J, Zhou CJ, Xie MY, et al. (2013) Structural transformation of the amyloidogenic core region of TAR DNA binding protein of 43 kDa (TDP-43) initiates its aggregation and cytoplasmic inclusion. J Biol Chem 288: 19614-19624.

Jiang, X., Buxbaum, J. N., and Kelly, J. W. (2001) *Proceedings of the National Academy of Sciences of the United States of America***98**, 14943-14948

Jiang, X., Smith, C. S., Petrassi, H. M., Hammarstrom, P., White, J. T., Sacchettini, J. C., and Kelly, J. W. (2001) *Biochemistry***40**, 11442-11452

Jicha GA, Bowser R, Kazam IG, Davies P (1997) Alz-50 and MC-1, a new monoclonal antibody raised to paired helical filaments, recognize conformational epitopes on recombinant tau. J Neurosci Res 48:128–132

Johnson BS, Snead D, Lee JJ, McCaffery JM, Shorter J, et al. (2009) TDP-43 is intrinsically aggregation-prone, and amyotrophic lateral sclerosis-linked mutations accelerate aggregation and increase toxicity. J Biol Chem 284: 20329-20339.

Johnson, S. M., Connelly, S., Fearns, C., Powers, E. T., and Kelly, J. W. (2012) *Journal of molecular biology***421**, 185-203

Junker M, Besingi RN, Clark PL. 2009. Vectorial transport and folding of an autotransporter virulence protein during outer membrane secretion. Mol Microbiol 71: 1323–1332.

Jürgen B, Breitenstein AA, Urlacher V, Büttner K, Lin H, et al. (2010) Quality control of inclusion bodies in Escherichia coli. Microb Cell Fact 9: 41.

K. Sörgjerd, B. Ghafouri, B.H. Jonsson, J.W. Kelly, S.Y. Blond, P. Hammarström. Retention of misfolded mutant transthyretin by the chaperone BiP/GRP78 mitigates amyloidogenesis, J. Mol. Biol. 356 (2006) 469-82.

K. Sörgjerd, T. Klingstedt, M. Lindgren, K. Kågedal, P. Hammarström. Prefibrillar transthyretin oligomers and cold stored native tetrameric transthyretin are cytotoxic in cell culture, Biochem. Biophys. Res Commun. 377 (2008) 1072-8.

Kabashi, E. *et al.* Gain and loss of function of ALS-related mutations of TARDBP (TDP-43) cause motor deficits *in vivo*. *Hum. Mol. Genet.* **19**, 671–683 (2010).

Kabashi, E. *et al.* TARDBP mutations in individuals with sporadic and familial amyotrophic lateral sclerosis. *Nature Genet.* **40**, 572–574 (2008)

Kawahara M, Kuroda Y, Arispe N, Rojas E (2000) Alzheimer's β-amyloid, human islet amylin, and prion protein fragment evoke intracellular free calcium elevation by a common mechanism in a hypopthalamic GnRH neuronal cell line. J Biol Chem 275:14077–14083

Kelly, J. W. (1996) *Current opinion in structural biology***6**, 11-17

Kelly, J. W., Colon, W., Lai, Z., Lashuel, H. A., McCulloch, J., McCutchen, S. L., Miroy, G. J., and Peterson, S. A. (1997) *Advances in protein chemistry***50**, 161-181

Kelly, S. M., Jess, T. J., and Price, N. C. (2005) *Biochimica et biophysica acta***1751**, 119-139

Kerman A, Liu HN, Croul S, Bilbao J, Rogaeva E, et al. (2010) Amyotrophic lateral sclerosis is a non-amyloid disease in which extensive misfolding of SOD1 is unique to the familial form. Acta Neuropathol 119: 335-344.

Kida E, Choi-Miura NH, Wisniewski KE, Deposition of apolipoproteins E and J in senile plaques is topographically determined in both Alzheimer's disease and Down's syndrome brain, Brain Res. 685 (1995) 211-216.

Kim HJ, Kim NC, Wang Y-D et al (2013) Mutations in prion-like domains in hnRNPA2B1 and hnRNPA1 cause multisystem proteinopathy and ALS. Nature 495(7442):467–473. doi:10.1038/nature11922

Kopke E, Tung YC, Shaikh S, Alonso AC, Iqbal K, Grundke- Iqbal I (1993) Microtubule-associated protein tau abnormal phosphorylation of a non-paired helical filament pool in Alzheimer disease. J Biol Chem 268:24374–24384

Kourie JI (2001) Mechanisms of amyloid β protein-induced modification in ion transport systems: implications for neurodegenerative diseases. Cell Mol Neurobiol 21:173–213

Kumita JR, Poon S, Caddy GL, Hagan CL, Dumoulin M, Yerbury JJ, Stewart EM, Robinson CV, Wilson MR, Dobson CM, The extracellular chaperone clusterin potently inhibits human lysozyme amyloid formation by interacting with prefibrillar species, J. Mol. Biol. 369 (2007) 157-167.

Kuznetsova, I. M., Turoverov, K. K., and Uversky, V. N. (2004) *Journal of proteome research***3**, 485-494

Kyle RA, Gertz MA, Linke RP (1992) Amyloid localized to tenosynovium at carpal tunnel release. Immunohistochemical identification of amyloid type. Am J Clin Pathol 97:250–253

L. Bojarski, J. Herms, J. Kuznicki. Calcium dysregulation in Alzheimer's disease, Neurochem Int 52 (2008) 621–633.

L. Liu, R.M. Murphy Kinetics of inhibition of beta-amyloid aggregation by transthyretin, Biochemistry (Mosc) 45 (2006) 15702-15709.

Lacor PN, Buniel MC, Chang L, Fernandez SJ, Gong Y, Viola KL, Lambert MP, Velasco PT, Bigio EH, Finch CE, Krafft GA, Klein WL, Synaptic targeting by Alzheimer's-related amyloid beta oligomers, J. Neurosci. 24 (2004) 10191-10200.

Laferla FM, Green KN, Oddo S, Intracellular amyloid-β in Alzheimer's disease. Nat. Rev.

Lagier-Tourenne C, Polymenidou M, Cleveland DW (2010) TDP-43 and FUS/TLS: emerging roles in RNA processing and neurodegeneration. Hum Mol Genet 19:R46–R64. doi:10.1093/ hmg/ddq137

Lai Z, Colón W, Kelly JW. The acid-mediated denaturation pathway of transthyretin yields a conformational intermediate that can self-assemble into amyloid. Biochemistry. 1996 May 21;35(20):6470-82.

Lai, Z., Colon, W., and Kelly, J. W. (1996) *Biochemistry***35**, 6470-6482

Lambert JC, Heath S, Even G, Campion D, Sleegers K, Hiltunen M, Combarros O, Zelenika D, Bullido MJ, Tavernier B, Letenneur L, Bettens K, Berr C, Pasquier F, Fievet N, Barberger- Gateau P, Engelborghs S, De Deyn P, Mateo I, Franck A, Helisalmi S, Porcellini E, Hanon O, de Pancorbo MM, Lendon C, Dufouil C,

Jaillard C, Leveillard T, Alvarez V, Bosco P, Mancuso M, Panza F, Nacmias B, Bossu P, Piccardi P, Annoni G, Seripa D, Galimberti D, Hannequin D, Licastro F, Soininen H, Ritchie K, Blanche H, Dartigues JF, Tzourio C, Gut I, Van Broeckhoven C, Alperovitch A, Lathrop M, Amouyel P (2009) Genome-wide association study identifies variants at CLU and CR1 associated with Alzheimer's disease. Nat Genet 41:1094–1099

Lambert MP, Barlow AK, Chromy BA, Edwards C, Freed R, Liosatos M, Morgan TE, Rozovsky I, Trommer B, Viola KL, Wals P, Zhang C, Finch CE, Krafft GA, Klein WL (1998) Diffusible, nonfibrillar ligands derived from Abeta1–42 are potent central nervous system neurotoxins. Proc Natl Acad Sci USA 95:6448–6453

Lesne S, Koh MT, Kotilinek L, Kayed R, Glabe CG, Yang A, Gallagher M, Ashe KH (2006) A specific amyloid-beta protein assembly in the brain impairs memory. Nature 440:352–357

Levinthal C. 1969. How to fold graciously, pp. 22-24. University of Illinois press Stefani M Protein folding and misfolding on surfaces. Int J Mol Sci. 2008 Dec;9(12):2515-42. doi:0.3390/ijms9122515. Epub 2008 Dec 9.

Li J, Hu J, Shao B, Zhou W, Cui Y, Dong C, Ezoulin JM, Zhu X, Ding W, Heymans F, Chen H, Protection of PMS777, a new AChE inhibitor with PAF antagonism, against amyloid-beta-induced neuronal apoptosis and neuroinflammation, Cell Mol. Neurobiol. 29 (2009) 589-595.

Li X, Masliah E, Reixach N, Buxbaum JN: Neuronal production of transthyretin in human and murine Alzheimer's disease: is it protective? J Neurosci 2011, 31:12483-12490.

Li, X., and Buxbaum, J. N. (2011) *Molecular neurodegeneration***6**, 79

Li, X., Masliah, E., Reixach, N., and Buxbaum, J. N. (2011) *The Journal of neuroscience : the official journal of the Society for Neuroscience***31**, 12483-12490

Li, X., Masliah, E., Reixach, N., and Buxbaum, J. N. (2011) *The Journal of neuroscience : the official journal of the Society for Neuroscience***31**, 12483-12490

Lim, K. H., Dyson, H. J., Kelly, J. W., and Wright, P. E. (2013) *Journal of molecular biology***425**, 977-988

Lin W-L, Dickson DW (2008) Ultrastructural localization of TDP-43 in filamentous neuronal inclusions in various neurodegenerative diseases. Acta Neuropathol 116:205–213. doi:10.1007/s00401-008-0408-9

Lindquist SL, Kelly JW. Chemical and biological approaches for adapting proteostasis to ameliorate protein misfolding and aggregation diseases: progress and prognosis. Cold Spring Harb Perspect Biol. 2011Dec 1;3(12). pii: a004507

Link, C. D. (1995) *Proceedings of the National Academy of Sciences of the United States of America***92**, 9368-9372

Liu L, Murphy RM: Kinetics of inhibition of beta-amyloid aggregation by transthyretin. Biochemistry (Mosc) 2006, 45:15702-15709.

Liu, L., and Murphy, R. M. (2006) *Biochemistry***45**, 15702-15709

Liu-Yesucevitz L, Bilgutay A, Zhang YJ, Vanderwyde T, Citro A, et al. (2010) Tar DNA binding protein-43 (TDP-43) associates with stress granules: analysis of cultured cells and pathological brain tissue. PLoS One 5: e13250.

Lovell MA, Markesbery WR, Amyloid beta peptide, 4-hydroxynonenal and apoptosis, Curr. Alzheimer Res. 3 (2006) 359-364.

Luheshi LM, Dobson CM. Bridging the gap: from protein misfolding to protein misfolding diseases. FEBS Lett. 2009 Aug 20;583(16):2581-6.

Luheshi LM, Hoyer W, de Barros TP, van Dijk Härd I, Brorsson AC, Macao B, Persson C, Crowther DC, Lomas DA, Ståhl S, Dobson CM, Härd T, Sequestration of the Abeta peptide prevents toxicity and promotes degradation in vivo, PLoS Biol. 8 (2010) e1000334.

M. Zampagni, R. Cascella, F. Casamenti, C. Grossi, E. Evangelisti, D. Wright, M. Becatti, G. Liguri, B. Mannini, S. Campioni, F. Chiti, C. Cecchi. A comparison of the biochemical modifications caused by toxic and nontoxic protein oligomers in cells, J. Cell Mol. Med. 15 (2011) 2106-2116.

Maachupalli-Reddy J, Kelley BD, De Bernardez Clark E (1997) Effect of inclusion body contaminants on the oxidative renaturation of hen egg white lysozyme. Biotechnol Prog 13: 144-150.

Mackenzie IRA, Bigio EH, Ince PG et al (2007) Pathological TDP-43 distinguishes sporadic amyotrophic lateral sclerosis from amyotrophic lateral sclerosis with SOD1 mutations. Ann Neurol 61:427–434. doi:10.1002/ana.21147,

Mannini B, Cascella R, Zampagni M, van Waarde-Verhagen M, Meehan S, Roodveldt C, Campioni S, Boninsegna M, Penco A, Relini A, Kampinga HH, Dobson CM, Wilson MR, Cecchi C, Chiti F, Molecular mechanisms used by chaperones to reduce the toxicity of aberrant protein oligomers, Proc. Natl. Acad. Sci. U. S. A. 109 (2012) 12479-12484.

Matagne A, Dobson CM. The folding process of hen lysozyme: a perspective from the 'new view'. Cell Mol Life Sci. 1998 Apr;54(4):363-71.

Matouschek A., and Fersht A.R. (1991) Protein engineering in analysis of protein folding pathways and stability. *Methods Enzymol* 202, 82-112.

Matouschek, A., Kellis, J. T., Jr., Serrano, L., Bycroft, M., and Fersht, A. R. (1990) *Nature***346**, 440-445

Mattson MP (1999) Impairment of membrane transport and signal transduction systems by amyloidogenic proteins. Methods Enzymol 309:733.768

Matus A (1990) Microtubule-associated proteins and the determination of neuronal form. J Physiol (Paris) 84:134–137

Mayor U, Guydosh NR, Johnson CM, Grossmann JG, Sato S, Jas GS, Freund SM, Alonso DO, Daggett V, Fersht AR The complete folding pathway of a protein from nanoseconds to microseconds. Nature.2003 Feb 20;421(6925):863-7.

Mazur-Kolecka Bcdae, Frackowiak J, Wisniewski HM: Apolipoproteins E3 and E4 induce, and transthyretin prevents accumulation of the Alzheimer's [beta]-amyloid peptide in cultured vascular smooth muscle cells. Brain Res 1995, 698:217-222.

Monaco HL. Three-dimensional structure of the transthyretin-retinol-binding protein complex. Clin Chem Lab Med. 2002; **40**: 1229-1236.

Moreira PI, Santos MS, Moreno A, Rego AC, Oliveira C (2002) Effect of amyloid beta-peptide on permeability transition pore: a comparative study. J Neurosci Res 15:257–267

Morimoto RI, Cuervo AM. 2009. Protein homeostasis and aging: Taking care of proteins fromthe cradle to the grave. J Gerontol, Ser A 64A: 167–170.

Morimoto RI, Proteotoxic stress and inducible chaperone networks in neurodegenerative disease and aging, Genes Dev. 22 (2008) 1427-1438.

Morimoto RI. 1998. Regulation of the heat shock transcriptional response: Cross talk between a family of heat shock factors, molecular chaperones, and negative regulators. Genes Dev 12: 3788–3796.

Morishima Y, Gotoh Y, Zieg J, Barrett T, Takano H, Flavell R, Davis RJ, Shirasaki Y, Greenberg ME (2001) Beta-amyloid induces neuronal apoptosis via a mechanism that involves the c-Jun N-terminal kinase pathway and the induction of Fas ligand. J Neurosci 21:7551–7560

N. Reixach , T.R. Foss , E. Santelli , J. Pascual , J.W. Kelly , J.N. Buxbaum. Human-murine transthyretin heterotetramers are kinetically stable and non-amyloidogenic. A lesson in the generation of transgenic models of diseases involving oligomeric proteins, J. Biol. Chem. 25 (2008) 2098-2107

N. Reixach, S. Deechongkit, X. Jiang, J.W. Kelly, J.N. Buxbaum. Tissue damage in the amyloidoses: Transthyretin monomers and nonnative oligomers are the major cytotoxic species in tissue culture, Proc. Natl. Acad. Sci. U. S. A. 101 (2004) 2817–2822.

N.A. Thornberry, T.A. Rano, E.P. Peterson, D.M. Rasper, T. Timkey, M. Garcia-Calvo, V.M. Houtzager, P.A. Nordstrom, S. Roy, J.P. Vaillancourt, K.T. Chapman, D.W. Nicholson. A combinatorial approach defines specificities of members of the caspase family and granzyme B. Functional relationships established for key mediators of apoptosis, J. Biol. Chem. 272 (1997) 17907–17911.

Narayan P, Meehan S, Carver JA, Wilson MR, Dobson CM, Klenerman D, Amyloid-β Oligomers are Sequestered by both Intracellular and Extracellular Chaperones, Biochemistry. 51 (2012) 9270-9276.

Narita M, Holtzman DM, Schwartz AL, Bu G, Alpha2-macroglobulin complexes with and mediates the endocytosis of beta-amyloid peptide via cell surface low-density lipoprotein receptor-related protein, J. Neurochem. 69 (1997) 1904-1911.

Nettleton, E. J., Sunde, M., Lai, Z., Kelly, J. W., Dobson, C. M., and Robinson, C. V. (1998) *Journal of molecular biology***281**, 553-564

Neumann M, Sampathu DM, Kwong LK et al (2006) Ubiquitinated TDP-43 in frontotemporal lobar degeneration and amyotrophic lateral sclerosis. Science 314:130–133. doi:10.1126/ science.1134108

Neumann, M. *et al.* Phosphorylation of S409/410 of TDP-43 is a consistent feature in all sporadic and familial forms of TDP-43 proteinopathies. *Acta Neuropathol.* **117**, 137–149 (2009).

Neumann, M. et al. Ubiquitinated TDP-43 in frontotemporal lobar degeneration and amyotrophic lateral sclerosis. Science 314, 130–133 (2006). TDP43 protein is identified biochemically, immunohistochemically and by amino acid sequence analysis as the major component of proteinaceous ubiquitin-positive inclusions in FTLD and ALS. Pathologic TDP43 is found to be ubiquitylated, phosphorylated and cleaved, and is associated with nuclear clearance of normal TDP43.

Neurosci. 8 (2007) 499–450.

Ng L, Bernard A, Lau C, Overly CC, Dong HW, Kuan C, Pathak S, Sunkin SM, Dang C, Bohland JW, et al: An anatomic gene expression atlas of the adult mouse brain. Nat Neurosci 2009, 12:356-362.

Nielsen HM, Veerhuis R, Holmqvist B, Janciauskiene S, Binding and uptake of A beta1-42 by primary human astrocytes in vitro, Glia. 57 (2009) 978-988.

Nishimura AL, Mitne-Neto M, Silva HCA et al (2004) A mutation in the vesicle-trafficking protein VAPB causes late-onset spinal muscular atrophy and amyotrophic lateral sclerosis. Am J Hum Genet 75:822–831. doi:10.1086/425287

NLomas DA,Carrell RW. Serpinopathies and the conformational dementias. at Rev Genet. 2002 Oct;3(10):759-68.

Nyrkova IA, Semenov AN, Aggeli A, Bell M, Boden N, et al. (2000) Self-assembly and structure transformations in living polymers forming fibrils. Eur Phys J B 17: 499-513.

Oberg K, Chrunyk BA, Wetzel R, Fink AL (1994) Native-like secondary structure in interleukin-1 beta inclusion bodies by attenuated total reflectance FTIR. Biochemistry 33: 2628-2634.

Oda T, Wals P, Osterburg HH, Johnson SA, Pasinetti GM, Morgan TE, Rozovsky I, Stine WB, Snyder SW, Holzman TF, Kraft GA, Finch CE, Clusterin (apoJ) alters the aggregation of amyloid beta-peptide (A beta 1-42) and forms slowly sedimenting A beta complexes that cause oxidative stress, Exp. Neurol. 136 (1995) 22-31.

Oddo S, Billings L, Kesslak JP, Cribbs DH, LaFerla FM, Abeta immunotherapy leads to clearance of early, but not late, hyperphosphorylated tau aggregates via the proteasome. Neuron. 43 (2004) 321-332.

Ojha J, Masilamoni G, Dunlap D, Udoff RA, Cashikar AG Sequestration of toxic oligomers by HspB1 as a cytoprotective mechanism, Mol. Cell Biol. 31 (2011) 3146-3157.

P. Hammarström, M. Persson, P.O. Freskgård, L.G. Mårtensson, D. Andersson, B.H. Jonsson, U. Carlsson. Structural mapping of an aggregation nucleation site in a molten globule intermediate. J. Biol. Chem. 274 (1999) 32897-32903.

P.N. Lacor, M.C. Buniel, L. Chang, S.J. Fernandez, Y. Gong, K.L. Viola, M.P. Lambert, P.T. Velasco, E.H. Bigio, C.E. Finch, G.A. Krafft, W..L Klein. Synaptic targeting by Alzheimer's-related amyloid beta oligomers, J. Neurosci. 24 (2004) 10191-10200.

Palha JA, Moreira P, Wisniewski T, Frangione B, Saraiva MJ: Transthyretin gene in Alzheimer's disease patients. Neurosci Lett 1996, 204:212-214.

Palmieri Lde, C., Lima, L. M., Freire, J. B., Bleicher, L., Polikarpov, I., Almeida, F. C., and Foguel, D. (2010) *The Journal of biological chemistry***285**, 31731-31741

Paxinos G, Watson CR, Emson PC, AChE-stained horizontal sections of the rat brain in stereotaxic coordinates, J. Neurosci. Methods. 3 (1980) 129-149.

Pensalfini A, Zampagni M, Liguri G, Becatti M, Evangelisti E, Fiorillo C, Bagnoli S, Cellini E, Nacmias B, Sorbi S, Cecchi C, Membrane cholesterol enrichment prevents Aβ-induced oxidative stress in Alzheimer's fibroblasts, Neurobiol. Aging. 32 (2011) 210-222.

Pickart CM, Cohen RE, Proteasomes and their kin: proteases in the machine age, Nat. Rev. Mol. Cell Biol. 5 (2004) 177-187.

Pitkanen P, Westermark P, Cornwell GGIII (1984) Senile systemic amyloidosis. Am J Pathol 117:391–399

Polymenidou, M. *et al.* Long pre-mRNA depletion and RNA missplicing contribute to neuronal vulnerability from loss of TDP-43. *Nature Neurosci.* **14**, 459–468 (2011).

Potter MA, Luxton G (2002) Transthyretin measurement as a screening tool for protein calorie malnutrition in emergency hospital admissions. Clin Chem Lab Med 40:1349–1354

Powers ET, Morimoto RI, Dillin A, Kelly JW, Balch WE. 2009. Biological and chemical approaches to diseases of proteostasis deficiency. Annu Rev Biochem 78: 23.21– 23.33.

Powers JM, Schlaepfer WW, Willingha MC, Hall BJ, An immunoperoxidase study of senile cerebral amyloidosis with pathogenetic considerations, J. Neuropathol. Exp. Neurol. 40 (1981) 592-612.

Price JM, Chi X, Hellermann G, Sutton ET: Physiological levels of betaamyloid induce cerebral vessel dysfunction and reduce endothelial nitric oxide production. Neurol Res 2001, 23:506-512.

Przybycien TM, Dunn JP, Valax P, Georgiou G (1994) Secondary structure characterization of beta-lactamase inclusion bodies. Protein Eng 7: 131-136.

Quintas, A., Vaz, D. C., Cardoso, I., Saraiva, M. J., and Brito, R. M. (2001) *The Journal of biological chemistry***276**, 27207-27213

R. Cascella, S. Conti, F. Tatini, E. Evangelisti, T. Scartabelli, F. Casamenti, M.R. Wilson, F. Chiti, C. Cecchi. Extracellular chaperones prevent $A\beta_{42}$-induced toxicity in rat brains, Biochim. Biophys. Acta 1832 (2013) 1217–1226.

R. Krishnan, S.L. Lindquist. Structural insights into a yeast prion illuminate nucleation and strain diversity, Nature 435 (2005) 765-772.

Radford SE, Dobson CM. From computer simulations to human disease: emerging themes in protein folding. Cell. 1999 Apr 30;97(3):291-8.

Ramshini H, Parrini C, Relini A, Zampagni M, Mannini B, et al. (2011) Large proteins have a great tendency to aggregate but a low propensity to form amyloid fibrils. PLoS One 6: e16075.

Rasband WS, ImageJ. US, National Institutes of Health, Bethesda, Maryland. (1997–2008) http://rsb.info.nih.gov/ij/

Raz A, Goodman DS. The interaction of thyroxine with human plasma prealbumin and with the prealbumin-retinol-binding protein complex. J Biol Chem. 1969; **244**: 3230-3237.

Reitz C1, Mayeux R2 Alzheimer disease: Epidemiology, diagnostic criteria, risk factors and biomarkers. Biochem Pharmacol. 2014 Jan 4. [Epub ahead of print]

Reixach N, Deechongkit S, Jiang X, Kelly JW, Buxbaum JN (2004) Tissue damage in the amyloidoses: transthyretin monomers and non-native oligomers are the major cytotoxic species in tissue culture. Proc Natl Acad Sci USA 101:2817– 2822

Reixach, N., Deechongkit, S., Jiang, X., Kelly, J. W., and Buxbaum, J. N. (2004) *Proceedings of the National Academy of Sciences of the United States of America***101**, 2817-2822

Religa T.L., Markson J.S., Mayor U., Freund S.M., and Fersht A.R. (2005) Solution structure of a protein denatured state and folding intermediate. *Nature* 437, 1053-1056.

Richartz E, Batra A, Simon P, Wormstall H, Bartels M, Buchkremer G, Schott K, Diminished production of proinflammatory cytokines in patients with Alzheimer's disease, Dement. Geriatr. Cogn. Disord. 19 (2005) 184-188.

Robinson JL, Geser F, Stieber A, Umoh M, Kwong LK, et al. (2013) TDP-43 skeins show properties of amyloid in a subset of ALS cases. Acta Neuropathol 125: 121-131.

Rocken C, Saeger W, Linke RP (1994) Gastrointestinal amyloid deposits in old age. Pathol Res Pract 190:641–649

Roder H., Elove G.A., and Englander S.W. (1988) Structural characterization of folding intermediates in cytochrome c by H-exchange labelling and proton NMR. *Nature* 335, 700-704.

Roselli F, Tirare M, Lu J, Hutzler P, Lamberti P, Livrea P, Morabito M, Almeida OF, Soluble beta-amyloid1-40 induces NMDA-dependent degradation of postsynaptic density-95 at glutamatergic synapses, J. Neurosci. 25 (2005) 11061-11070.

Rosen DR, Siddique T, Patterson D et al (1993) Mutations in Cu/Zn superoxide dismutase gene are associated with familial amyotrophic lateral sclerosis. Nature 362:59–62. doi:10.1038/362059a0

Rosi MC, Luccarini I, Grossi C, Fiorentini A, Spillantini MG, Prisco A, Scali C, Gianfriddo M, Caricatole A, Terstappen GC, Casamenti F, Increased Dickkopf-1 expression in transgenic mouse models of neurodegenerative disease, J. Neurochem. 112 (2010) 1539-1551.

Ross CA (2002) Polyglutamine pathogenesis: emergence of unifying mechanisms for Huntington's disease and related disorders. Neuron 35:819–822

S. Campioni, B. Mannini, M. Zampagni, A. Pensalfini, C. Parrini, E. Evangelisti, A. Relini, M. Stefani, C.M. Dobson, C. Cecchi and F. Chiti. A causative link between the structure of aberrant protein oligomers and their ability to cause cellular dysfunction, Nat. Chem. Biol. 6 (2010) 140-147.

S. Choi, N. Reixach, S. Connelly, S.M. Johnson , I.A. Wilson , J.W. Kelly. A substructure combination strategy to c reate potent and selective transthyretin kinetic stabilizers that prevent amyloidogenesis and cytotoxicity, J. Am. Chem. Soc. 132 (2010) 1359-70.

S. Orrenius, B. Zhovotovsky, P. Nicotera. Regulation of cell death: the calciumapoptosis link. Nat. Rev. 4 (2003) 552–565.

Sabaté R, Espargaró A, Saupe SJ, Ventura S (2009) Characterization of the amyloid bacterial inclusion bodies of the HET-s fungal prion. Microb Cell Fact 8: 56.

Saini A, Chauhan VS (2011) Delineation of the core aggregation sequences of TDP-43 C-terminal fragment. Chembiochem 12: 2495-2501.

Santoro, M. M., and Bolen, D. W. (1988) *Biochemistry***27**, 8063-8068

Schmid, F. X. (2001) *Advances in protein chemistry***59**, 243-282

Schultz K, Nilsson K, Nielsen JE, Lindquist SG, Hjermind LE, Andersen BB, Wallin A, Nilsson C, Petersen A: Transthyretin as a potential CSF biomarker for Alzheimer's disease and dementia with Lewy bodies: effects of treatment with cholinesterase inhibitors. Eur J Neurol 2010, 17:456-460.

Schwarzman AL, Goldgaber D: Interaction of transthyretin with amyloid beta-protein: binding and inhibition of amyloid formation. Ciba Found Symp 1996, 199:146-160.

Schwarzman AL, Gregori L, Vitek MP, Lyubski S, Strittmatter WJ, Enghilde JJ, Bhasin R, Silverman J, Weisgraber KH, Coyle PK: Transthyretin sequesters amyloid beta protein and prevents amyloid formation. Proc Natl Acad Sci USA 1994, 91:8368-8372.

Schwarzman AL, Tsiper M, Wente H, Wang A, Vitek MP, Vasiliev V, Goldgaber D: Amyloidogenic and anti-amyloidogenic properties of recombinant transthyretin variants. Amyloid 2004, 11:1-9.

Schwarzman, A. L., Gregori, L., Vitek, M. P., Lyubski, S., Strittmatter, W. J., Enghilde, J. J., Bhasin, R., Silverman, J., Weisgraber, K. H., Coyle, P. K., and et al. (1994) *Proceedings of the National Academy of Sciences of the United States of America***91**, 8368-8372

Sebastião MP, Saraiva MJ, Damas AM. The crystal structure of amyloidogenic Leu55 --> Pro transthyretin variant reveals a possible pathway for transthyretin polymerization into amyloid fibrils. J Biol Chem. 1998 Sep 18;273(38):24715-22.

Sekijima, Y., Wiseman, R. L., Matteson, J., Hammarstrom, P., Miller, S. R., Sawkar, A. R., Balch, W. E., and Kelly, J. W. (2005) *Cell***121**, 73-85

Selkoe DJ (2002) Alzheimer's disease is a synaptic failure. Science 298:789–791

Selkoe DJ Alzheimer's disease: genes, proteins, and therapy. Physiol Rev. 2001 Apr;81(2):741-66.

Selkoe DJ. Alzheimer's disease. Cold Spring Harb Perspect Biol. 2011 Jul 1;3(7).

Selkoe DJ. Alzheimer's disease. In the beginning... Nature. 1991 Dec 12;354(6353):432-3.

Serag, A. A., Altenbach, C., Gingery, M., Hubbell, W. L., and Yeates, T. O. (2002) *Nature structural biology***9**, 734-739

Serot JM, Christmann D, Dubost T, Couturier M: Cerebrospinal fluid transthyretin: Aging and late onset Alzheimer's disease. J Neurol Neurosurg Psychiatry 1997, 63:506-508.

Serpell LC, Sunde M, Benson MD, Tennent GA, Pepys MB, Fraser PE The protofilament substructure of amyloid fibrils. J Mol Biol. 2000 Jul 28;300(5):1033-9.

Shastry M.C., Luck S.D., and Roder H. (1998) A continuous-flow capillary mixing method to monitor reactions on the microsecond time scale. *Biophys J* 74, 2714-2721.

Shirahama T, Skinner M, Westermark P, Rubinow A, Cohen AS, Brun A, Kemper TL: Senile cerebral amyloid. Prealbumin as a common constituent in the neuritic plaque, in the neurofibrillary tangle, and in the microangiopathic lesion. Am J Pathol 1982, 107:41-50

Sicorello A, Torrassa S, Soldi G, Gianni S, Travaglini-Allocatelli C, et al. (2009) Agitation and high ionic strength induce amyloidogenesis of a folded PDZ domain in native conditions, Biophys J 96: 2289-2298.

Sorgjerd, K., Klingstedt, T., Lindgren, M., Kagedal, K., and Hammarstrom, P. (2008) *Biochemical and biophysical research communications***377**, 1072-1078

Sousa JC, Cardoso I, Marques F, Saraiva MJ, Palha JA: Transthyretin and Alzheimer's disease: where in the brain? Neurobiol Aging 2007, 28:713-718

Sousa MM, Cardoso I, Fernandes R, Guimaraes A, Saraiva MJ (2001) Deposition of transthyretin in early stages of familial amyloidotic polyneuropathy: evidence for toxicity of nonfibrillar aggregates. Am J Pathol 159:1993–2000

Sousa, M. M., Cardoso, I., Fernandes, R., Guimaraes, A., and Saraiva, M. J. (2001) *The American journal of pathology***159**, 1993-2000

Sousa, M. M., Fernandes, R., Palha, J. A., Taboada, A., Vieira, P., and Saraiva, M. J. (2002) *The American journal of pathology***161**, 1935-1948

Squier TC (2001) Oxidative stress and protein aggregation during biological aging. Exp Gerontol 36:1539–1550

Sreedharan, J. *et al.* TDP-43 mutations in familial and sporadic amyotrophic lateral sclerosis. *Science* **319**, 1668–1672 (2008))

Stefani M, Dobson CM. Protein aggregation and aggregate toxicity: new insights into protein folding, misfolding diseases and biological evolution. J Mol Med (Berl). 2003 Nov;81(11):678-99.

Stefani M. Protein folding and misfolding on surfaces. Int J Mol Sci. 2008 Dec;9(12):2515-42.

Stein TD, Anders NJ, Decarli C, Chan SL, Mattson MP, Johnson JA: Neutralization of transthyretin reverses the neuroprotective effects of secreted amyloid precursor protein (APP) in APP(Sw) mice resulting in tau phosphorylation and loss of hippocampal neurons: Support for the amyloid hypothesis. J Neurosci 2004, 24:7707-7717.

Stéphan A, Laroche S, Davis S Generation of aggregated beta-amyloid in the rat hippocampus impairs synaptic transmission and plasticity and causes memory deficits. J. Neurosci. 21 (2001) 5703-5714.

Strauss S, Bauer J, Ganter U, Jonas U, Berger M, Volk B, Detection of interleukin-6 and alpha 2-macroglobulin immunoreactivity in cortex and hippocampus of Alzheimer's disease patients, Lab. Invest. 66 (1992) 223-230.

Strauss S, Bauer J, Ganter U, Jonas U, Berger M, Volk B, Detection of interleukin-6 and alpha 2-macroglobulin immunoreactivity in cortex and hippocampus of Alzheimer's disease patients, Lab. Invest. 66 (1992) 223-230.

Strittmatter WJ, Weisgraber KH, Huang DY, Dong LM, Salvesen GS, Pericak- Vance M, Schmechel D, Saunders AM, Goldgaber D, Roses AD: Binding of human apolipoprotein E to synthetic amyloid beta peptide: isoformspecific effects and implications for late-onset Alzheimer disease. Proc Natl Acad Sci USA 1993, 90:8098-8102.

Strong, M. J. *et al.* TDP43 is a human low molecular weight neurofilament (hNFL) mRNA-binding protein. *Mol. Cell. Neurosci.* **35**, 320–327 (2007).

Taipale M, Jarosz DF, Lindquist S. 2010. HSP90 at the hub of protein homeostasis: Emerging mechanistic insights. Nat Rev Mol Cell Biol 11: 515–528.

Teng MH, Yin JY, Vidal R, Ghiso J, Kumar A, Rabenou R, Shah A, Jacobson DR, Tagoe C, Gallo G, Buxbaum J (2001) Amyloid and nonfibrillar deposits in mice transgenic for wild-type human transthyretin: a possible model for senile systemic amyloidosis. Lab Invest 81:385–396

Ternstrom, T., Mayor, U., Akke, M., and Oliveberg, M. (1999) *Proceedings of the National Academy of Sciences of the United States of America***96**, 14854-14859

Terry, C. J., Damas, A. M., Oliveira, P., Saraiva, M. J. M., Alves, I. L., Costa, P. P., Matias, P. M., Sakaki, Y., and Blake, C. C. F. (1993) *EMBO J.* **12,** 735–741

Thomas PJ, Qu BH, Pedersen PL Defective protein folding as a basis of human disease. Trends Biochem Sci. 1995 Nov;20(11):456-9.

Tollervey JR, Curk T, Rogelj B et al (2011) Characterizing the RNA targets and position-dependent splicing regulation by TDP-43. Nat Neurosci 14:452–458. doi:10.1038/nn.2778

Travaglini-Allocatelli C., Gianni S., and Brunori M. (2004) A common folding mechanism in the cytochrome c family. *Trends Biochem Sci* 29, 535-541.

Travaglini-Allocatelli, C., Gianni, S., Morea, V., Tramontano, A., Soulimane, T., and Brunori, M. (2003) *The Journal of biological chemistry***278**, 41136-41140

Trougakos IP, Gonos ES Regulation of clusterin/apolipoprotein J, a functional homologue to the small heat shock proteins, by oxidative stress in ageing and age-related diseases, Free Radic. Res. 40 (2006) 1324-1334.

Tsuzuki K, Fukatsu R, Yamaguchi H, Tateno M, Imai K, Fujii N, Yamauchi T: Transthyretin binds amyloid [beta] peptides, A[beta]1-42 and A[beta]1- 40 to form complex in the autopsied human kidney - possible role of transthyretin for A[beta] sequestration. Neurosci Lett 2000, 281:171-174.

Umetsu M, Tsumoto K, Ashish K, Nitta S, Tanaka Y, et al. (2004) Structural characteristics and refolding of in vivo aggregated hyperthermophilic archaeon proteins. FEBS J 557: 49-56.

Uversky, V. N., and Fink, A. L. (2004) *Biochimica et biophysica acta***1698**, 131-153

Valax P, Georgiou G (1993) Molecular characterization of beta-lactamase inclusion bodies produced in Escherichia coli. 1. Composition. Biotechnol Prog 9: 539-547.

Walsh DM, Klyubin I, Fadeeva JV, Cullen WK, Anwyl R, Wolfe MS, et al. Naturally secreted oligomers of amyloid beta protein potently inhibit hippocampal long-term potentiation in vivo. Nature 2002; 416:535-9.

Walsh DM, Selkoe DJ, Deciphering the molecular basis of memory failure in Alzheimer's disease, Neuron. 44 (2004)181-193.

Van Deerlin VM, Leverenz JB, Bekris LM et al (2008) TARDBP mutations in amyotrophic lateral sclerosis with TDP-43 neuropathology: a genetic and histopathological analysis. Lancet Neurol 7:409–416. doi:10.1016/S1474-4422(08)70071-1)

Wang L (2009) Towards revealing the structure of bacterial inclusion bodies. Prion 3: 139-145.

Wang L, Maji SK, Sawaya MR, Eisenberg D, Riek R (2008) Bacterial inclusion bodies contain amyloid-like structure. PLoS Biol 6: e195.

Varadarajan S, Yatin S, Aksenova M, Butterfield DA, Review: Alzheimer's amyloid beta-peptide-associated free radical oxidative stress and neurotoxicity, J. Struct. Biol. 130 (2000) 184-208.

Vardy ERLC, Catto AJ, Hooper NM. Proteolytic mechanisms in amyloid-beta metabolism: therapeutic implications for Alzheimer’s disease. Trends Mol Med 2005; 11:464-72.

Vatassery GT, Quach HT, Smith WE, Benson BA, Eckfeldt JH: A sensitive assay of transthyretin (prealbumin) in human cerebrospinal fluid in nanogram amounts by ELISA. Clin Chim Acta 1991, 197:19-25

Wegiel J, Kuchna I, Nowicki K, Frackowiak J, Mazur-Kolecka B, Imaki H, Wegiel J, Mehta PD, Silverman WP, Reisberg B, Deleon M, Wisniewski T, Pirttilla T, Frey H, Lehtimäki T, Kivimäki T, Visser FE, Kamphorst W, Potempska A, Bolton D, Currie JR, Miller DL, Intraneuronal Aβ immunoreactivity is not a predictor of brain amyloidosis-β or neurofibrillary degeneration. Acta Neuropathol. (Berl) 113 (2007) 389–402.

Weibezahn J, Schlieker C, Tessarz P, Mogk A, Bukau B, Novel insights into the mechanism of chaperone-assisted protein disaggregation, Biol. Chem. 386 (2005) 739-744.

Vendruscolo M, Dobson CM Towards complete descriptions of the free-energy landscapes of proteins. Philos Trans A Math Phys Eng Sci. 2005 Feb 15;363(1827):433-50; discussion 450-2.

Vendruscolo M, Dobson CM. Structural biology: Protein self-assembly intermediates. Nat Chem Biol. 2013 Apr;9(4):216-7. doi: 10.1038/nchembio.1210.

Went, H. M., Benitez-Cardoza, C. G., and Jackson, S. E. (2004) *FEBS letters***567**, 333-338

Ventura S, Villaverde A (2006) Protein quality in bacterial inclusion bodies. Trends Biotechnol 24: 179-185.

Verkhratsky A, Olabarria M, Noristani HN, Yeh CY, Rodriguez JJ, Astrocytes in Alzheimer's disease, Neurotherapeutics 7 (2010) 399-412.

Westermark P, Benson MD, Buxbaum JN, Cohen AS, Frangione B, Ikeda S, Masters CL, Merlini G, Saraiva MJ, Sipe JD (2007) A primer of amyloid nomenclature. Amyloid 14:179–183

Westermark P, Benson MD, Buxbaum JN, Cohen AS, Frangione B, Ikeda S, Masters CL, Merlini G, Saraiva MJ, Sipe JD; Amyloid. Amyloid: toward terminology clarification. Report from the Nomenclature Committee of the International Society of Amyloidosis.2005 Mar;12(1):1-4.

White, J. T., and Kelly, J. W. (2001) *Proceedings of the National Academy of Sciences of the United States of America***98**, 13019-13024

Wiseman, R. L., Powers, E. T., and Kelly, J. W. (2005) *Biochemistry***44**, 16612-16623

Wisniewski T, Castano E, Ghiso J, Frangione B: Cerebrospinal fluid inhibits Alzheimer beta-amyloid fibril formation in vitro. Ann Neurol 1993, 34:631-633.

Wisniewski T, Frangione B: Apolipoprotein E: a pathological chaperone protein in patients with cerebral and systemic amyloid. Neurosci Lett 1992, 135:235-238.

Wright JR, Calkins E, Breen WJ, Stolte G, Schultz RT: Relationship of amyloid to aging. Review of the literature and systematic study of 83 patients derived rom a general hospital population. Medicine 1969, 48:39-60

Wyatt AR, Yerbury JJ, Berghofer P, Greguric I, Katsifis A, Dobson CM, Wilson MR, Clusterin facilitates in vivo clearance of extracellular misfolded proteins, Cell Mol. Life Sci. 68 (2011) 3919-3931.

Wyatt AR, Yerbury JJ, Dabbs RA, Wilson MR. Roles of extracellular chaperones in amyloidosis. J Mol Biol.2012 Aug 24;421(4-5):499-516.

Wyatt AR, Yerbury JJ, Ecroyd H, Wilson MR. Extracellular chaperones and proteostasis. Annu Rev Biochem. 2013;82:295-322.

X. Li, E. Masliah, N. Reixach, J.N. Buxbaum. Neuronal production of transthyretin in human and murine Alzheimer's disease: is it protective?, J. Neurosci. 31 (2011) 12483-12490.

Yankner BA, Caceres A, Duffy LK. Nerve growth factor potentiates the neurotoxicity of beta amyloidProc Natl Acad Sci U S A. 1990 Nov;87(22):9020-3.

Yerbury JJ, Kumita JR, Meehan S, Dobson CM, Wilson MR, alpha2-Macroglobulin and haptoglobin suppress amyloid formation by interacting with prefibrillar protein species, J. Biol. Chem. 284 (2009) 4246-4254.

Yerbury JJ, Kumita JR, Meehan S, Dobson CM, Wilson MR, alpha2-Macroglobulin and haptoglobin suppress amyloid formation by interacting with prefibrillar protein species, J. Biol. Chem. 284 (2009) 4246-4254.

Yerbury JJ, Poon S, Meehan S, Thompson B, Kumita JR, Dobson CM, Wilson MR, The extracellular chaperone clusterin influences amyloid formation and toxicity by interacting with prefibrillar structures, FASEB J. 21 (2007) 2312-2322.

Zampagni M, Cascella R, Casamenti F, Grossi C, Evangelisti E, et al. (2011) A comparison of the biochemical modifications caused by toxic and non-toxic protein oligomers in cells. J Cell Mol Med 15: 2106-2116.

Zampagni M, Wright D, Cascella R, D'Adamio G, Casamenti F, Evangelisti E, Cardona F, Goti A, Nacmias B, Sorbi S, Liguri G, Cecchi C, Novel S-acyl glutathione derivatives prevent amyloid oxidative stress and cholinergic dysfunction in Alzheimer disease models, Free Radic. Biol. Med. 52 (2012) 1362-1371.

Zlokovic BV, Cerebrovascular transport of Alzheimer's amyloid beta and apolipoproteins J and E: possible anti-amyloidogenic role of the blood-brain barrier, Life Sci. 59 (1996) 1483-1497.